1 Status Report on the FINUDA offline software - 11.11.98

1.1 General structure of the software

The off-line software of the FINUDA experiment is composed of four main parts:

1. The Monte Carlo simulation of the apparatus and of the physical events that will be recorded by the apparatus : hypernuclear events, physical background events, cosmic rays for calibration.

2. The Reconstruction Program composed by local (detector) and global (apparatus) Pattern Recognitions and Track Fitting Procedures. The Reconstruction Program is equipped by an Event Display essential both for the development phase of the software and for the debugging and analysis phase on the real data. Moreover the Reconstruction Program is designed to work both off-line on files of recorded events and on-line, with a proper interface with the data acquisition system, for on-line monitor of the data.

3. The Calibration Programs that have to read sets of real data (cosmic rays or calibration events on the beam) and produce calibration constants both for the different detectors (e.g. t_0 for the drift chambers) and for the whole apparatus (e.g. geometric calibrations). These sets of calibration constants must be stored in a data base and used by the reconstruction programs.

4. Physical analysis programs to be used for the analysis of the reconstructed data (DST's). These programs are in general developed using a package of physical analysis like PAW or Root.

The FINUDA Monte Carlo is essentially complete and stable whereas the Reconstruction Program is complete and tested with Monte Carlo events for what concerns the basic algorithms and the design of the data structures and their transport. The calibration programs are, on the contrary, in progress, since their their development follows the possibility of recording calibration data (cosmic rays or calibration events).

In this report the main results already obtained in the design of the apparatus and in the evaluation of its performances will be summarized. Specific reference will be made to the corresponding reports previously presented, which will be annexed to this document. On the contrary the latest results obtained in the evaluation of the rates for the exclusive measurement of the non-mesonic decay of hypernuclei will be illustrated in some detail.

Concerning the Reconstruction Program the results obtained in the evaluation of the efficiency of the reconstruction algorithms will be summarized. For this latter topic specific reference to the reports previously presented will be done too.

1.2 Tools, platforms, distribution

The off-line software is based on some tool of very general use: the basic simulation package is GEANT3.21: the (back)tracking package is GEANE3.21 closely correlated with the GEANT environment: the source code manager is CMZ and the memory manager is ZEBRA.

The programming language used is FORTRAN for the part of the code strictly off-line (Monte Carlo and Reconstruction algorithms), whereas the connection with the data acquisition, in particular for the on-line version of the Reconstruction Program, is written in C++. Similarly the off-line event display is based on KUIP and HIGZ (PAW Package), whereas the on-line Event Display is based on the use of the ROOT package.

The programs are running on different operating systems and platforms: on VaxStations and AlphaStations with Open VMS, on UNIX system on AlphaStations and finally on PC's using LINUX Operating System. The installation and distribution of the software is provided by information and material loaded in a Web page accessible by the members of the collaboration (http://fidabs.ing.unibs.it).

1.3 Monte Carlo simulation

The Monte Carlo simulation program is essentially complete and stable. The basic features of the FINUDA simulation program have been described in the FINUDA *Technical Report* (**Doc.1**). There the first design of the apparatus geometry and the first results concerning expected acceptance, momentum resolution for different type of particles coming from hypernucleus formation and decay, trigger rates and rejection powers have been reported.

A more realistic description of the apparatus was performed and studied in the *Status Report of May 95* (**Doc.2**). The improved design of the apparatus was aimed, on one side, to accurately evaluate and to optimize the acceptance and trigger rates and on the other to describe as well as possible the detector geometry and their support mechanical structures. The introduction of the mechanical structure in the Monte carlo description was important in order to evaluate accurately the effects of the machine induced background on trigger efficiency and pattern recognition procedures.

In the design of the interaction target region a particular attention was devoted to the study of the expected resolution in the vertex position. This is particularly relevant since the ultimate momentum resolution on the pion coming from the hypernucleus formation depends on the accuracy of the correction for the energy lost in crossing the target material. This study is reported in **Doc.3** and leaded to important indications for the design of microstrip target assembly.

The simulation of the response of the detectors is described in the *Status Reports of Sept 95* and *April 96* (**Doc.4** and **Doc.5**). A particular attention was devoted to the study of the silicon microstrips, since the performances requested to this device in FINUDA are more severe than in applications to other experiments. Moreover an accurate simulation of the response was an essential tool to develop efficient algorithms

for the detector pattern recognition. In the *Status Report of October 96* **(Doc.6)** the representation of the simulated response of the drift chambers and of the straw tube system is shown in the Event Display of the Reconstruction program and the description of the track fitting algorithm which accounts for the simulated signals is given.

Finally the Monte Carlo simulation program was used to perform calculations of the expected performances of the apparatus and to plan physical measurements. After the first evaluations of rates and resolutions for the measurements of hypernuclear spectra reported in the *Progress Report* **(Doc.1)** a extensive simulation of hypernuclear spectra from different hypernuclei was performed and reported in the *Status Report of June 97* **(Doc.7)**. In this study possible strategies of physical background suppression were studied, based on the unique possibility offered by the FINUDA apparatus to detect, with a large solid angle, both the pion coming from the hypernucleus formation and the proton coming from the hypernuclear decay or from background processes.

Recently the effort in simulation of physical processes was devoted to the more accurate simulation of performances and rates in the measurement of the non-mesonic decay of the hypernuclei. The results of this study will be briefly described in the following section.

1.4 Simulation of the measurement of the non-mesonic decay of hypernuclei

An accurate simulation of the measurement of the non-mesonic decay of hypernuclei in the FINUDA apparatus has been performed. It is worth recalling that the measurement of the non mesonic decay of hypernuclei is one of the most important physical achievements of the experiment since the data available are scarce and affected by large statistical and systematic errors. On the other side this measurements presents consistent difficulties, since it requests, at least for the neutron-neutron case, the measurement of two neutrons coming from the non mesonic decay of the hypernucleus. However the challenge is particularly attracting, since FINUDA is the only experimental apparatus which is potentially able to measure the complete hypernuclear event: the pion from the hypernuclar formation and the two nucleons from the hypernucleus decay.

To study the performances of the apparatus for the measurement of the non-mesonic decay of hypernuclei, a generator of the hypernucleus decay was needed. A very simplified model was adopted: in the framework of the DWIA a point like two hadron interaction was considered and the amplitude for one specified initial and final state was written as : $V_{fi} \int d^3r \Psi^*_{f1} \Psi^*_{f2} \Psi_{i1} \Psi_{i2}$. In this formula $\Psi_{i1} \Psi_{i2}$ represent the nuclear bound states for the colliding nucleon and hyperon and $\Psi^*_{f1} \Psi^*_{f2}$ are the distorted plane waves for the two outgoing nucleons. An incoherent sum over the different initial and final states of the nucleons was then performed; in this sum the V_{if} point like interaction is factorised away. Finally the transition amplitude is obtained by multipling this sum times a phase space factor.

The transition amplitude obtained accounts for the nuclear wave function of the

colliding nucleon and hyperon (Fermi momentum), for the adsorbtion of the nucleon in crossing the nuclear medium and for the phase space. In Fig. 1 the results of the generator for the nucleon energy and momentum and for the nucleon angular correlation are shown for the decay of the ${}^{12}_{\Lambda}C$. It is seen that the momentum of the outgoing nucleons is smeared by the Fermi momentum whereas a certain angular correlation between the two outgoing directions is conserved. It is useful to remark that the quantity that better keeps memory of the elementary hyperon-nucleon interaction is the sum of the energies of the two nucleons; it is very close to the available energy generated by the exothermic interaction, since the residual nucleus carries very small kinetic energy.

Let us recall that in the reconstruction of the emitted nucleons the proton is tracked in the spectrometer and its energy is reconstructed with an energy resolution of $1.3MeV$. On the other side the neutron can be reconstructed thanks to the signals induced in the outer scintillator array. The detection efficiency of the scintillator array, measured in calibration tests, was accounted for in the simulation; on average it amounts to 10%. The energy of the neutron was reconstructed on the basis of an estimated error on time of flight of $500ps$ (fwhm) and on a resolution on the zeta coordinate of the hit of the neutron on the scintillator slab of $6cm$ (fwhm). Under these condition the energy of the neutron is reconstructed with an average uncertainty of $5MeV$ (fwhm) depending, of course, on the neutron energy.

1.4.1 Measurement of the hypernucleus lifetime.

The measurement of the hypernucleus lifetime is based on the measurement of the difference between the time of flight of the delayed proton on the external scintillator array and the time of flight of the prompt pion coming from the hypernucleus formation. Both these time of flights have, naturally, to be corrected for the flight path of the particles.

An accurate simulation of the process and of the reconstruction procedure showed that, at a luminosity of $10^{32}cm^{-2}s^{-1}$ and a capture rate of 10^{-3}, the FINUDA apparatus is able to collect $18event/hour$ useful for the measurement of the hypernucleus lifetime. At this rate, in a week of data taking, hypernucleus lifetimes with statistical errors of some percent can be obtained. In fig. 2 the distributions of the time differences between proton and pion are shown for two different hypernucleus lifetimes. Additionally the fitting function adopted is shown; it is the convolution of a gaussian resolution function and of an exponential decay law where the hypernuclus lifetime is the fitting parameter.

1.4.2 Measurement of non-mesonic decay

In the measurement of non mesonic decay of the hypernuclei both nucleons produced by the decay of the hypernucleus have to measured; as mentioned before the proton coming from the proton-neutron decay is mode tracked in the apparatus whereas the neutron is produced by the proton-neutron or the neutron-neutron decay mode is recognized

as an isolated hit in the outer scintillator array of the apparatus, not connected with a charged signal, i.e. a charged track coming from the interaction region.

In the study of the efficiency in the recognition of the non-mesonic decay a particular attention has been devoted to the identification of the possibile physical backgrounds that can fake the recognition of the decay events. One of the most important source of background was recognized to be the neutral signals in the outer scintillator array generated by the photons coming from the decay of the π^0 produced by the decay of the K^+. This background is particularly dangerous since the time of flight distribution of these photons is superimposed to the time of flight distribution of the neutrons. In this condition, for the proton-neutron decay mode, the signal/background ratio is of the order of 0.6. Fortunately one may profit of some correlations that characterize the signals coming from the hypernuclear decay: in particular the angular correlation between the two nucleons and their total kinetic energy, which conserve memory of the elementary interaction (see Fig. 1).

In Fig. 3 The distributions of the time of flight, the angular correlation, and the total energy for the signal and the background in the proton-neutron decay mode are shown. One can see as the time of flight distributions are superimposed, whereas the angular and the total energy distributions are quite different. Appropriate cuts on the three distributions allow the background to be reduced to the 2.5% whereas the signal is reduced only to the 80%. This means that, at a luminosity of $10^{32} cm^{-2} s^{-1}$, the FINUDA apparatus is able to collect 2 event/hour of proton-neutron non-mesonic decay (at 10^{-3} capture rate). In one week of data taking 300 decay events can be recorded obtaining a statistical error of some percent on the ratio Γ_p/Γ_Λ.

The same study has been performed for the neutron-neutron decay mode where two neutrons have to be measured in the final state. In that case the effects of the background originated by the decay of the π^0 is particularly severe and, without any cuts, the signal/background ratio is of the order of 0.2. Cuts on time of flight, angular correlation and total energy allow this ratio to be increased to 11, which is a reasonable level of background. In Fig. 4 the angular distributions and the total energy for the signal and the background are shown. With the appropriate cuts the signal is reduced to the 93% and the background to the 1.5%. In these conditions at a luminosity of $10^{32} cm^{-2} s^{-1}$ and with a capture rate of 10^{-3} the FINUDA apparatus is able to collect 0.5 event/hour of neutron-neutron hypernuclear decay mode. This means that in a month of data taking 300 neutron-neutron events may be collected and 1300 proton-neutron events; this allows an important observable of the non mesonic decay, the neutron over proton induced decay ratio Γ_n/Γ_p to be measured with some percent statistical error.

1.5 Reconstruction Program

The basic algorithms of the reconstruction procedures, the data structure in ZEBRA format and the data transport inside the program from input (RDT) to output (DST), have been written and tested using sets of Monte Carlo generated events.

The structure of the reconstruction program is composed by :

1. Local Pattern Recognition procedures for two detectors : straw tube arrays and silicon microstrip modules.
2. Global Pattern Recognition for the full apparatus, which has been developed and tested for hypernuclear events and cosmic rays. The Pattern Recognition for other types of events like Bhabha scattering and Kaon-nucleon interaction are still in progress.
3. Vertex identification procedure and measurement of the vertex position.
4. Track Fitting procedures involving the four layers of detectors composing the spectrometer. Two different algorithms have been developed and tested: an iterative procedure based on the Wind spline algorithm (non uniform magnetic field) and a numerical integration procedure. Both the numerical integration procedure and the backtracking toward the vertex are based on the GEANE tracking package.
5. Event Display allowing both the Monte Carlo event and the reconstructed one to be shown in the same picture.

The basic structure of the reconstruction algorithms were designed and described in the FINUDA *Technical Report* (**Doc.1**). In particular it was pointed out the important role played, in the recognition of the kaons coming from the decay of the ϕ, by the silicon microstrip detector. In the same report the local Pattern Recognition for the straw tube detector was described as well as the global Pattern recognition for track identification in the full apparatus. In spite of the very low redundancy of the spatial information available and thanks to the simplicity of the triggered events and the low level of the physical noise, the Pattern Recognition procedures provided a good global efficiency, larger than 95%. Further tests of the effects of the machine induced background on the Pattern Recognition Procedures showed that they are practically negligible.

The description and the performance of the local Pattern Recognition of the silicon microstrip detector are illustrated in the *Status Report of April 96* (**Doc.5**). This reconstruction procedure implies different steps: clusterization of the struck strips on each module face, cluster association on z and ϕ sides and the reconstruction of the spatial coordinates by means of a weighted average of the strip positions. Finally an algorithm for particle identification based on both the charge released in the microstrip volume by the crossing track and the number of struck strips in the cluster has been developed, with the aim of recognizing the hit of the crossing kaons against the hits of inclined pions or protons.

Extensive tests of these algorithms with Monte Carlo generated events are described in the *Status Report of November 97* (**Doc.8**) where the efficiency reduction of the Global Pattern Recognition by the inefficiency of the microstrip local Pattern

Recognition is evaluated not more than 10%. This reduction is mainly due to a more correct estimation of the sensitive area of the microstrip modules; in fact, at the border of the sensitive area of each detector, the efficiency is reduced as a part of the deposited charge is not collected.

Concerning the Track Fitting procedure two main algorithms were developed:

1. a numerical integration of the track trajectory based on a Runge Kutta method and using the GEANE package. This method, which is described in the *Status Report of April 96* (**Doc.5**), has the advantage of exploiting at best the information coming from each detectors and of accounting accurately for the energy loss of the track along the trajectory. The disadvantages are well known: a certain instability against bad starting point of the fitting procedures and the need of a lot of computing time.

2. an iterative method of track fitting coupling the Wind spline algorithm for the microstrips, the drift chambers and the longitudinal straw tubes with a procedure of minimization of the residuals relative to the stereo straws. This latter method gave good results in term of stability, accuracy and computing time. For the backtracking towards the vertex the GEANE tracking package was used. The description and the performances of this track fitting algorithm are given in the *Status Report of October 96* (**Doc.6**).

1.6 Pattern Recognition and track fitting cosmic rays

The description and the performances of the procedures for Pattern Recognition and Track Fitting of cosmic rays crossing the apparatus in absence of magnetic field are given in the *Status Report of June 97* (**Doc.7**). Using sets of simulated cosmic rays it is shown that the spatial resolution which can be obtained with a geometrical calibration based on cosmic rays crossing straw tubes and drift chambers is of the order of $100\mu m$, in the plane orthogonal to the beam direction, and $250\mu m$ in the zeta direction.

1.7 Fitting of the measured magnetic field map; effect on the momentum resolution

In the *Status Report of November 97* (**Doc.8**) the procedure adopted for a first fitting of the measured magnetic field of the FINUDA solenoid has been described. Moreover the effects on the momentum resolution of possible uncertainties in the measurement and in the fitting of the magnetic field have been evaluated by Monte Carlo simulation. In particular several different situations were simulated : from the extreme cases were the tracks were generated accounting for the measured components of the magnetic field and reconstructed using a perfectly uniform field to the working situation in which the magnetic field is accounted both in the simulation and in the reconstruction.

The results are reported in Table 1 of the quoted Report. Summarizing the conclusions one can state that with a reasonably accurate measurement of the FINUDA

magnetic field and a good interpolation of the data, the required momentum resolution can be easily fulfilled in the whole tracking volume. However, even disregarding, in the reconstruction the non uniformity of the magnetic field, thanks to the low value of the transverse components, the nominal momentum resolution is completely preserved in the central region of the apparatus.

1.8 Off-line on-line connection

In conclusion it is worth mentioning that, recently, the off-line reconstruction programs have been completely integrated with the on-line programs for data acquisition and monitoring. At present the reconstruction programs are used to process off-line data coming from cosmic ray tests of a part of the apparatus and may be connected on-line for the monitoring of the data acquisition.

$$^{12}_{\Lambda}C \rightarrow {}^{10}B_{g.s.} + p + n \qquad ^{12}_{\Lambda}C \rightarrow {}^{10}C_{g.s.} + n + n$$

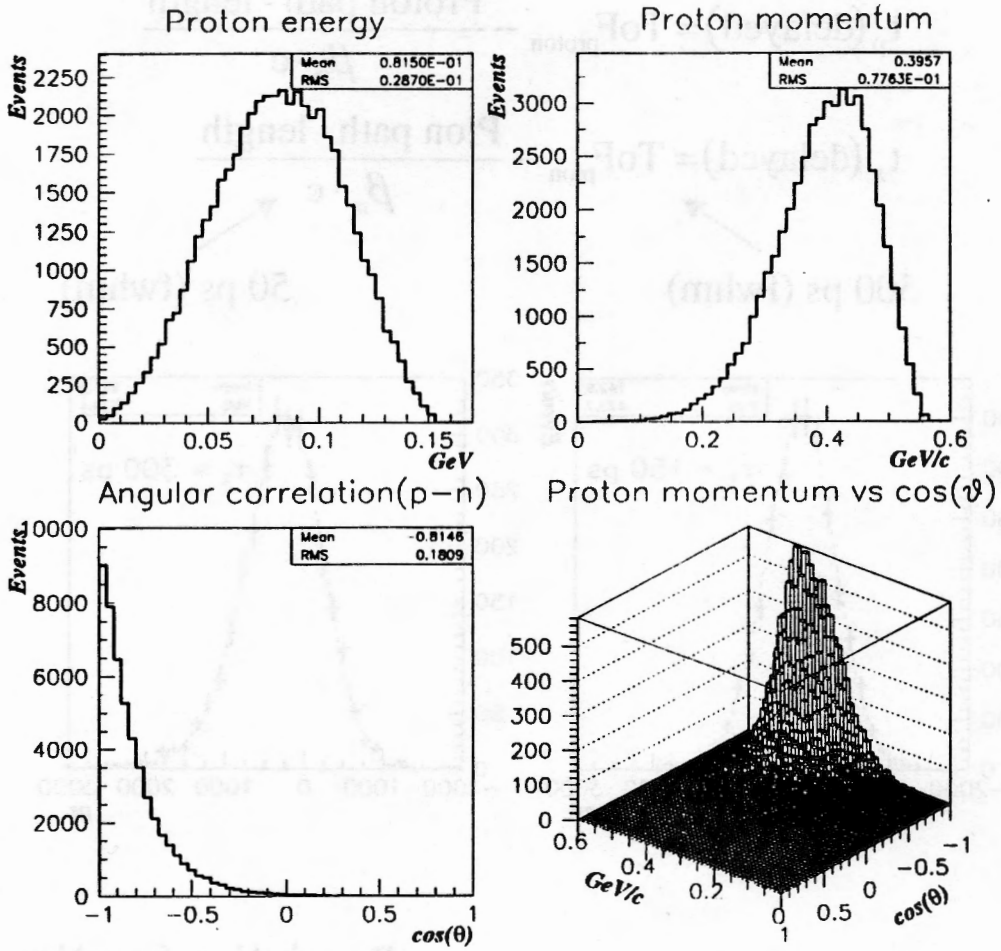

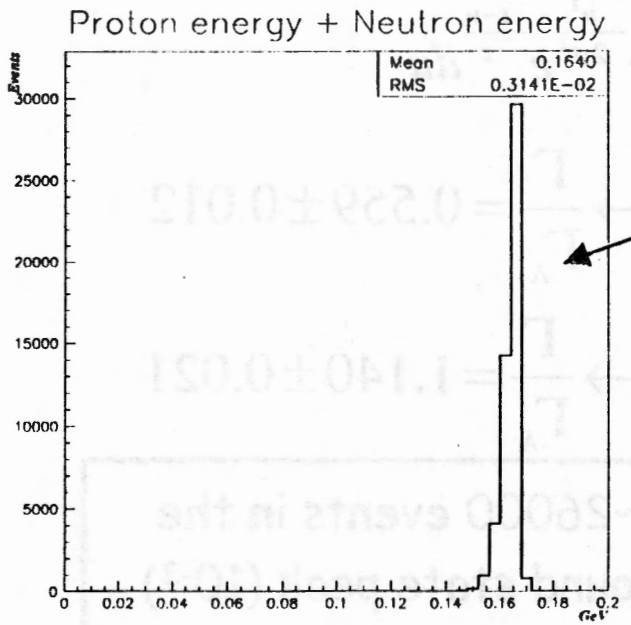

It keeps memory of the elementary interaction

Adsorbtion due to FSI :

Hypernucleus lifetime measurement

$$t_p(\text{delayed}) = \text{ToF}_{\text{proton}} - \frac{\text{Proton path - length}}{\beta_p \cdot c}$$

$$t_\pi(\text{delayed}) = \text{ToF}_{\text{pion}} - \frac{\text{Pion path - length}}{\beta_\pi \cdot c}$$

500 ps (fwhm)

50 ps (fwhm)

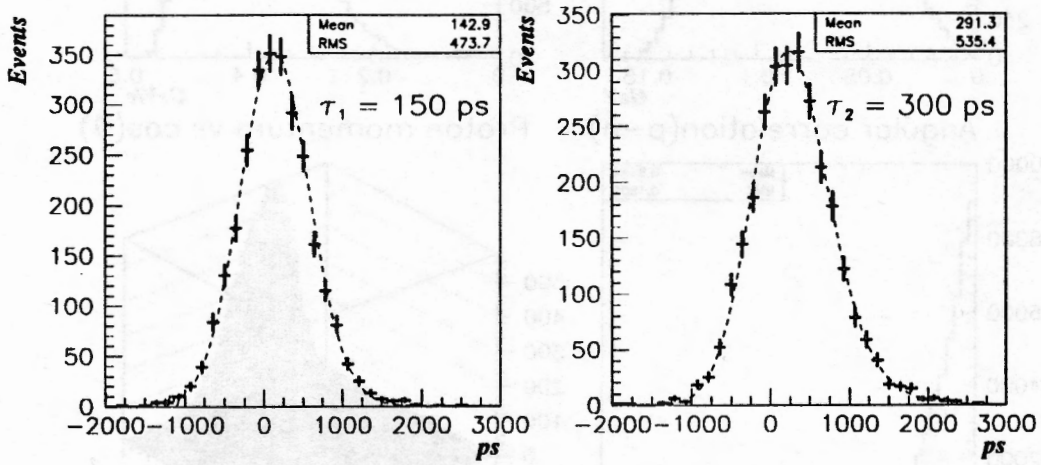

Fitting function :

Resolution function

Exponential decay

$$S(t) = \frac{1}{\sigma\sqrt{2\pi}} \frac{1}{\tau} \int_{-\infty}^{t} e^{-\frac{u^2}{2\sigma^2}} e^{-\frac{t-u}{\tau}} du$$

Results : $\tau_1 = (147 \pm 3)\text{ps} \rightarrow \frac{\Gamma}{\Gamma_\Lambda} = 0.559 \pm 0.012$

$$\tau_2 = (300 \pm 5)\text{ps} \rightarrow \frac{\Gamma}{\Gamma_\Lambda} = 1.140 \pm 0.021$$

Obtained with ~26000 events in the hypernuclear ground state peak (10^{-3})

1 week at L=10^{32} cm^{-2}s^{-1}

$\Lambda + p \rightarrow n + p$ decay reconstruction

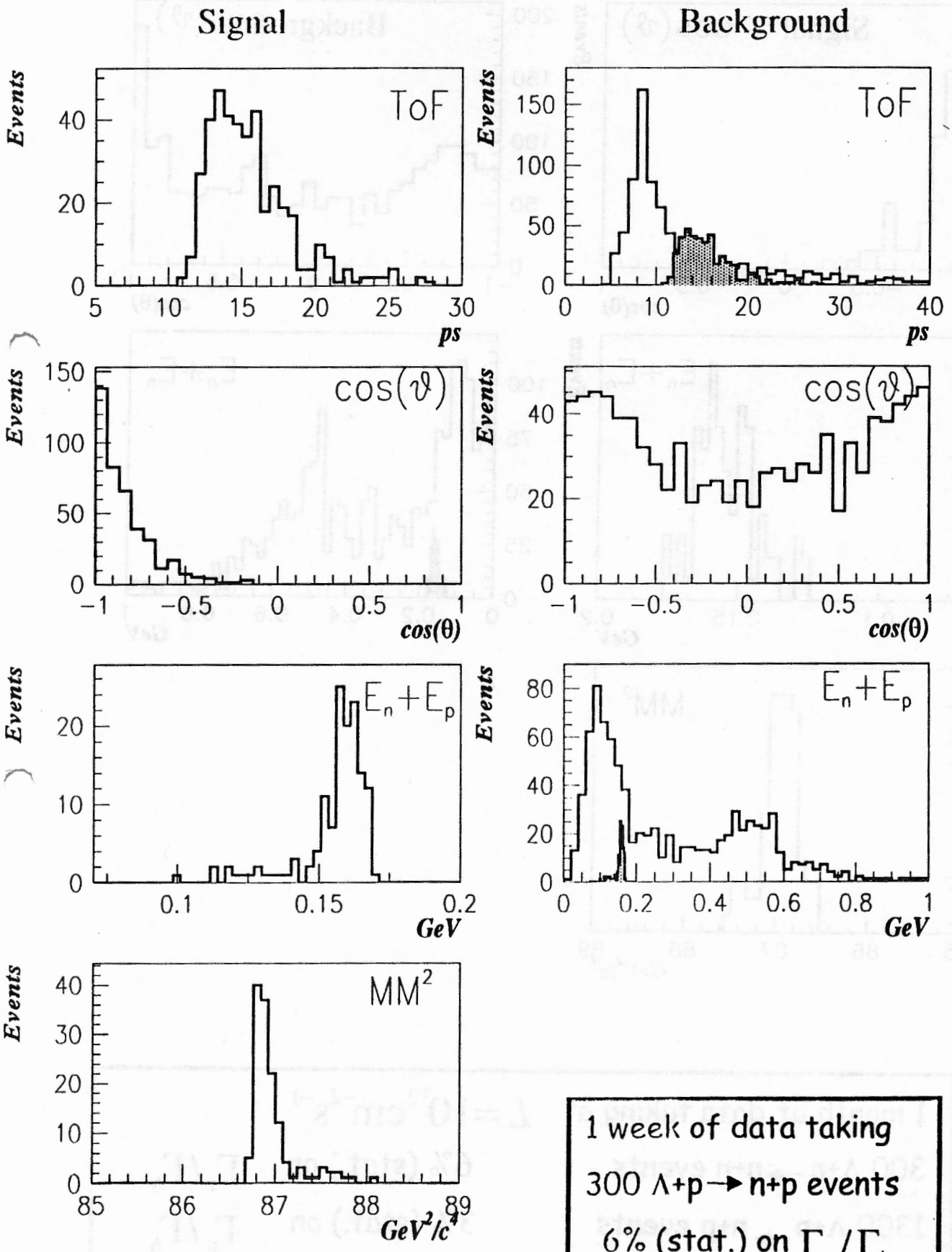

1 week of data taking

300 $\Lambda + p \rightarrow n + p$ events

6% (stat.) on $\Gamma_n / \Gamma_\Lambda$

$\Lambda + n \rightarrow n + n$ decay reconstruction

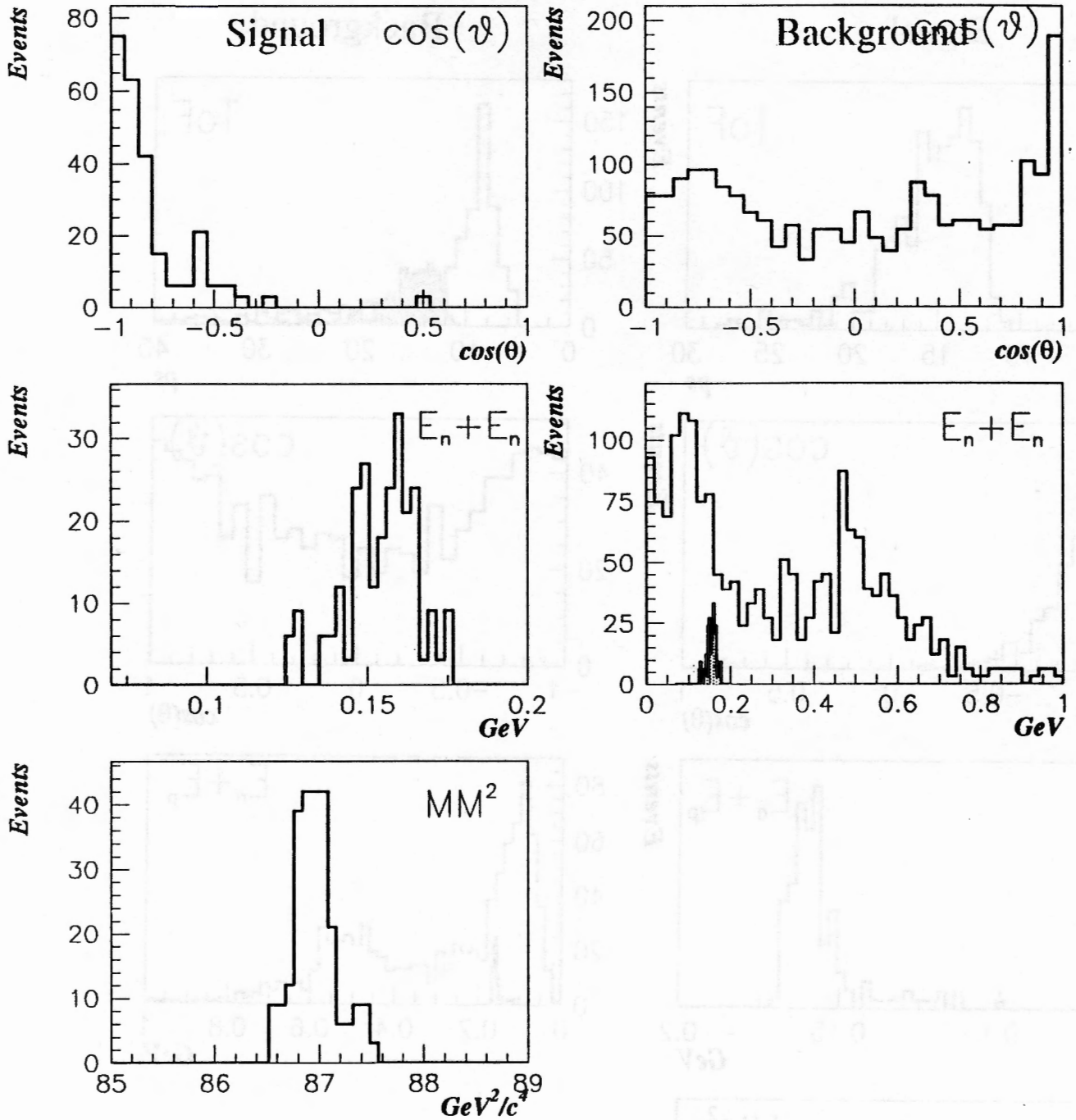

1 month of data taking at $L = 10^{32} cm^{-2} s^{-1}$

300 Λ+n → n+n events — 6% (stat.) on $\Gamma_n / \Gamma_\Lambda$

1300 Λ+p → n+p events — 3% (stat.) on $\Gamma_p / \Gamma_\Lambda$

6% (stat.) on Γ_n / Γ_p

Chapter 8

PHYSICS PERFORMANCES

8.1 Apparatus simulation

As mentioned in the proposal of the experiment [1], the simulation of the FINUDA apparatus was performed in the framework provided by the CERN simulation package GEANT3 [2].

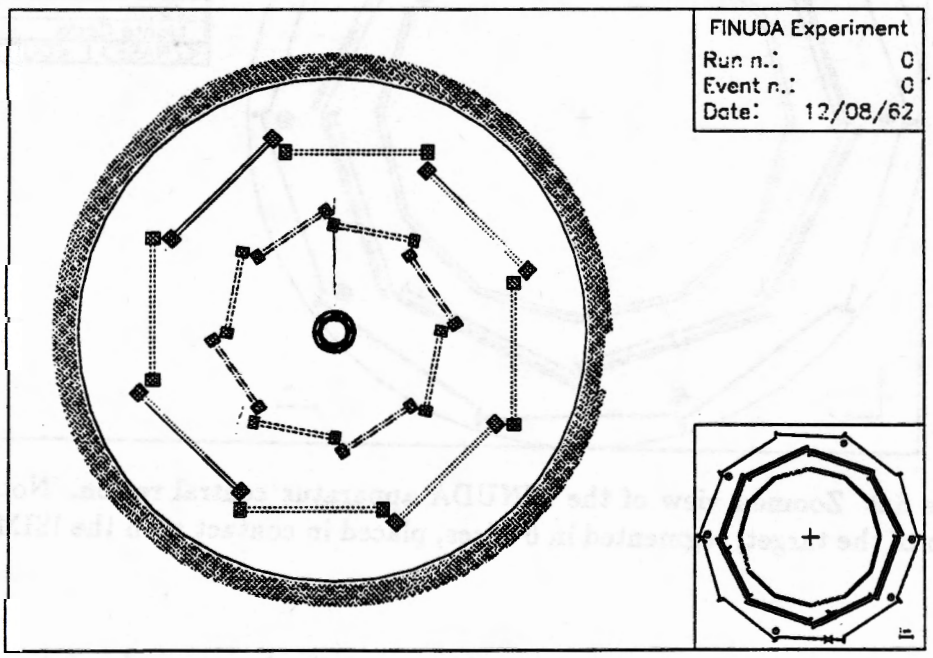

Figure 8.1: Front view of the new configuration of the FINUDA apparatus (only the first straw tubes double-array is drawn for simplicity). The inset shows the interaction region in more detail.

In this design stage the Monte Carlo simulation was mainly finalized to the evaluation, as realistically as possible, of trigger efficiency andrejection, spectrometer

acceptance and resolution and to their optimization. Moreover the simulated events, in terms of hits of the tracks in the sensitive volumes of the detectors, are used as input to the reconstruction and fitting processes which are, at present, under development.

All the relevant physical volumes of the apparatus, detectors structures and sensitive parts, as well as the mechanical supports interposed on the particle paths, were modeled with appropriate level of detail and different geometrical configurations were tested in order to optimize acceptances and resolutions.

The kinematics of the $e^+ + e^- \rightarrow \phi$ formation and the ϕ decay in the different decay channels was simulated using the GEANFI code [3], developed by the KLOE collaboration, whereas the kinematics of the formation and decay of the hypernuclei was generated in a dedicated process.

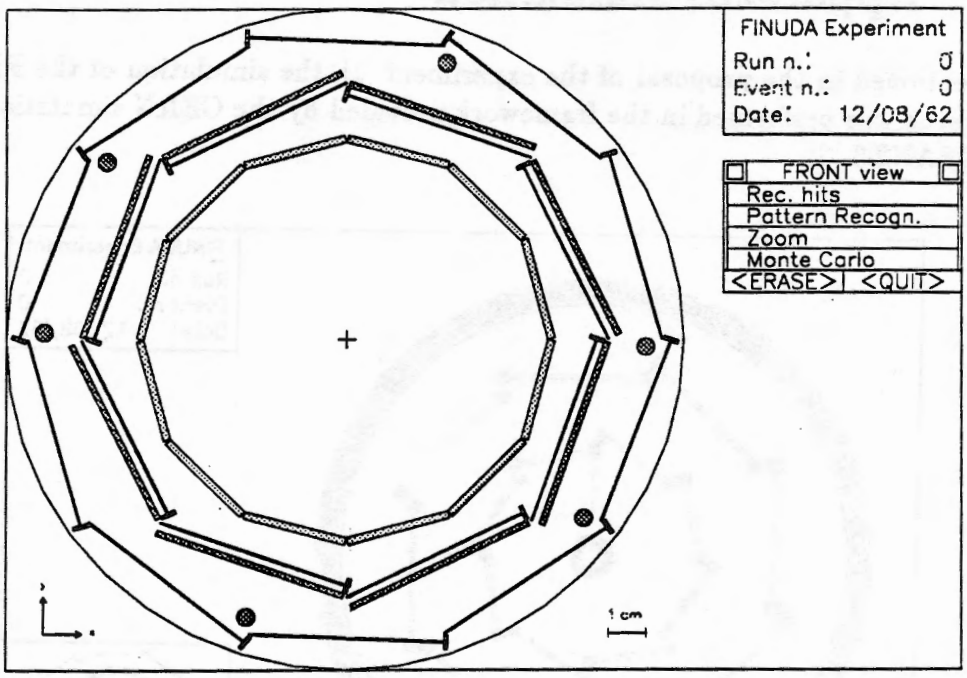

Figure 8.2: Zoomed view of the FINUDA apparatus central region. Note the new design of the target, segmented in 6 slices, placed in contact with the ISIM modules.

The particles produced in the ϕ decay and in the successive interactions are tracked through the various volumes of the apparatus by the GEANT3 tracking package. Energy loss in the different materials with Vavilov and Landau fluctuations, multiple scattering and decay of unstable particles, as well as electromagnetic interaction and showering of light charged particles and photons are taken into account by the tracking package.

In fig. 8.1 and fig. 8.2, respectively, the structure of the full apparatus and the details of the interaction region are shown as they are simulated in the Monte

Carlo program. This final design, which is the result of several tests of different configurations, optimizes the trigger efficiency, the acceptance and the resolution of the apparatus for hypernucleus formation events while keeping, at the same time, easiness of mechanical construction and care.

The simulation of the structure of the apparatus was performed with greater detail for the sensitive parts of the detectors, whereas the mechanical supports and structures are only schematically designed when they are relevant for the acceptance or transparency of the apparatus to the tracked particles.

In previous chapters the detailed description of the structure of the different detectors and their assembly were already given and it will be not reviewed here. We only remark that the main structural modifications relative to the original apparatus design [1] concern the shape of the target (fig. 8.2), whose cylindrical cross section was changed to octogonal in order to position the target material as close as possible to the ISIM microstrips. Moreover, the internal layer of drift chambers was rotated by 11 degrees around the axis of the apparatus. For the calculations presented in this section an octogonal Carbon target of 1.5 mm thickness was assumed.

As it will be better illustrated in the following, the change of the target geometry allows a better accuracy in the determination of the stopping point of the K^- inside the target (vertex position) and makes easier the mechanical construction and assembly of the interaction region. The rotation of the internal layer of drift chambers results in a 30% relative increase in the spectrometer acceptance.

8.2 Detector resolutions and spectrometer momentum resolution and acceptance

The performances of the different detectors in term of time, energy and spatial resolution were measured in tests performed with prototypes, as described in the previous sections, or assumed as a reasonable extrapolation of standard performances of the present technology.

The appropriate resolution functions were inserted in the Monte Carlo simulation of the apparatus as a smearing of the hits of the tracks on the sensitive parts of the detectors.

-) Internal scintillator array (TOFINO) (see Chap. 5.1):

A time resolution of 0.5 ns $FWHM$ is assumed, whereas the resolution on the signal amplitude is evaluated on the estimated gathering of 50 photoelectrons for minimum ionizing particles (pions) and 200 photoelectrons (4 times more) for kaons of 16.1 MeV coming from the ϕ decay.

-) Silicon microstrip detectors (ISIM/OSIM) (see Chap. 4.1):

A spatial resolution and detector granularity with $\sigma = 50$ μm along both the microstrip axes is assumed, whereas the resolution on $\Delta E/\Delta X$ of the kaons

is evaluated at 20% $FWHM$.

-) Low mass drift chambers (LMDC) (see Chap. 4.2):

The spatial resolution is assumed to be 100 μm in the direction octhogonal to the wire (ρ, φ plane), as obtained by the measurement of the drift time. A much coarse resolution ($\sigma \sim 1\%$ of the wire length) is obtained by charge division along the wire direction.

-) External scintillator barrel (TOFONE) (see Chap. 5.2):

The time resolution is assumed 0.5 ns $FWHM$ and within 5 cm $FWHM$ for the zeta coordinate obtained with a suitable treatment of the signals of the two PMs looking at the same scintillator slab.

-) Straw tube array (ST) (see Chap. 4.3):

A spatial resolution $\sigma \sim 100\mu m$ is assumed in the radial direction (drift line direction) relative to the wire. No measurement of the coordinate along the wire direction by means of charge division is foreseen, since the charge division technique cannot provide the needed spatial resolution. In fact, in order to achieve the desired momentum resolution, at least two zeta coordinates (OSIM and ST) have to be measured with high spatial resolution; the OSIM microstrip provide a resolution of 50 microns while a resolution of the order of the millimeter is requested for the ST array. For this reason the zeta coordinate of the impact of the particle on the Straw Tube array will be determined fitting the particle path through the three straw tube super-layers. One of these layers is longitudinal and fixes the particle trajectory in the (ρ, φ) plane, the other two are tilted by 15 degrees each relative to the longitudinal direction and determine the position of flying path of the particle in the zeta direction. The resolution which can be reached using this technique was evaluated with Monte Carlo events and result of the order of 500 μm.

The momentum resolution of the spectrometer can be evaluated on the basis of well known standard formulae [4], usign the above spatial resolution, an evaluation of the radiation length of the different materials along the particle paths in the spectrometer, assuming the proper average length of the track and a homogeneous magnetic field of 1.1 $Tesla$.

The amount of material along the particle path is kept to the minimum in order to minimize the effect of multiple scattering. For these reasons the windows of the chambers are very thin and the tracking volume is filled with helium. As a result, the radiation length of the complete tracking volume is around 170000 cm to be compared with 570000 cm for pure helium and 30400 cm for air.

In fig. 8.3 a) and b) the $\Delta p/p$ $FWHM$ predicted resolution for pions is plotted versus the pion momentum at polar angles respectively of 90 and 50 $degrees$.

In fig. 8.3 a) the full line represents the total resolution, the dotted line represents the contribution from multiple scattering and the dashed line the contribution from

the helix fit of the track trajectory. The two contributions are summed quadratically. The dashed-dotted lines in fig. 8.3 b) represent the same contributions for the straight line fit in in the (z, s) plane where s is the path length along the track trajectory.

The plots show that for pions of 270 MeV/c the design momentum resolution of $0.2 - 0.3\%$ $FWHM$ is achieved by the present configuration of the apparatus. Besides, it appears that the momentum resolution is dominated by multiple scattering distorting effect and not by the uncertainty in the track fitting. Therefore the momentum resolution of the apparatus will not be critical under possible worsening of the spatial resolutions.

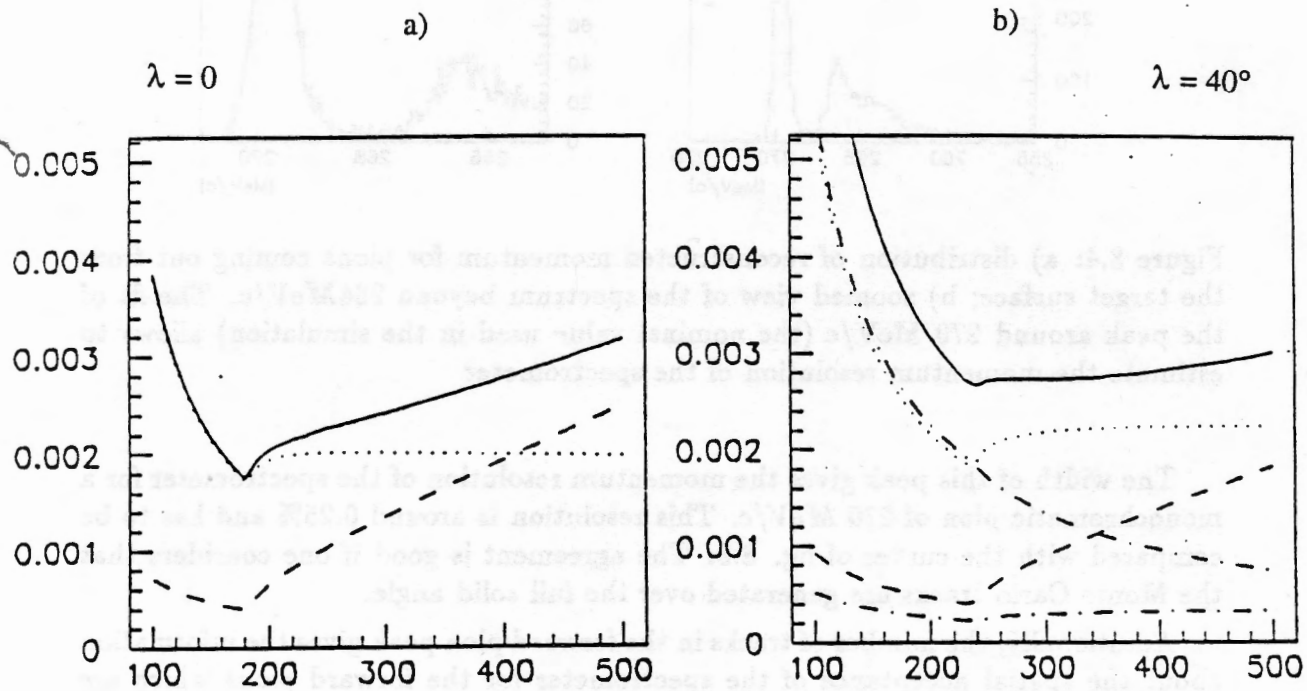

Figure 8.3: Comparison of the various terms that contribute to the spectrometer resolution as a function of the momentum (see text for further details).

The prediction of the standard formula for the momentum resolution was checked by simulating with the FINUDA Monte Carlo program populations of monochromatic pion and proton tracks starting from the external surface of the target and isotropically generated in space. The hits of the tracks with the different detectors are smeared with appropriate resolution functions and used to reconstruct the momentum of the particles by means of a helix fit procedure.

Figs. 8.4 and 8.5 show the reconstructed momentum distributions for pions of 270 MeV/c and protons of 416 MeV/c, respectively. In fig. 8.4 the reconstructed momentum distribution of the pions shows a peak around 270 MeV/c and a broad structure at lower momentum. This latter bump corresponds to the pions that have crossed the structure of the interaction region before entering in the tracking volume

and have lost a part of their energy (backward pions). The peak at 270 MeV/c represents the pions that have entered the spectrometer without crossing the target or the structure of the interaction region (forward pions).

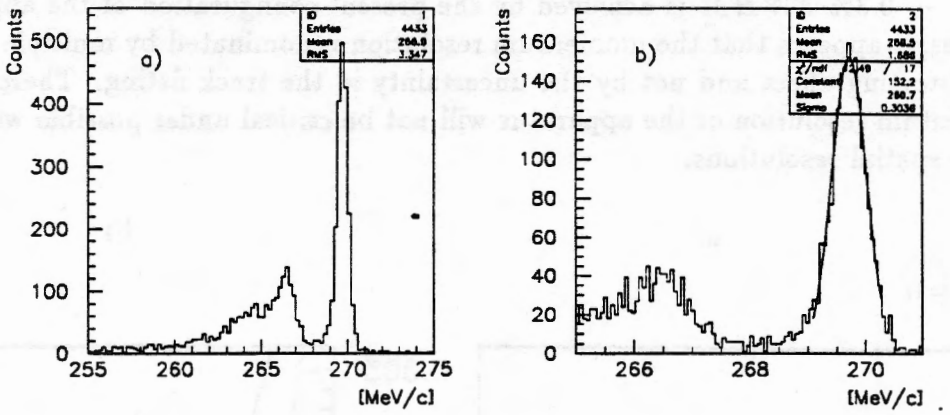

Figure 8.4: a) distribution of reconstructed momentum for pions coming out from the target surface; b) zoomed view of the spectrum beyond 264MeV/c. The fit of the peak around 270 MeV/c (the nominal value used in the simulation) allows to estimate the momentum resolution of the spectrometer

The width of this peak gives the momentum resolution of the spectrometer for a monochromatic pion of 270 MeV/c. This resolution is around 0.25% and has to be compared with the curves of fig. 8.3. The agreement is good if one considers that the Monte Carlo tracks are generated over the full solid angle.

Additionally, the number of tracks in the forward pion peak gives the information about the spatial acceptance of the spectrometer for the forward pions which are those useful for high resolution hypernuclear spectroscopy. This number takes into account the geometric acceptance of the spectrometer as well as the reduction in acceptance due to the mechanical structure of the chambers and their dead zones. This overall acceptance for forward pions amounts to 22%, 30% greater than in the previous configuration of the chamber internal layer. It is worth to remark that, in the absence of dead zones and mechanical structures in the two chamber layers the geometrical acceptance of the spectrometer for the forward pions amounts to about 28%.

In fig. 8.5 the same plots for a proton of 416 MeV/c are shown. The resolution for the proton tracks is 0.7%, worse that the for pions, since protons are subjected to more multiple Coulomb scattering deviations.

The present evaluation of the spectrometer resolution was performed with a homogeneous magnetic field and using a helix fit procedure for momentum reconstruction. In fact, the design magnetic field will not be completely homogeneous. However, the deviation from uniformity will be of the order of some percent and localized mainly at the edges or out of the tracking volume. In the final reconstruction

program a track fitting algorithm, which make use of a quintic spline interpolation of the track trajectory [5] and takes into account the non uniformity of the magnetic field, will be used. Several tests with Monte Carlo events and different forms of magnetic fields much more inhomogeneous than the one used by the experiment, demonstrated that the design momentum resolution is preserved when an accurate measurement of the magnetic field components (0.1%) is available.

To give an example, a population of pions of 270 MeV/c was tracked in the apparatus through a rather inhomogeneous magnetic field (up to 10% of the nominal value at the edges of the tracking volume for the three Bx, By, Bz components). In fig. 8.6 a comparison between the distribution of the momentum reconstructed with helix fit (a) and spline (b) algorithm is shown.

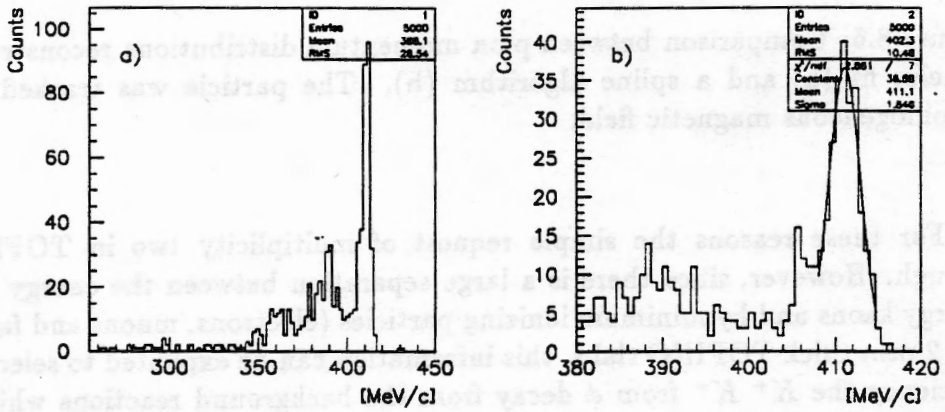

Figure 8.5: a) Distribution of reconstructed momentum for proton coming out from the target surface; b) zoomed view of the spectrum beyond $380 MeV/c$. The fit of the peak around 416 MeV/c (the nominal value used in the simulation) allows to estimate the momentum resolution of the spectrometer.

8.3 Trigger efficiency and background rejection

The goal of the trigger system is to select the $K^+ K^-$ decay of the ϕ formed in the $e^+ e^-$ collision from background events as Bhabha scattering, other ϕ decays and cosmic rays. Furthermore, the trigger system must select hypernuclear events where a prompt pion, coming from the hypernucleus formation, has crossed the tracking volume of the spectrometer.

It is worthwhile to recall that, at the top luminosity $\mathcal{L} = 10^{33}\ cm^{-2}\ s^{-1}$ the expected total rate for ϕ production is about 4.4 kHz and that, in the angular range covered by TOFINO, the Bhabha scattering cross section is some order of magnitudes lower than in the forward and backward directions. Rates of $(K^+ K^-)$ and $(e^+ e^-)$ will be then of the same order of magnitude (few kHz). Rates due to other ϕ decays are considerably smaller.

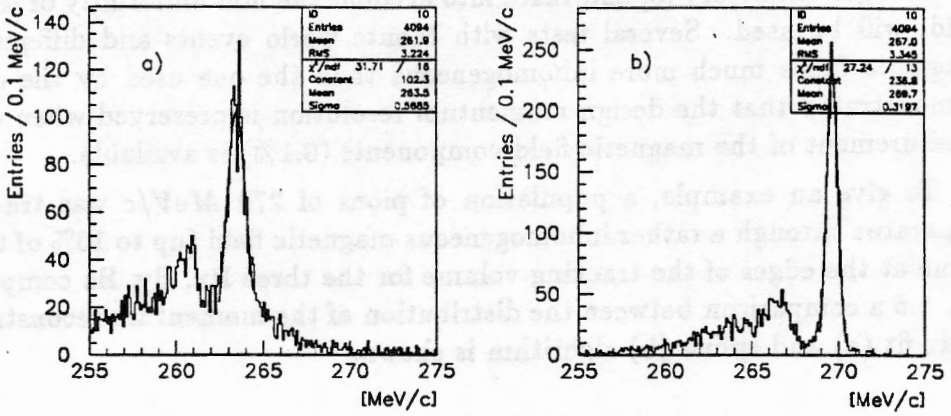

Figure 8.6: Comparison between pion momentum distributions reconstructed using a helix fit (a) and a spline algorithm (b). The particle was tracked in a quite inhomogeneous magnetic field.

For these reasons the simple request of multiplicity two in TOFINO is not enough. However, since there is a large separation between the energy lost by low energy kaons and by minimum ionizing particles (electrons, muons and fast pions) in the 2 mm thick TOFINO slabs, this information can be exploited to select with high efficiency the K^+ K^- from ϕ decay from the background reactions which produce light relativistic particles.

A further constraint can be provided by the request of a "back to back" topology in the interaction region, by simply requiring a coincidence between one TOFINO slab and the axially symmetric one or its two neighboring (extended back to back), in order to account for the curvature of the trajectory of K^+ K^- tracks and the uncertainty of the e^+ e^- interaction point. The latter is characterized in fact by a dispersion with a $\sigma = 2$ mm in the horizontal coordinate.

Once the K^+ K^- event has been recognized by means of amplitude discrimination on TOFINO signals and slab topology, the occurrence of a K^- interaction in the target with emission of a prompt pion crossing the tracking volume can be selected by the request of at least one fired slab of TOFONE within a narrow timing gate. It is worth to recall that muons of 236 MeV/c coming from the decay of the K^+ stopped in the target are delayed by the kaon mean life which is of about 12 ns.

In summary, the first level trigger is based on TOFINO and TOFONE and requires the coincidence of the following occurrence :

-) TOFINO

a) "extended" back to back topology (BTB)

b) energy lost above a fixed threshold

-) TOFONE

a) prompt coincidence $\leq$ 10 ns

b) multiplicity $\geq$ 1 (optional)

This trigger strategy has been extensively tested with Monte Carlo simulations. For the timing and amplitude resolutions of the scintillators the values quoted in Chap. 5 were adopted, and furthermore, being the crucial part of the trigger logic based on amplitude threshold discrimination, a possible fluctuation of the electronic threshold of 5% $FWHM$ has been assumed. In terms of energy lost in a single slab by the particles this corresponds to a fluctuation of 0.175 MeV for a threshold of 3.5 MeV.

To evaluate the trigger efficiency a population of hypernuclear formation reactions was simulated, in particular : a ϕ is formed from e^+ e^- collision; it decays in K^+ K^-; when the K^- is emitted into the acceptance volume and stops in the target an hypernucleus is formed and a prompt pion of 270 MeV/c is emitted; after that the hypernucleus decays in non-mesonic mode with a mean life of 0.3 ns emitting a proton and a neutron of 416 MeV/c.

Besides, several background reactions were simulated to evaluate the trigger rejection power.

The results of these calculations are presented in tables 8.1 and 8.2. In table 8.1 the results for the trigger efficiency are shown: the high angular acceptance of the TOFINO barrel and the large energy lost by kaons allows the selection of 75% of the K^+ K^- events which fulfill the topological and threshold conditions. The 25% loss is due to angular acceptance (12%) and decay in flight of the kaons (13%).

The dead zones in the interaction region, the limited solid angle coverage of the spectrometer for particles coming from the interaction region, and the timing gate, reduce the triggered events to 40%.

Table 8.1: Trigger efficiency for $\phi \rightarrow K^+ K^- +$ hypernucleus events

TOFINO $\equiv$ (energy loss * extended BTB)	75%
TRIGGER $\equiv$ TOFINO * TOFONE (prompt coincidence)	40%

It is worthwhile to recall that not all of the triggered events result useful for physics, since the trigger condition can be fulfilled by spurious events too. For instance, the prompt coincidence on one TOFONE slab can be provided by a fast muon from K^+ decay, whereas the pion from hypernucleus decay escapes from the spectrometer acceptance. A detailed analysis of the different classes of events within the triggered ones will be given below.

In table 8.2 the trigger rejection for background events is shown giving the expected rates for some processes; it appears that the trigger strategy allows an efficient background rejection. Within the different conditions imposed by the trigger logic

the most powerful one is, without any doubt, the threshold discrimination on the particle energy loss in TOFINO. In fact it is very unlikely that a couple of minimum ionizing particles coming from the background reactions can release as much energy in the scintillator slabs as a couple of slow kaons coming from the ϕ decay.

Table 8.2: Background events accepted by the trigger

Bhabha scattering	$< 10^{-2} Hz$
$\phi \rightarrow K_S\, K_L$	$< 10^{-1} Hz$
$\phi \rightarrow \rho\, \pi$	$< 10^{-2} Hz$
$\phi \rightarrow \pi^+\, \pi^-\, \pi^0$	$< 10^{-3} Hz$

As noticed above, within the class of triggered events only a subsample corresponds to "useful events", that is events in which the K^- stops in the target, forms the hypernucleus and produces a negative pion which gives the prompt coincidence in TOFONE and deposits hits in the four detectors of the spectrometer (OSIM, two LMDC and ST). Four hits are considered the minimum needed to obtain the best recognition of the track and resolution in momentum. For tracks with 3 hits, recognition and track fitting are possible as well, but with lower quality warrant and worse momentum resolution.

Among the 40% triggered events, 25.5% are useful ones, whereas for 7.5% of them the negative pion gives the prompt coincidence but has less then 4 hits, having hit a structural part. For 7.0% of them the negative pion is out of the acceptance and the prompt coincidence is given by another particle (positive muon, in general).

Finally, half of the 25.5% useful events have forward pions and can be utilized for high resolution hypernuclear spectroscopy.

8.4 Pattern recognition and event reconstruction

The pattern recognition process of the FINUDA apparatus is mainly aimed to the identification, within the events selected by the trigger, of the "useful events" that is the ones in which the stop of a K^- in the target is followed by the emission of a prompt pion crossing the four detector layers of the spectrometer. The measurement of the momentum of the pion emitted from the K^- interaction allows the hypernuclear spectroscopy studies.

Additionally, other charged and neutral products of the interactions or decays such as protons and neutrons from the hypernucleus decay or muons and pions from the K^+ decay, may be recognized in order to perform measurements of the lifetime of the hypernucleus or simply for detector calibration.

The efficiency of this pattern recognition process can greatly affect the capability of the experiment to efficiently separate hypernuclear events from spurious ones and

to utilize at the best the potentiality of the machine and of the apparatus.

The worry is justified, to a greater extent, by the fact that, in order to reduce, as much as possible, the amount of materials along the particle paths, the redundancy of the track position sampling within the spectrometer is reduced to the minimum.

For this reason Monte Carlo simulated events were used to develop and test a number of pattern recognition and event reconstruction procedures designed to fully exploit the information on the event recorded by the FINUDA detectors.

To this aim a first version of the reconstruction program for the apparatus was written, which performs the following tasks:

a) Read in, from the Monte Carlo events, of the description of the hits of the tracks in the different detectors (Raw Data Tape). The hits were smeared by proper resolution functions.

b) Read in, from the Monte Carlo program, of the geometry and material composition of the detectors and structures in the apparatus. Being the reconstruction program based on the GEANT package, the GEANT/GEANE [6] environment can be exploited to perform tracking and back-tracking of particle trajectories through the apparatus volumes, with calculation of energy lost and error matrix transport, with great easiness and accuracy.

c) Management of a data base for the hits in the detectors, reconstructed event structure and calibration data, based on the ZEBRA package.

d) Supply of an user interactive interface, additional to the batch mode, based on the KUIP package [7], as well as of an event display process based on Xwindow/GKS package. The event display is able to show to the user the Monte Carlo generated event, the hits in the detector and the results of the reconstruction process at the same time. The pattern recognition and reconstruction strategies can be tested event by event and adapted to the particular features of the apparatus and to the characteristics of the event topology under study.

e) Connection of the pattern recognition process to the track fitting procedures.

f) Production of a data summary tape containing the results of the reconstruction in terms of recognized topology, interaction and decay point position (K^- and K^+ stopping points in the target) and directions and momenta of the tracks, in the form of ZEBRA banks and PAW n-tuples.

In the following, a short description of the pattern recognition strategy adopted in the first version of the reconstruction program is given, as well as the results concerning its efficiency.

For typical hypernuclear events (useful events) the pattern recognition flow is organized in two successive steps:

a) Identification of the "beam" K^+ K^- couple which crosses the interaction region and deposits hits in two opposite TOFINO slabs and in two correspondent ISIM microstrips. Reconstruction of the "beam" trajectory in the space and extrapolation of the K^- and K^+ tracks inside the target to estimate their stopping points. (Interaction Vertex and K^+ decay point, respectively)

b) Identification, inside the spectrometer, of the helical trajectories which start from one hit in OSIM and cross the other three detector layers of the spectrometer (two LMDC and ST) and possibly TOFONE. These helical trajectories, if they correspond to physical tracks, are connected with the K^- or K^+ stopping points too. For "backward" tracks which cross the interaction region before entering into the spectrometer, the additional hits in the internal detectors (ISIM and TOFINO) are placed near the helical trajectory too. The little amount of material interposed inside the tracking volume and the uniformity of the magnetic field largely allows to approximate the particle trajectories as helices, at least for pattern recognition purposes.

The low level of background and the high rejection power of the trigger allows to expect clean events and promise a high efficiency for the pattern recognition process, in spite of the limited number of hits available.

Tracks with only three points can be identified and reconstructed as well, but with worse recognition quality and momentum resolution. The recognition of the "beam" and, consequently, the reconstruction of the Vertex is considered, on the contrary, essential to validate an useful event and to allow the identification of "backward" and "forward" tracks.

Moreover, the reconstruction of the Interaction Vertex allows the correction of the negative pion momentum, for the energy lost in the already thin target and leads to the best performances the momentum resolution of the apparatus.

8.5 K^+ K^- "beam" identification in the interaction region

The recognition of the K^+ K^- beam in the interaction region starts from the two back to back TOFINO slabs in which the signal amplitude has overcome the requested threshold and triggered the acquisition of the event. Assuming that these two slabs have been fired by kaons from the ϕ decay, the hits of these kaons in the ISIM microstrips in the angular region subtended by the two slabs are searched for.

In fig. 8.7 the interaction region for a typical hypernuclear event is shown; the two TOFINO back to back slabs and the hits of the K^+ K^- beam on ISIM are indicated. They can be distinguished from other hits on ISIM, in the same angular region (see the proton hit near the K^- one), using the information on specific energy loss provided by the Silicon microstrip detector. The $\Delta E/\Delta x$ of the stopping Kaon (average energy at the incident point on ISIM $\sim$ 12 MeV) is $\sim$ 1.5 MeV,

around 4 times the minimum ionizing one. A specific energy loss resolution around 20% $FWHM$, assumed for the Silicon microstrip detectors, results to be largely sufficient to separate the hits produced by slow kaons from those by other particles produced in the interactions.

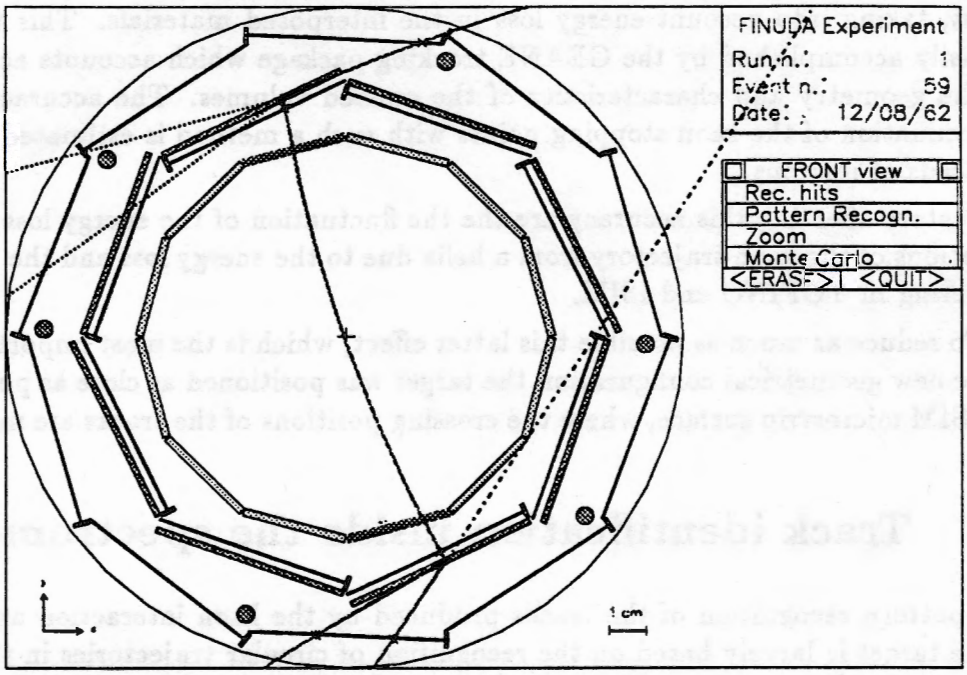

Figure 8.7: A typical FINUDA event: zoomed view of the central part of FINUDA apparatus showing the K^- and K^+ interacting in the target.

Monte Carlo calculations using hypernuclear events with a proton–neutron decay of the hypernucleus, demonstrated that the efficiency for this separation is around 96%.

Once the hits of the beam tracks on ISIM have been recognized, the trajectory of the K^+ K^- couple inside the interaction region can be reconstructed imposing that a helical trajectory corresponding to a nominal momentum of the kaons crosses the two hit points. Having measured, in each point, the three spatial coordinates (x, y, z) with high spatial resolution, this is enough to determine completely the beam trajectory, apart from an ambiguity on the sign of the radius of curvature or, in other words, on the concavity of the curve.

This ambiguity can be easily solved comparing the two alternative trajectories with the e^+ e^- interaction region ($\sigma = 0.2$ cm in the horizontal plane and $\sigma = 0.002$ cm in the vertical one). The true beam trajectory must cross this region in the e^+ e^- annihilation point. The rare cases for which this ambiguity survives are solved by checking the sign of the particles emitted in the kaon interactions or decay in the target.

The efficiency of this beam identification process was estimated to be $\sim$ 99%

of the K^+ K^- couples which have hit the ISIM microstrip and stopped inside the target.

When the beam trajectory is reconstructed, the stopping position of the K^+ and K^- in the target can be estimated by simple extrapolation of the trajectory to the target, taking into account energy loss in the interposed materials. This task can be easily accomplished by the GEANE tracking package which accounts accurately for the geometry and characteristics of the crossed volumes. The accuracy in the determination of the kaon stopping points with such a method is estimated in some hundreds of microns.

Factors affecting this accuracy are the the fluctuation of the energy loss and the deviations of the kaon trajectory from a helix due to the energy loss and the multiple scattering in TOFINO and ISIM.

To reduce as much as possible this latter effect, which is the most important one, in the new geometrical configuration the target was positioned as close as possible to the ISIM microstrip surface, where the crossing positions of the tracks are measured.

8.6 Track identification inside the spectrometer

The pattern recognition of the tracks produced by the kaon interaction and decay in the target is largely based on the recognition of circular trajectories in the plane orthogonal to the axis of the apparatus, trajectories that start from the target region and cross the sensitive volumes of the different detectors sufficiently close to the projection of the hit points on the same plane. As already mentioned, the uniformity of the magnetic field is sufficient to allow the use of a helix approximation for the track trajectories.

In addition, the simple topology of the searched events and the minimum redundancy of the track position sampling (average number of hits or clusters per event $\sim$ 24) make the use of a simple local pattern recognition method (road method) more appropriate and economic than global pattern recognition methods like the inverse conformal transformation method [8] often used to recognize circular paths with a common origin.

The tracks searched for are supposed to start from one of the two kaon stopping points in the target (vertices) and must cross the sensitive parts of OSIM, internal LMDC, external LMDC, ST (in the order) and possibly ISIM for backward tracks.

Hence the pattern recognition process starts the analysis of the hits considering one hit in OSIM detector. After that it constructs one circle from every possible combination of this hit and two hits in the two LMDC arrays. Since the measurements of the coordinates in the transversal plane is very accurate for the three mentioned detectors, the combination of three hits coming from a true track corresponds to a circular trajectory passing very close to one of the two vertices and close to the hit of the longitudinal straw tubes when they are fired by the track. This first request on the alignment on a circular path of three hits with one of the two vertices and

the ST defines a track candidate to be submitted to further tests.

The OSIM detector provides an accurate determination of the z (longitudinal) coordinate of the hit, while the z coordinate of the vertex is estimated with a good precision by kaon track extrapolation. The two LMDCs provide a coarser accuracy in zeta determination (1% of the wire length). However, the check of the alignment of the z coordinates of these four points along a straight line in the (z, s) plane (s is the path length along the track) is very useful in resolving possible ambiguities and mainly in rejecting spurious candidates.

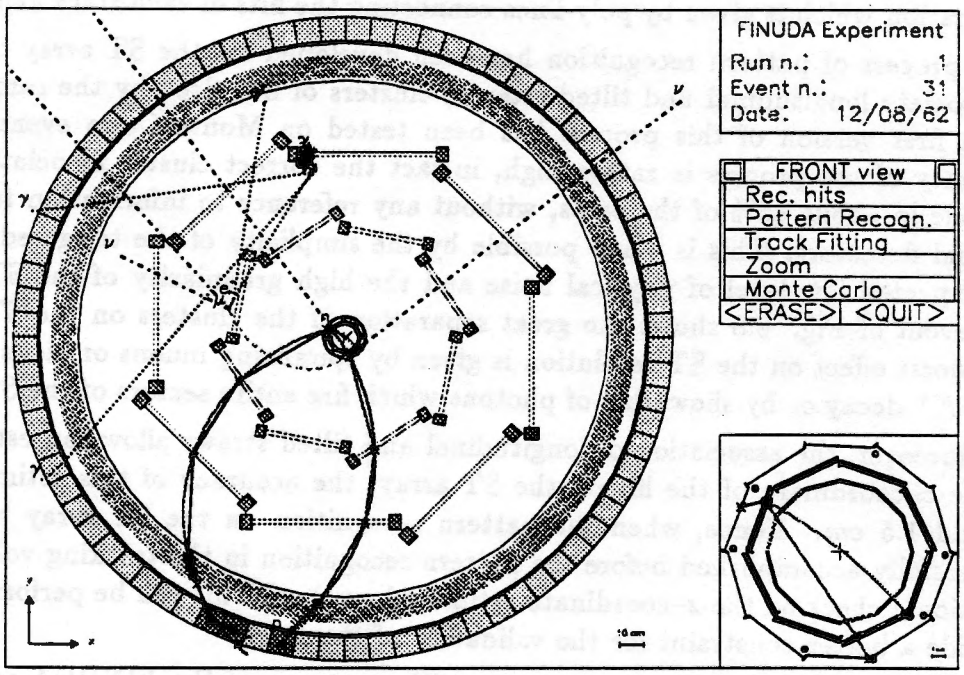

Figure 8.8: A typical FINUDA event: the hypernucleus formation is followed by a n-p non-mesonic decay. The poly-lines superimposed to the Monte Carlo particle trajectories represent the results of the pattern recognition algorithms.

When one track candidate fulfills the requested conditions within tolerances depending on the assumed spatial resolutions, it is validated as a good track and connected in the event structure to the corresponding vertex. The corresponding hits are discarded from the input data structure and no longer considered in the search for track candidates. Additionally the circle parameters provide a first estimation of charge, momentum and direction of the validated track. The process is then repeated for all other hits on OSIM looking for good candidate tracks; residual hits are considered as noise or submitted to search for track candidates of lower quality.

Good candidate tracks may have four measured points (OSIM,LMDCs,ST) if they cross the ST array or three measured points, if not. In the latter case the track may have escaped the tracking volume acceptance or may have such a low

momentum that spiralizes inside the spectrometer; in this case other corresponding hits in the LMDC layers are searched for and connected.

For backward tracks possible hits on ISIM and TOFINO are searched for, as well as hits on TOFONE for both backward and forward tracks. It is worth to remark that once the track has been validated and connected to the corresponding vertex, it becomes possible to distinguish backward from forward tracks.

In fig. 8.8 a hypernuclear event fully recognized by the pattern recognition process is shown; the Monte Carlo tracking is superimposed to the pattern recognition information which is given by poly-lines connecting the hits of each track candidate.

A process of pattern recognition has been developed for the ST array in order to associate longitudinal and tilted (stereo) clusters of ST, fired by the same track and a first version of this process has been tested on Monte Carlo events. The efficiency of the process is rather high, in fact the correct cluster association can be done in about 85% of the cases, without any reference to information from the internal detectors. This is made possible by the simplicity of the triggered events, the expected low level of physical noise and the high granularity of the ST array. The event of Fig. 8.8 shows the great separation of the clusters on the ST array. The worst effect on the ST resolution is given by spiralizing muons or pions coming from K^+ decay or by showering of photons which fire entire sectors of the ST array.

Moreover, the association of longitudinal and tilted straws allows an estimation of the z–coordinate of the hit on the ST array; the accuracy of this estimation is around 1.5 cm. Hence, when the pattern recognition on the ST array has been successfully accomplished before the pattern recognition in the tracking volume, an additional check on the z–coordinate estimated on the ST hit can be performed and provide a better constraint for the validation of the track.

The first version of the pattern recognition process of the FINUDA apparatus was tested on Monte Carlo events and provides an efficiency larger than 95% for tracks crossing the full spectrometer. As expected, the efficiency is very high and the process is not time consuming. Being this the first version of the process, both efficiency and economy can be improved by more clever and refined algorithms.

The reliability of the algorithm in presence of a high level of noise on the detectors is at present under study. First tests show that, owing to the high accuracy of the spatial positions on the detectors, it is unlikely that spurious hits can contaminate a true track or even create a fake track.

8.7 Track fitting and momentum reconstruction

As mentioned before, the track fitting process is accomplished by a helix fit process or by an efficient spline algorithm; OSIM and LMDCs provide measurements of the three spatial coordinates though with less accuracy for the zeta coordinate when the LMDCs are concerned. Besides, reconstructed hit coordinates for the LMDCs in the (ρ, φ) plane depend slightly on the incident angle of the track. This dependence

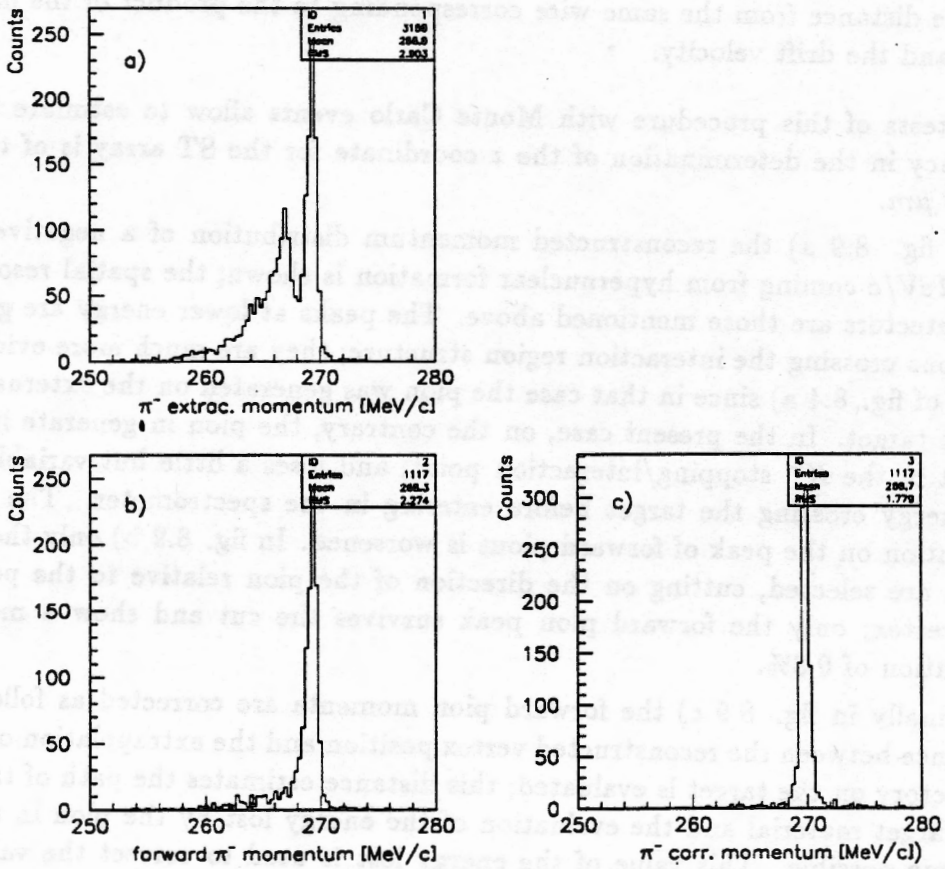

Figure 8.9: The sequences of plots shows the capability of selecting the "useful events" (b) and of correcting the π momentum for the energy lost in the target (c), starting from the global spectrum (a).

will be accurately taken into account in the final fit procedure.

The accurate determination of the longitudinal coordinate for the ST array will be performed by fitting the extrapolation of the track trajectory through the hit stereo tubes; this is done by minimizing the sum of the squares of the differences between :

a) the distance of the trajectory (helix) from the wire of a hit tube;

b) the distance from the same wire corresponding to the product of the drift time and the drift velocity.

First tests of this procedure with Monte Carlo events allow to estimate that the accuracy in the determination of the z coordinate for the ST array is of the order of 500 μm.

In fig. 8.9 a) the reconstructed momentum distribution of a negative pion of 270 MeV/c coming from hypernuclear formation is shown; the spatial resolution of the detectors are those mentioned above. The peaks at lower energy are generated by pions crossing the interaction region structure; they are much more evident that those of fig. 8.4 a) since in that case the pion was generated on the external surface of the target. In the present case, on the contrary, the pion in generate inside the target in the K^- stopping/interaction point, and loses a little but variable part of its energy crossing the target before entering in the spectrometer. The resulting resolution on the peak of forward pions is worsened. In fig. 8.9 b) only the forward pions are selected, cutting on the direction of the pion relative to the position of the vertex; only the forward pion peak survives the cut and show a momentum resolution of 0.3%.

Finally in fig. 8.9 c) the forward pion momenta are corrected as follows. The distance between the reconstructed vertex position and the extrapolation of the pion trajectory on the target is evaluated; this distance estimates the path of the pion in the target material and the evaluation of the energy lost by the pion in the target became possible. This value of the energy lost is used to correct the value of the pion momentum measured by the spectrometer. The resulting distribution is shown in fig. 8.9 c); the peak is now centered around 270 MeV/c and its width correspond to the nominal resolution of 0.25%.

8.8 Hypernuclear spectroscopy resolution

Given the performances illustrated above for the resolution of the different detectors, the pattern recognition and event reconstruction, it is possible to use Monte Carlo simulated events to estimate the resolution and sensitivity of detection of hypernuclear levels in presence of a physical background. As an example, a Monte Carlo calculation was performed in which the K^- originated by the ϕ decay and then stopping in the target, generates a spectrum of negative pions similar to the ones of fig. 1.1, which is a typical spectrum obtained at KEK with a $(CH)_{12}$ target.

The only difference is that the two peaks at 273 and 261 MeV/c were generated as monochromatic lines in the same proportion, relative to the background, as the areas of the two peaks relative to the area of the full spectrum, as seen by fig. 8.10. They correspond to the standard capture rate of 10^{-3}/stopped K^- respectively. Furthermore two additional peaks at 265 MeV/c and 270 MeV/c have been generated corresponding to capture rates of $2 \cdot 10^{-4}$ and 10^{-4} stopped k^- respectively. They would correspond to the excited states at $\sim$ 2.6 MeV and 6.8 MeV in ${}^{12}_{\Lambda}C$, observed with the (π^+, K^+) reaction in flight (see fig. 1.2

The simulated Monte Carlo spectrum was then passed through the full chain of programs described in this Chapter and the final results are shown in fig. 8.11, where the two peaks at 10^{-3} stopped K^- are clearly visible over a flat background, with a resolution and a signal / background ratio as expected and anticipated in Chapter 1 and the peaks at 10^-/ $stoppedk^-$ can still be distinguished from the background. Concerning the expected counting rates, we may finally obtain the following evaluation. At $\mathcal{L} = 10^{32}\ cm^{-2}\ s^{-1}$ we expect $\sim 216\ K^- s^{-1}$; for a production rate of hypernuclei of $10^{-3} K^-_{stopped}$ we expect then 2.16×10^{-1} hypernuclear states s^{-1}. The trigger efficiency is 0.255 and the reconstruction one is 0.95. Furthermore, we have to take into account the circumstance that only the forward pions are useful for fine spectroscopy (a factor ~ 0.5) and that the total transparency of the LMDCs is 0.8. The final rate is then 2.09×10^{-2} hypernuclear states s^{-1}, corresponding to 75 h^{-1}: it means that the spectra shown in fig. 8.11 would be obtained in $\sim 7\ h$ at $\mathcal{L} = 10^{32}\ cm^{-2}\ s^{-1}$, in $\sim 1\ h$ at $\mathcal{L} = 10^{33}\ cm^{-2}\ s^{-1}$, a quite impressive result.

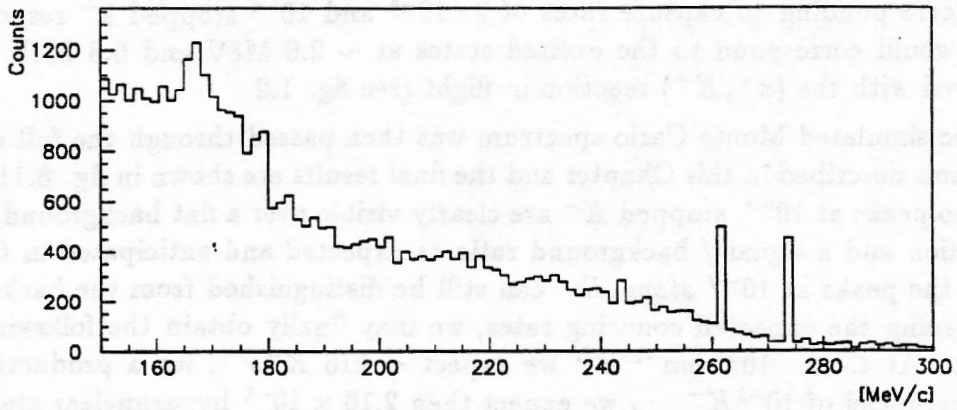

Figure 8.10: Simulated π^- momentum spectrum used as input for the FINUDA Monte Carlo program.

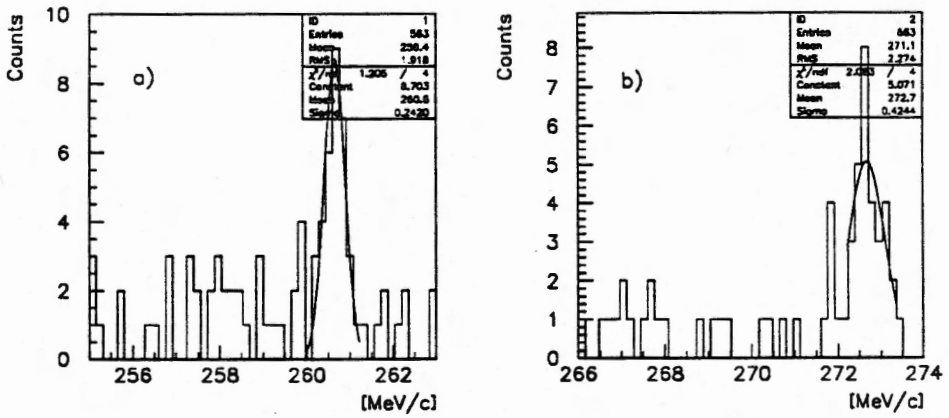

Figure 8.11: The capability of resolving narrow peaks is showed. Note how, despite the not very high statistics, the peaks are clearly emerging from the background.

1 Monte Carlo simulation of the FINUDA apparatus.

The performances of the FINUDA apparatus concerning trigger efficiency, apparatus acceptance and momentum resolution, have been evaluated by a Monte Carlo simulation of the final, more realistic design of the different detectors and supporting mechanics . Concerning the details about the Monte Carlo program, the general structure of the apparatus, the amount of materials in the spectrometer placed along the particle paths, we refer to what already illustrated in the FINUDA proposal[1] and the FINUDA Technical Report[2]. The spatial and time resolutions assumed for the different detectors are the same as those given in the Technical Report, exception made for the spatial resolution of the drift chambers and the zeta resolution of the straw tubes, for which the pessimistic values of σ = 150 μm and σ = 1.0 mm respectively, have been assumed.

1.1 Simulation of the realistic structure of the apparatus.

The final design of the structure of the FINUDA apparatus in terms of dimensions and positions of the different detectors and shapes, sizes and constituent materials of the supporting structures, has been worked out by the mechanical design group in close collaboration with the Monte Carlo simulation group. This coordinated effort resulted in a final design of the different parts of the apparatus, which improves the global transparency and acceptance of the structure and, consequently, the trigger and reconstruction efficiency.

All the sensitive and structural volumes belonging to the different detectors, in their final sizes and shapes, have been modelled inside the Monte Carlo program with the proper level of detail. The same has been done for all the mechanical structures supporting the detectors or, in general, placed inside the magnet gap and along the beam pipe. The accurate simulation of the supporting structures is needed to evaluate, as closely as possible, the effects of the machine background on trigger efficiency and rejection and on the Pattern Recognition efficiency.

In Fig.1 the longitudinal cross section of the apparatus is shown as it is simulated in the Monte Carlo program. The magnet and coil structures together with the beam pipe, the compensating magnets and the flasks supporting the central detector region, appear clearly in the picture. A part of the mechanical structure supporting the drift chambers and the straw tubes appears too. This latter structure is better seen in Fig. 2, where an axonometric view of the chamber supports is shown. The same structure is seen in a frontal view in Fig 3 together with the drift chamber cross sections.

The frontal cross section of the entire detector volume is seen in Fig.4; the support structures at each side of the chambers account both of the vetronite framework of the chambers and of the supporting aluminum slides. The angle of

rotation of the internal drift chamber barrel relative to the the external one has been optimized to maximize the acceptance of the system for negative pions of about 270 MeV/c coming from the target.

The best improvements in terms of transparency has been obtained for the internal detector region where most part of the mechanical structure supporting the microstrip detectors has been suppressed. The remaining stainless steel pillars connecting the two side flasks are seen in Fig.5, where the central region cross section is shown. The silicon microstrip modules, whose number has increased from six to eight in the internal ring and from eight to ten in the external one, due to geometric constraints around the beam pipe, are now supported only by very thin lateral plastic beams.

With the more realistic structure of detectors and supports described in the Monte Carlo program, the trigger efficiency and the apparatus acceptance have been estimated by simulation.

1.2 Spectrometer acceptance and momentum resolution

The acceptance of the spectrometer has been evaluated for particles coming from hypernucleus formation and decay and from K^+ decay. As mentioned before, the design of the apparatus has been optimized to improve the acceptance for π^- of 270 MeV/c momentum; protons of 417 MeV/c, typical momentum for the particles emitted by non-mesonic proton-neutron decay, and μ^+ of 236 MeV/c originating from K^+ decay at rest, have been considered too.

The particles have been generated from a ideal cylindrical surface with radius of 7.5 cm and length 15.0 cm placed around the polyhedral target. The direction of each track is extracted randomly over the solid angle. The track enters the acceptance of the spectrometer when it deposits four hits in the four detector layers.

In Table 1.1 the results for the particle acceptances are resumed; they are compared with the geometric acceptance of the apparatus, which is evaluated counting the number of particles which hit the first straw tube layer in the absence the two drift chamber barrels. If one request that the particle also hits the external scintillator barrel, the acceptance decreases to 40%, 29% and 21% for pions, protons and muons respectively, owing to the reduced solid angle covered and to the curvature of the trajectories. It is worth recalling that, for unstable particles, the acceptance is reduced also by the decay in flight, that, for π^- of 270 MeV/c, amounts to around 10%.

It appears from the Table that the final geometric design of the spectrometer maximizes the acceptance for negative pions whereas positive particles, in particular very curved μ^+, are intercepted by the structural supports of the chambers to a greater extent.

Concerning the momentum resolution, as mentioned in the FINUDA Technical Report, with the assumed spatial resolutions of the different detectors and the

Table 1.1: Acceptances for different particles evaluated for the full apparatus and for the straw tubes only (geometrical acceptance)

Particles	Full apparatus	Geometric acceptance
π^- 270 MeV/c	(45±1)%	(54±1)%
p 417 MeV/c	(32±1)%	(60±1)%
μ^+ 236 MeV/c	(31±1)%	(53±1)%

Table 1.2: Momentum resolution of the spectrometer for different particles

Particles	Momentum resolution "forward particles"
π^- 270 MeV/c	0.28%
p 417 MeV/c	0.79%
μ^+ 236 MeV/c	0.24%

minimum amount of materials interposed along the particle paths, the resolution in momentum is dominated by the multiple scattering. Therefore, it will not be critical under possible worsening spatial resolutions of the detectors. The radiation length of the complete tracking volume is less than 170,000 cm (it would be 570,000 cm for pure helium and 30,400 cm for air), the radial dimension of the spectrometer is around 102 cm and the value of the homogeneous magnetic field is 1.1 Tesla. The momentum resolutions for different particles calculated with a Monte Carlo simulation are resumed in Tab. 1.2; they are estimated from the width of the reconstructed momentum distribution for "forward particles".

The Table shows that, in the final apparatus design, the expected momentum resolution for negative pions is slightly worse than the one estimated in the Technical Report for the previous apparatus configuration. This slight worsening of the resolution is caused by the decrease of the size of the spectrometer due to the change in the geometry of the internal detector region and to the increase of the radius of the straw tubes. Nevertheless, this momentum resolution still largely fulfills the goal of the experiment, whose main aim is to perform with an energy resolution of ≈ 0.7 MeV, a factor ≈ 4 better than the best present experiment[3] in the field.

In Fig. 6 the spectrum of the reconstructed momentum of a π^- of 270 MeV/c coming from the formation of an hypernucleus in a $\phi \to K^+K^-$ event is shown. The peak at around 270 MeV/c is due to pions which enter the spectrometer without crossing the structures of the internal detector region whereas the other peaks at lower energy are due to pions which cross one or more layers of these structures. The momentum resolution of the peak is of the order of 0.3% which can be improved, as illustrated in the Technical Report, by correction of the

energy lost by the π^- crossing the very thin target volume.

1.3 Trigger efficiency and rejection and trigger rates

The trigger strategy for the selection of hypernucleus formation events against the background, is based, as mentioned in the Technical Report, on three main requests concerning the topology of the decay products of the ϕ, the energy release of these products in the tofino slabs and a time coincidence between the internal and external scintillator barrels.

The first two conditions are verified on the internal scintillator barrel, where an "extended" back to back topology is demanded (coincidence of one slab with one of the three in front of it), as well as a condition of energy lost above a fixed threshold in at least two slabs. The latter condition results the most powerful in accepting K^+K^- decay events and rejecting the background ones. In fact the energy release of the slow kaons inside the tofino slabs, 2 mm thick, is several time greater than the minimum ionizing particles of the concurrent reactions.

The last condition demands for a time coincidence between the hits in the tofino back to back slabs and the first slab hit by a particle in the external scintillator barrel. The time coincidence requests a delay of not more than 10 ns between the two barrels. This conditions selects the events where a particle has crossed the spectrometer and in particular the fast pions coming from hypernucleus formation. On the contrary most of the μ^+ coming from the K^+ decay and crossing the apparatus are rejected, since they are delayed by the K^+ mean life which is about 12 ns.

In Tab. 1.3 the trigger efficiency for events where the ϕ decays into K^+K^- is shown; it is worth recalling that, in the simulated events, each time the K^- stops inside the target it is assumed that an hypernucleus is formed with the emission of a prompt pion of 270 MeV/c. Then, with a mean life time of about 0.300 ns, a non-mesonic hypernuclear decay is simulated, where a neutron and a proton of 417 MeV/c momentum are emitted. On the other hand the K^+, in flight or stopping in materials, decays with its proper lifetime.

In Tab. 1.3 the fraction of events satisfying the different trigger conditions is shown; the three mentioned conditions are simultaneously satisfied by 39% of the events, which gives the trigger efficiency for hypernucleus formation events. The inefficiency of the trigger strategy is due mostly to the angular acceptance of the π^- relative to the external scintillator barrel and, to a lesser extent, to angular acceptance of the K^+K^- and to kaon decay in flight.

In the 29% of the events, out of the 39% triggered, the π^- produced by the hypernucleus formation hits the four detector layers ("useful events"). In the other events, either the π^- has crossed one of the non sensitive volumes of the detectors, or the time coincidence on the external barrel has been given by a μ^+ from K^+ decay or by the conversion of a gamma ray.

Finally, about half of the 29% "useful events" have "forward pions" (pions

that have entered the spectrometer without crossing the target or the structure of the interaction region), and can be used for high resolution hypernuclear spectroscopy.

It is worth remarking that the final configuration of the apparatus has improved the percentage of "useful events" from the 25% evaluated in the Technical Report to 29%, while keeping the total trigger efficiency to around the 40%. This is due to the greater transparency of the internal detector region, which makes the "Back to Back + Energy Threshold" percentage increase from 75% to 80%, and the optimization of the apparatus geometry for negative pion trajectories.

In Tab. 1.4 the trigger rejection powers of the most important background processes are reported. Several reactions compete with the K^+K^- production from ϕ decay; indeed, in the angular range covered by the tofino scintillators, the rate of the Bhabha scattering events is expected to be of the same order of magnitude than $\phi \rightarrow K^+K^-$ decays, whereas other ϕ decays have comparable but smaller frequency. Nevertheless, the trigger strategy and, in particular, the energy threshold condition, give rise to an efficient rejection of these background events.

For the evaluation of the total trigger rate it is important to consider those events in which the K^- stops inside the target without formation of the hypernucleus. The trigger conditions can be satisfied by such events, since the fast time coincidence on the external scintillator barrel can be given both by the negative pion, which is emitted in the K^- interaction on a wide momentum spectrum (see Fig. 1.1 of the Technical Report), or by the μ^+ from the K^+ decay. Fortunately most of the spectrum of the emitted π^- is at momenta lower than 180 MeV/c and does not enter in the external barrel acceptance. These events, selected by the trigger, can give origin to an important source of background, since they are typically 10^3 times more frequent than the hypernucleus formation events.

In Tab. 1.5 the expected trigger rates for hypernucleus formation events and main background processes are given for a luminosity $L = 10^{32} cm^{-2} s^{-1}$. As an example let us calculate the rate for hypernucleus formation events. At the given luminosity we expect $\approx 440\ \phi s^{-1}$ and then, taking into account the Branching Ratio of the ϕ into K^+K^-, about 216 $K^+K^- s^{-1}$; the rate of hypernucleus formation is about $10^{-3} K^-_{stopped}$ and the trigger efficiency for events where the hypernucleus is formed, when the K^- stops inside the target, is 39%. The product of all these factors give a trigger rate of about 0.1 Hz. Finally, $\frac{29\%}{39\%} = 74\%$ of these events are "useful events" and about half of them have "forward pions", which are useful for high resolution hypernuclear spectroscopy.

1.4 Pattern Recognition Efficiency

Since the qualitative features of the final design of the apparatus remain essentially unchanged, the strategy of the Pattern Recognition process of the apparatus signals and its performances remain the same as those described in the

Table 1.3: Trigger efficiency for hypernucleus formation events. Percentages are relative to all generated events.

Extended back to back, energy threshold and 10 ns time delay	
Back to back	(89.3.±1.3)%
Energy threshold	(81.2±1.3)%
B.t.B * Energy	(80.6±1.3)%
Time coincidence	(46.2±1.0)%
TRIGGER	(38.6±1.0)%
Four hits	(36.0±0.9)%
TRIGGER + 4 hits	(29.4±0.8)%

Table 1.4: Trigger rejection powers for background processed. Percentages are relative to all generated events.

Extended back to back, energy threshold and 10 ns time delay	
Bhabha scattering	$< 10^{-2}$%
$\phi \rightarrow K_S K_L$	$(3 \pm 1)10^{-2}$%
$\phi \rightarrow \rho\pi$	$(4 \pm 1)10^{-2}$%
$\phi \rightarrow \pi^+\pi^-\pi^o$	10^{-2}%
K^- interaction without hypernucleus formation	(7.3±0.5)%

Table 1.5: Trigger rates at luminosity $L = 10^{32} cm^{-2} s^{-1}$.

Extended back to back, energy threshold and 10 ns time delay	
Hypernucleus formation	$8 \cdot 10^{-2}$Hz
Bhabha scattering	$< 4 \cdot 10^{-2}$Hz
$\phi \rightarrow K_S K_L$	$\approx 5 \cdot 10^{-2}$Hz
$\phi \rightarrow \rho\pi$	$\approx 2 \cdot 10^{-2}$Hz
$\phi \rightarrow \pi^+\pi^-\pi^o$	$\approx 10^{-3}$Hz
K^- interaction without hypernucleus formation	15 Hz

Technical Report. Work is in progress to perform a more accurate simulation of the response of the different detectors, based on experimental tests on prototypes. This simulation would allow, in a short time, to perform a more realistic estimation of the efficiency of Pattern Recognition and Track Fitting procedures.

References

[1] *FINUDA Proposal*

[2] *FINUDA Technical Report*

[3] *KEK Experiment*

Fig. 1

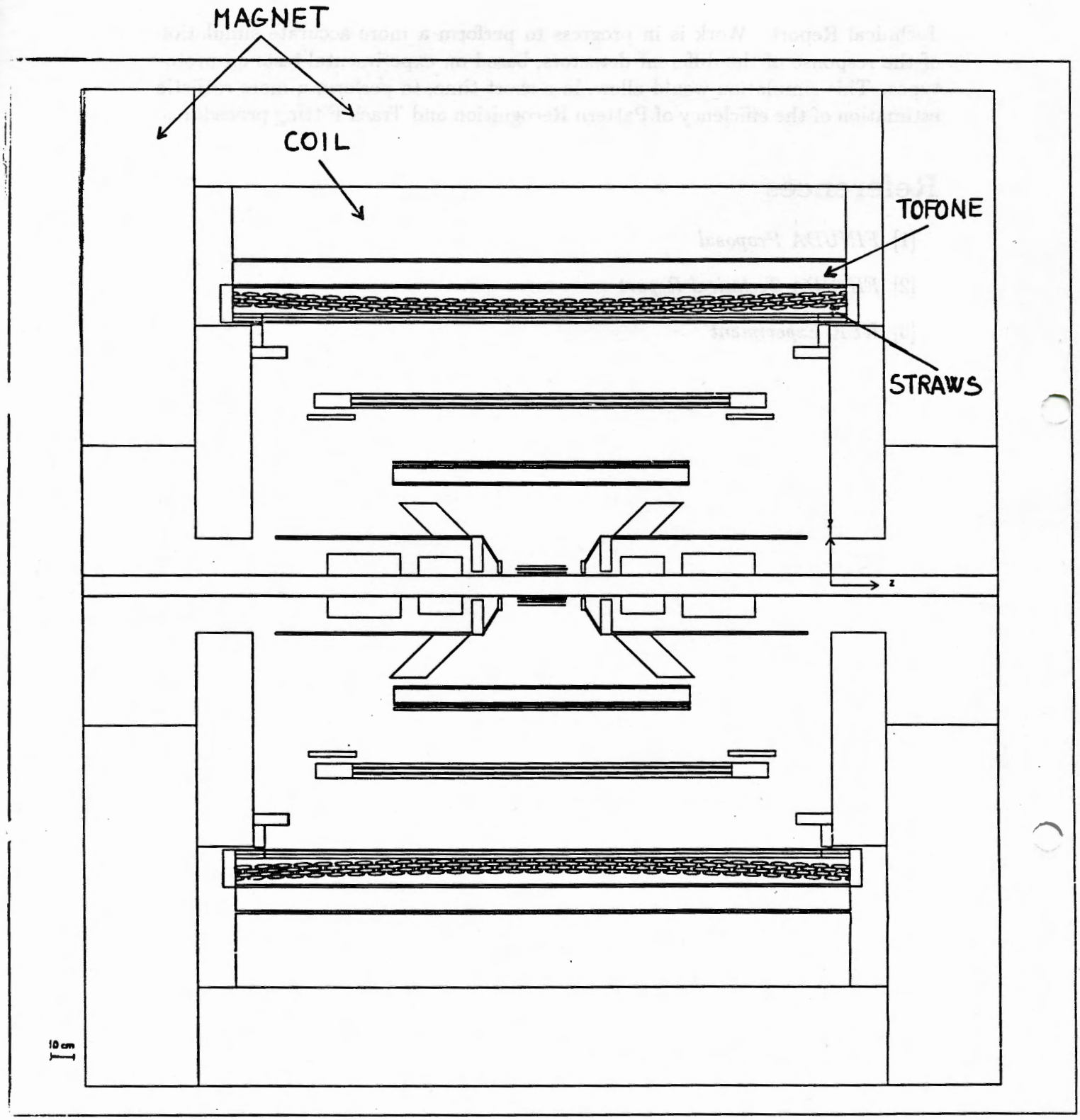

Fig. 2

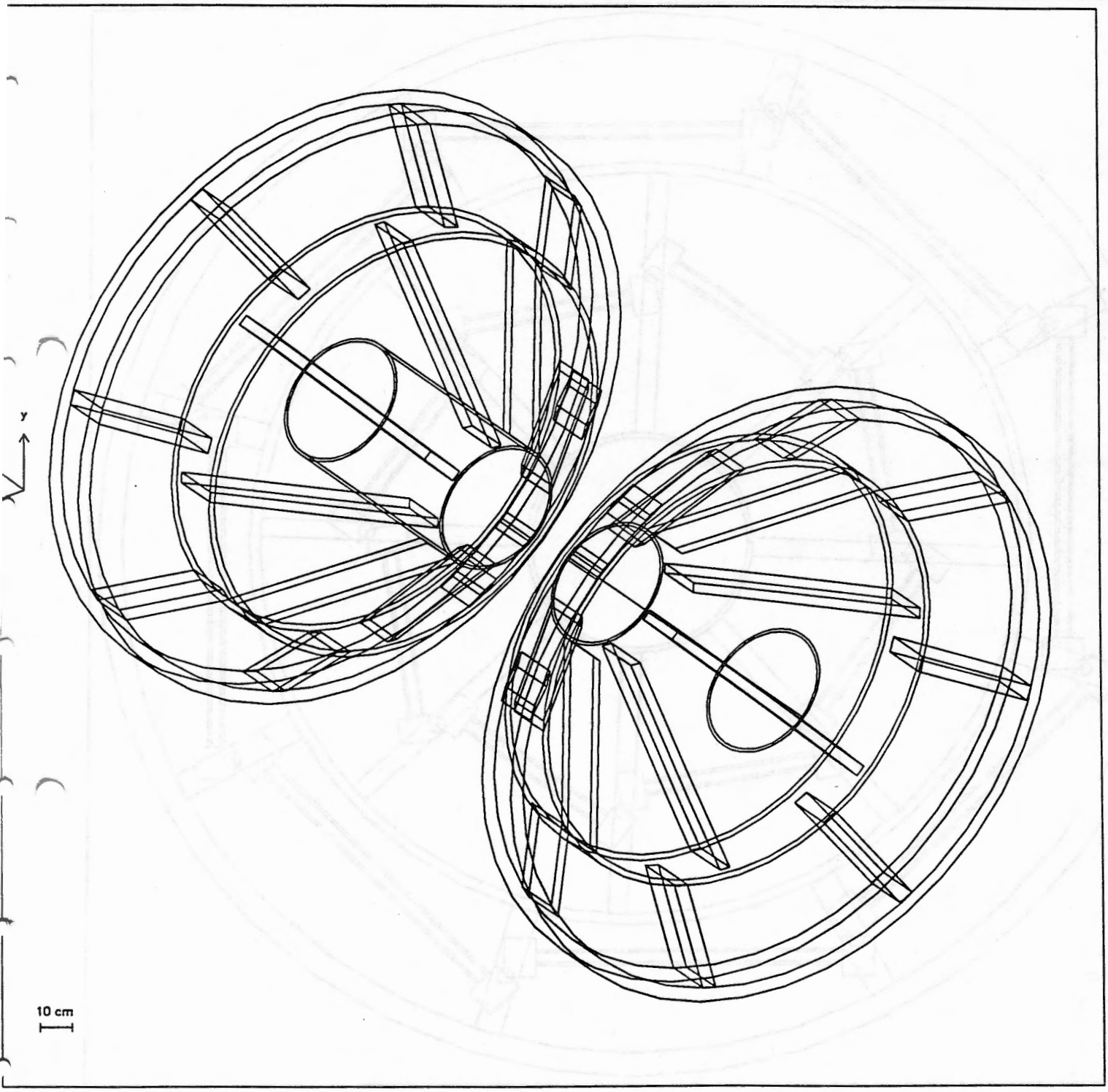

Fig. 3

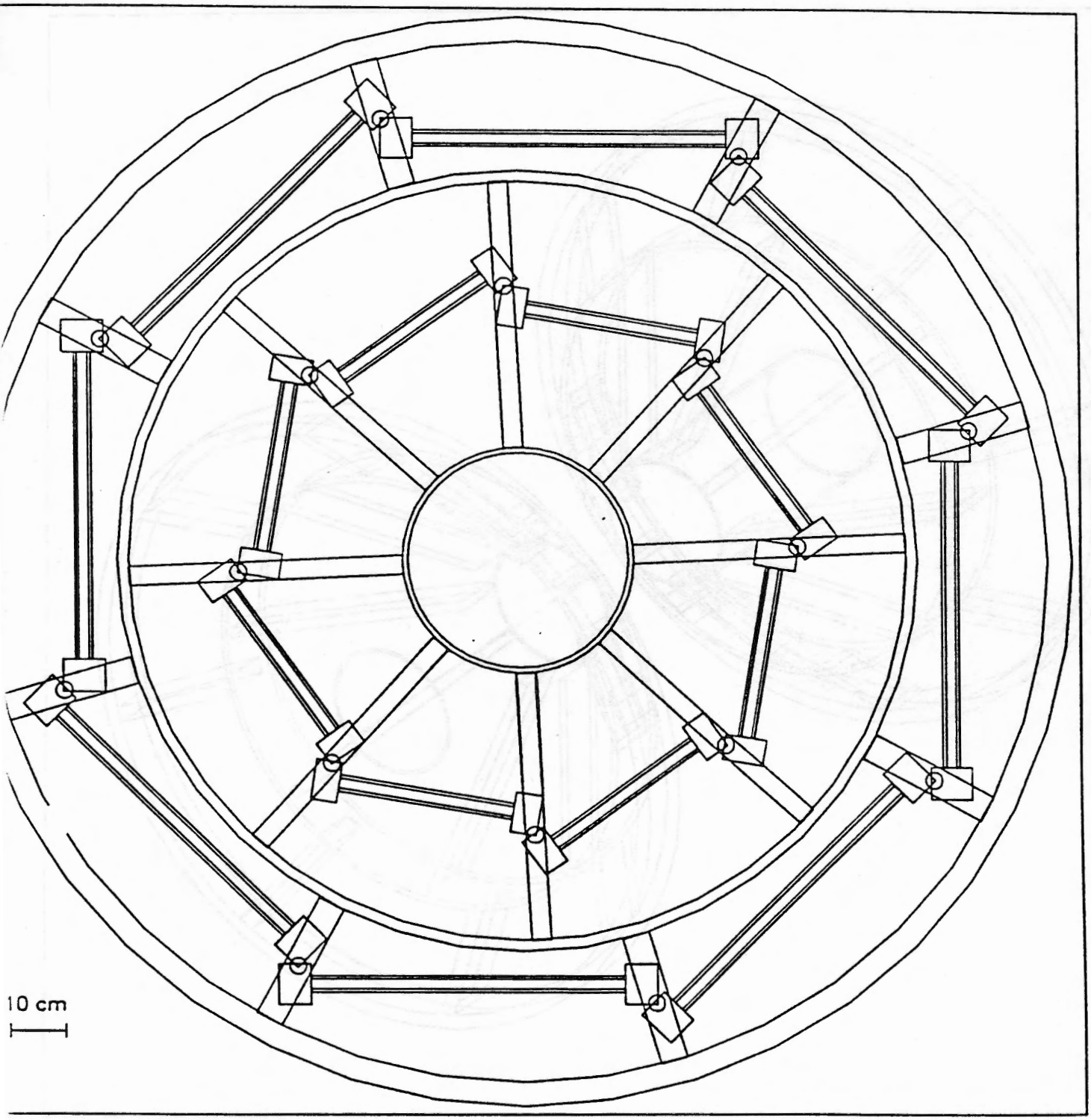

Fig. 4

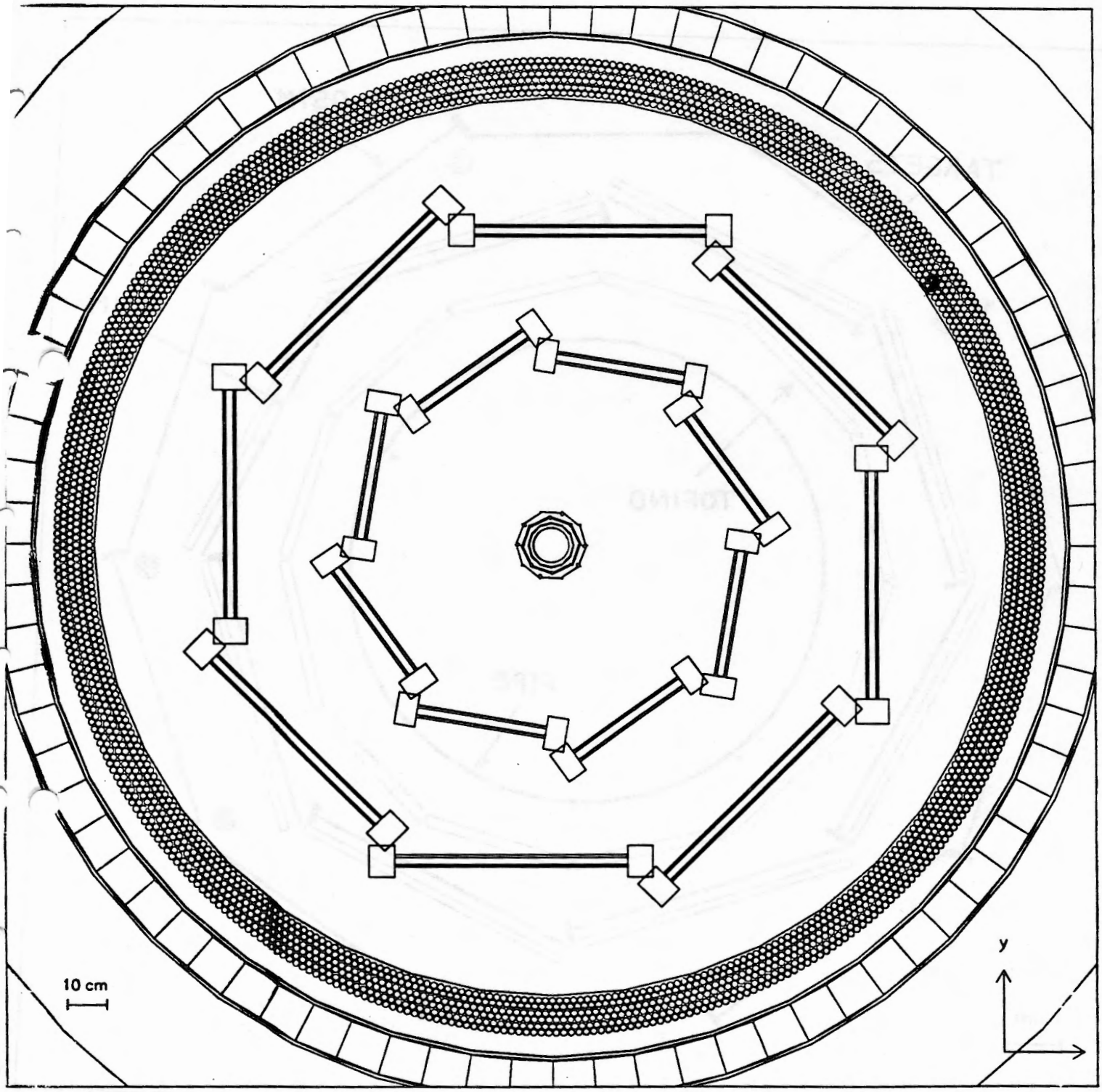

Fig. 5

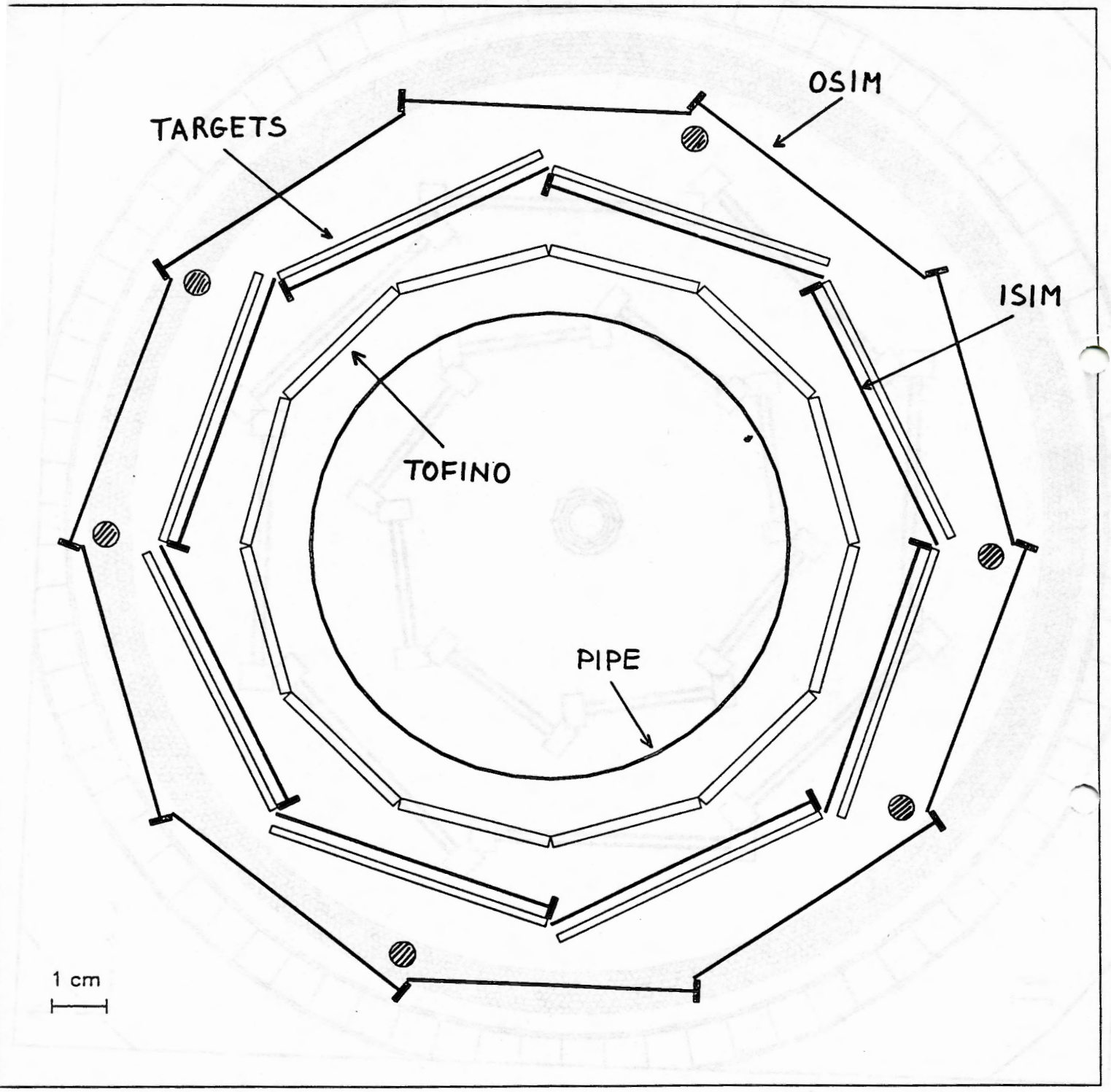

Fig. 6

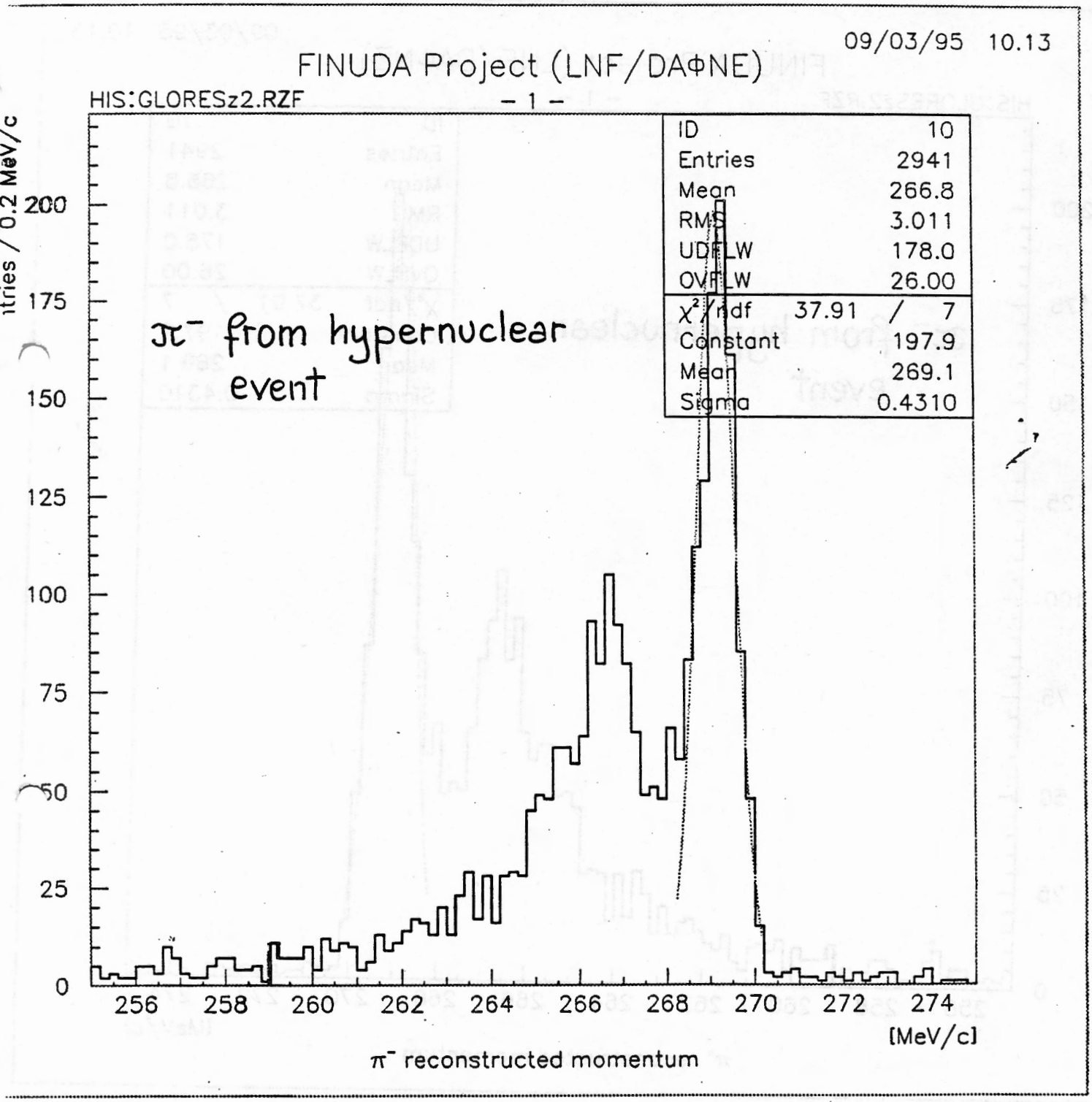
09/03/95 10.13
FINUDA Project (LNF/DAΦNE)
HIS:GLORESz2.RZF
- 1 -
ID 10
Entries 2941
Mean 266.8
RMS 3.011
UDFLW 178.0
OVFLW 26.00
χ²/ndf 37.91 / 7
Constant 197.9
Mean 269.1
Sigma 0.4310
π⁻ from hypernuclear event
tries / 0.2 MeV/c
200
175
150
125
100
75
50
25
0
256
258
260
262
264
266
268
270
272
274
[MeV/c]
π⁻ reconstructed momentum

Doc. 3

CERN 7.5.95

Caro Calvetti, mi scuso se non mi sono ancora fatto vivo, ma ho avuto un periodo denso di lezioni ed esami (fortunatamente le elezioni a Cremona sono andate bene... per me).

Rispondo quindi con un certo ritardo ad alcuni quesiti che lei mi aveva posto circa il tracciamento dei K^- dal decadimento della ϕ in FINUDA, approfittandone per studiare più nel dettaglio, come era già mia intenzione, l'efficienza del processo di ricostruzione del vertice. Stiamo infatti, in questo momento, scrivendo l'algoritmo definitivo per tale processo.

Una questione da lei posta riguardava la dispersione per scattering multiplo e perdita di energia dei K^- che si arrestano nel bersaglio.

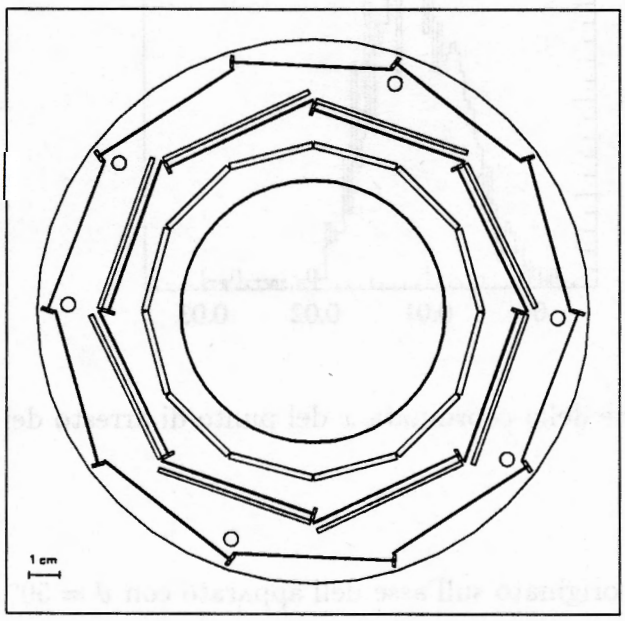

Figura 1: vista frontale dell'attuale configurazione della regione centrale dell'apparato

Abbiamo simulato delle popolazioni di K^- di impulso opportuno, ottenendo i seguenti risultati.

Condizioni:
- bersaglio a 2 mm di distanza da ISIM (Fig. 1)
- Impulso del K^- al valore centrale della distribuzione

- K^- originato sull'asse dell'apparato con $\vartheta = 90°$

Dispersione nella profondità del punto di arresto nel bersaglio a causa delle fluttuazioni di perdita di energia lungo il percorso: $\sim 100\ \mu m$ FWHM (Fig. 2). Dispersione laterale del punto di stop complessiva (a partire dal centro dell' apparato) $\sim 1.3\ mm$ FWHM (Fig. 3). Va tuttavia ricordato che il passaggio delle traccia è registrato su ISIM immediatamente prima del bersaglio con una risoluzione migliore di $\sim 50\ \mu m$ in sigma.

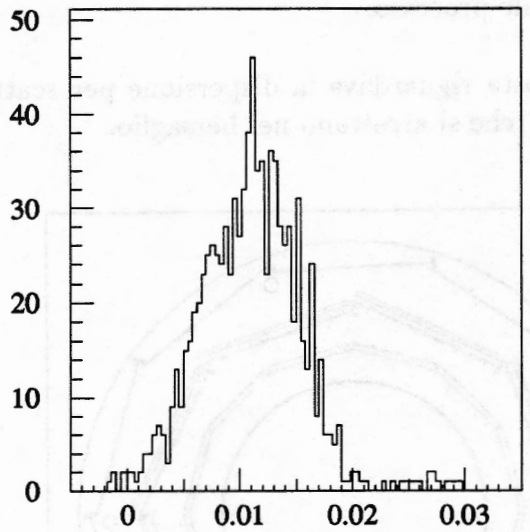

Figura 2: distribuzione della coordinata x del punto di arresto dei K^- [cm]

- K^- originato sull'asse dell'apparato con $\vartheta = 50°$

In questo caso, a causa del maggiore spessore dei materiali attraversati, del maggiore sviluppo geometrico della traccia e della sua inclinazione rispetto al bersaglio, la dispersione longitudinale (parallela all'asse del fascio) risulta essere maggiore, dell'ordine di 2.5 mm FWHM. Queste dispersioni sono quelle cumulate lungo tutto il percorso della traccia; i contributi relativi all'attraversamento di ISIM (dove il K^- arriva all'incirca con 10.9 MeV di energia contro i 16.3 MeV di valore centrale), al percorso ISIM-bersaglio ed al frenamento nel bersaglio, sono stati valutati separatamente.

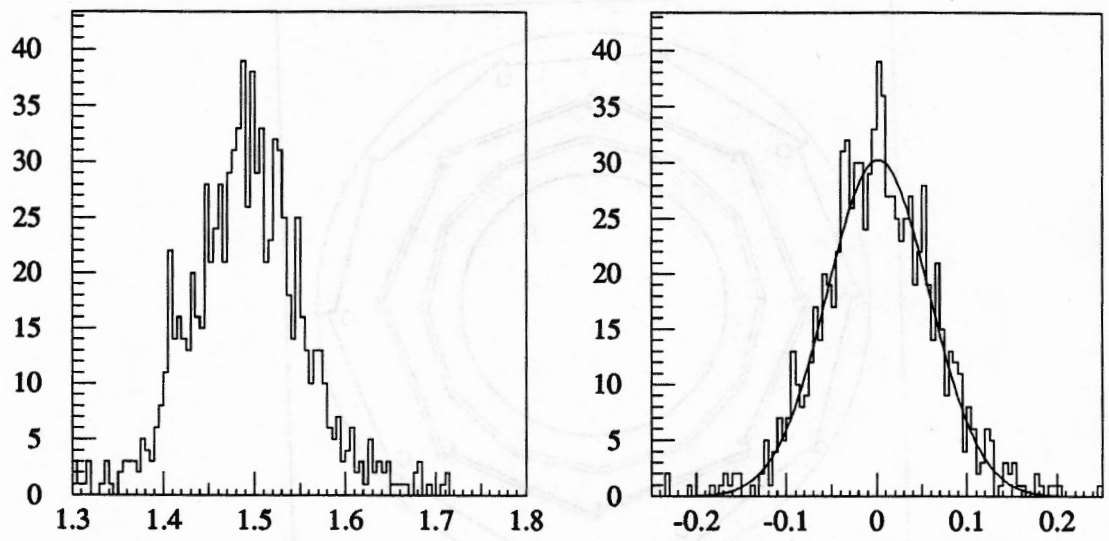

Figura 3: distribuzione della coordinata y (sinistra) e z (destra) del punto di arresto dei K [cm]

- K originato prima di ISIM (T $\sim 10.9 MeV$) con $\vartheta = 90°$

Dispersione in profondità per straggling: $\sim 50\ \mu m$ FWHM
Dispersione laterale per scattering multiplo: $\sim 300\ \mu m$ FWHM

- K originato prima di ISIM (T $\sim 8.7 MeV$) con $\vartheta = 50°$

Dispersione in profondità per straggling: $\sim 50\ \mu m$ FWHM
Dispersione longitudinale per scattering multiplo: $\sim 600\ \mu m$ FWHM

Queste dispersioni laterali sono dovute all'ultimo tratto di percorso della traccia dopo ISIM. Esse possono essere ridotte avvicinando il più possibile il bersaglio alla superficie di ISIM.

Con il bersaglio aderente alla superficie della μstrip (Fig. 4) si ottiene:

- K originato prima di ISIM (T $\sim 10.9 MeV$) con $\vartheta = 90°$

Dispersione laterale per scattering multiplo: $\sim 130\ \mu m$ FWHM

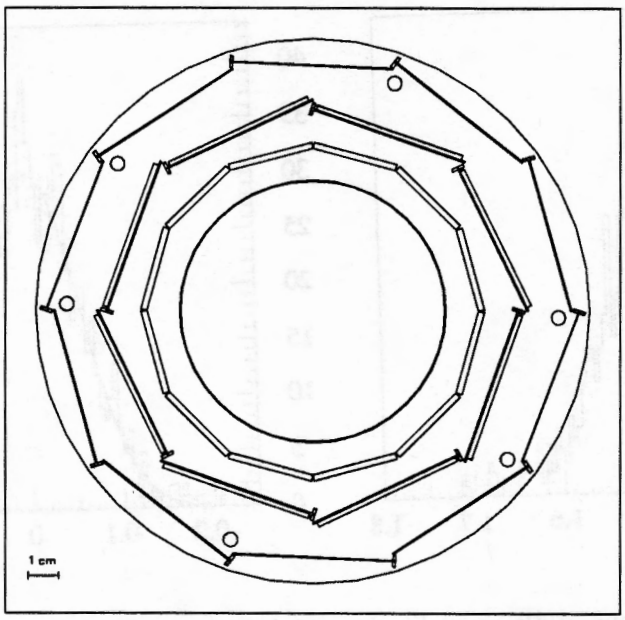

Figura 4: vista frontale della *possibile* configurazione della regione centrale dell'apparato

- K originato prima di ISIM (T $\sim 8.7 MeV$) con $\vartheta = 50°$

Dispersione longitudinale per scattering multiplo: $\sim$ 90 μm FWHM. Il valore inferiore della dispersione longitudinale rispetto al caso precedente e' da attribuire al minore range residuo della particella.

Considerato il sensibile miglioramento nella dispersione si cercherà di realizzare il massimo avvicinamento del bersaglio ad ISIM, in dipendenza dalla natura del materiale costituente i bersaglio stesso.

Va comunque precisato che la risoluzione finale sull'individuazione del vertice dipenderà anche dalla precisione di ricostruzione della traiettoria del K^+K^- a partire dai due punti misurati su ISIM. Stiamo, in questo momento, valutando le prestazioni dell'algoritmo finale adottato.

Un altro elemento importante, che influenza la dispersione dei vertici di arresto dei kaoni, è la fluttuazione del valore dell'impulso del K generato dal decadimento della ϕ. Tale fluttuazione è originata dalla convoluzione della larghezza intrinseca della ϕ con la dispersione della energia di centro di massa dovuta ai fenomeni radiativi nella collisione. Secondo l'algoritmo di calcolo di tale disper-

sione, sviluppato dalla collaborazione KLOE, la larghezza indotta sull'impulso del kaone emesso è di 3.3 MeV/c FWHM su 127.8 MeV/c di impulso centrale.

Questa fluttuazione di impulso determina un'ulteriore dispersione in profondità della distribuzione di arresto, che si allarga a $\sim$ 250 μm FWHM, mentre non influenza apprezzabilmente la dispersione laterale dovuta allo scattering multiplo.

Stiamo attualmente completando e collaudando una procedura definitiva di individuazione del vertice di arresto del kaone nella geometria finale della regione interna di rivelatori. Essa permetterà di apportare, all'impulso del pione misurato nello spettrometro, la correzione per l'attraversamento del bersaglio. Oltre che sulla stima della posizione di arresto del kaone la procedura si basa sulla estrapolazione della traccia del pione verso la superficie del bersaglio. Tale estrapolazione può essere fatta, grazie alla precisione nella misura della traiettoria, con una precisione sul punto estrapolato dell'ordine di 100 μm.

Non appena i risultati del collaudo di questo processo saranno disponibili provvederò a farglieli pervenire.

Cordiali saluti

Aldo Zenoni
Alessandro Feliciello

22/9/95

Doc. 4

PROGRESS REPORT ON THE FINUDA OFFLINE SOFTWARE

Monte Carlo simulation

The study of the performances and the optimization of the design of the mechanical structure of the apparatus, in terms of acceptance and of momentum resolution, has been completed. Trigger efficiency and background contamination for the different concurrent reactions have been studied and work is still in progress for the optimization of the trigger rejection, in particular for the Bhabha and Touschek events.

The possible application of the FINUDA apparatus to the investigation of the Kaon-Nucleon scattering has been studied too. It involves some changes of the apparatus and will be a possible physical aim for a second stage of the experimental activity. A detailed proposal concerning this subject will be presented in the future.

Most of the work concerning the apparatus simulation has been devoted to the simulation of the behaviour and the response of the different detectors. A particular attention has been dedicated to the study of the silicon microstrips, since the performances requested to this device, in the FINUDA experiment, result to be more severe that in the applications to other experiments. In fact, the silicon microstrips in FINUDA have to detect both minimum ionizing and highly ionizing particles and have to allow the recognition of the crossing points of their trajectories without the support of redundant information from other detectors; moreover, they have to accurately measure the specific energy loss of the different tracks for recognizing the minimum ionizing particles from highly ionizing slow ones.

The simulation of the signals produced by the silicon microstrips has been done starting from an accurate description of the energy loss in silicon. Each track element in the silicon volume is subdived into a number of small track elements. The length of the elementary track element is 10 μm. The energy released by each elementary track element is determined as a Landau distribution, computed by an algorithm developed by the ALEPH Collaboration. It is a modification of the GEANT routine GLANDZ adapted to accurately reproduce the experimental data. It has been tested by the ALEPH group for minimum ionizing particles and it works well. The behavior for highly ionizing slow particles has to be checked. Tests on prototypes are foreseen in November 95 at TRIUMF.

The ionization charge associated to the energy released by each elementary track element is distribuited between the interested strips following a gaussian function, with a standard deviation depending on the position of the small track element and on the physical parameters of the detector (the effects of the magnetic field have to be included). The signal detected by the amplifiers (positioned every 2 strips) is a fraction of the charge collected by the strips connected to the amplifiers and a fraction of the charge collected by neighbouring strips (these

fractions must be determined). The simulation of the electronic noise is implemented too. It is distribuited according to a gaussian function with a standard deviation (not yet determined) given by the equivalent noise charge (ENC) of the detector-amplifier system.

Concerning the drift chambers, the electric and drift time structure of the cell have been largely studied and optimized accounting for the magnetic field and the specific gas mixture utilized; the drift cell simulation program GARFIELD has been used for accomplishing this task. Extended tests of the drift chamber prototype with a pion beam have been performed and will allow the reliability of these simulations to be verified. The mapping of the drift cell, in terms of space drift time relationship and the experimental results for what concerns the time resolution of the chamber at different track incident angles, will be inserted in the Monte Carlo program in order to reproduce, as realistically as possible, the response of the chamber. The work is in progress.

The simulation of the digitized signals from the different detectors finalized to the accurate reproduction of the structure of the event (the Raw Data Tape) is in progress too, in close collaboration with the ONLINE group.

Reconstruction algorithms

After having determined the final geometry of the interaction zone, the vertex reconstruction algorithm has been developed and tested in its final version. It makes use, for the estimation of the stopping points of the K^- and K^+ inside the target, of the tracking package GEANE, which accounts, in a accurate way, of the geometry of the detectors and mechanical supports, of the magnetic field and of the average energy loss of the particles. In the reconstruction algorithm first the approximate trajectory of the K^+, K^- beam is evaluated interpolating the crossing points of the K^+ and K^- in ISIM with a helix; then, with the GEANE tracking package, the average path of the Kaon is tracked starting from the estimated vertex position and direction, until the stop of the tracks in the target. As a result the penetration depth of the Kaon in the target can be evaluated.

Finally this penetration depth is used to determine the stopping point of the Kaon in the approximate helical trajectory which intersects the ISIM crossing points. Owing to the very low energy of the stopping Kaons, the effect of the multiple scattering in the final part of the trajectory is relevant; however, thank to the short path from the ISIM detector to the target, the K^+ and K^- stopping points can be determined with a spatial resolution of about 600 μm along the target length and width and $\sim$150 μ in target depth.

Using the information on the K^- stopping point and the extrapolation of the π^- trajectory on the target surface, the measured momentum of the π^- can be corrected for the energy lost by the pion in crossing the target material. The results from the Monte Carlo simulation show that, with this correction of the measured momentum, the design resolution of the spectrometer can be fully exploited.

Concerning the reconstruction algorithms of the different detectors, they are being designed and implemented. For the silicon microstrips, the cluster-finding algorithms will be done following the Monte Carlo results (in particular depending from the signal-noise ratio and the geometry of the tracks). For what concerns the position-finding algorithm, the use of the "centre of gravity method" is foreseen. If needed different algorithms, selected in dependence of the inclinations of the tracks, can be implemented in order to increase the spatial resolution.

For the drift chamber reconstruction, the proper time vs space relationships for different angle of incidence have been obtained from the GARFIELD simulation program. They can easily be inserted in the reconstruction program to convert the drift time in spatial crossing positions.

Finally, concerning the track fitting algorithm, a relevant improvement of the present one is under test. In fact the present algorithm provides the fit, with a spline algorithm, of the spatial information obtained from the OSIM detector, the Drift Chambers and the longitudinal straw tubes; the stereo straw tubes are only utilized for the determination of the zeta coordinate of the track trajectory at the longitudinal straw tube radius.

However, most of the spatial information carried by the stereo straw tubes is still in the $(\rho\phi)$ plane, where the curvature of the track develops and where the information about the track momentum is available. Moreover, the stereo straw tubes are placed at a radius greater than the longitudinal ones. Consequently, if the stereo straw tubes could be inserted in the fitting procedure too, the momentum resolution of the track should be sensibly improved; very optimistically it could be improved by the square of the ratio between the radius of the stereo straw tubes and the longitudinal ones which is about 1.4.

For this reason, a new fitting algorithm is being implemented, where the trajectory of the π^- track through full apparatus set-up is calculated with a Runge-Kutta method, accounting for the energy loss in the different volumes. This tentative trajectory is compared with the crossing points (or distances from wires) of the track in the different detectors and an estimator of the agreement is evaluated. Minimizing this estimator, the best fitting of the track trajectory inside the full apparatus can be obtained; in the fitting procedure a careful account for the deviations due to detector spatial resolution and multiple scattering has to be applied. The work on this new fitting procedure is in progress.

Brescia, 10/4/96

Short summary of the present status of the FINUDA off-line software

The off-line software of the FINUDA experiment is, at present, composed of two main parts :

- The Monte Carlo simulation of the apparatus based on GEANT3 package. In this program the mechanical and physical structure of the apparatus and of all the detectors is described in proper detail and different event generators are available for simulating hypernuclear events, physical background and machine background.

  In the present version of the Monte Carlo, the expected resolutions of the detectors have been simply simulated as smearings of the geometrical hits, the crossing times and the deposited energies.

  The program has been largely utilised for the design of the apparatus and for the evaluation of its performances.

- The Reconstruction Program, which accepts in input the smeared hits and the information on the geometrical structure of the apparatus from the Monte Carlo program and performs the reconstruction of the events and the visualisation of the results.
  The Reconstruction Program works through different phases :
  - The decoding of the simulated RDT in a input data structure based on ZEBRA data banks.
  - The local Pattern Recognition of the detectors for which a preliminary analysis of the raw information is needed. The Pattern Recognition of the straw tube arrays is already written and working; it clusters together the fired tubes corresponding to the same track and performs an estimation of the zeta coordinate of the crossing of the track in the first layer of straw tubes (longitudinal straws).
    The resolution on the zeta coordinate obtained with this method is of the order of σ=1.5 *cm*; the efficiency for correct clustering of the tubes and reconstruction of the zeta coordinate is better than 85%.
    The Pattern Recognition of the silicon microstrip detectors is in progress (see below). The other detectors do not need a local Pattern Recognition.
  - the General Pattern Recognition of the event; it is performed through different successive tasks : (1) reconstruction of the K^+K^- beam basing on the hits in the TOFINO slabs and the hits on the silicon microstrips (dE/dX and particle recognition in the microstrips are needed); (2) reconstruction of the points of interaction of the kaons inside the target (vertices) by extrapolation of the beam trajectory (the GEANE package is used, in order to account for the energy loss in the materials); (3) Pattern Recognition of the curved tracks leaving the vertices and crossing four detector layers: OSIM, the two drift chambers and the longitudinal straw tube arrays. Short tracks crossing only the first three detectors are recognised as well.

An output data structure in form of ZEBRA banks is produced and contains the logical correlations of the geometrical hits and the event structure found by the Pattern Recognition.

- The fitting of the tracks by means of a helix fit or a spline algorithm. These two algorithms need in input the (x,y,z) coordinates of spatial points. The geometrical information used is : the crossing point coordinates in OSIM (x,y,z with high spatial resolution); the crossing points in the drift chambers, where the left-right ambiguity is solved by the doublet of sense wires (x,y with high spatial resolution and z with a looser one - σ=1 or 2 cm); x and y crossing point coordinates (distance to the wires) of the first layer of straw tubes; for these detectors the left-right ambiguity has to be solved by the local Pattern Recognition.

  A first approximation of the z coordinate of the track at the first layer of straw tubes is given by the straw tube local Pattern Recognition. A better estimation of this coordinate is found with the following procedure.

  First a helix trajectory starting at the estimated crossing point of the track at the first layer of straw tubes, with the same ϕ and θ angles and the same projected curvature of the track fitted in first approximation, is considered. Then, the z coordinate of the crossing point is adjusted in order to minimise the differences between the estimated distances to the wires and the measured ones. An iterative procedure is adopted to improve the result. The resolution on the z coordinate that can be obtained with this method is of the order of σ= 1 mm.

  The need of using separate procedures for straw tubes and other detectors, in order to fit the track through the full apparatus, originates from the fact that a straw tube provide, as spatial information, the distance to a wire and not a spatial point. For this reason this information cannot be inserted directly in a fitting procedure using a helix fit or a spline method. Alternatively, in order to fit the spatial information from all the detectors at the same time, a numerical fitting procedure is needed (see below).
- The result of the analysis (and the input from the Monte Carlo) can be visualised by an Event Display inserted in the Reconstruction Program. The Program, in fact, can be run both interactively for event debugging and in batch for event processing. The final results (the DST) are written on tape in the form of ZEBRA data structures.

- The expected performances of the apparatus concerning the resolution on momentum and hypernuclear lifetime and the efficiencies for trigger, background rejection and event reconstruction, have been estimated with the Monte Carlo and have been presented in the FINUDA Technical Report and other Status Reports of the experiment.

Progress in the FINUDA offline software

In the developing the FINUDA offline software, the recent effort has been mainly devoted to two main tasks :

1) The simulation of the analogical response of the detectors and the corresponding reconstruction algorithms.

2) A numerical method of track fitting using a Runge-Kutta numerical integration of the track trajectory.

Additionally, the existing software has been transported and is now working on the Unix operating system, which will be largely used in the on-line and off-line processing computers. Moreover, the choice of the general data base tool *mini SQL* has been made, and the geometrical data of the different detectors, in particular the straw tube ones, are being inserted at present.

- Simulation/reconstruction of the detectors. The work has been mostly concentrated on the silicon microstrip detector. For these detectors a local Pattern Recognition is needed for the reconstruction of the detector information and the ability in exploiting its particle recognition capability is crucial for the global Event Reconstruction.

  The analogical signal expected from the detectors has been simulated as follows, along the same lines followed by the Aleph Collaboration. First, by means of the GEANT tracking system, the particles of the generated events are tracked through the active detector volume in very small steps and, at each step, the energy deposition is calculated.

  At present, provisionally, the Landau distribution has been utilised, just to develop the basic reconstruction algorithms. Experimental data from tests on the detectors are waited, especially for what concerns the highly ionising particles, since the saturation characteristics of the detectors and of their amplification chains are not well known. The data available from other experiments concern exclusively minimum ionising particles, while one of the major tasks of these detectors, in the FINUDA context, is the recognition of highly ionising slow kaons.

  In a second time, the charge created by ionisation in the different positions inside the detector active volume, are projected onto the system of strips with a gaussian distribution whose width depends on the diffusion coefficient D=35.1 cm^2/s for electrons and D=12.5 cm^2/s for holes (see Fig. 1, ϕ side).

  Finally the charge collected on the amplified strips is calculated, accounting also for the charge induced by the adjacent non amplified strips. This is done both for the ϕ and z sides of each microstrip module. All the active strips of the two sides in all the modules are numbered and correctly positioned in the space, therefore each signal can be put in correspondence to a precise spatial position in the reconstruction phase.

  The detector noise has been accounted for by injecting in each strip, randomly, a gaussian noise of nominal value. This nominal noise can be calculated as a function of the detector thickness, the condition of polarisation and the amplification chain characteristics. For minimum ionising particles crossing orthogonally the detector module, this results in a signal to noise ratio of around 40. In Fig. 2 the signal induced on the ϕ side strips by an orthogonal relativistic pion is seen.

  The values of the charge collected by all the active strips are transferred to the reconstruction algorithm; the algorithm works out the information in four successive steps : (1) finding of the strip

clusters on the ϕ and z sides of each module; (2) association of the clusters, on the two sides of a module, which correspond to the crossing of the same track; (3) reconstruction of the spatial coordinates of a hit; (4) particle recognition by dE/dX and by cluster characteristics.

The cluster finding algorithm has been already written and tested and it seems to work with high efficiency in the simulated condition of noise and event topology. Fig. 3 shows the number of clusters per event (on the ϕ side), when hypernuclear events are generated; the average number of clusters per event is around 6; 0.5 per module in ISIM and 0.2 per module in OSIM. In Fig. 4 a) and b) the difference between the number of generated clusters on a module and the number of reconstructed ones is shown, for the ϕ and z sides respectively.

The negative channels indicate spurious clusters, which are generated by the physical noise of spiralizing tracks hitting many contiguous strips in the same module. This type of events is, in any case, difficult to reconstruct. The positive channels indicate the number of lost clusters, which is not negligible (the total number of cluster is around 6000, the lost ones are around 500).

However, an inspection of the characteristics of the lost clusters shows that they are mostly placed at the border of the sensitive area of the detectors, where a part of the ionisation is not collected. Additionally, some of the lost clusters correspond to ambiguities in the cluster finding algorithm occurring when two clusters are too close. Considering the high granularity of the detectors, these ambiguites can be avoided by a proper tuning of the parameters of the algorithm.

The cluster association on the ϕ and z sides is based on the fact that the positive and negative charge, deposited by the track in the sensitive volume of the microstrip, are totally collected by the strips on the two sides of the module, without multiplication or relevant recombination effects (in absence of saturation). Therefore, one may expect that the two clusters, generated by the same track in the two sides of the module, have the same value of collected charge.

In effect in Fig. 5, from experimental data of Aleph, the scatter plot of the charge collected on one side of a microstrip module versus the charge collected on the other side, for hits of the same minimum ionising track is shown. Fig. 6 the same scatter plot is shown, for the FINUDA microstrip detectors, for simulated hits in hypernuclear events. The deviations from a straight line, in the simulated scatter plot, are due only to the detector noise or to a loss of a part of the charge for clusters close to the border of the module. Considering that, in FINUDA, the particles generated in hypernuclear events have very different specific energy loss, a good association of the clusters in the ϕ and z sides should be possible. Ambiguities in the association can be generated by a high level of noise or by a high number of hits on the same module.

The reconstruction of the spatial coordinates of the hits is performed by means of a weighted average of the strip positions inside the clusters. Simple and efficient algorithms for coordinate reconstruction have been developed by Aleph and can be adopted by FINUDA. The only relevant difference consists in the fact that, in the FINUDA situation, the tracks may be very inclined and the number of strips in one cluster may be high. This may be a disadvantage from the

point of view of the determination of the spatial position but can be an advantage from the point of view of the Pattern Recognition and track identification. It is worth reminding that, in any case, the spatial resolution requests of FINUDA are less stringent than the spatial resolutions potentially reachable by the microstrip detectors. The code for the cluster association and point coordinate reconstruction has been already written and is currently under test.

The particle identification in the microstrip detectors is of crucial importance for the global Event Reconstruction, since the starting point of the general Pattern Recognition is the identification of the two hits generated on ISIM by the slow kaons. This identification can, in principle, be easily performed basing on the high dE/dX of the slow kaons relative to the minimum ionising particles (around 25 times larger) and by the cluster structure typical of the different particles. In fact, the kaons come from the axis of the apparatus and cross almost radially the ISIM microstrips, while the other particles are isotropically emitted from the target.

In Fig. 7 a),b) the charge collected in the clusters for a population of kaons coming from the ϕ decay is shown, together with the distribution of the number of active strips hit on the ϕ side; in Fig. 8 a),b) and Fig. 9 a),b) the same distributions are shown for protons and pions. It is evident the larger mean energy released by the kaons and the much lower multiplicity of its strip clusters.

In Fig. 10 the ratio of the energy lost over the number of strips hit on the ϕ side is shown for the different particles; kaons appear clearly separated from pions and also from protons. Moreover, the cluster multiplicity can be used as well for particle recognition. The code needed to accomplish this task has already be written and is under test.

Concerning the low mass drift chambers, the simulation of the drift cell by means of the GARFIELD package has already been performed and both the mapping of the cell and the space-time relationship have been calculated. They have to be checked experimentally in the proper magnetic field and introduced in the Reconstruction Program.

Concerning the scintillators of the outer scintillator barrel (TOFONE), a number of experimental test have been performed to characterise the efficiency of all detectors and their time and energy resolutions. The results of these tests are being analysed at present and will provide the proper resolution and efficiency functions to be inserted in the Monte Carlo simulation and in the Reconstruction Program.

In particular, a calibration experiment was performed in TRIUMF, Vancouver, to measure the neutron detection efficiency of the TOFONE scintillators for neutrons of energy from 20 to 70 MeV, coming from a source-detector geometry similar to that of FINUDA.

A negative pion beam was stopped in a polietilene target and the two neutrons coming from the $\pi^- + {}^{12}C$ reaction were detected in two scintillator slabs placed in opposite sides, in coincidence with the trigger given by a pion stopping in the beam telescope. Data analysis is

in progress and the neutron response function at various energies have already been extracted from single counting, for selected neutron energies and impact positions on the long detectors. In the meantime a complete simulation of the experimental set up is being performed by means of GEANT; in this simulation the amplitude resolution and the attenuation data versus flashing position, obtained with a reference moving scintillator tracked with cosmic rays, have been implemented. As a result of the comparison of the simulated neutron response functions with the experimental ones, the neutron detection efficiency will be deduced.

From this analysis the neutron detection efficiency versus energy, threshold and position will be extracted, in order to obtain a lookup table for the FINUDA data analysis.

The neutron coincidences between the two TOFONE elements of the calibration experiment will be furtherly analysed to obtain a second evaluation of the neutron detection efficiency. In this case the normalisation will be deduced from the known quasi-deuteron π^- interaction mechanism. If the reaction description and the collected statistics will be satisfactory, the extracted data will support, at a very high level of confidence, the data extracted from single counting.

Neither the low mass drift chambers nor the scintillator barrels TOFINO and TOFONE need a local Pattern Recognition procedure.

- Numerical method for track fitting. As stated before, the geometrical information coming from the different arrays of detectors, in the FINUDA apparatus, cannot be fitted together with the same helix or spline fitting algorithm. In fact, while the OSIM detectors and the drift chambers provide the coordinate of a spatial crossing point x,y,z (z with loose resolution for the chambers), the straw tubes provide the distances to the wires at which the track is passed. The spatial information is a condition of tangency to cylinders in the space.

  For these reason different algorithms must be adopted for OSIM, drift chambers and longitudinal straws (spline) and for longitudinal and stereo straws (minimisation of distances to the wires of a helix trajectory) and the two algorithms must be matched by means of an iterative procedure.

  Alternatively, a fitting of the track trajectory by numerical integration can be used; such a procedure should work along the following lines. First, approximated parameters of the track (momentum, θ and ϕ angles and coordinates of the starting point) must be provided to the algorithm. Then, using these first approximation parameters, the trajectory of the tentative track is calculated numerically through the apparatus, taking into account the inhomogeneous magnetic field, the geometrical structure of the apparatus and detectors and the energy loss in the crossed materials.

  Geometrical points along the trajectory, at the sensitive volumes of the detectors, are recorded; at the same points the covariance matrix of the errors on the coordinates generated by the multiple scattering along the tracking path, are calculated; this is the only way in which the deviations of the trajectory due to the multiple scattering can be accounted for.

Once the tentative track has been computed, an estimator of the goodness of the track trajectory can be calculated. For each measured position or distance, the square of the difference between the measured quantity (position or distance to a wire) and the corresponding quantity for the tentative track is calculated; then it is divided by the square of the expected spatial resolution of the detector plus the cumulated spatial variance due to the multiple scattering. The sum of these quantities, for each detector, provides an estimator of the closeness of the tentative track to the measured trajectory; essentially the χ^2 of the track. Finally, usual minimisation algorithm can be used to find the best agreement between the tentative track and the measured trajectory.

The method provides several advantages : (1) the information coming from all the detectors is fitted within the same procedure and exploited at best; (2) in particular, the full spatial information from straw tubes is used, not only the one concerning the zeta coordinate of the track, but also the one in the (ρ,ϕ) plane. The latter could improve, in principle, the resolution on the track momentum; (3) the numerical algorithm accounts for the energy loss of the track, consequently the accuracy in the determination of the track momentum should be improved; (4) finally, the correct account for the errors due to the multiple scattering, which are dominant in the FINUDA case, should provide a statistical significance to the calculated χ^2 of the track.

The disadvantages of such a method are well known: the instability against bad starting point of the fitting (first approximation values of the parameters) and the need of a lot of computing time. Concerning this last point, it is worth mentioning that the computing time can be considerably reduced if the fitting procedure is adopted only to estimate some crucial track parameters, like the θ angle, and not all the parameter at the same time.

A first version of numerical fitting algorithm has already be developed; it is based on GEANE package as tracking package and error transport and, provisionally, on MINUIT as minimisation algorithm. In Fig. 11 a), b) the results for the fitting of a population of tracks of pions of 270 MeV/c, generated in the plane orthogonal to the beam axis is shown; in a) the spline algorithm is used with an error in the zeta coordinate at the first layer of longitudinal straws of σ=1,5 *cm* (the error from the local Pattern Recognition), in b) the numerical fitting has been used with the full information from longitudinal and stereo straws. The starting values of the track parameters for the numerical algorithm are obtained smearing the true values of the parameters with reasonable errors. Fig. 12 a) and b) show the distribution of the distances of the tentative track from the straw tube wires at the first call of the minimisation algorithm and after the minimisation.

The results for the reconstructed momentum using the two different algorithms are similar as expected; the non negligible number of events where the numerical fitting has given a poor result are probably due to problems in the computation of the estimator that should be easily solved. On the other side, the mean value of the distribution of the momentum is correctly centred at 270 MeV/c for the

numerical fitting which accounts for the energy loss of the particle, whereas it is underestimated for the spline fitting method.

It is worth recalling that, when the tracks are in the plane orthogonal to the beam axis, the error in the zeta coordinate of the last point of the track does not affect significantly the resolution on the track momentum. On the contrary, it becomes important for inclined tracks: in Fig. 13 a) and b) the same picture as in Fig. 11 a),b) are shown for a population of pion tracks with θ angle of 60°. The result for the spline algorithm is much worse, whereas the numerical fitting method provides a constant resolution on the momentum.

The work for the development of a numerical track fitting procedure is still in progress.

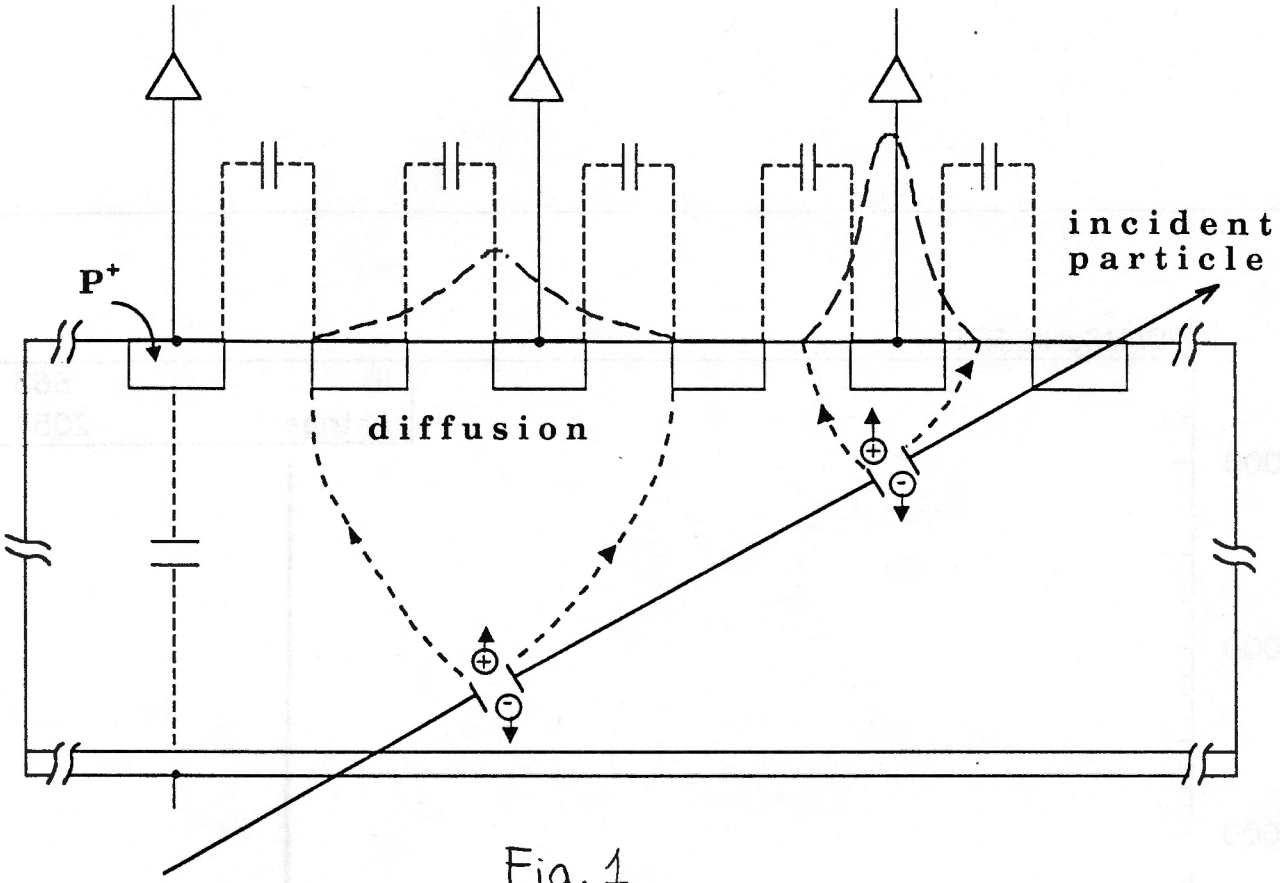

Fig. 1

ϕ side 25 μm pitch

z side 50 μm pitch

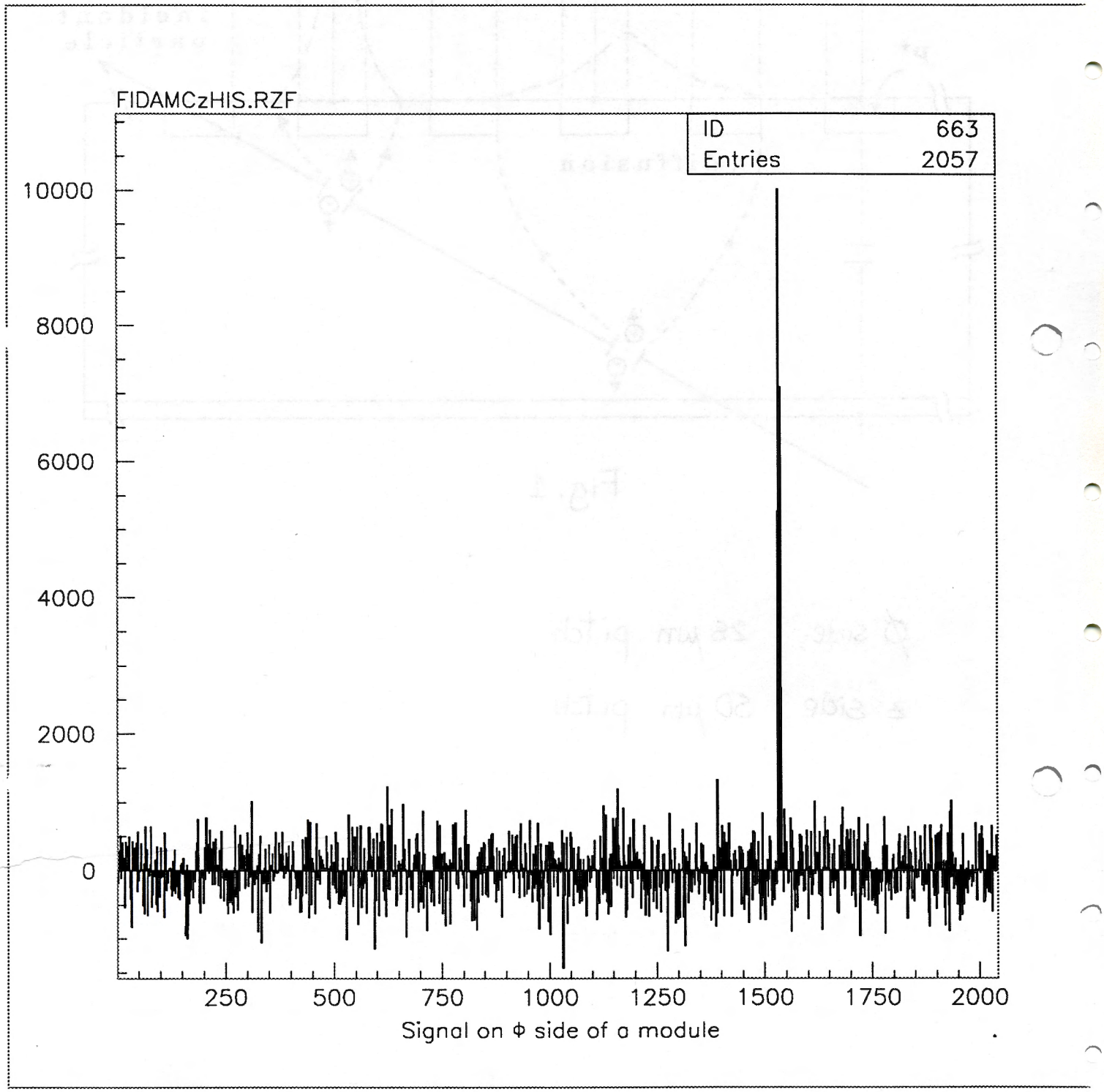
FIDAMCzHIS.RZF
ID 663
Entries 2057
10000
8000
6000
4000
2000
0
250
500
750
1000
1250
1500
1750
2000
Signal on Φ side of a module

Fig. 2

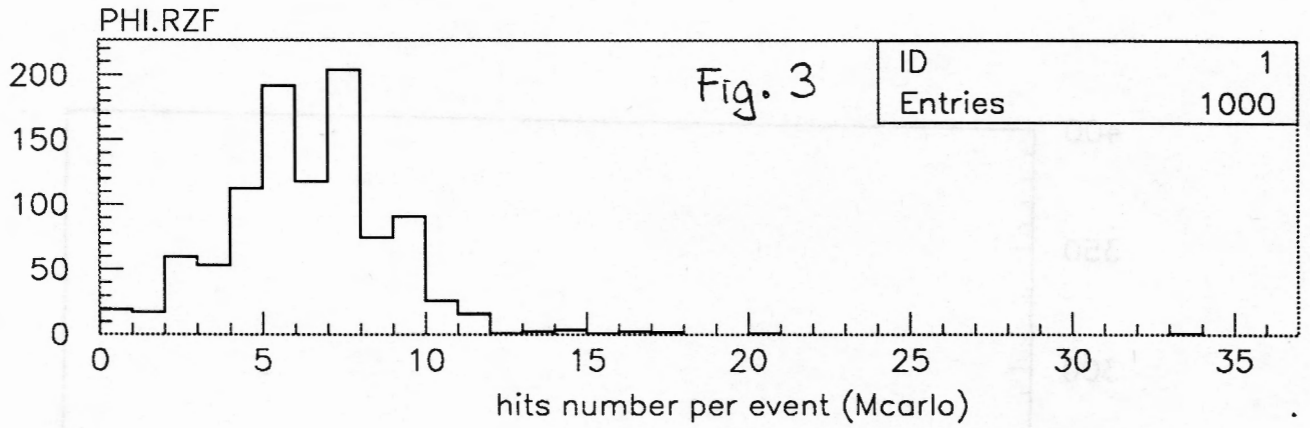
PHI.RZF
Fig. 3
ID 1
Entries 1000
200
150
100
50
0
0 5 10 15 20 25 30 35
hits number per event (Mcarlo)

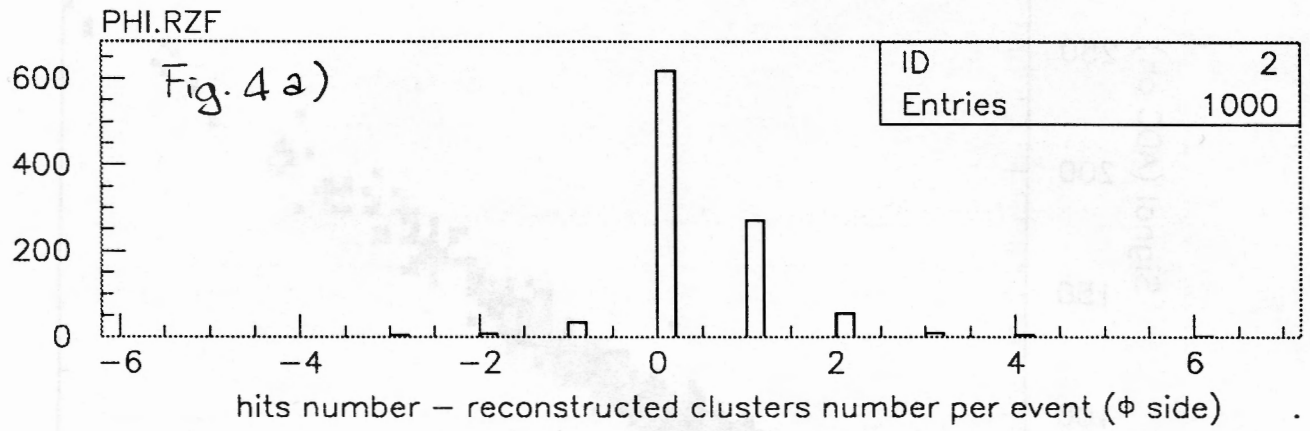
PHI.RZF
Fig. 4 a)
ID 2
Entries 1000
600
400
200
0
−6 −4 −2 0 2 4 6
hits number − reconstructed clusters number per event (ϕ side)

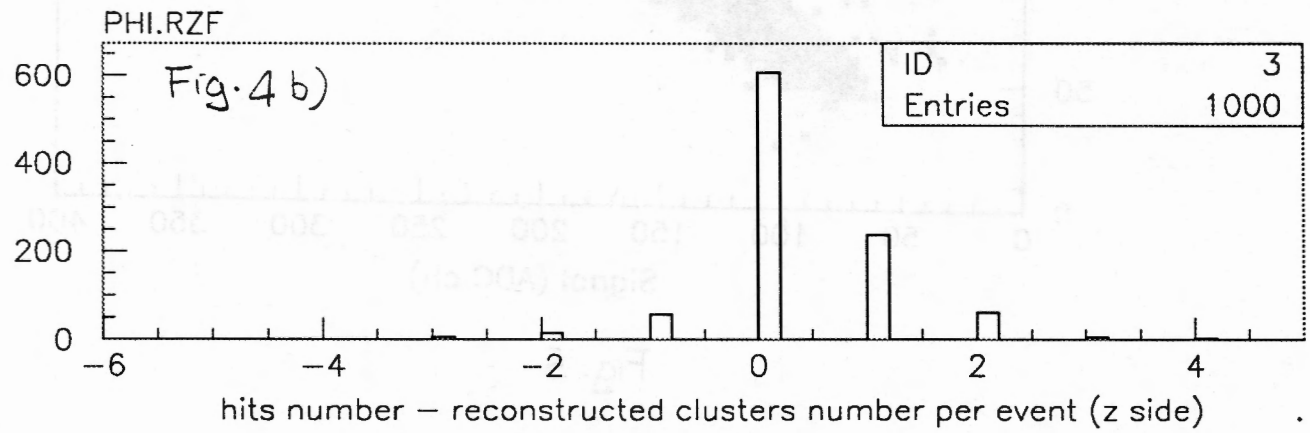
PHI.RZF
Fig. 4 b)
ID 3
Entries 1000
600
400
200
0
−6 −4 −2 0 2 4
hits number − reconstructed clusters number per event (z side)

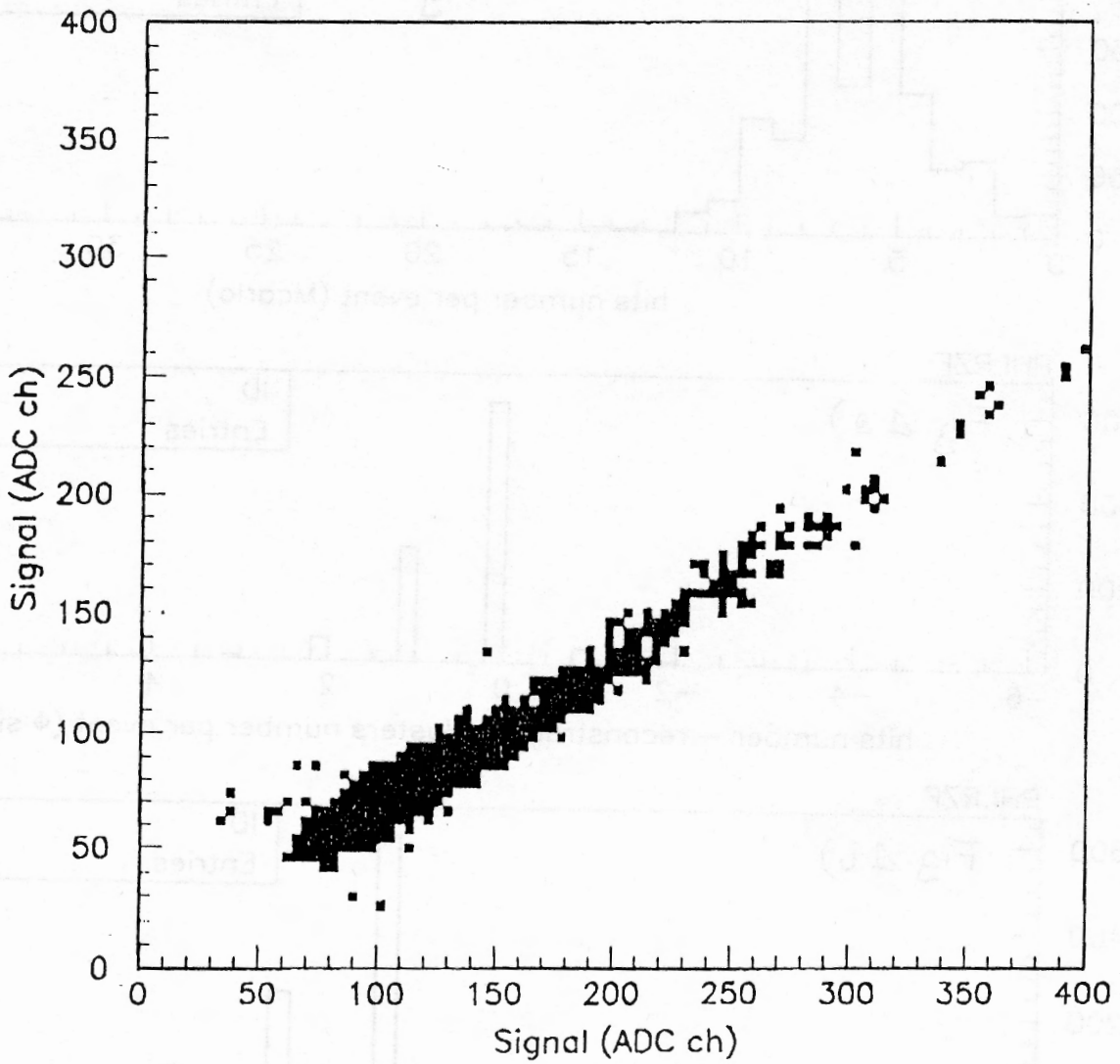

Fig. 5

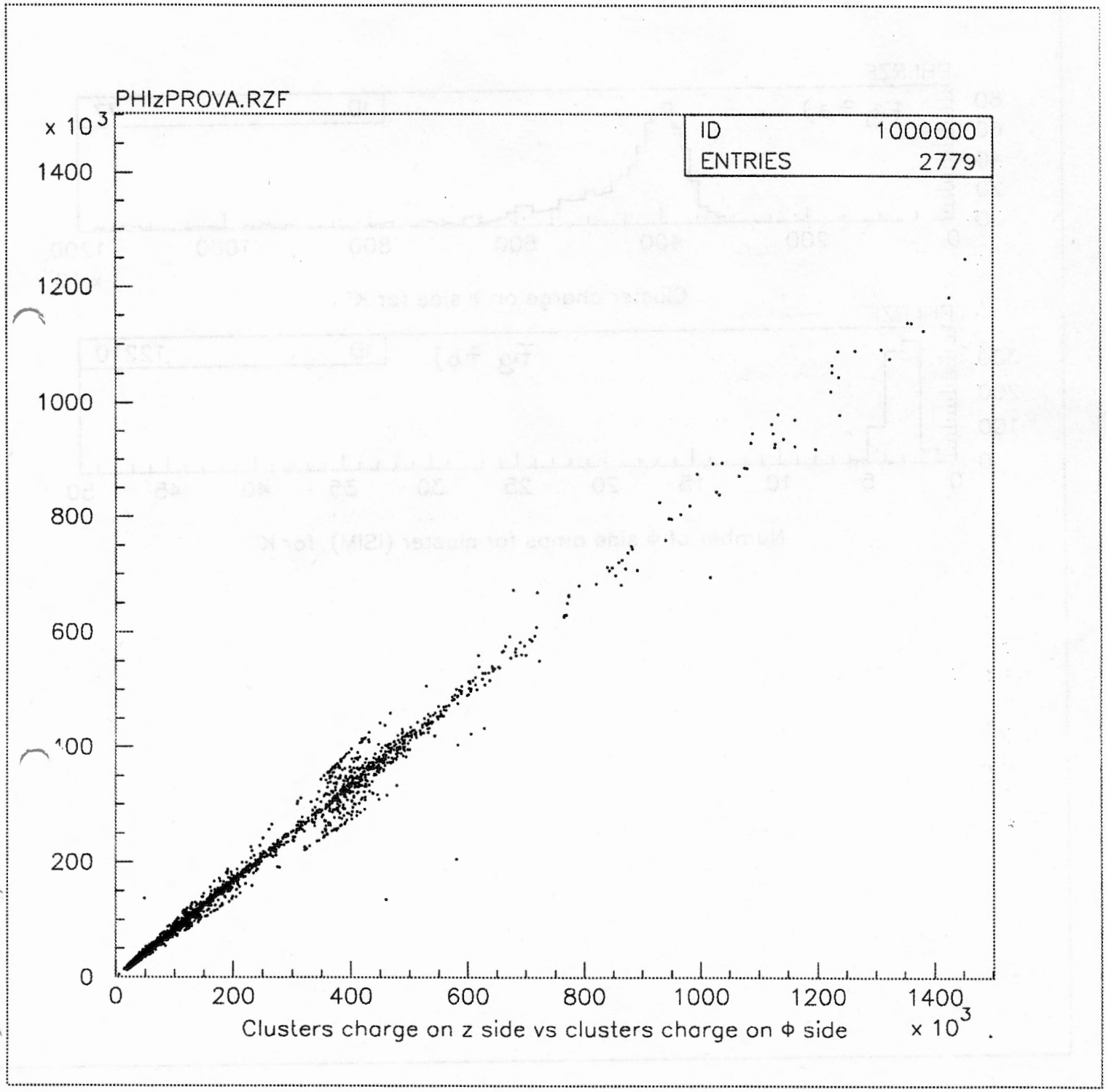
PHIzPROVA.RZF
x 10 3
ID 1000000
ENTRIES 2779
1400
1200
1000
800
600
400
200
0
0
200
400
600
800
1000
1200
1400
Clusters charge on z side vs clusters charge on Φ side
x 10 3

Fig.6

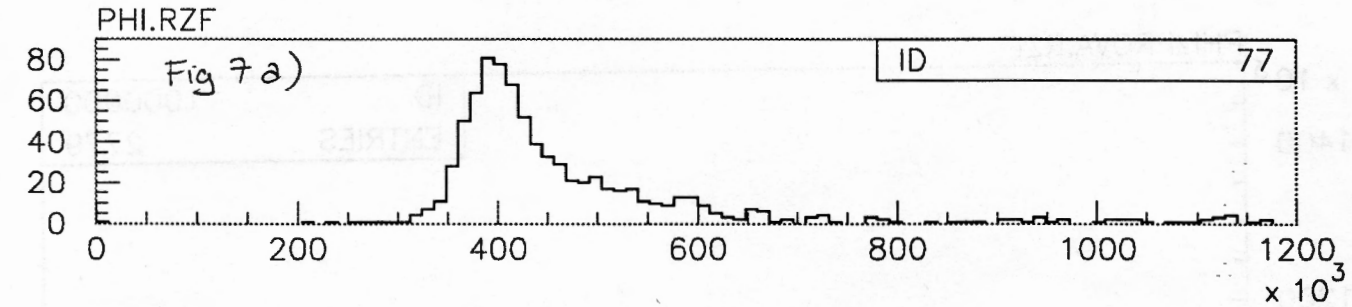

Cluster charge on Φ side for K^-

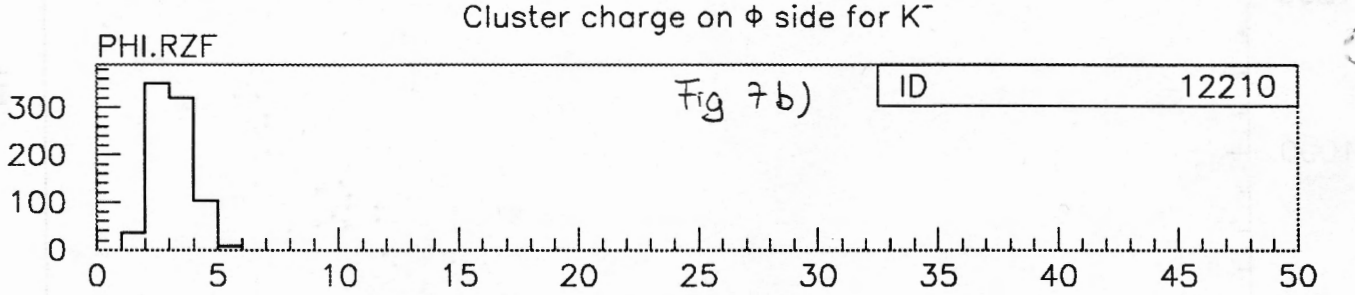

Number of Φ side amps for cluster (ISIM) for K^-

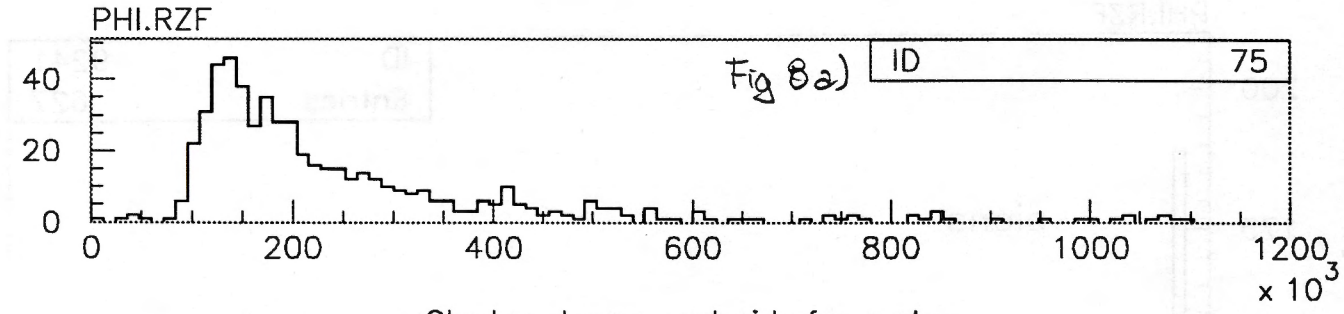

Fig 8a)

Cluster charge on Φ side for proton

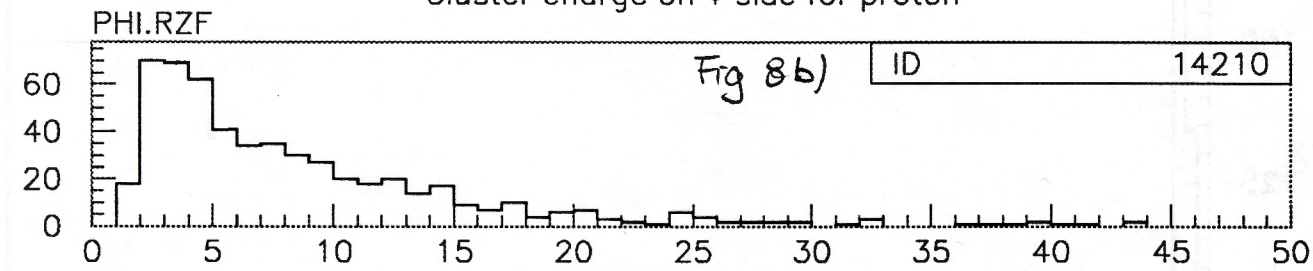

Fig 8b)

Number of Φ side amps for cluster (ISIM) for proton

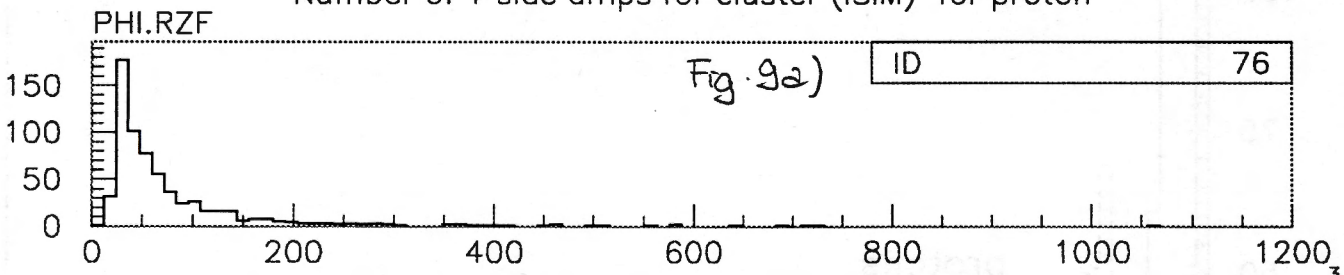

Fig 9a)

Cluster charge on Φ side for π^-

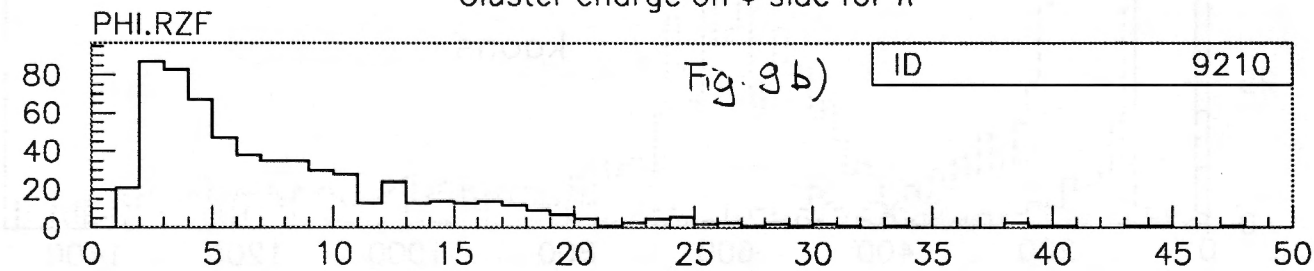

Fig 9b)

Number of Φ side amps for cluster (ISIM) for π^-

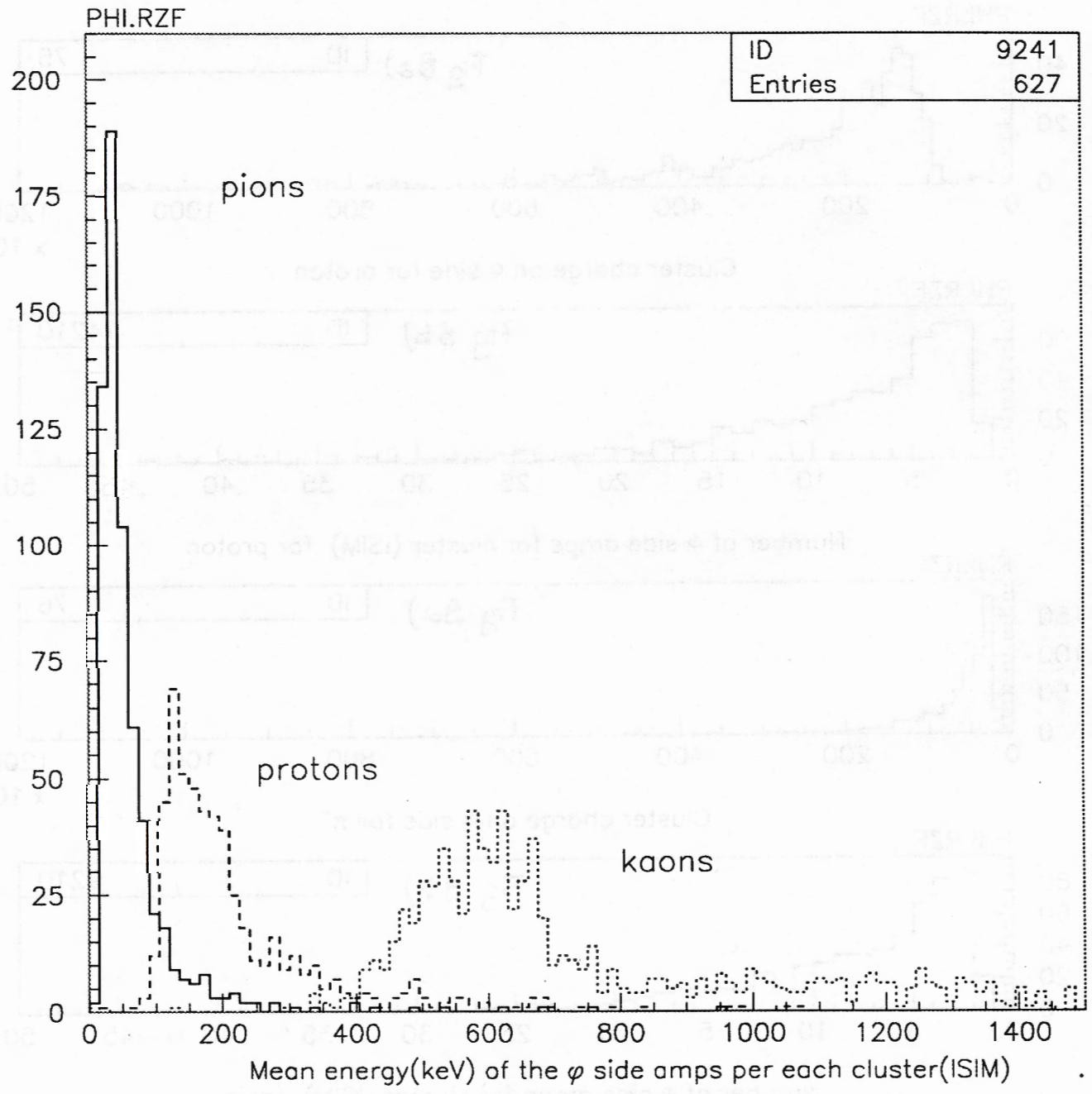
PHI.RZF
ID 9241
Entries 627
pions
protons
kaons
200
175
150
125
100
75
50
25
0
0
200
400
600
800
1000
1200
1400
Mean energy(keV) of the φ side amps per each cluster(ISIM)

Fig 10

Input tracks ϑ = 90 degrees

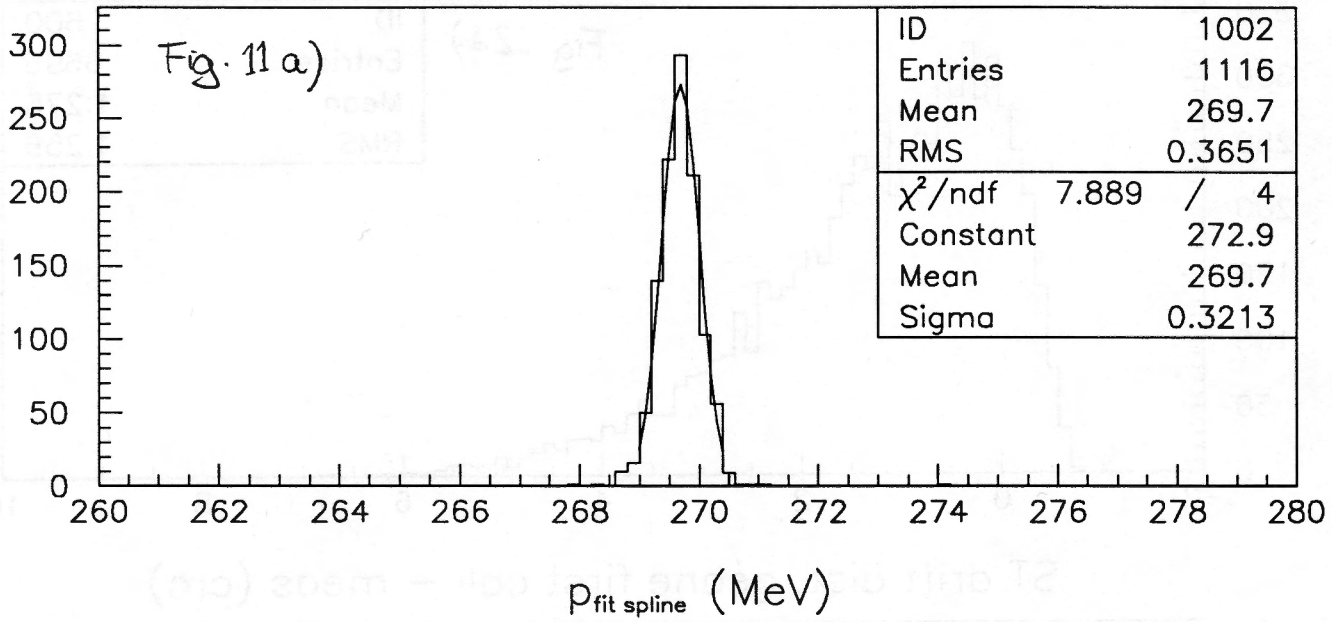

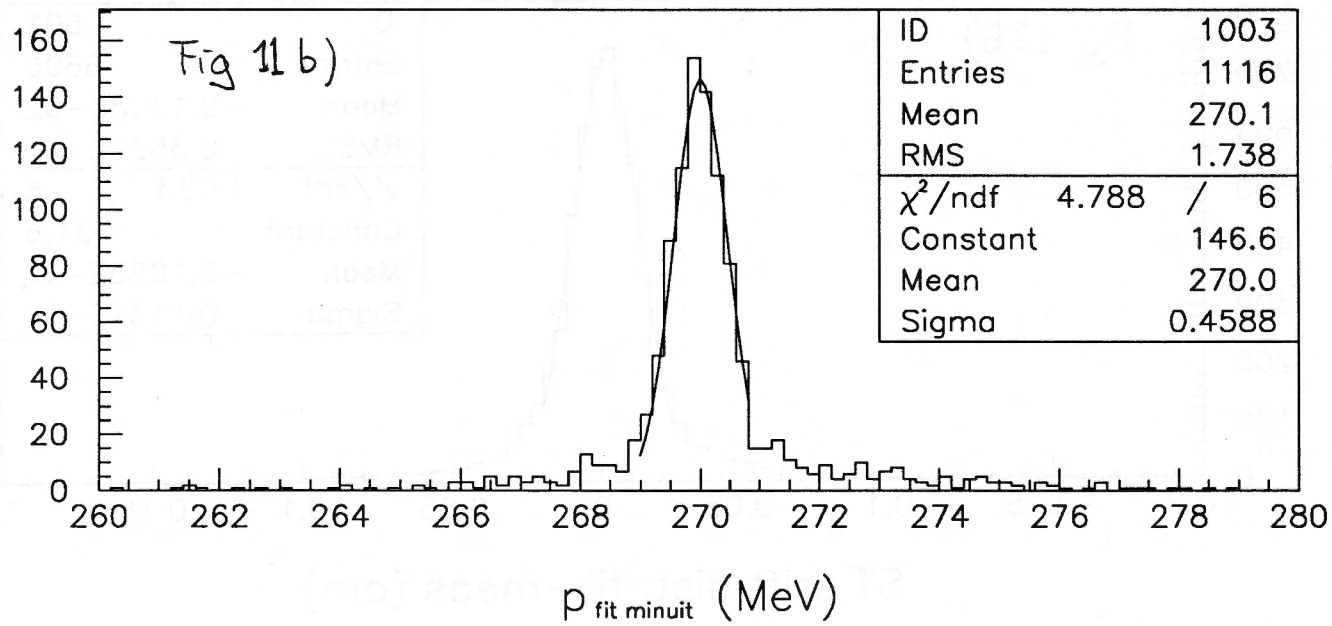

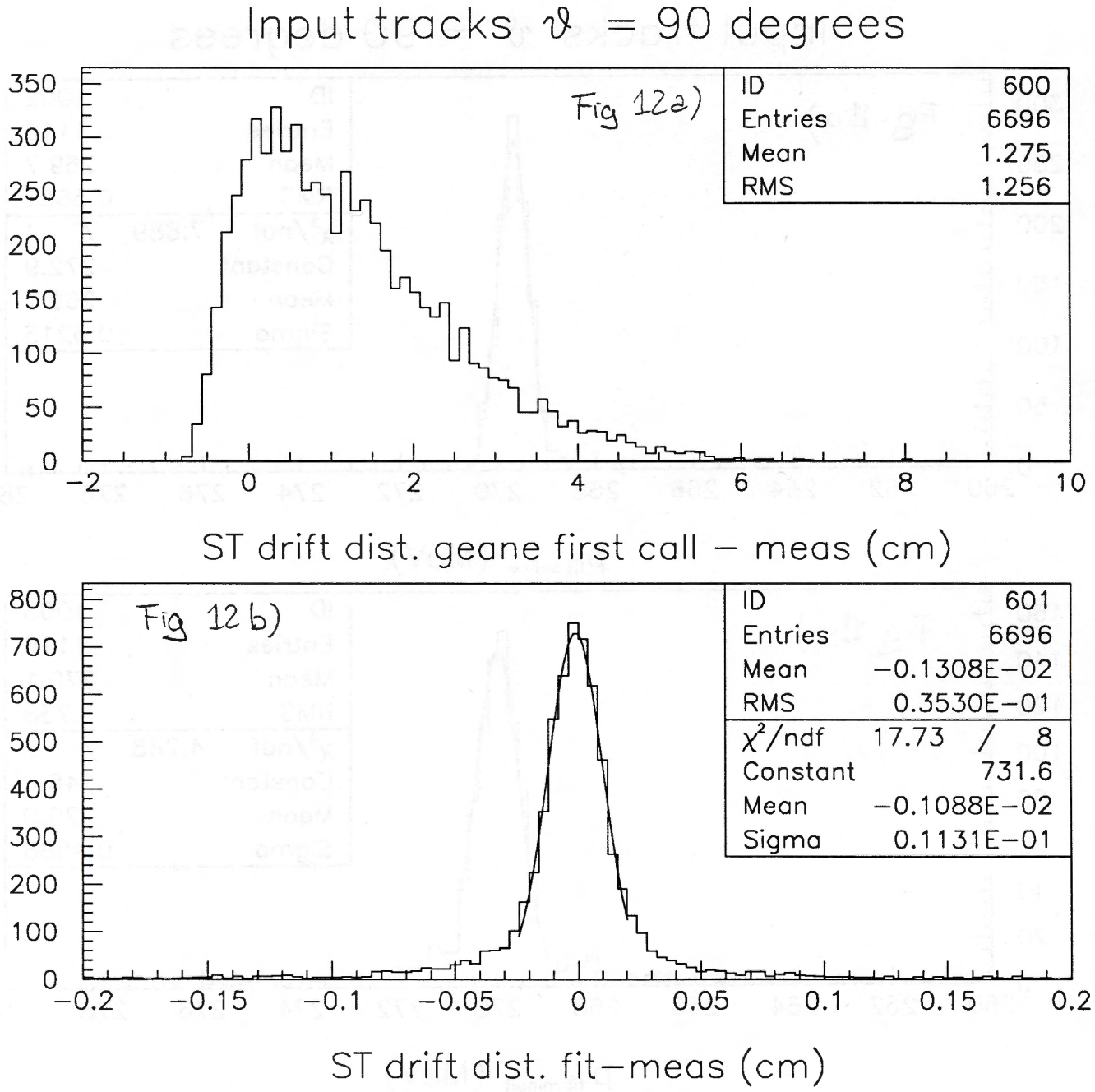
Input tracks ϑ = 90 degrees
Fig 12a)
ID 600
Entries 6696
Mean 1.275
RMS 1.256
ST drift dist. geane first call − meas (cm)
Fig 12 b)
ID 601
Entries 6696
Mean −0.1308E−02
RMS 0.3530E−01
χ^2/ndf 17.73 / 8
Constant 731.6
Mean −0.1088E−02
Sigma 0.1131E−01
ST drift dist. fit−meas (cm)

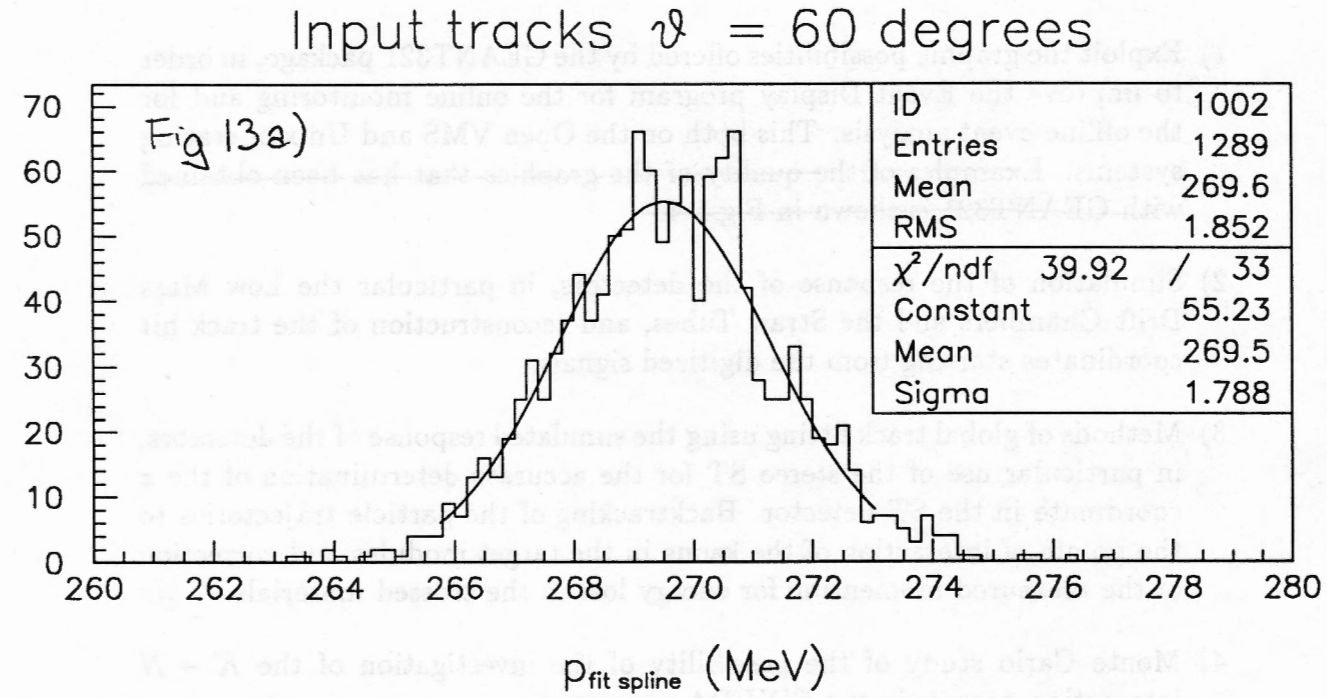
Input tracks ϑ = 60 degrees
Fig 13a)
ID 1002
Entries 1289
Mean 269.6
RMS 1.852
χ^2/ndf 39.92 / 33
Constant 55.23
Mean 269.5
Sigma 1.788
$p_{fit\ spline}$ (MeV)

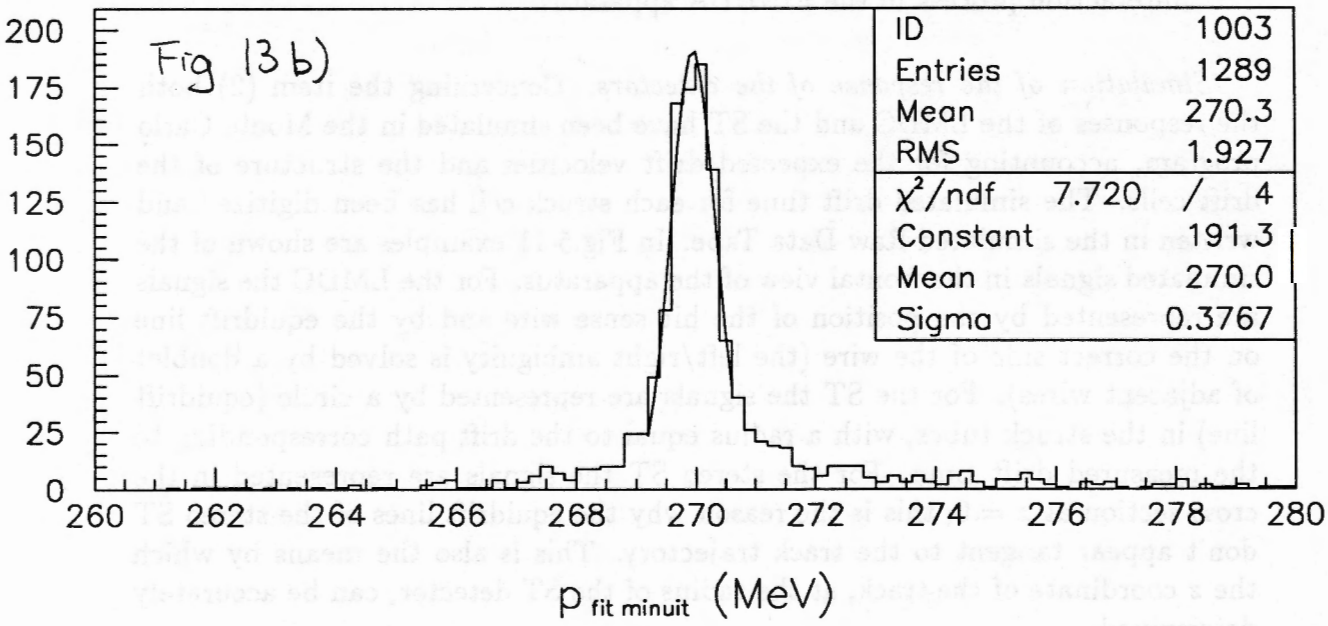
Fig 13b)
ID 1003
Entries 1289
Mean 270.3
RMS 1.927
χ^2/ndf 7.720 / 4
Constant 191.3
Mean 270.0
Sigma 0.3767
$p_{fit\ minuit}$ (MeV)

FINUDA STATUS REPORT October 96 : OFFLINE SOFTWARE

The work on the offline software for the FINUDA experiment has been carried on, in the last months, along the following lines :

1) Exploit the graphic possibilities offered by the GEANT321 package, in order to improve the Event Display program for the online monitoring and for the offline event analysis. This both on the Open VMS and Unix operating systems. ~~Examples of the quality of the graphics that has been obtained with GEANT321 is shown in Fig.1-4.~~

2) Simulation of the response of the detectors, in particular the Low Mass Drift Chambers and the Straw Tubes, and reconstruction of the track hit coordinates starting from the digitized signals.

3) Methods of global track fitting using the simulated response of the detectors, in particular use of the stereo ST for the accurate determination of the z coordinate in the ST detector. Backtracking of the particle trajectories to the points of interaction of the kaons in the target modules and correction of the measured momentum for energy loss in the crossed materials.

4) Monte Carlo study of the possibility of the investigation of the $K - N$ interaction process in the FINUDA apparatus.

Simulation of the response of the detectors. Concerning the item (2) both the responses of the LMDC and the ST have been simulated in the Monte Carlo program, accounting for the expected drift velocities and the structure of the drift cells. The simulated drift time for each struck cell has been digitized and written in the simulated Raw Data Tape. In Fig.5-11 examples are shown of the simulated signals in the frontal view of the apparatus. For the LMDC the signals are represented by the position of the hit sense wire and by the equidrift line on the correct side of the wire (the left/right ambiguity is solved by a doublet of adjacent wires). For the ST the signals are represented by a circle (equidrift line) in the struck tubes, with a radius equal to the drift path corresponding to the measured drift time. For the stereo ST the signals are represented in the cross section at $z = 0$; this is the reason why the equidrift lines of the stereo ST don't appear tangent to the track trajectory. This is also the means by which the z coordinate of the track, at the radius of the ST detector, can be accurately determined.

For the ISIM/OSIM microstrip detectors the simulation of the response and the methods of local Pattern Recognition have already be studied and have still to be inserted in the General Reconstruction Program.

Track fitting methods. The item (3) is of the greatest importance, since the momentum resolution of the apparatus depends on the ability in exploiting the spatial information coming from the different detectors. We have investigated two methods.

A numerical integration of the track trajectory based on Runge-Kutta formulas and accounting for the energy loss in the tracking volume (GEANE package), with minimization (MINUIT program) of the square differences between measured drift radii around the LMDC and ST wires and the calculated distances between the track trajectory and the wires. This numerical method has some advantages :

(1) it fully exploits the spatial information provided by the stereo ST which is most in the x, y plane,

(2) it accounts for the energy loss in the tracking volume, allowing the track momentum to be determined more accurately. The main disadvantage is the computing time needed; the algorithm that has been currently implemented gives good results, but requires tens of seconds per track on a AlphaVax 250. This amount of computing time is evidently too large and studies are in progress to reduce it to acceptable values.

A second iterative technique has been implemented. It is based on the iteration of two procedures : a fitting (with a spline method) of the spatial information coming from the OSIM microstrip, the LMDC and the longitudinal ST and the correction of the z coordinate on the longitudinal ST by fitting the track extrapolation on the stereo ST. This method has been found rather fast and efficient and some results are shown in the following.

Schematically the iterative fit procedure goes on along the following steps.

(1) A first fit of the track trajectory is done using the coordinates of the OSIM point, the first approximation of the points of crossing of the track on the sense wire planes in the LMDC and the x, y coordinates of the wire of the first longitudinal ST hit by the track. An estimation of the corresponding z coordinate is obtained by the ST local Pattern Recognition with a resolution of 2-3 cm. From this first fit an evaluation of the incident angle of the track on the LMDC and on the ST is obtained.

(2) The left/right ambiguity on the first longitudinal ST hit by the track is solved using the multiple hits of the track on the longitudinal tubes or, in case of single hit, by comparing the χ^2 of the fit on stereo ST in both the left/right hypotheses.

(3) The estimated crossing points of the track on the wire plane of the chambers is corrected, accounting for the track incidence angle.

(4) The track trajectory is extrapolated with a helix in the stereo ST volume and a χ^2 is evaluated for the differences between the measured drift radii and the computed distances between the track trajectory and the wires. This χ^2 is minimized varying the value of the z coordinate of the extrapolated track at the radius of the longitudinal ST.

(5) A spline fitting is performed with the improved values of the coordinates of the track hits on the different detectors

(6) Points (3), (4), and (5) are repeated iteratively up to convergence.

Backtracking towards the vertex. The fitting procedure determines the average momentum of the track in the tracking volume and its direction at the OSIM point. Using the geometrical and physical information about the structure of the apparatus described in the FINUDA Monte Carlo program and the GEANE package, the trajectory is backtracked towards the target module where the vertex was found. The procedure allows the recognition of whether the track is either a "forward" or a "backward" one and allows the correction of the momentum of the track for energy loss in the materials and of the track direction for curvature. At the end of the procedure the best estimate of the track momentum is obtained, together with some estimators of the track quality (distance to the vertex, angle of incidence on the target, amount of target material crossed).

Results of fitting and backtracking procedures. A population of tracks of π^- of 270 MeV/c momentum, starting from points inside the target modules, has been simulated by the FINUDA simulation program, with the following localization errors on the different detectors : (1) 50 μm for the OSIM modules, (2) 150 μm average error across the drift cell of the chambers and 1.5 - 2.0 cm along the z coordinate, (3) 100 μm along the radial direction for the longitudinal and stereo ST. In Fig.12-21 the results of the momentum reconstruction obtained by the procedures illustrated above are shown.

Fig.12 shows the raw reconstructed spectrum is shown; it has been obtained in the hypothesis of using only a raw evaluation of the z coordinate on the longitudinal ST (2.0 cm) from the ST local Pattern Recognition. The two peaks corresponding to the "forward" and "backward" tracks are seen with rough resolution. Fig.13 shows the same spectrum with the z coordinate at longitudinal ST determined by means of the fitting of the track extrapolation on the stereo ST. The momentum resolution appears clearly improved; in particular, in Fig.14, the difference between the "true" Monte Carlo value of the z coordinate and its reconstructed value shows that the latter can be determined with a resolution of 600 μm.

Fig.15 shows the momentum spectrum when the correction for energy loss in the material crossed along the particle path between the target and OSIM is applied. The peak at lower energy, produced by "backward" pions, disappears under the peak of the "forward" ones. In Fig.16 the additional correction for target crossing is applied and the peak shrinks furtherly. The resulting resolution for the full population of tracks ("forward" plus "backward") is seen in Fig.17 and amounts to 0.33% FWHM.

Obviously the momentum resolution must be smaller for the "forward" tracks, since the "backward" ones crosses a larger amount of material and their momen-

tum is spread by the fluctuation in energy loss, that cannot be corrected for. Indeed, in Fig.18, the peak for "forward" tracks shows a momentum resolution of 0.28% FWHM; the peak of the "backward" ones is shown in Fig.19; their momentum resolution is not less than 0.47%, which is not enough for high resolution hypernuclear spectroscopy, but can be enough for the recognition of the hypernuclear ground state in studying the hypernuclear decays.

Moreover, with further cuts on track quality, the momentum resolution for "forward" tracks can be improved: for example in Fig.20-22 the peak for "forward" tracks is shown with successive cuts on the track incidence angle on the target: 80, 60 and 30 degrees. The ultimate momentum resolution for "forward" tracks can be of the order of 0.26% FWHM.

The iterative algorithm for track fitting in the FINUDA apparatus and of backtraking towards the vertex looks efficient and very economic too: the average time for track fitting and backtraking for one track results of about 220 ms per track on a VAXstation 4000/90.

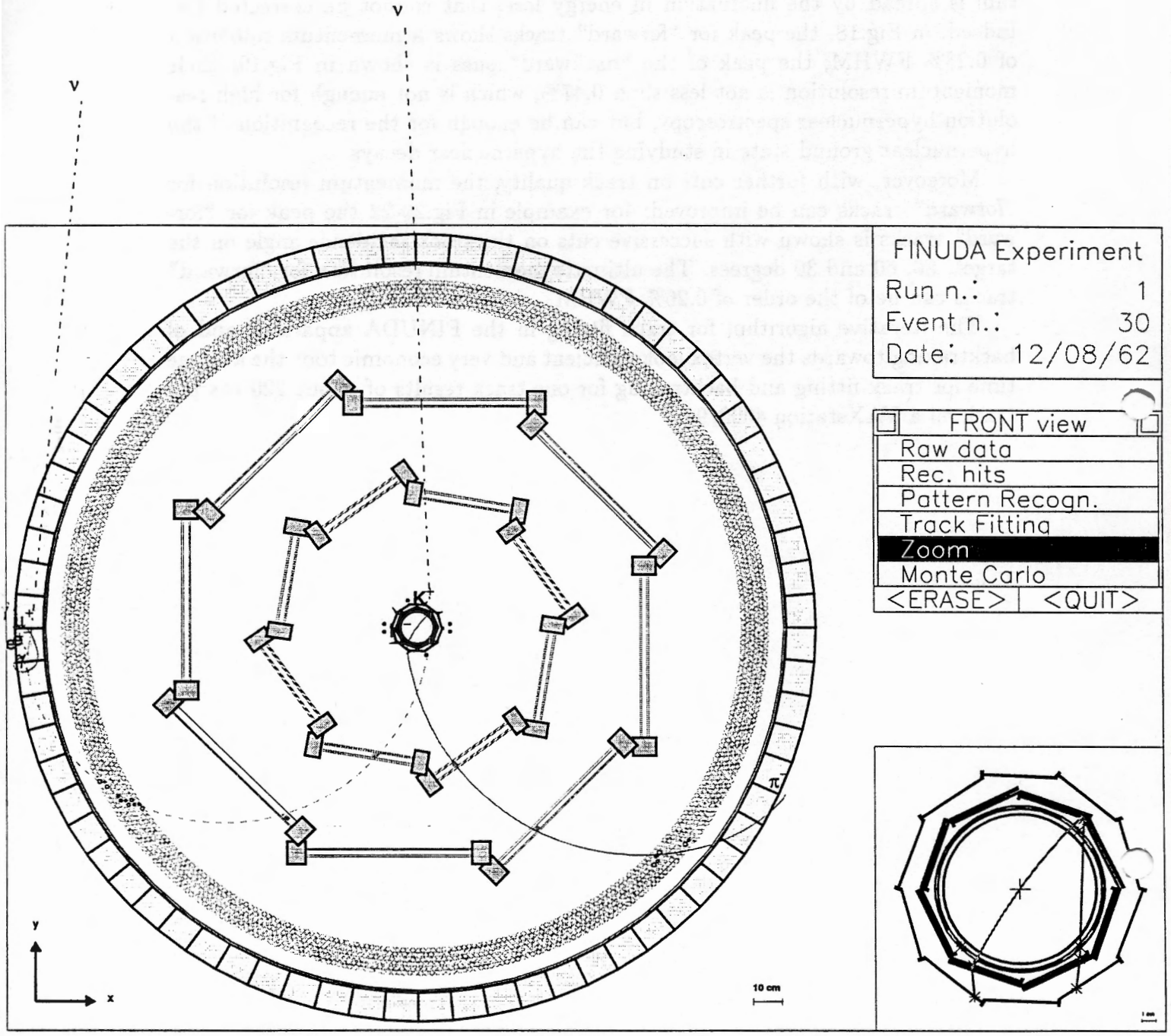
ν
ν
K+
π
y
x
10 cm
FINUDA Experiment
Run n.: 1
Event n.: 30
Date: 12/08/62
FRONT view
Raw data
Rec. hits
Pattern Recogn.
Track Fitting
Zoom
Monte Carlo
<ERASE>
<QUIT>
1 m

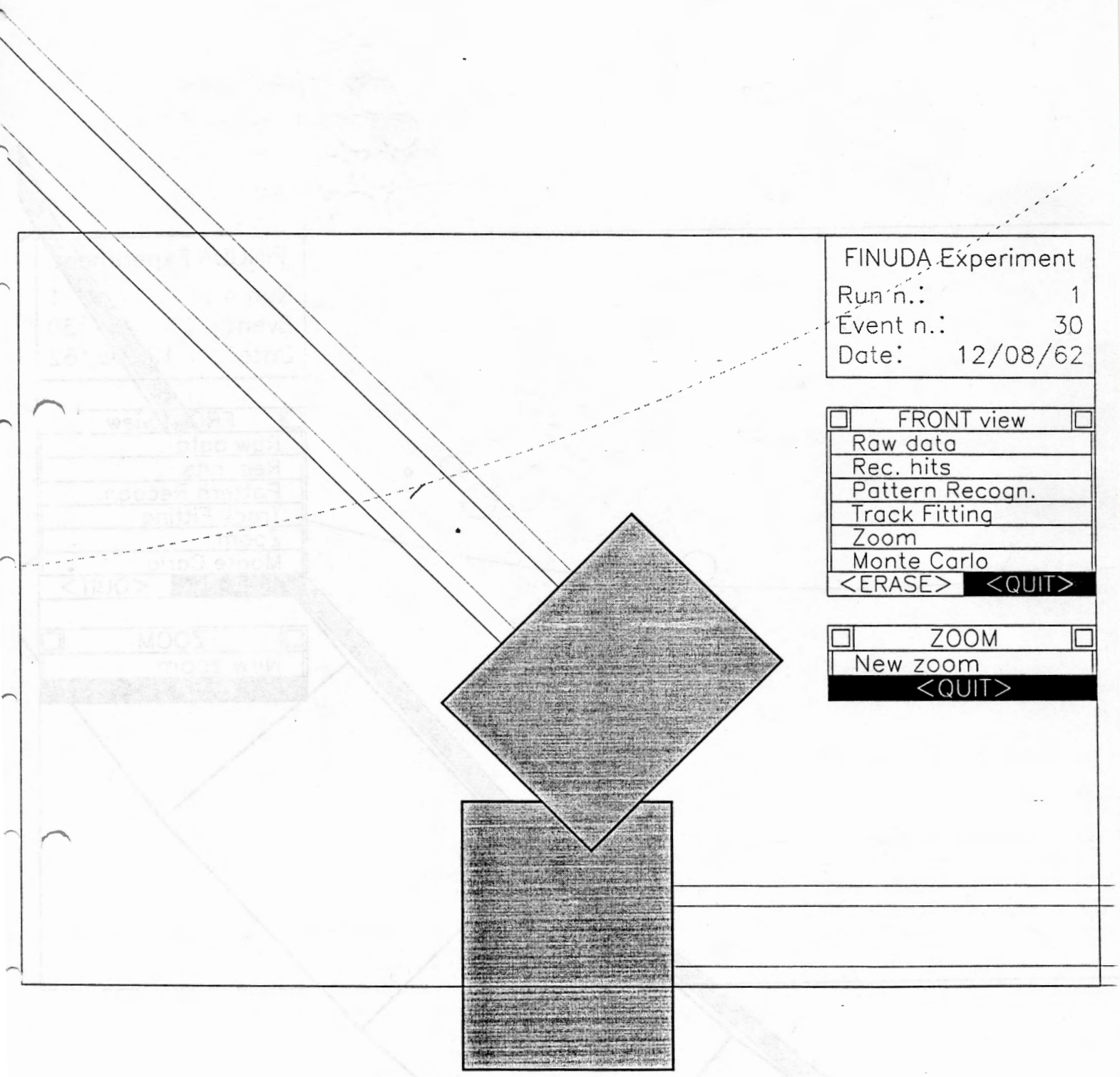
FINUDA Experiment
Run n.: 1
Event n.: 30
Date: 12/08/62
FRONT view
Raw data
Rec. hits
Pattern Recogn.
Track Fitting
Zoom
Monte Carlo
<ERASE>
<QUIT>
ZOOM
New zoom
<QUIT>

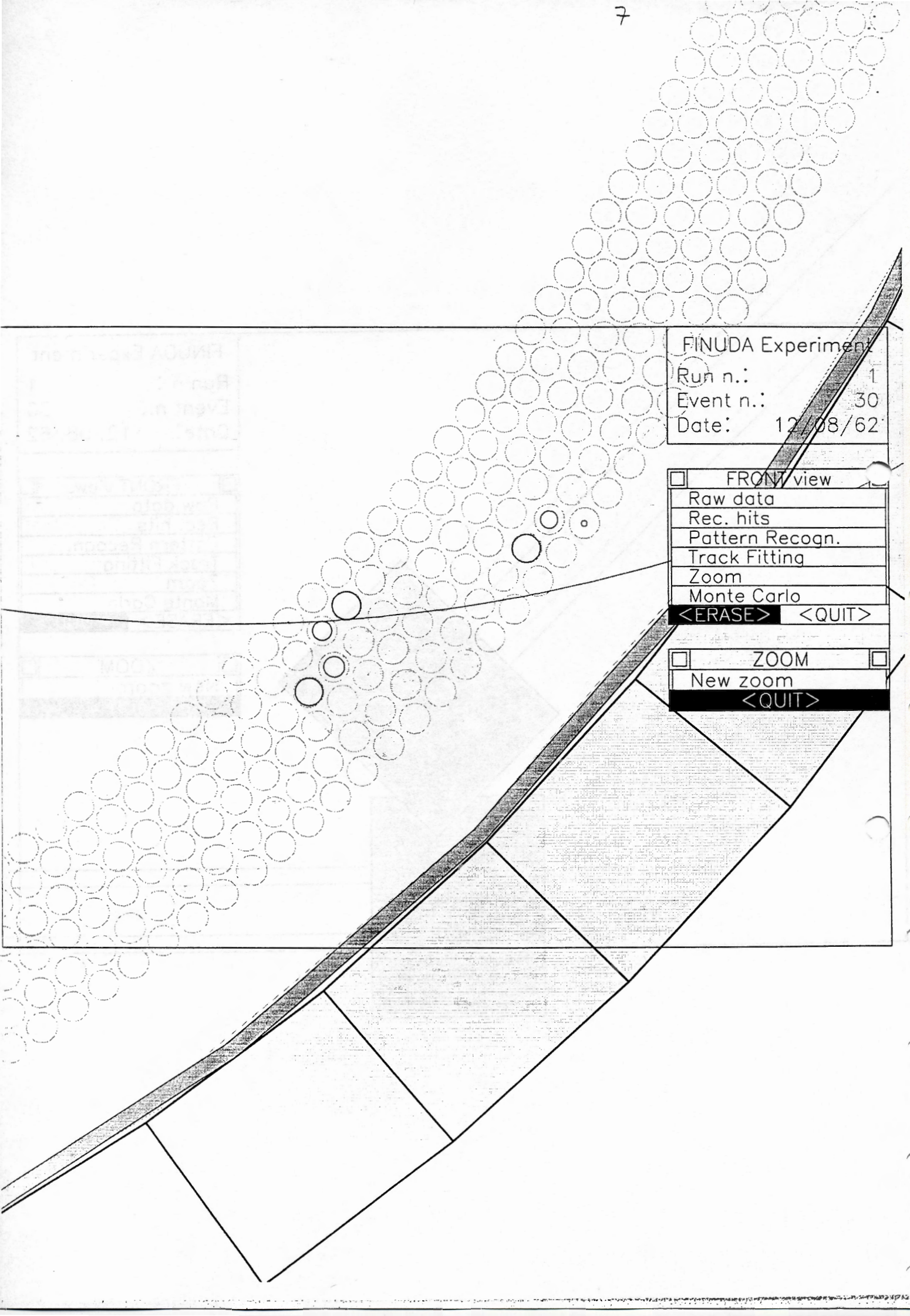
FINUDA Experiment
Run n.: 1
Event n.: 30
Date: 12/08/62
FRONT view
Raw data
Rec. hits
Pattern Recogn.
Track Fitting
Zoom
Monte Carlo
<ERASE>
<QUIT>
ZOOM
New zoom
<QUIT>

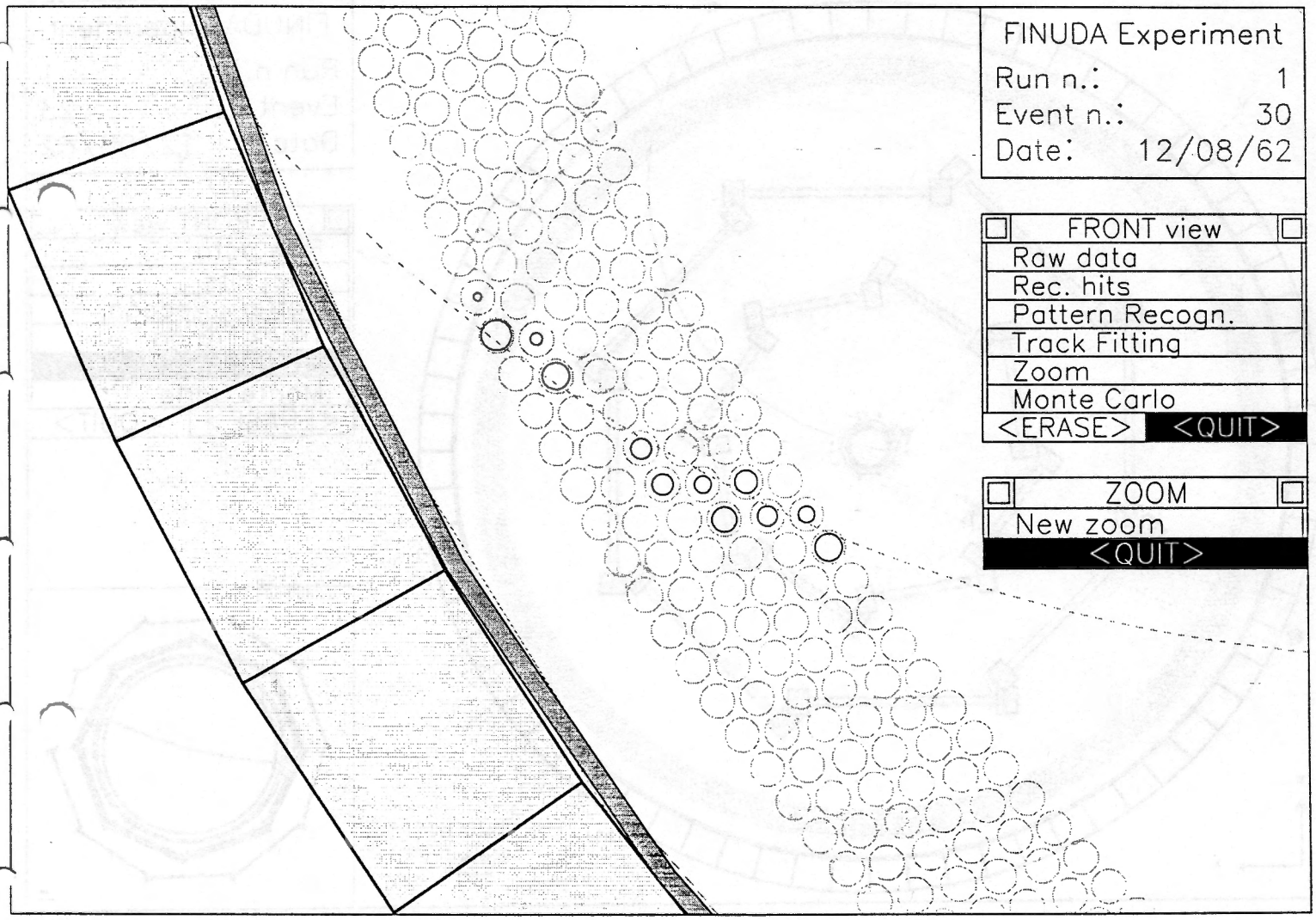
FINUDA Experiment
Run n.: 1
Event n.: 30
Date: 12/08/62
FRONT view
Raw data
Rec. hits
Pattern Recogn.
Track Fitting
Zoom
Monte Carlo
<ERASE>
<QUIT>
ZOOM
New zoom
<QUIT>

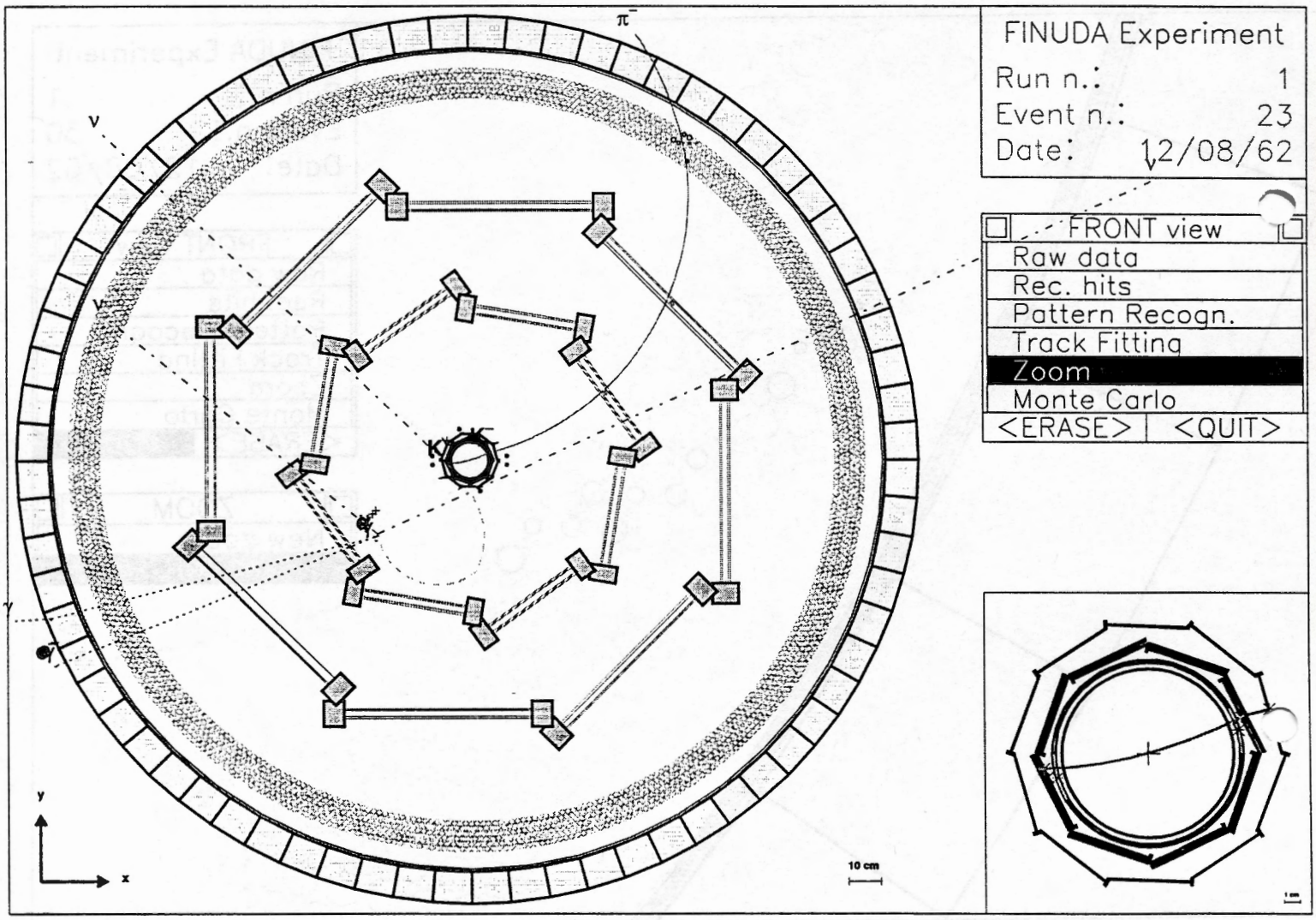
FINUDA Experiment
Run n.: 1
Event n.: 23
Date: 12/08/62
FRONT view
Raw data
Rec. hits
Pattern Recogn.
Track Fitting
Zoom
Monte Carlo
<ERASE>
<QUIT>
π⁻
ν
10 cm
y
x

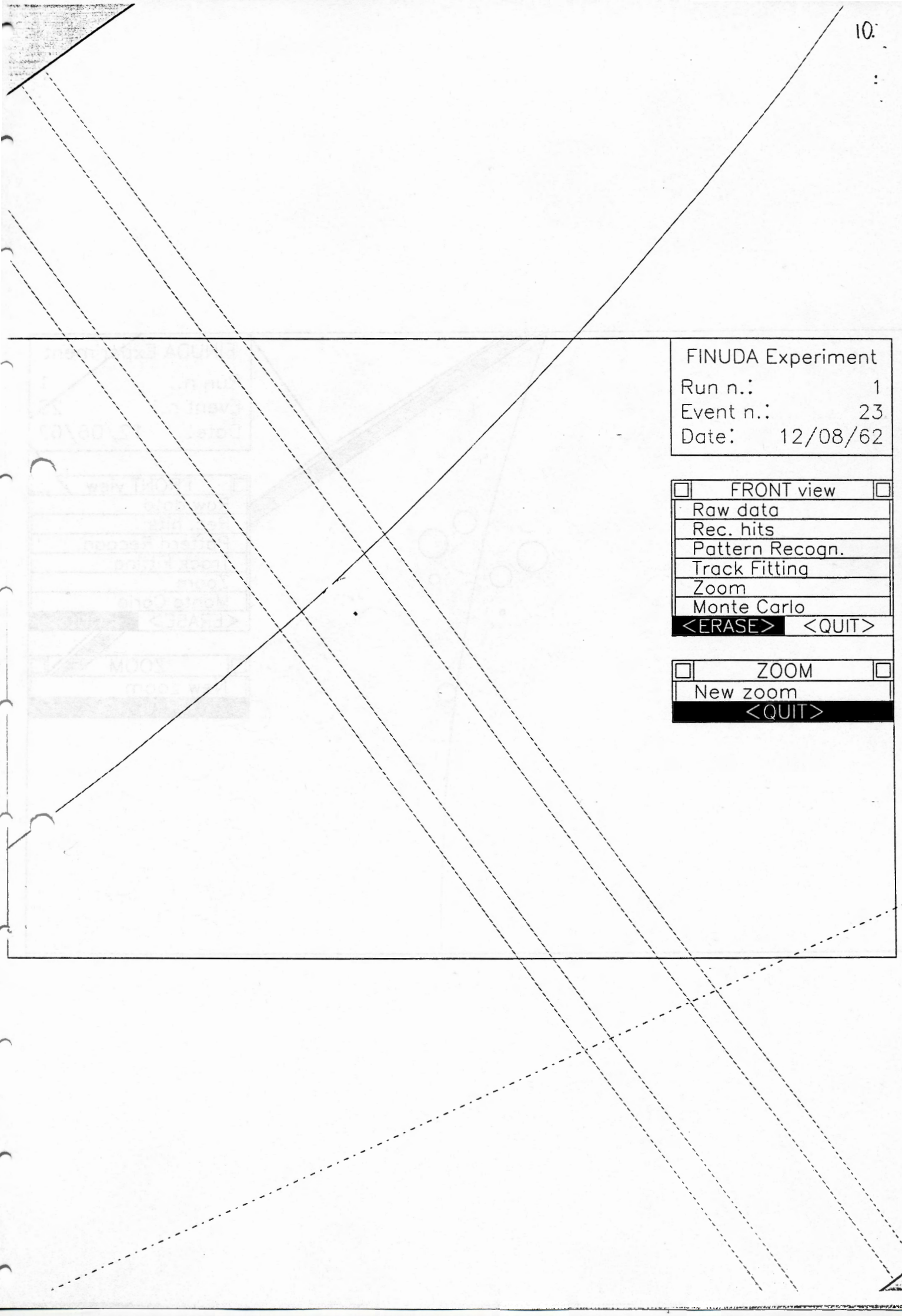
FINUDA Experiment
Run n.: 1
Event n.: 23
Date: 12/08/62
FRONT view
Raw data
Rec. hits
Pattern Recogn.
Track Fitting
Zoom
Monte Carlo
<ERASE>
<QUIT>
ZOOM
New zoom
<QUIT>

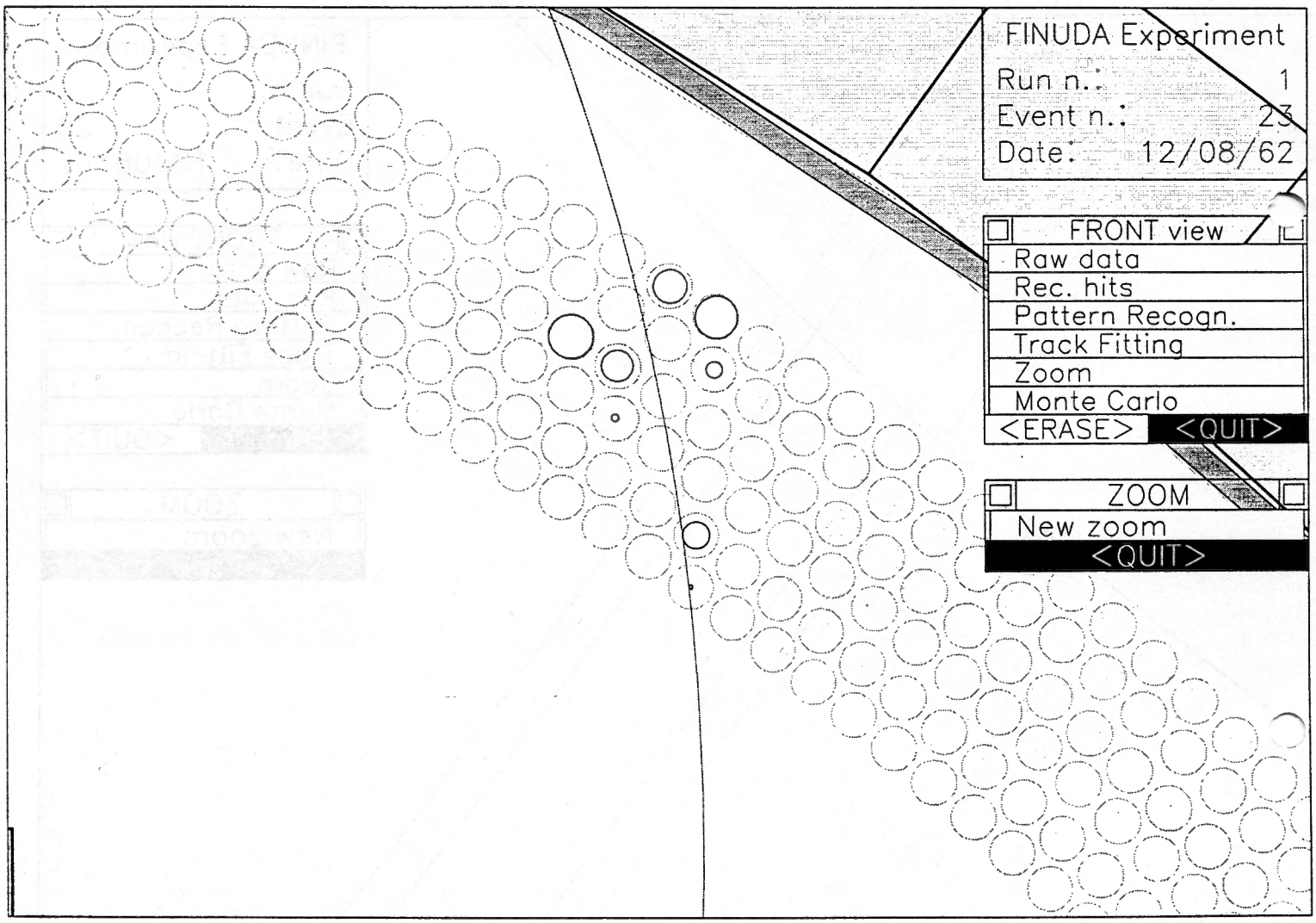
FINUDA Experiment
Run n.: 1
Event n.: 23
Date: 12/08/62
FRONT view
Raw data
Rec. hits
Pattern Recogn.
Track Fitting
Zoom
Monte Carlo
<ERASE>
<QUIT>
ZOOM
New zoom
<QUIT>

22/09/96 16.02

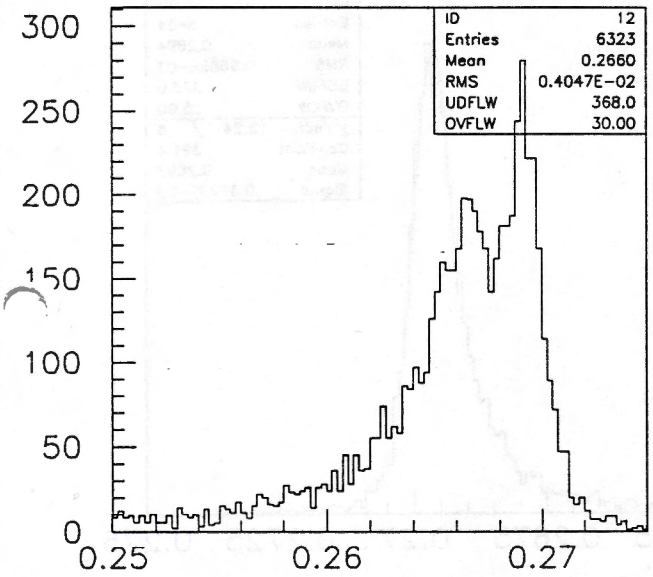

P not corr. σ_z straw 2.0 cm

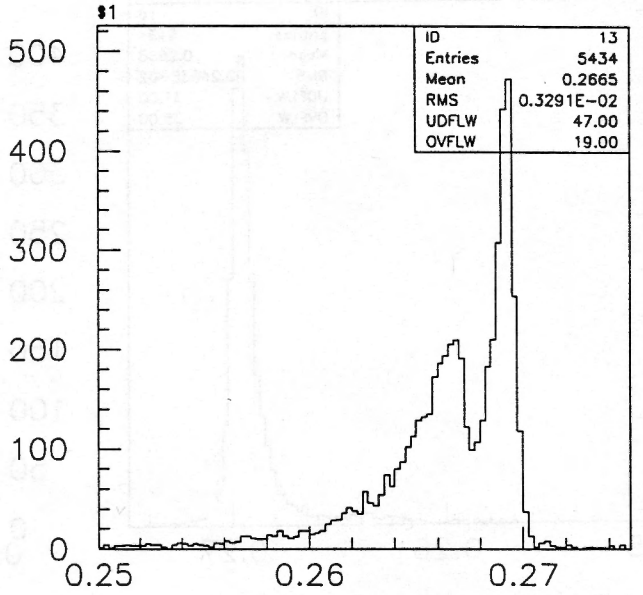

P not corr. σ_z straw from stereo

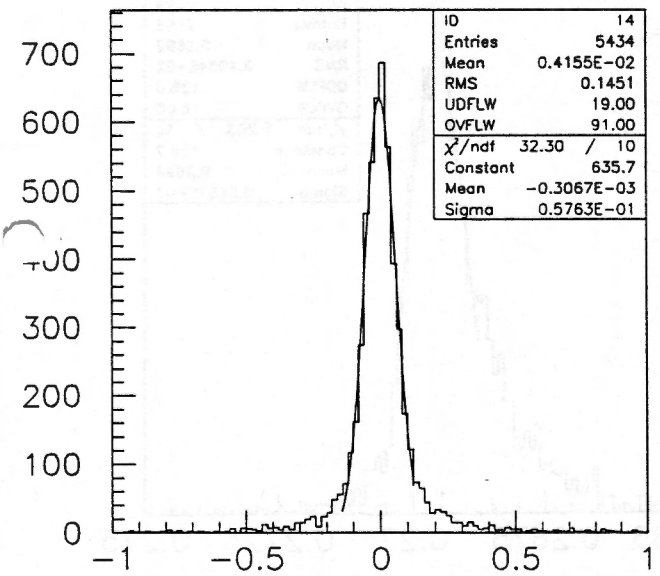

(Zstraw mc)−(Zstraw rec.)

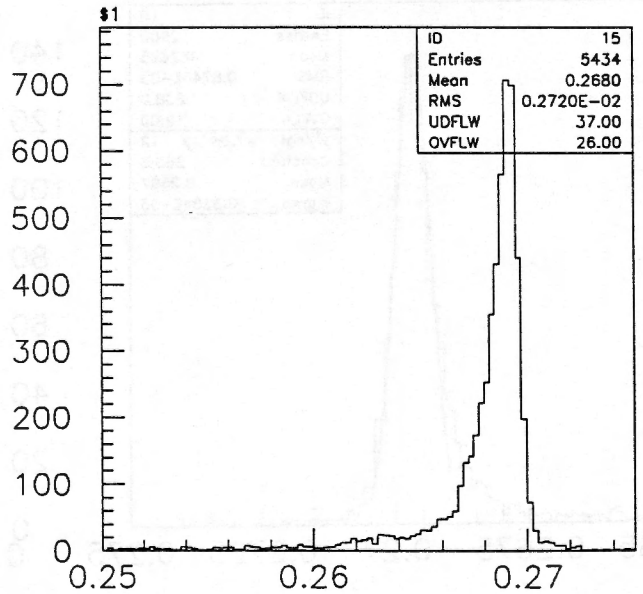

P corr. for backt

22/09/96 16.03

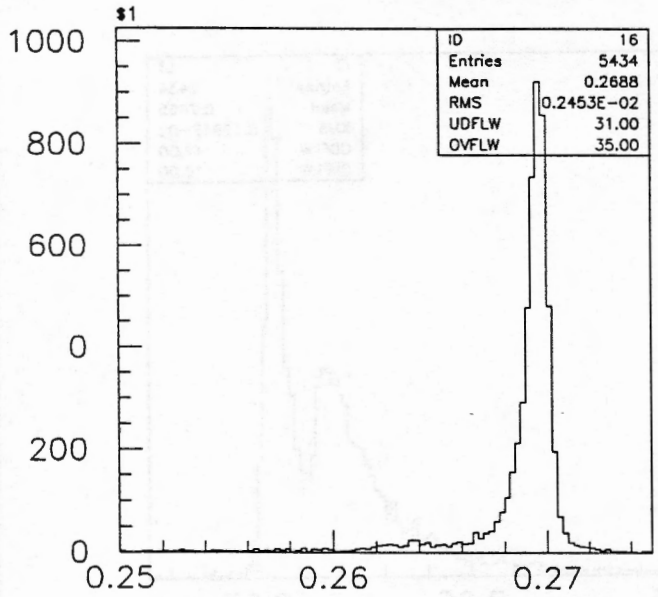

P corr. for backt and tcross

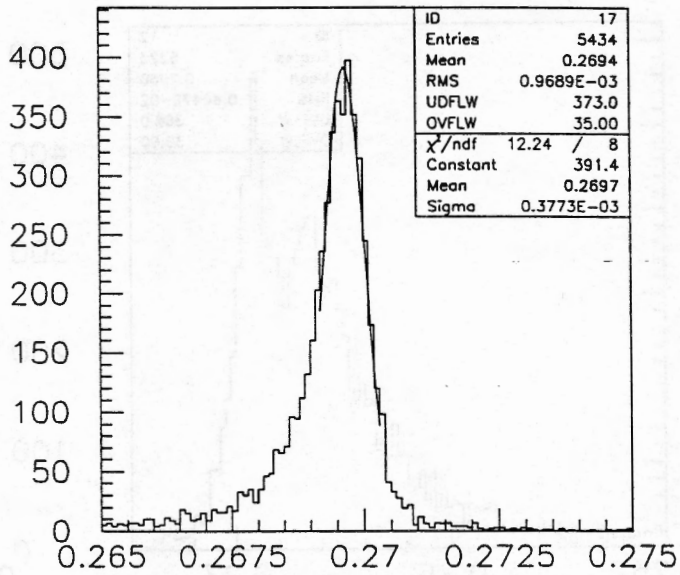

P corr. for backt and tcross

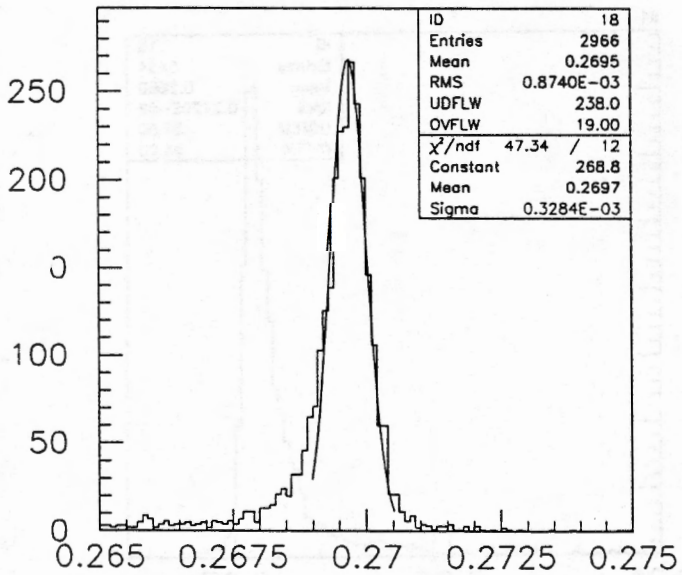

P corr. for backt and tcross – forward

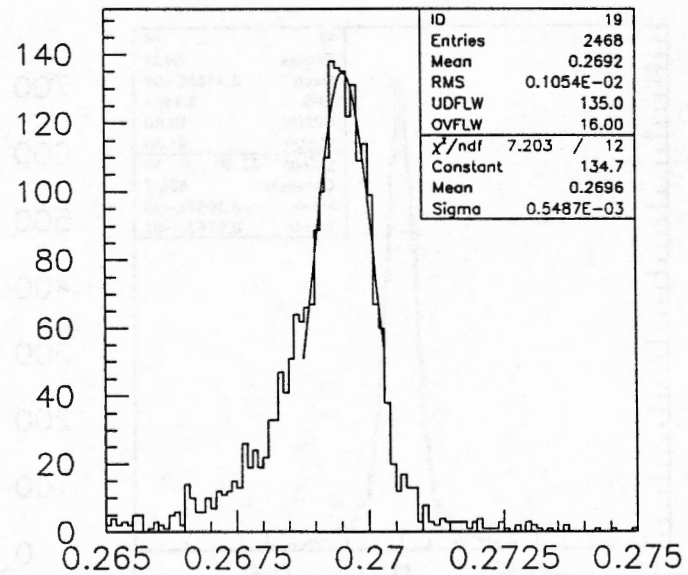

P corr. for backt and tcross – backward

22/09/96 16.03

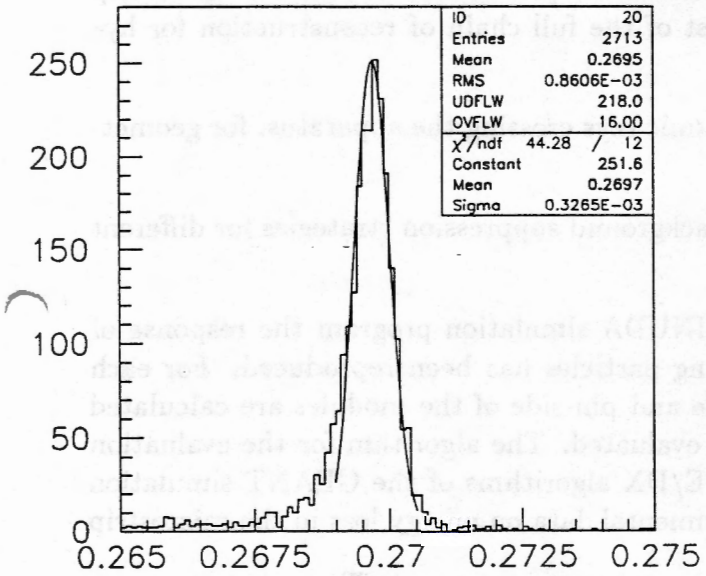

P corrected – forward – angle<80°

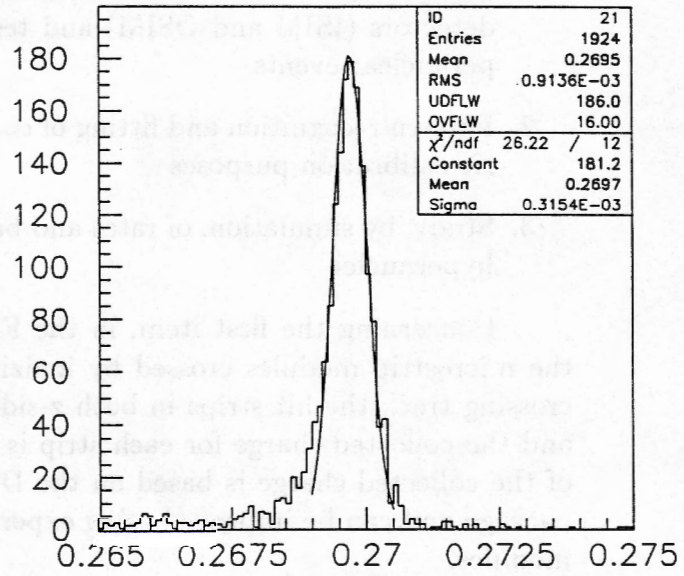

P corrected – forward – angle<60°

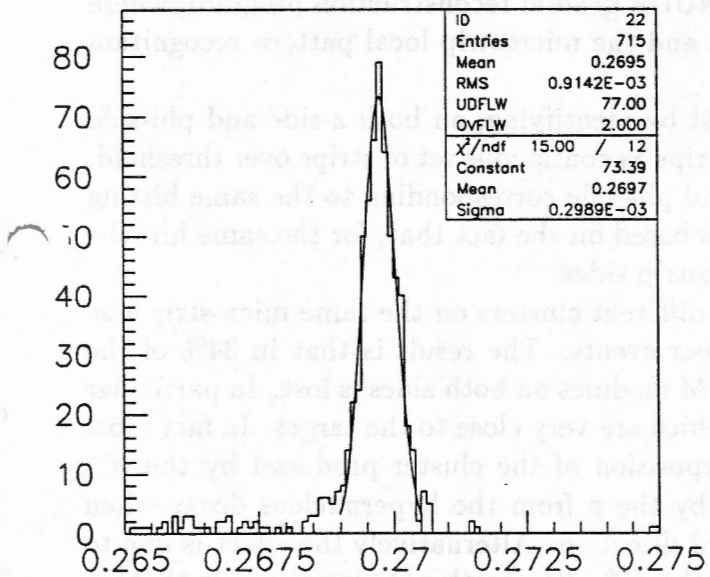

P corrected – forward – angle<30°

1 FINUDA offline software status report - 10.6.97

The work on the FINUDA offline software has progressed along three main lines :

1. Completion of the simulation/reconstruction process for the silicon microstrip detectors (ISIM and OSIM) and test of the full chain of reconstruction for hypernuclear events
2. Pattern recognition and fitting of cosmic rays crossing the apparatus, for geometric calibration purposes
3. Study, by simulation, of rates and background suppression strategies for different hypernuclei

Concerning the first item, in the FINUDA simulation program the response of the microstrip modules crossed by ionizing particles has been reproduced. For each crossing track the hit strips in both z-side and phi-side of the modules are calculated and the collected charge for each strip is evaluated. The algorithm for the evaluation of the collected charge is based on the DE/DX algorithms of the GEANT simulation package and can be improved using experimental data on energy loss in the microstrip modules.

The information about the hit strips and charge collected, together with a simulation of the strip noise (signal/noise=30 for min. ion.) is written on the simulated RDT. The simulated RDT is read in by the FINUDA general reconstruction program, where the procedures for the hit reconstruction and the microstrip local pattern recognition have been installed.

The hit reconstruction proceeds first by identifying, on both z-side and phi-side of each module, the different clusters of strips as contiguous set of strips over threshold. Second, the clusters of strips on z-side and phi-side corresponding to the same hitting particle are recognized; this recognition is based on the fact that, for the same hit, the same charge drifts towards the two microstrip sides.

The efficiency in the recognition of different clusters on the same microstrip side has been evaluated in typical hypernuclear events. The result is that in 34% of the events one clusters over all ISIM and OSIM modules on both sides is lost. In particular the effect is relevant for ISIM modules, which are very close to the target. In fact most of the lost clusters are due to the superposition of the cluster produced by the K^- and the cluster produced by the π^- or by the p from the hypernucleus decay when they exit from the target in the backward direction. Alternatively the effect is due to the μ^+ produced by the decay at rest of the K^+. It's worth noticing however that, in the case of backward π^-, the event cannot, in any case, be used for high resolution spectroscopy, whereas, in the case of backward protons, the effect of the inefficiency doesn't affect the fitting of the forward pion.

The coupling of the phi-side and z-side clusters fails in some percent of the events. Nevertheless the efficiency is much higher in the case of kaons, which are highly ionizing particles.

Once the pair of phi-side and zeta-side clusters produced by the same track have been coupled, the geometrical position of the hit on the module is reconstructed and, basing on the amount of the charge collected and on the cluster structure, the identification of the crossing particle is performed. The main aim of the particle recognition is the identification of the hits generated by the kaons on ISIM. In fact, the kaon beam recognition is the starting point of the Global Pattern Recognition for the hypernuclear event.

In principle the separation by energy loss of kaons crossing the microstrip modules from other particles can be easily obtained, since the ionization of slow kaons is much higher than the one of pions and protons (Fig. 1). However, the different inclinations of the tracks relative to the microstrip modules and, in consequence, the different crossing paths, produce some identification ambiguities (Fig.2). Nevertheless the cluster structure of kaons and protons is expected to be different; in fact kaons are expected to cross the modules orthogonally and hit few strips, whereas the protons may cross several strips. Coupling the information about collected charge and the information from the number of strips in the cluster, a good separation of kaons from protons is achieved (Fig. 3). The percentage of kaon-proton confusion on ISIM is evaluated in 2% of the events.

The effect of the inefficiencies of the microstrip local pattern recognition and particle identification on the Global Pattern Recognition is under study on a sample of simulated hypernuclear events. We estimate that the reduction of the Global Pattern Recognition efficiency will be not more than 10%.

Concerning the second item, a procedure of pattern recognition and track fitting for cosmic rays without magnetic field has been written, in preparation of the test of the apparatus with cosmic rays. In Fig. 4 a cosmic ray tracked in the apparatus is seen; the trigger for the cosmic ray is designed to be given either by two clusters of slabs in TOFONE ring or, with lower rate, by TOFINO slabs, in order to check the alignment of all the detectors.

The fitting procedure utilizes the information from longitudinal straws and drift chamber to fit the cosmic ray as a straight line in the (X, Y) plane and the information from the stereo straw tubes and the charge division from the drift chambers to obtain the polar angle of the cosmic ray relative to the axis of the apparatus (X, Z and Y, Z planes). In particular the simulated cosmic rays are a population of muons of around 2 GeV energy crossing the apparatus and hitting three chambers without hitting any internal structural part. In Fig. 5 the comparison between the Monte Carlo X and Z coordinates of the point of crossing of a longitudinal straw tube by the cosmic ray and the same point reconstructed by the fit is shown. It can be seen that the X coordinate is reconstructed within the intrinsic resolution of the straw tube ($100\mu m$) and the Z coordinate is reconstructed with a resolution of $250\mu m$.

In Fig. 6, in the hypothesis of a perfect alignment of all the detectors, the comparison between the measured distances from the hit wires (drift path) and the crossing position reconstructed by the fitting procedure is shown, as well as the comparison between the zeta coordinate measured by charge division and the value reconstructed by

the fit. It can be seen that the agreement of the measured and reconstructed values is within the intrinsic resolution of the detectors. Since the calibration with cosmic rays will be mainly devoted to check the geometrical alignment of the detectors, we intentionally moved one of the chambers of $300\mu m$ along the drift plane. The results of the comparison between the measured positions and the reconstructed ones are shown in Fig. 7. It is clearly seen that such a systematic error in the position of the chamber can be easily detected by the calibration procedure.

Concerning the third item a number of simulations of relevant physical cases have been performed. In these simulations a large statistics of hypernuclear events with different targets ^{12}C,^{89}Y,^{139}La,^{208}Pb have been generated and passed through the reconstruction procedures. In Fig. 8 the injected spectrum of pions for the reference case of ^{12}C is shown and the hypernuclear peaks with the experimental background are seen. In Fig.9 the reconstructed spectrum of the π^- is shown: in a) the raw spectrum is seen, whereas in b) the spectrum of forward pions is presented; the four peaks of $^{12}C_\Lambda$ are clearly seen over the background.

A possible way of suppress the background under the peaks is based on some reasonable hypotheses about the nature of this background. In fact this backgroud should be mainly due, in the momentum region under the peaks, to formation and decay in flight of the Σ^- and to quasi-free Λ production. The proton emitted in these processes are correlated in momentum and direction with the emitted π^- (H.Tamura et al. P.L. **160B** (1985)32). The possibility of FINUDA to detect and measure the proton coming from the K^- interaction in the target together with the π^-, allows this background to be suppressed as shown in the following pictures of Fig.9.

Fig 1

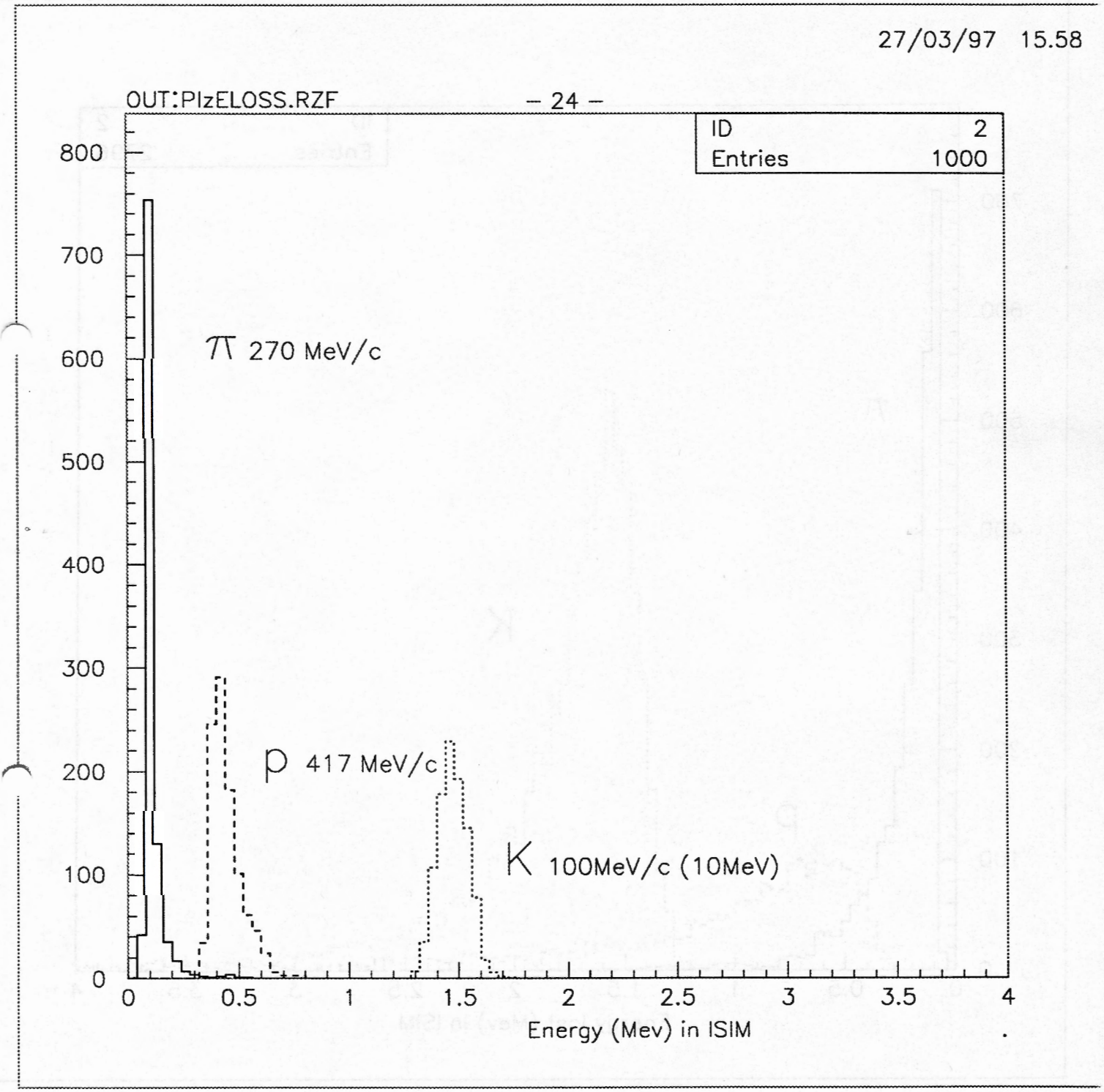
27/03/97 15.58
OUT:PIzELOSS.RZF
– 24 –
ID 2
Entries 1000
π 270 MeV/c
p 417 MeV/c
K 100MeV/c (10MeV)
800
700
600
500
400
300
200
100
0
0
0.5
1
1.5
2
2.5
3
3.5
4
Energy (Mev) in ISIM

Fig. 2

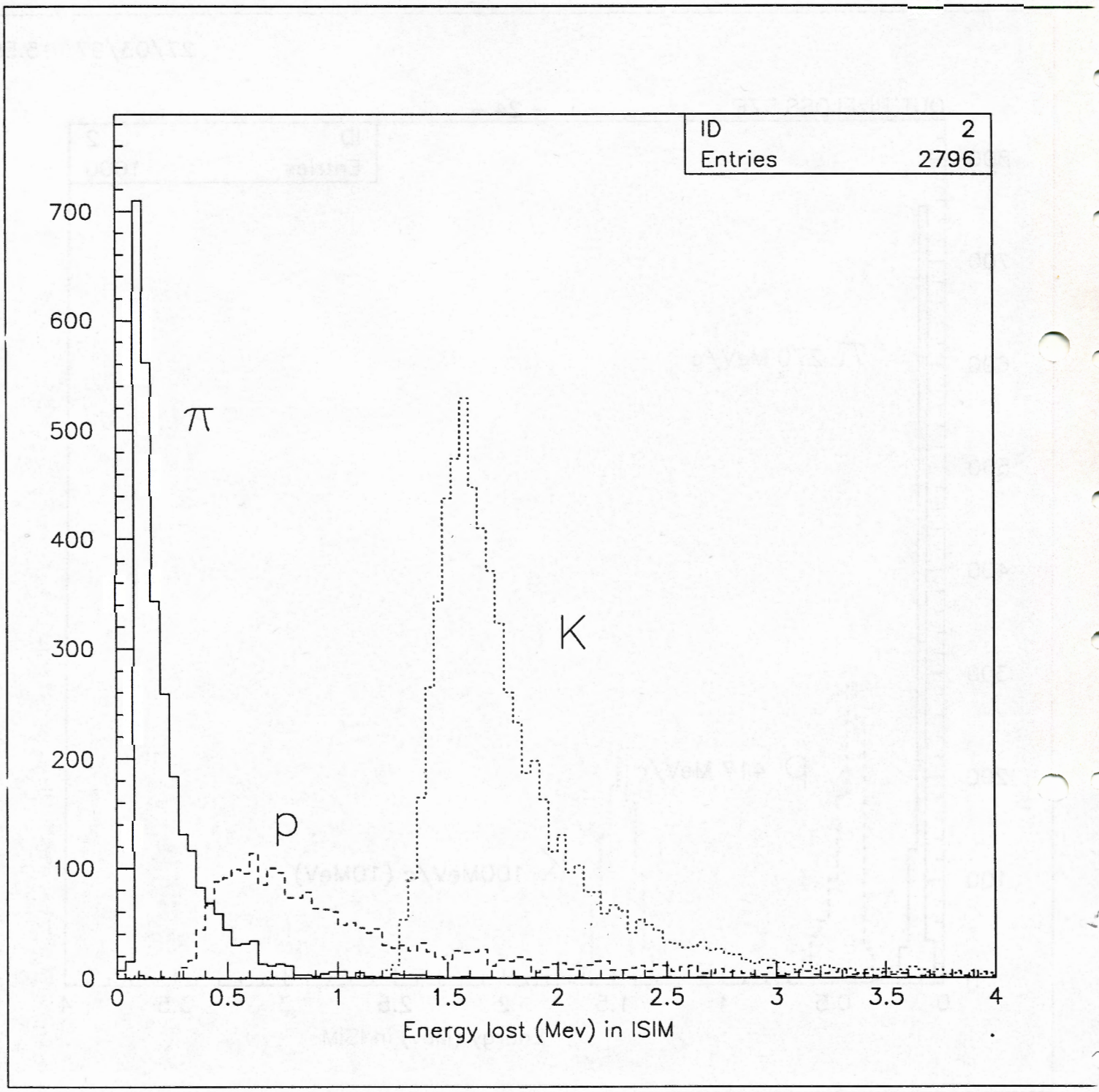
ID 2
Entries 2796
700
600
500
400
300
200
100
0
π
p
K
0
0.5
1
1.5
2
2.5
3
3.5
4
Energy lost (Mev) in ISIM

Fig. 3

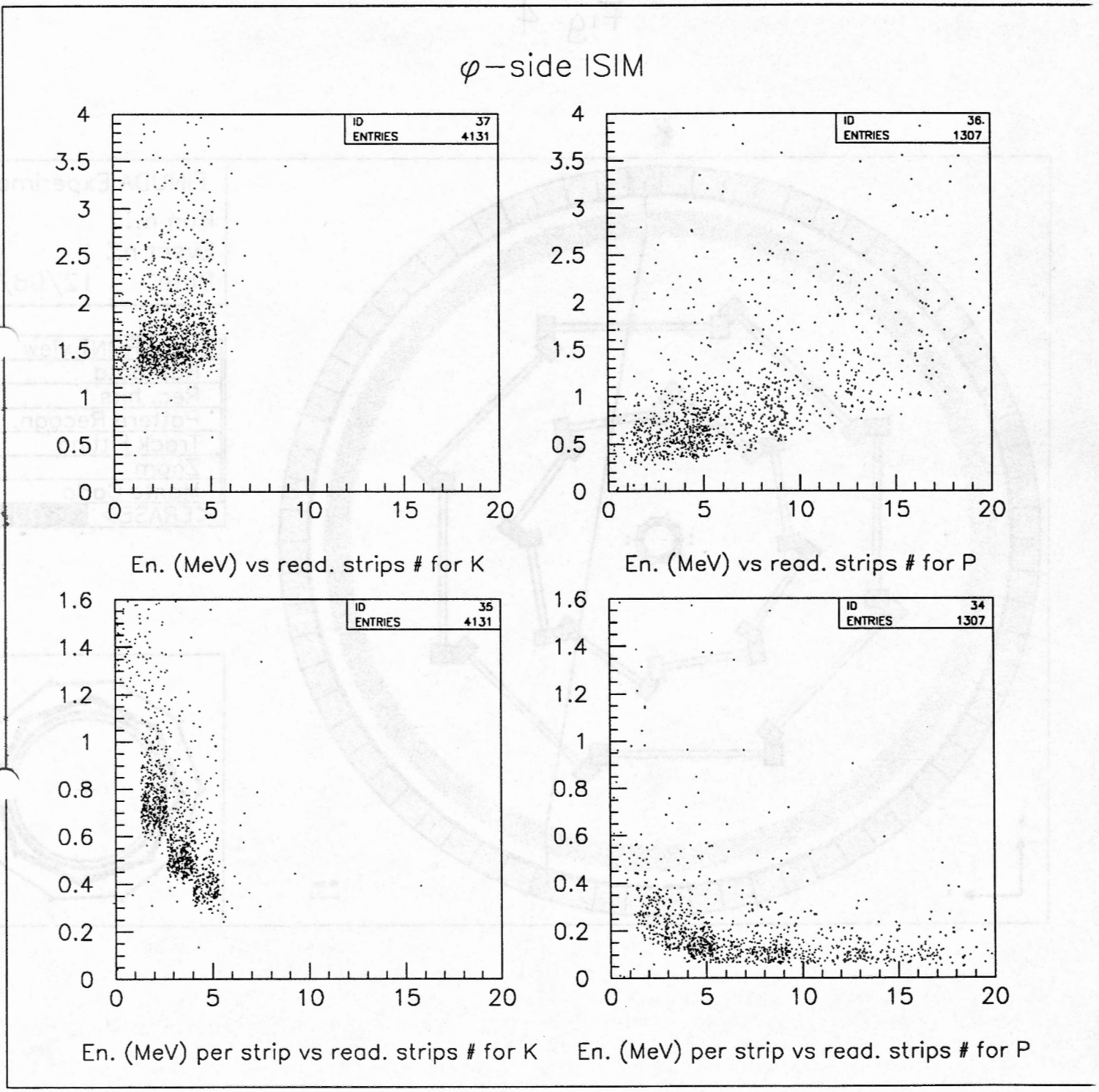
φ−side ISIM
ID 37
ENTRIES 4131
En. (MeV) vs read. strips # for K
ID 36.
ENTRIES 1307
En. (MeV) vs read. strips # for P
ID 35
ENTRIES 4131
En. (MeV) per strip vs read. strips # for K
ID 34
ENTRIES 1307
En. (MeV) per strip vs read. strips # for P

Fig. 4

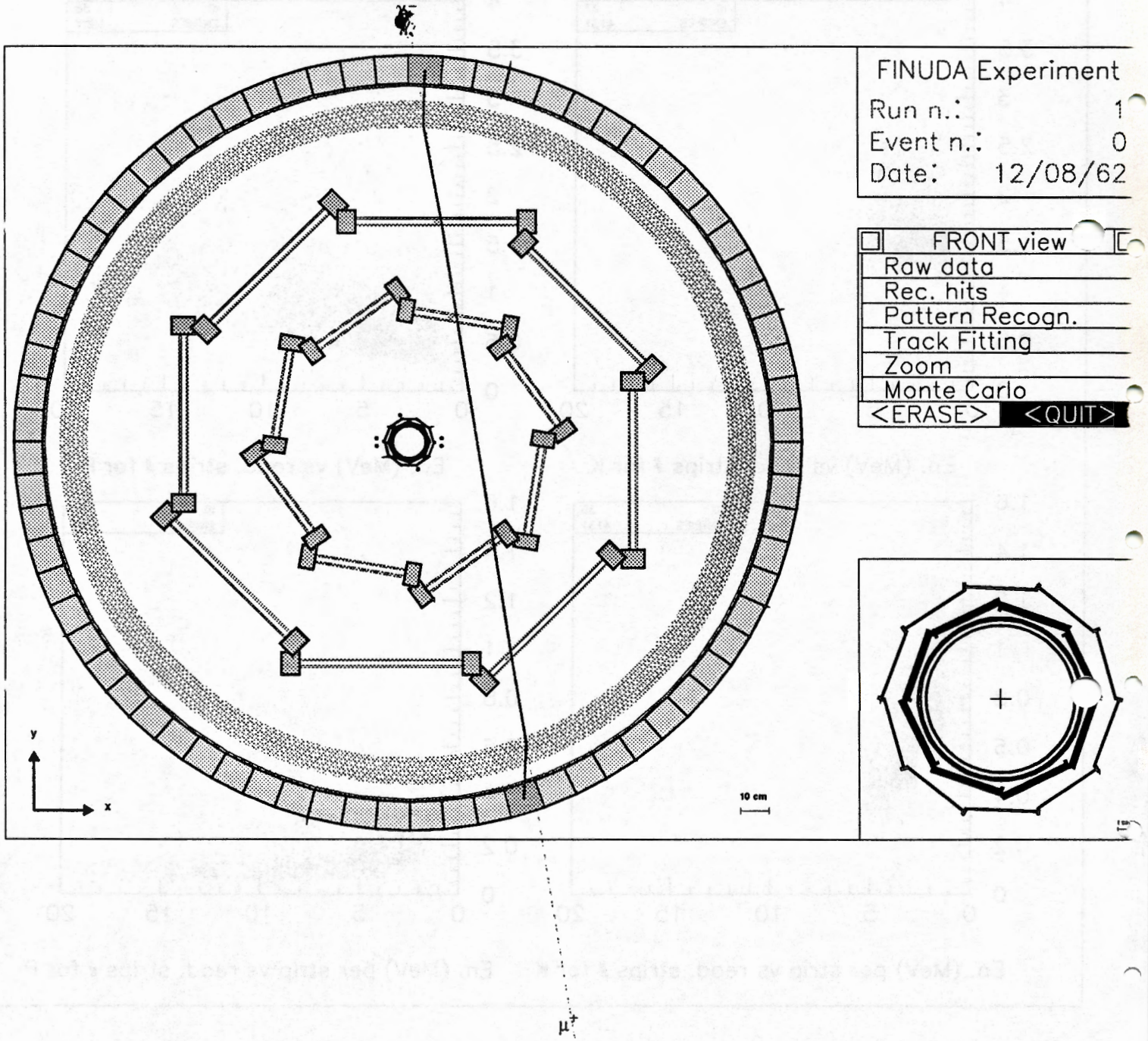
FINUDA Experiment
Run n.: 1
Event n.: 0
Date: 12/08/62
FRONT view
Raw data
Rec. hits
Pattern Recogn.
Track Fitting
Zoom
Monte Carlo
<ERASE>
<QUIT>
y
x
10 cm
μ+

Fig. 5

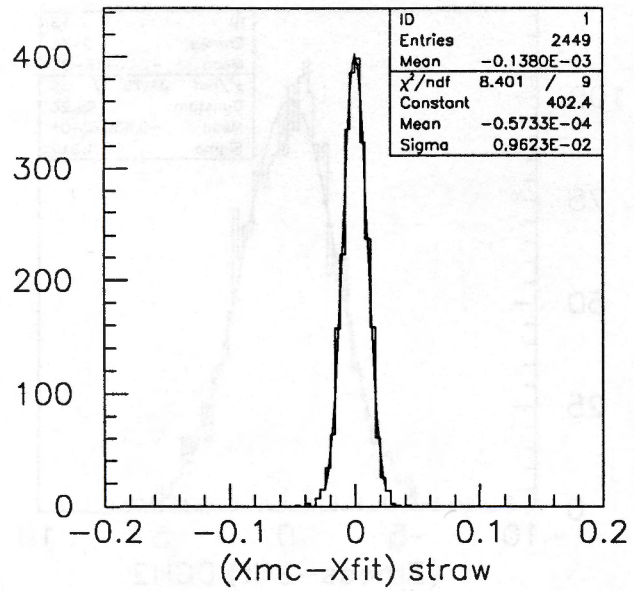
ID 1
Entries 2449
Mean −0.1380E−03
χ²/ndf 8.401 / 9
Constant 402.4
Mean −0.5733E−04
Sigma 0.9623E−02
400
300
200
100
0
−0.2
−0.1
0
0.1
0.2
(Xmc−Xfit) straw

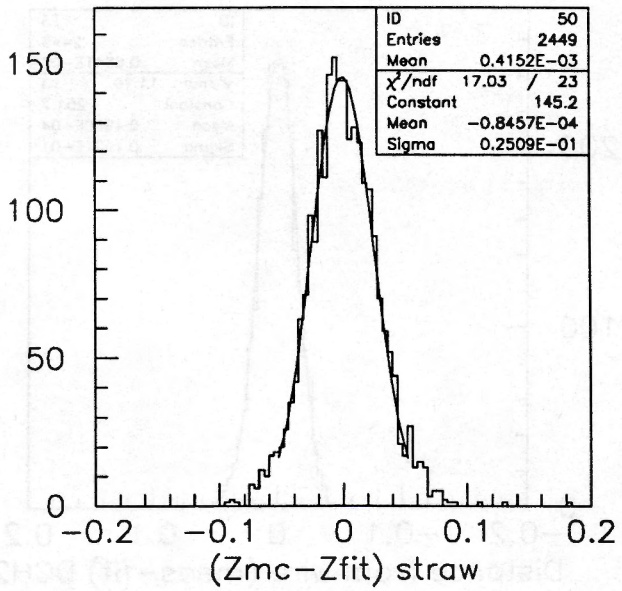
ID 50
Entries 2449
Mean 0.4152E−03
χ²/ndf 17.03 / 23
Constant 145.2
Mean −0.8457E−04
Sigma 0.2509E−01
150
100
50
0
−0.2
−0.1
0
0.1
0.2
(Zmc−Zfit) straw

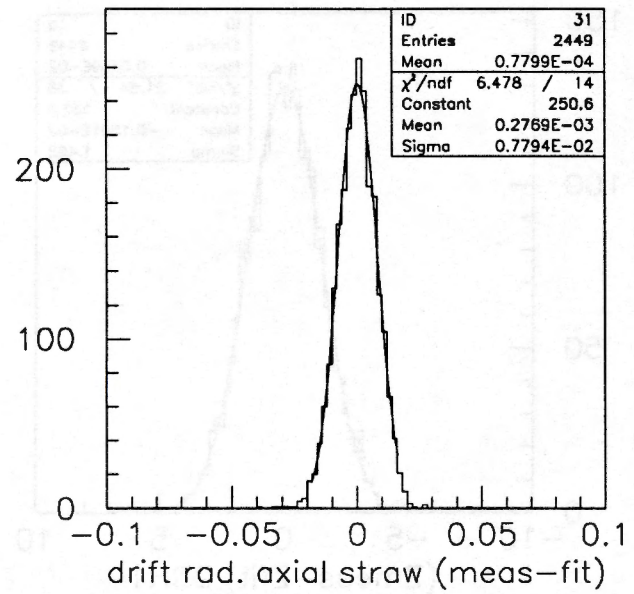
ID 31
Entries 2449
Mean 0.7799E−04
χ²/ndf 6.478 / 14
Constant 250.6
Mean 0.2769E−03
Sigma 0.7794E−02
200
100
0
−0.1
−0.05
0
0.05
0.1
drift rad. axial straw (meas−fit)

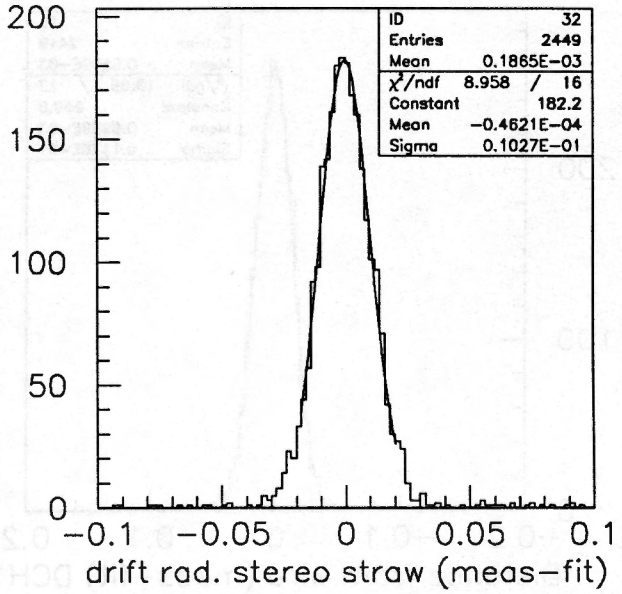
ID 32
Entries 2449
Mean 0.1865E−03
χ²/ndf 8.958 / 16
Constant 182.2
Mean −0.4621E−04
Sigma 0.1027E−01
200
150
100
50
0
−0.1
−0.05
0
0.05
0.1
drift rad. stereo straw (meas−fit)

Fig. 6

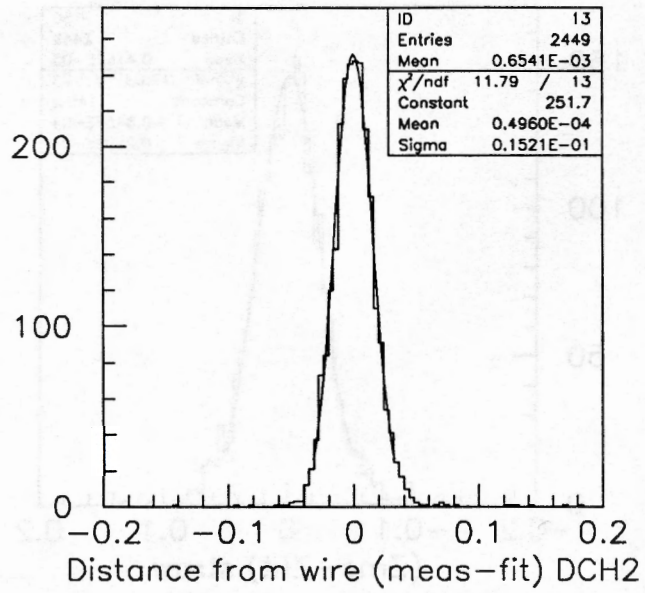
ID 13
Entries 2449
Mean 0.6541E-03
χ²/ndf 11.79 / 13
Constant 251.7
Mean 0.4960E-04
Sigma 0.1521E-01
Distance from wire (meas−fit) DCH2

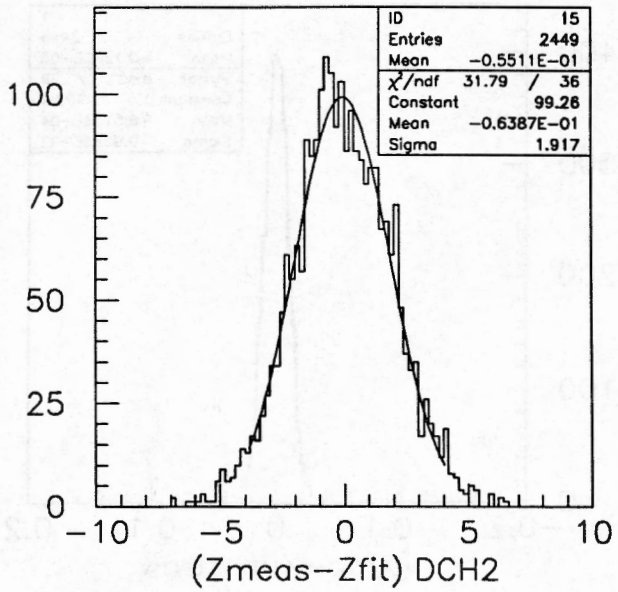
ID 15
Entries 2449
Mean −0.5511E-01
χ²/ndf 31.79 / 36
Constant 99.26
Mean −0.6387E-01
Sigma 1.917
(Zmeas−Zfit) DCH2

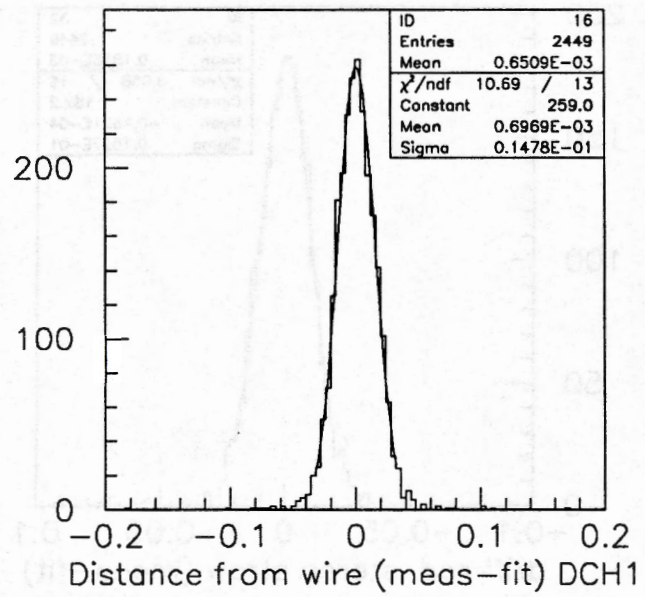
ID 16
Entries 2449
Mean 0.6509E-03
χ²/ndf 10.69 / 13
Constant 259.0
Mean 0.6969E-03
Sigma 0.1478E-01
Distance from wire (meas−fit) DCH1

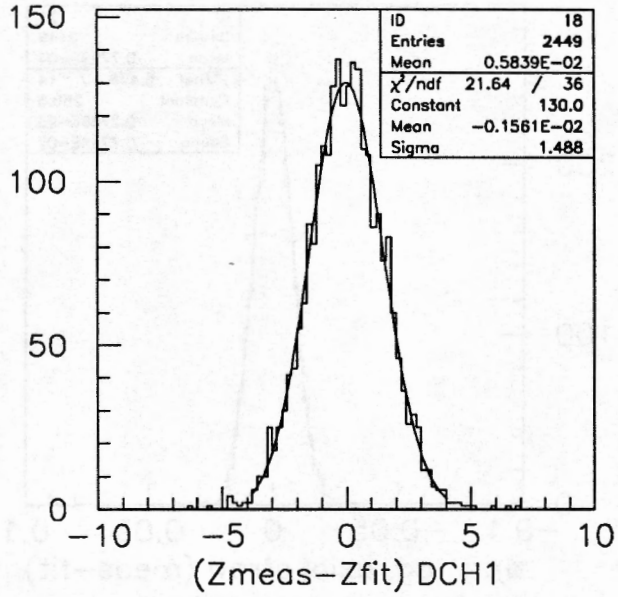
ID 18
Entries 2449
Mean 0.5839E-02
χ²/ndf 21.64 / 36
Constant 130.0
Mean −0.1561E-02
Sigma 1.488
(Zmeas−Zfit) DCH1

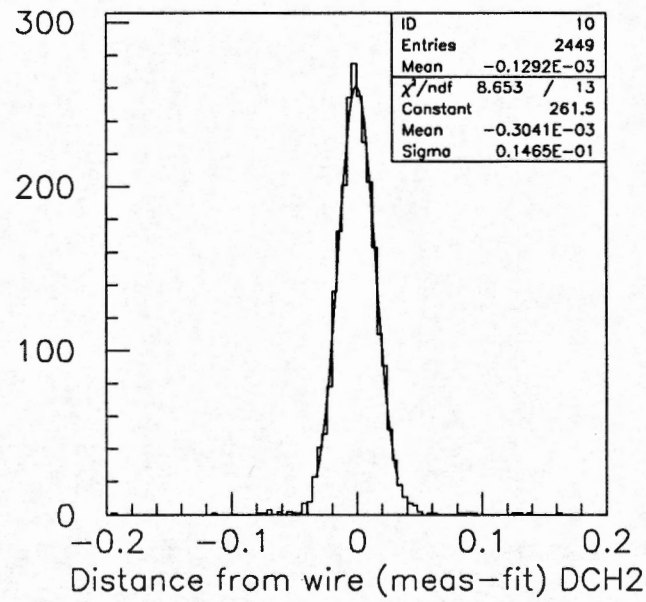
ID 10
Entries 2449
Mean −0.1292E-03
χ²/ndf 8.653 / 13
Constant 261.5
Mean −0.3041E-03
Sigma 0.1465E-01
Distance from wire (meas−fit) DCH2

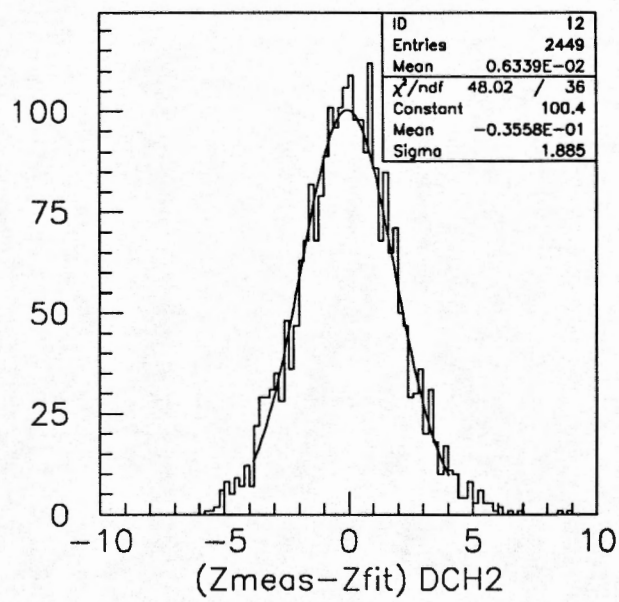
ID 12
Entries 2449
Mean 0.6339E-02
χ²/ndf 48.02 / 36
Constant 100.4
Mean −0.3558E-01
Sigma 1.885
(Zmeas−Zfit) DCH2

Fig. 7

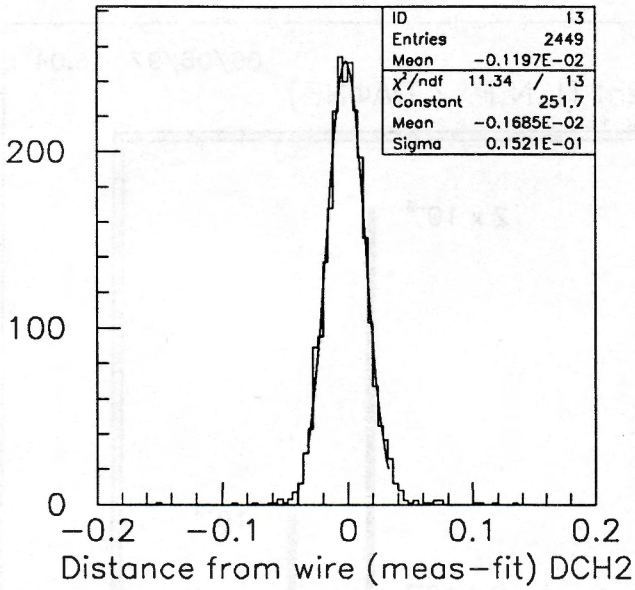
ID 13
Entries 2449
Mean −0.1197E−02
χ²/ndf 11.34 / 13
Constant 251.7
Mean −0.1685E−02
Sigma 0.1521E−01
Distance from wire (meas−fit) DCH2

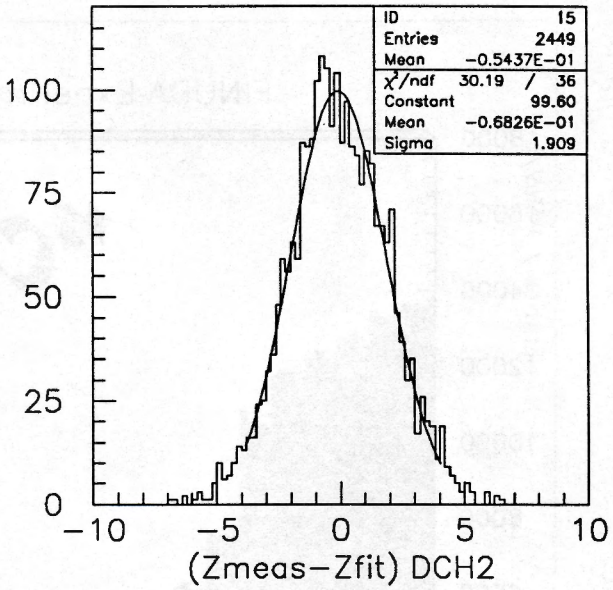
ID 15
Entries 2449
Mean −0.5437E−01
χ²/ndf 30.19 / 36
Constant 99.60
Mean −0.6826E−01
Sigma 1.909
(Zmeas−Zfit) DCH2

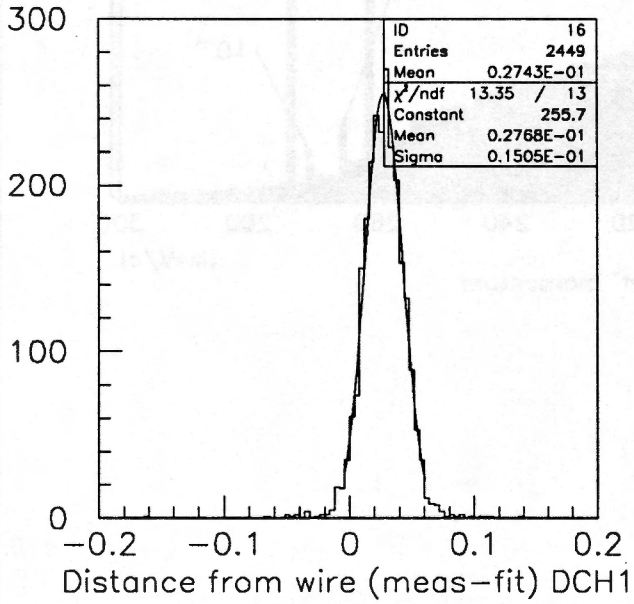
ID 16
Entries 2449
Mean 0.2743E−01
χ²/ndf 13.35 / 13
Constant 255.7
Mean 0.2768E−01
Sigma 0.1505E−01
Distance from wire (meas−fit) DCH1

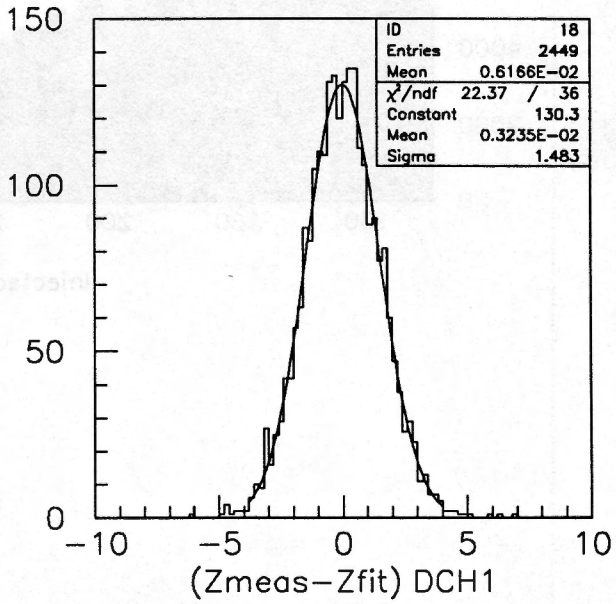
ID 18
Entries 2449
Mean 0.6166E−02
χ²/ndf 22.37 / 36
Constant 130.3
Mean 0.3235E−02
Sigma 1.483
(Zmeas−Zfit) DCH1

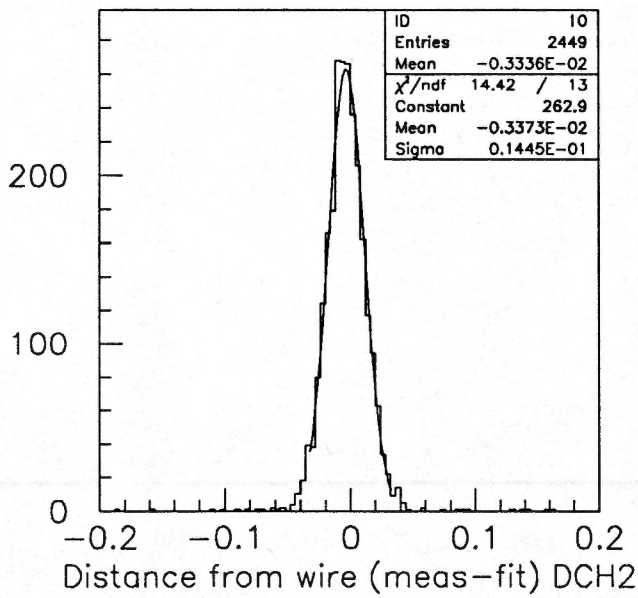
ID 10
Entries 2449
Mean −0.3336E−02
χ²/ndf 14.42 / 13
Constant 262.9
Mean −0.3373E−02
Sigma 0.1445E−01
Distance from wire (meas−fit) DCH2

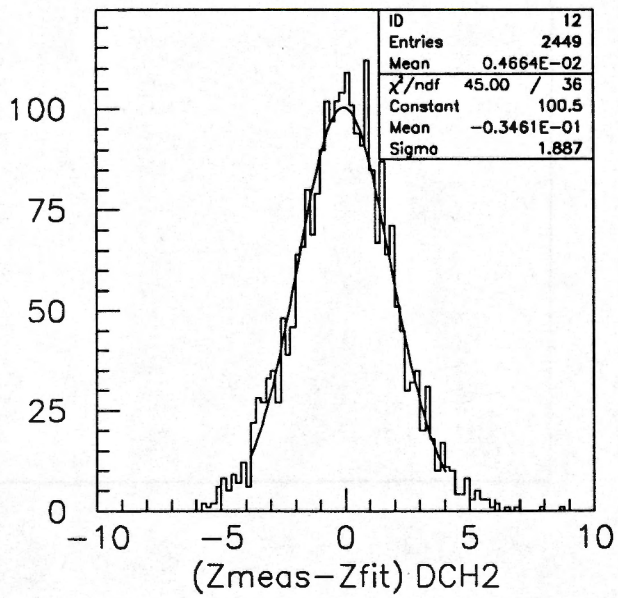
ID 12
Entries 2449
Mean 0.4664E−02
χ²/ndf 45.00 / 36
Constant 100.5
Mean −0.3461E−01
Sigma 1.887
(Zmeas−Zfit) DCH2

Fig 8

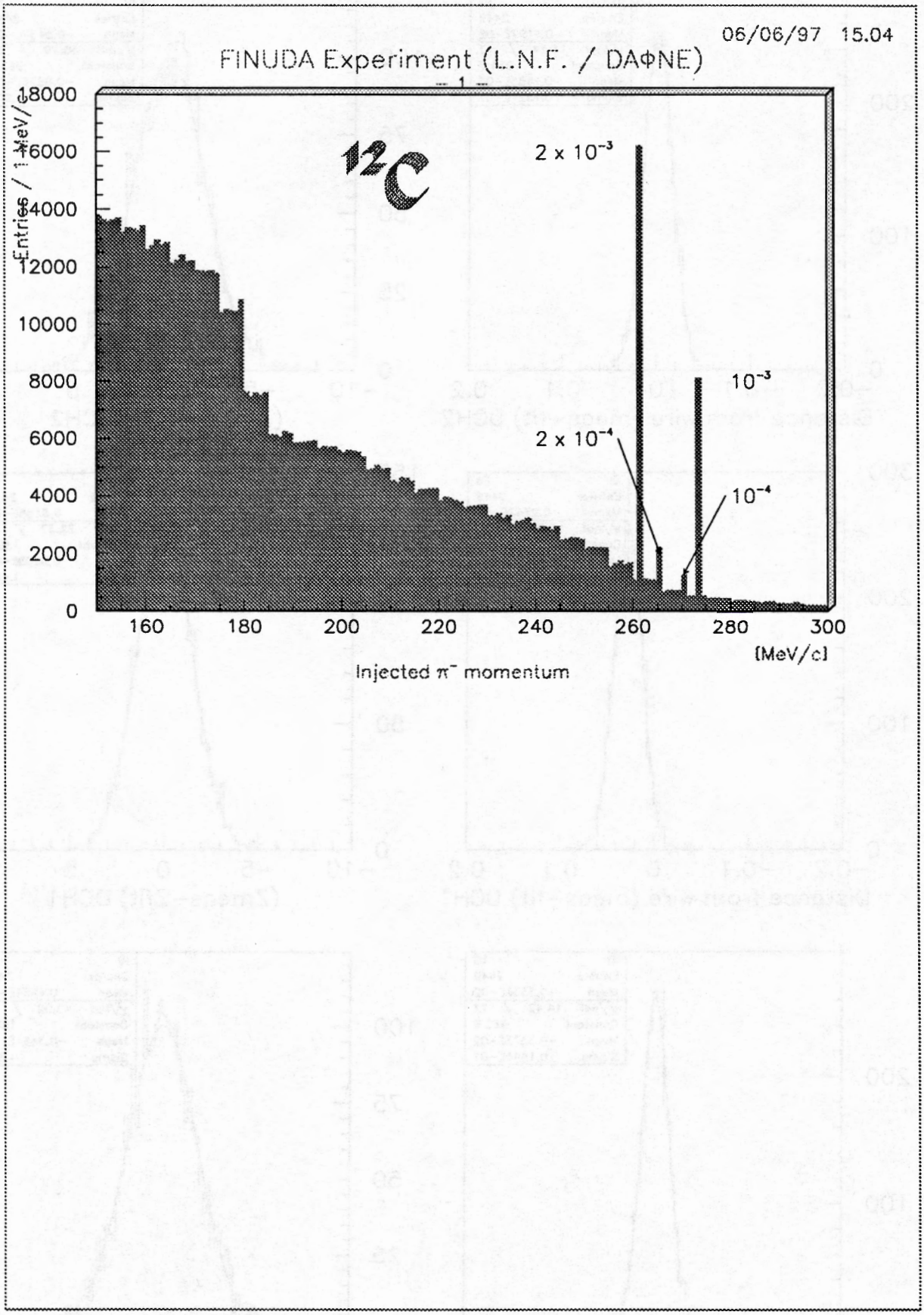
06/06/97 15.04
FINUDA Experiment (L.N.F. / DAΦNE)
– 1 –
^{12}C
2×10^{-3}
10^{-3}
2×10^{-4}
10^{-4}
Entries / 1 MeV/c
18000
16000
14000
12000
10000
8000
6000
4000
2000
0
160
180
200
220
240
260
280
300
[MeV/c]
Injected π^- momentum

Fig. 9

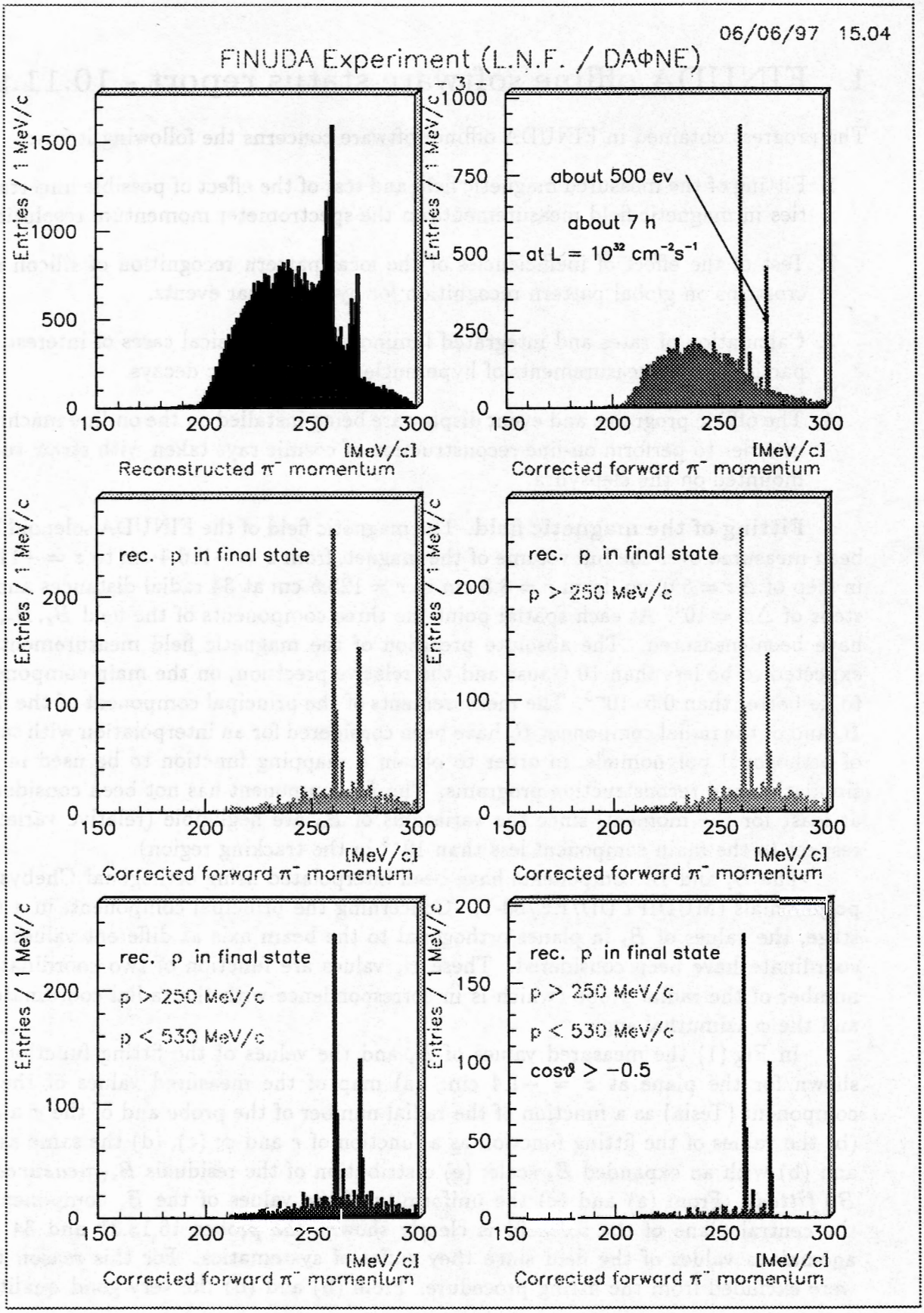
06/06/97 15.04
FINUDA Experiment (L.N.F. / DAΦNE)
Entries / 1 MeV/c
Reconstructed π⁻ momentum
about 500 ev
about 7 h
at L = 10³² cm⁻²s⁻¹
Corrected forward π⁻ momentum
rec. p in final state
p > 250 MeV/c
p < 530 MeV/c
cosϑ > −0.5
[MeV/c]

1 FINUDA offline software status report - 10.11.97

The progress obtained in FINUDA offline software concerns the following items:

1. Fitting of the measured magnetic field and test of the effect of possible uncertainties in magnetic field measurements on the spectrometer momentum resolution.
2. Test of the effect of inefficiencies of the local pattern recognition of silicon microstrips on global pattern recognition for hypernuclear events.
3. Calculation of rates and integrated luminosities for physical cases of interest. In particular for measurements of hypernuclear non-mesonic decays.
4. The offline programs and event display are being installed on the on-line machines in order to perform on-line reconstruction of cosmic rays taken with straw tubes mounted on the clepsydra.

Fitting of the magnetic field. The magnetic field of the FINUDA solenoid has been measured over the full volume of the magnet, from $z = -116.4$ cm to $z = +115.2$ in step of $\Delta z = 5.0$ cm, from $r = 8.5$ cm to $r = 125.5$ cm at 34 radial distances and in steps of $\Delta\phi = 10^0$. At each spatial point the three components of the field B_z, B_r, B_ϕ have been measured. The absolute precision of the magnetic field measurements is expected to be less than 10 Gauss and the relative precision, on the main component, to be better than $0.5 \cdot 10^{-3}$. The measurements of the principal component of the field B_z and of the radial component B_r have been considered for an interpolation with series of orthogonal polynomials, in order to obtain a mapping function to be used in the simulation and reconstruction programs. The B_ϕ component has not been considered, at least for the moment, since the variations of B_ϕ are negligible (relative variation respect to the main component less than 10^{-3} in the tracking region).

The B_z and B_r components have been interpolated using orthogonal Chebyshev polynomials (MUDIFI DD/EE/80-1). Concerning the principal component, in a first stage, the values of B_z in planes orthogonal to the beam axis at different values of z coordinate have been considered. These B_z values are function of two coordinates : number of the radial probe (which is in correspondence with the radial coordinate r) and the ϕ azimuthal angle.

In Fig.(1) the measured values of B_z and the values of the fitting function are shown for the plane at $z = -1.4$ cm: (a) map of the measured values of the B_z component (Tesla) as a function of the radial number of the probe and of the ϕ angle; (b) the values of the fitting function as a function of r and ϕ; (c), (d) the same as (a) and (b) with an expanded B_z scale; (e) distribution of the residuals $B_z(measured) - B_z(fitted)$. From (a) and (c) the uniformity of the values of the B_z component at the central plane of the solenoid is clearly shown; the probes 16,18,31 and 34 give anomalous values of the field since they suffer of systematics. For this reason they were excluded from the fitting procedure. From (b) and (d) the very good quality of

the interpolation is shown. From (e) it is seen that the average residual is actually of the order of 10 gauss.

The field remains essentially flat in r and ϕ coordinates up to $z = -90.0$ cm, whereas at larger distances from the center of the solenoid the effects of the finite length of the solenoid, of the current density of the external coils which is twice the current density of the central one, and of the presence of the end caps of the magnet distort the field lines and introduce a modulation in the B_z behaviour. In figg.(2) and (3) the same plots as Fig.(1) are shown at $z = -86.4$ cm and $z = -116.4$. The fitting function interpolates quite well the mapped values of the field but at the extreme value of z where the residuals greatly increase. Better results may be obtained in this region, where the field values vary rapidly, by using different interpolating functions in different areas and connecting them at the boundaries. However it has to be considered that this region is nearly completely out of the tracking volume, where the momentum reconstruction is performed.

Another information that can be drawn from Figg.(1) to (3) is that the values of B_z are very flat when the ϕ angle varies. For this reason, for the aim of obtaining a fitting function of the field for simulation and reconstruction, the B_Z field values may be interpolated with a function of two variables z and r using for B_z the values at some representative ϕ angle or the averaged values over the ϕ angle.

In Fig.(4) the mapped values of B_z as a function of z and of the radial number of the probes are shown together with the values of the interpolating function sampled in the corresponding (z, r) space. The map of the measured values and the function are plotted only in the half-space with negative z values, the other half-space being symmetrical. Plots (a) and (b) represent the measured values of the B_z component at two different ϕ angles with the field scale starting from zero. The field is rather uniform in the central part of the solenoid but shows dramatic border effects near the end cap (a region, however, outside the FINUDA tracking volume). In plot (c) the measurements at $\phi = 10^0$ are shown with an enlarged field scale. Systematic effects of probes 16,18,31 and 34 appears clearly.

In plot (d) the values of the interpolating function are shown in the same (z, r) region. The fit is not completely satisfactory since a unique polynomial function has been used for the entire region. In this case too, much better results may be obtained by discarding from the fit the region which stay out of the tracking volume or by fitting separately different sub regions with different polynomial functions. This will be necessary for obtaining the final interpolating function. For the moment, this first approximation function fulfills the limited purpose of testing the effect of magnetic field uncertainties on the momentum resolution.

Concerning the B_r component of the field, it has much lower absolute values than the main one (about 10^{-3}) in the central part of the solenoid whereas, near to the edges of the magnet, where the field is distorted by the need to enter the magnet yoke through the end-caps, its absolute value may reach thousands of gauss. As it was done for the main component B_z, the values of B_r have been considered in planes orthogonal

to the beam axis at different values of the z coordinate.

In Fig.(5) the values of B_r at $z = -11.4$ cm, near the center of the solenoid, are plotted as a function of the radial number of the probe and of the azimuthal angle ϕ. In order to avoid plotting negative values the field values are incremented by 1.0 tesla. As it is seen from the picture (a) the field values show a certain dispersion which is averaged by the fitting function (b); in picture (c) the superposition of measured data and fitting function is seen. The data show also a modulation along the ϕ coordinate, which is due to the 1 mrad tilt of the magnetic axis relative to the mechanical one; this modulation has been reproduced by the interpolating function.

In Fig.(6) the same plots are shown for the plane at value of $z = -56.4$ cm, where the modulation in ϕ is clearly seen too. Owing to the dependence of the values of the B_r component on the ϕ angle the global interpolating function for B_r was calculated as function of the three variables (z, r, ϕ), fitting separately different volume regions and connecting the values at the boundaries.

Test of momentum resolution. The interpolating functions for the two field components B_z and B_r have been used to test, by Monte carlo simulation, the effects on the momentum resolution of possible uncertainties in the measurements or fitting of the realistic magnetic field. With this aim in mind, populations of hypernuclear events have been simulated using the mapped field components; in the reconstruction program this events have been analysed either using the mapped field or using a uniform field or a mapped field with some distortion, in order to evaluate the effect on the momentum resolution.

The results of these tests are summed up in Table (1). Each line of the Table corresponds to a particular test. In column (2) the conditions for the magnetic field in the simulation are reported. It can be seen that some tests have been performed with a perfectly uniform magnetic field, in order to obtain an ideal reference. In column (3) the field conditions for the reconstruction are listed for each test. Column (3) and (4) show whether the multiple scattering or the measurement errors have been accounted for. Some tests indeed have been performed disregarding about these effects in order to separate the effects of the distortions of the magnetic field. In columns (5) and (6) the momentum resolution is reported for respectively forward pions and for a selected population of tracks crossing the central part of the solenoid (central tracks), where the effects of field distortions are minimal.

Tests (1A,1B) show the ideal condition of perfectly uniform magnetic field. Tests (2A,2B) show what happens in the extreme condition of disregarding about the modulation of the principal components B_z; the required resolution (less than 3 per mille) is obtained only for central tracks. In tests (3A,3B,3C) where the B_z map is used in the reconstruction, the required resolution is found again.

From test (5A) the effects of B_r component are introduced. In (5A,5B) the presence of a B_r component is disregarded completely in reconstruction; the effects on resolution are less relevant than they are for the main component and affect only the most inclined tracks. The required resolution is found again in tests (7A,7B,7C)

where the map of B_r is considered too, whereas the effect of a systematic error of 30 gauss (which is a large error) on the evaluation of the B_r component is seen in tests (6A,6B,6C). Finally in tests (8A,8B,8C) random errors have been added to the values of the two components; the results show that these type of errors (fluctuations in the field measurements) average away and don't affect significantly the resolution. In conclusion one can infer from these studies that, with a reasonably accurate measurement of the FINUDA magnetic field and a good field interpolation, the required momentum resolution can be easily fulfilled.

Global Pattern Recognition efficiency with microstrips. Recently the procedures for simulation and reconstruction of silicon microstrips have been completed and inserted in the general FINUDA programs. In particular the reconstruction procedure needs a Local Pattern Recognition which performs the following tasks : (1) cluster identification of z and ϕ sides of each microstrip module; (2) cluster association on the two sides and identification of the hit position; (3) hit coordinate reconstruction; (4) particle identification, in particular identification of kaon hits on ISIM. The last task, which corresponds to the identification of the K^+K^- beam, is essential for the start of the Global Pattern Recognition procedure.

The microstrip Local Pattern Recognition may present a number of inefficiency in its different steps: loss of cluster due to closeness of tracks or border effects, ambiguity in coupling z clusters with ϕ clusters, wrong identification of the kaon with a proton in ISIM, etc. These inefficiencies have an impact on the Global Pattern Recognition, which has to be evaluated on the complete hypernuclear event. In fact, for instance, the loss of a cluster has minimal effect when it concerns a muon, whereas it has a fatal effect when it concerns a forward pion.

For this reason a population of simulated hypernuclear events fulfilling the trigger condition has been processed through the full reconstruction program, either accounting for the microstrip simulation/reconstruction or using, for the microstrip, the Monte Carlo hits. In this way the impact of the microstrip pattern recognition on the Global Pattern Recognition has been checked directly. The results are summed up in two numbers giving the efficiency of the Pattern Recognition in the two cases.

When the Monte Carlo hits are used for the microstrips, the Pattern Recognition procedure (straw tubed + spectrometer) has an efficiency of about 90%. The efficiency is defined as the ratio of the recognized π^- over the hypernuclear events which passed the trigger and have a π^- with 4 hits in the 4 layers of detectors (recognizable events). The efficiency decreases to 80% when the microstrip local pattern recognition is used. The reasons for the losses are mainly due to the border effects, which are now taken into account correctly, and to the loss of clusters due to the closeness of track hits on the microstrips. Indeed, one has to consider that ISIM is very close to the target (2 mm) and a cluster is lost when, either in one coordinate or in the other on the module, two hits are closer than the hit dimension, which is several strips (hundreds of microns). It is worth remarking anyway that the present procedure is a first approximation one and could be improved once the data will be available.

Calculations of rates for physical cases of interest. Calculations of rates and integrated luminosities for hypernuclear spectroscopy have been presented in the last status report and appears rather encouraging. As an example, assuming for the ground state of ${}^{12}_{\Lambda}C$ a capture rate of 10^{-3} and a machine luminosity of 10^{32} cm^{-2} s^{-1} the experiment is able to cumulate 500 events in the ground state peak in less than 10 hours of data taking. In these conditions states with capture rates of the order of 10^{-5} are attainable in reasonable beam time.

New calculations have been performed for the measurement of hypernuclear non-mesonic decays in (n,n) and (n,p) for the standard hypernucleus ${}^{12}_{\Lambda}C$. The calculations have been done under the following hypotheses : machine luminosity of 10^{32} cm^{-2} s^{-1}; 8 carbon targets (we recall that FINUDA has the possibility of using targets of different materials at the same time); efficiency of TOFONE slabs for neutron recognition estimated to 10%; ratio of (n,n) over (n,p) decays of about 50%.

Under these conditions the estimated rates are the following: (1) events useful for high resolution spectroscopy: 80 event/hour in the ground state; (2) events where a proton is recognized and hits a TOFONE slab: 14 event/hour (hypernuclear life time measurement); (3) events in the ground state where a proton is recognized together with the corresponding hit of the neutron in TOFONE: 2 event/hour; (4) events in the ground state where two neutrons back to back are recognized in TOFONE slabs: 0.5 event/hour. This means that, with an integrated luminosity of 144 pbarn^{-1} which corresponds to 17 days of data taking, FINUDA can collect $3.2 \cdot 10^4$ events for high resolution spectroscopy, $5.6 \cdot 10^3$ events for mean life measurement, $8 \cdot 10^2$ events of (n,p) decay and $2 \cdot 10^2$ events of (n,n) decay.

Fig. 1

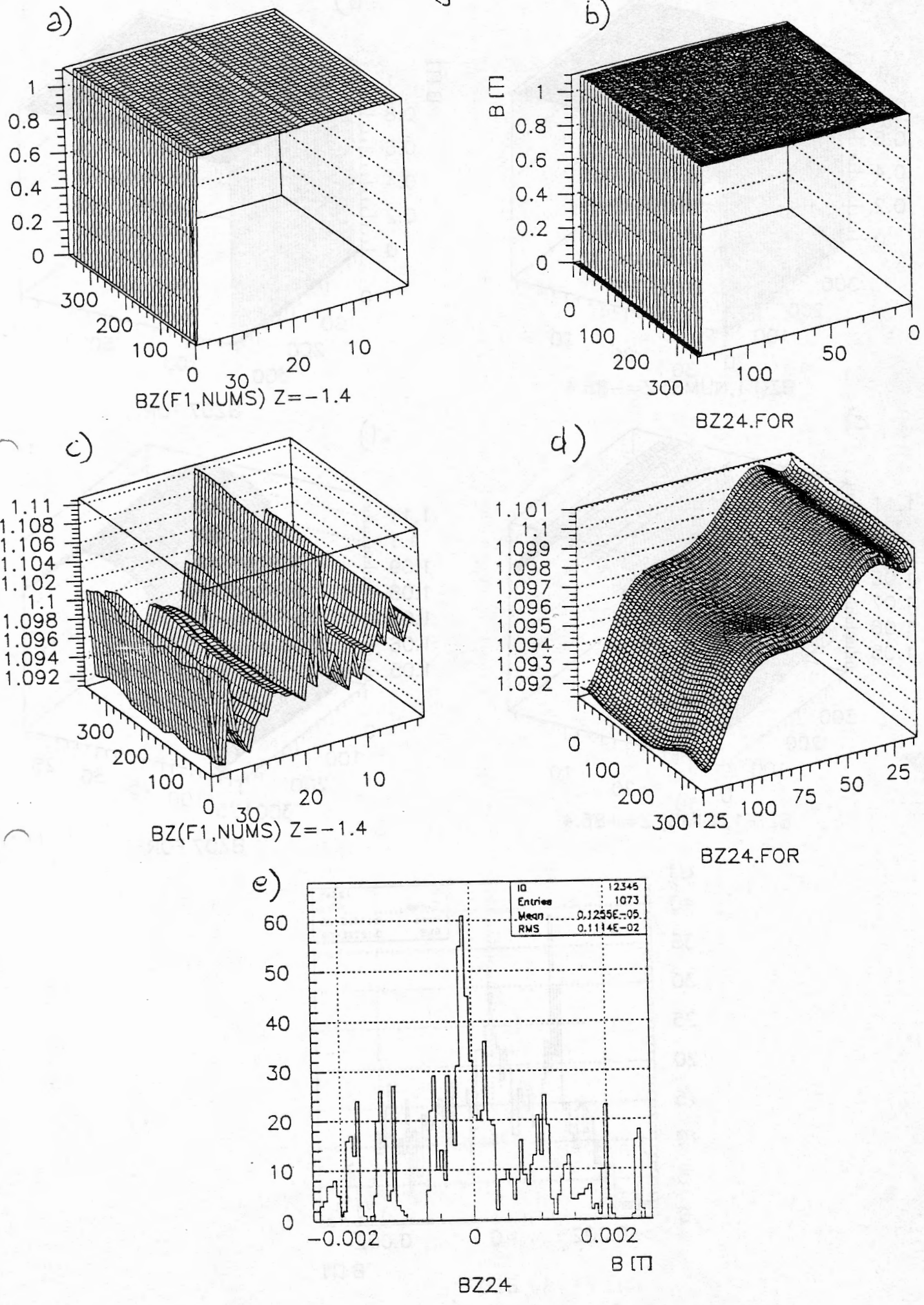
a)
1
0.8
0.6
0.4
0.2
0
300
200
100
0
30
20
10
BZ(F1,NUMS) Z=-1.4
b)
B [T]
1
0.8
0.6
0.4
0.2
0
0
100
200
300
100
50
0
BZ24.FOR
c)
1.11
1.108
1.106
1.104
1.102
1.1
1.098
1.096
1.094
1.092
300
200
100
0
30
20
10
BZ(F1,NUMS) Z=-1.4
d)
1.101
1.1
1.099
1.098
1.097
1.096
1.095
1.094
1.093
1.092
0
100
200
300
125
100
75
50
25
BZ24.FOR
e)
ID 12345
Entries 1073
Mean 0.1255E-05
RMS 0.1114E-02
60
50
40
30
20
10
0
-0.002
0
0.002
B [T]
BZ24

Fig. 2

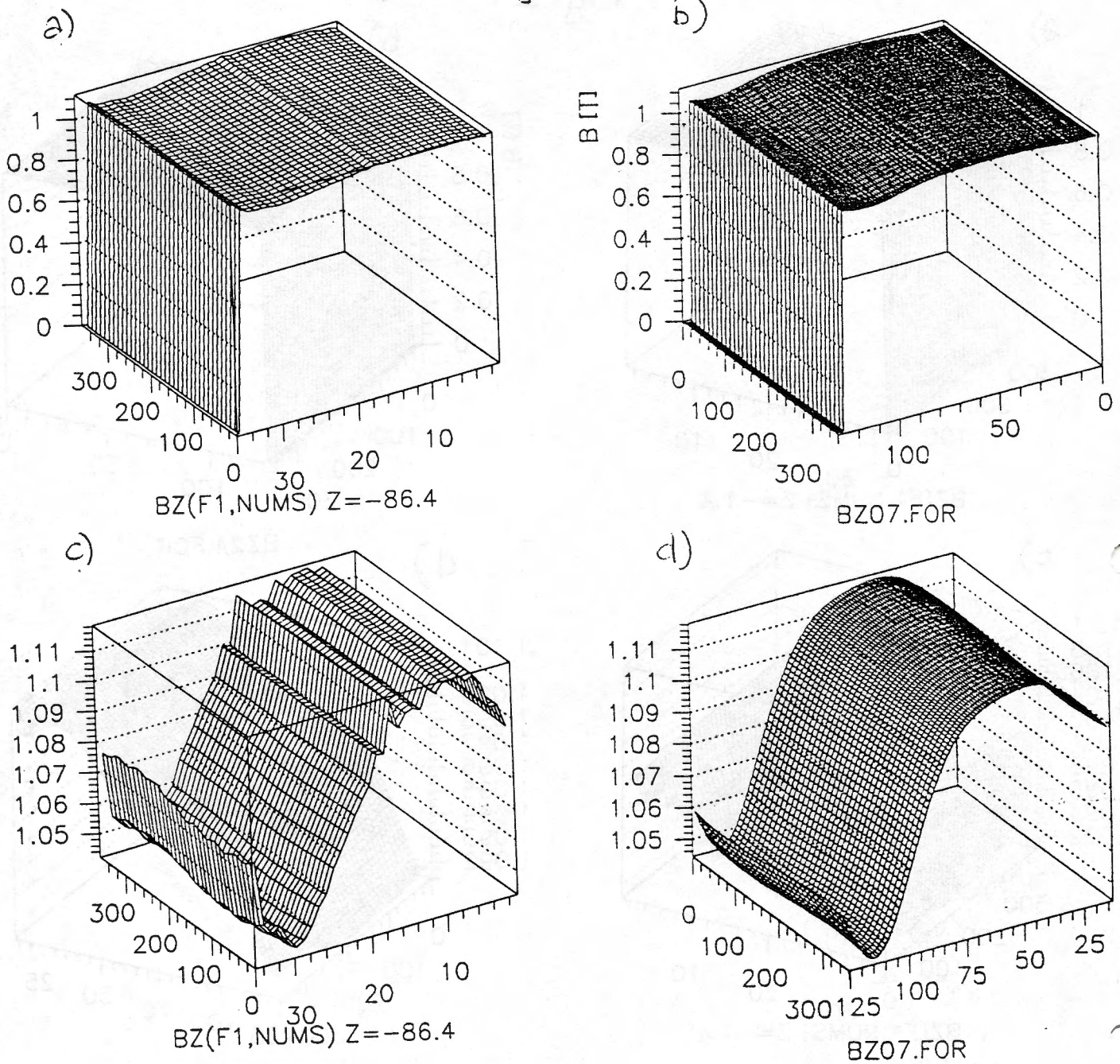
a)
1
0.8
0.6
0.4
0.2
0
300
200
100
0
30
20
10
BZ(F1,NUMS) Z=-86.4
b)
B [T]
1
0.8
0.6
0.4
0.2
0
0
100
200
300
100
50
0
BZ07.FOR
c)
1.11
1.1
1.09
1.08
1.07
1.06
1.05
300
200
100
0
30
20
10
BZ(F1,NUMS) Z=-86.4
d)
1.11
1.1
1.09
1.08
1.07
1.06
1.05
0
100
200
300
125
100
75
50
25
BZ07.FOR

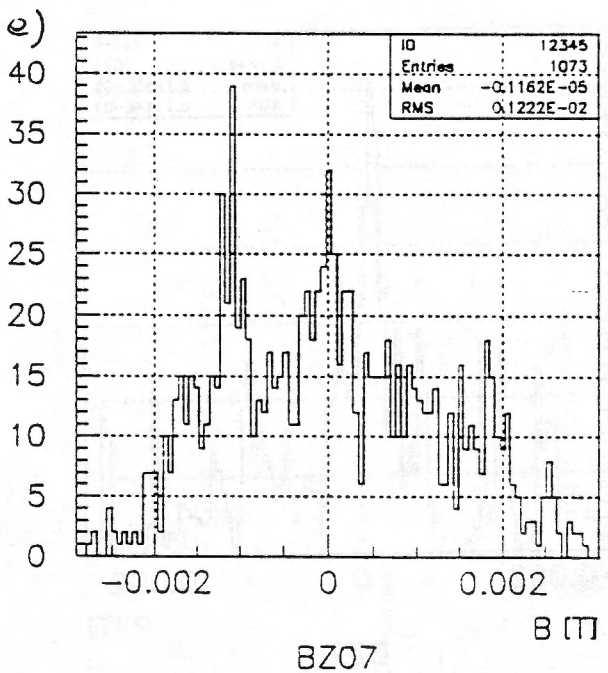
e)
ID 12345
Entries 1073
Mean -0.1162E-05
RMS 0.1222E-02
40
35
30
25
20
15
10
5
0
-0.002
0
0.002
B [T]
BZ07

Fig. 3

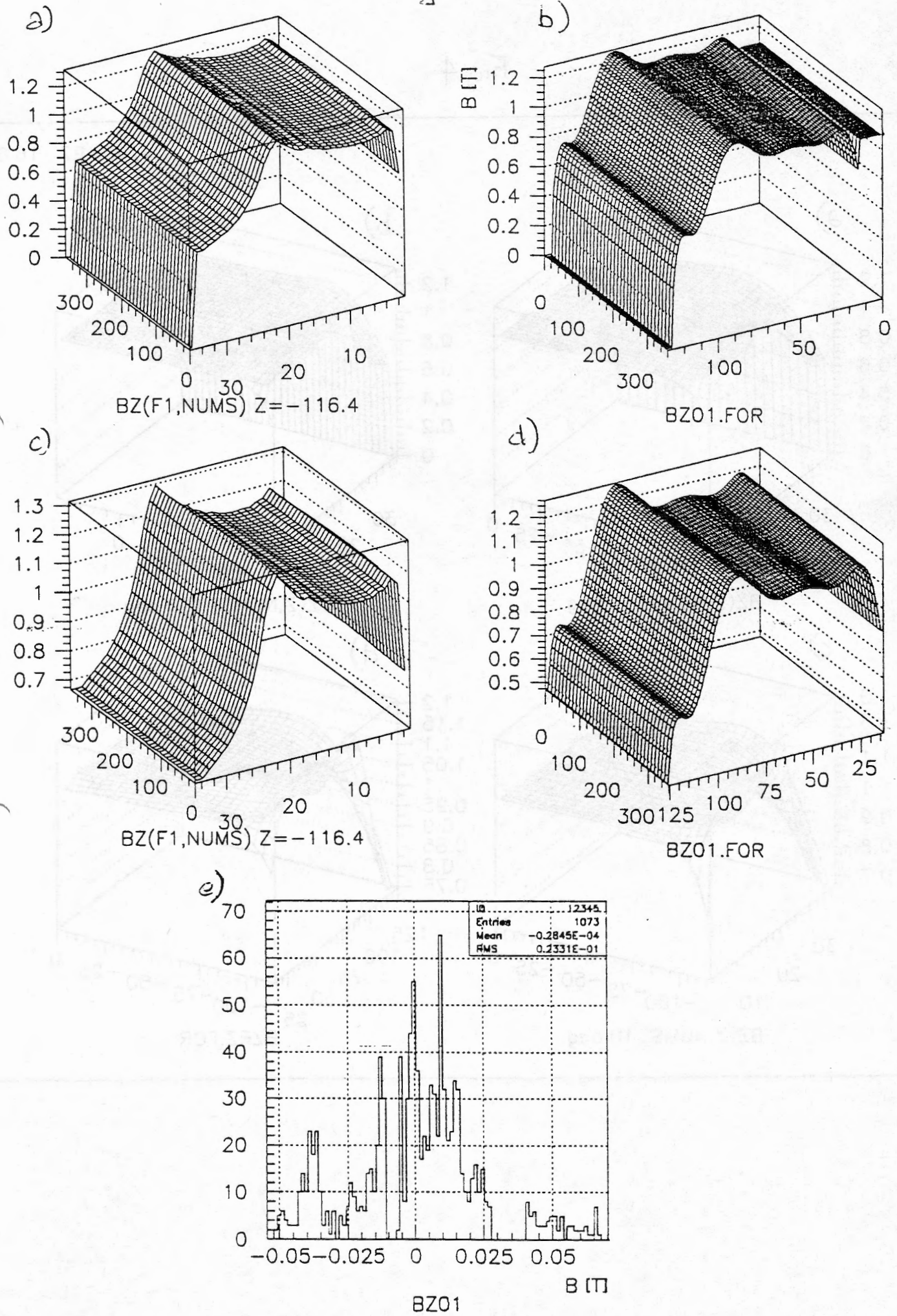
a)
1.2
1
0.8
0.6
0.4
0.2
0
300
200
100
0
30
20
10
BZ(F1,NUMS) Z=-116.4
b)
B [T]
1.2
1
0.8
0.6
0.4
0.2
0
0
100
200
300
100
50
0
BZ01.FOR
c)
1.3
1.2
1.1
1
0.9
0.8
0.7
300
200
100
0
30
20
10
BZ(F1,NUMS) Z=-116.4
d)
1.2
1.1
1
0.9
0.8
0.7
0.6
0.5
0
100
200
300
125
100
75
50
25
BZ01.FOR
e)
70
60
50
40
30
20
10
0
Entries 1073
Mean -0.2845E-04
RMS 0.2331E-01
-0.05
-0.025
0
0.025
0.05
B [T]
BZ01

Fig 4

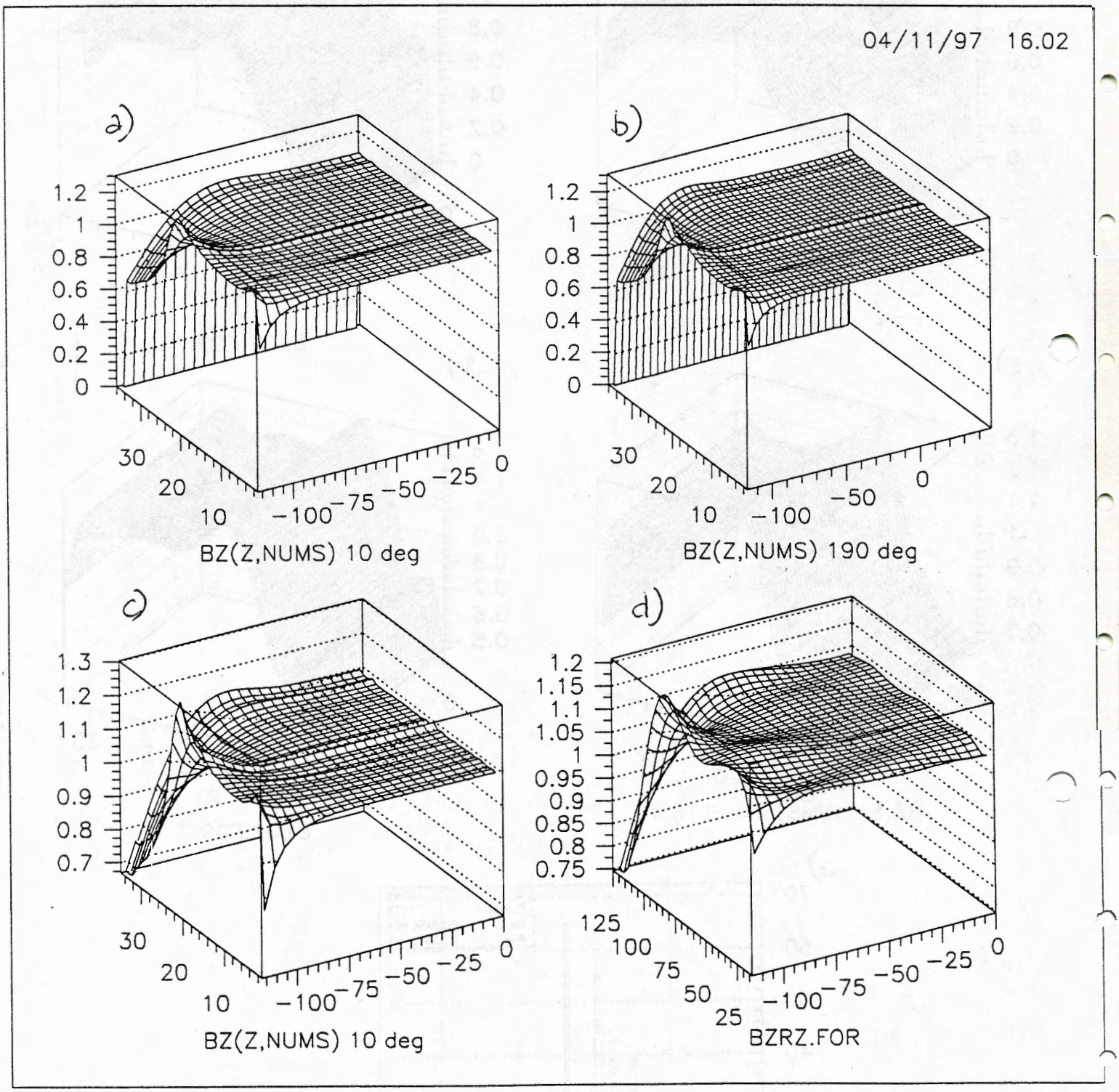
04/11/97 16.02
a)
1.2
1
0.8
0.6
0.4
0.2
0
30
20
10
−100
−75
−50
−25
0
BZ(Z,NUMS) 10 deg
b)
1.2
1
0.8
0.6
0.4
0.2
0
30
20
10
−100
−50
0
BZ(Z,NUMS) 190 deg
c)
1.3
1.2
1.1
1
0.9
0.8
0.7
30
20
10
−100
−75
−50
−25
0
BZ(Z,NUMS) 10 deg
d)
1.2
1.15
1.1
1.05
1
0.95
0.9
0.85
0.8
0.75
125
100
75
50
25
−100
−75
−50
−25
0
BZRZ.FOR

Fig. 5

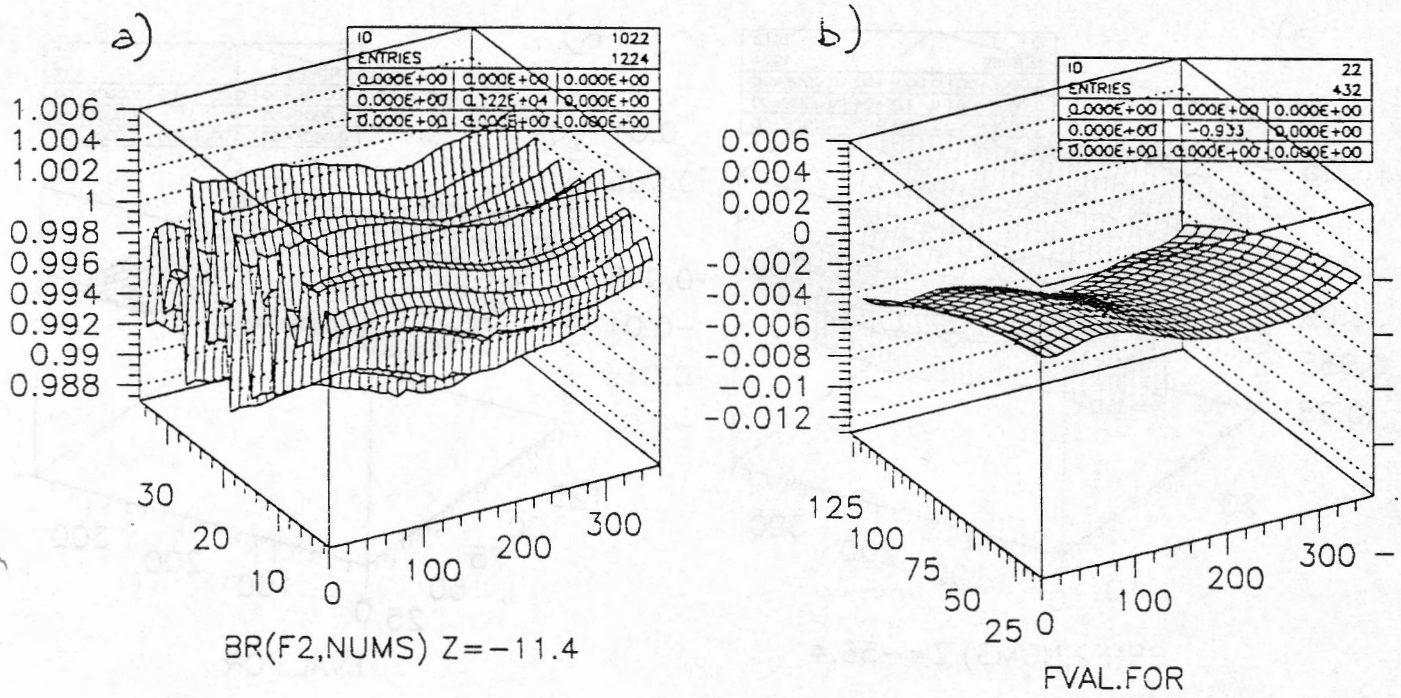
a)
ID 1022
ENTRIES 1224
1.006
1.004
1.002
1
0.998
0.996
0.994
0.992
0.99
0.988
30
20
10
0
100
200
300
BR(F2,NUMS) Z=-11.4
b)
ID 22
ENTRIES 432
0.006
0.004
0.002
0
-0.002
-0.004
-0.006
-0.008
-0.01
-0.012
125
100
75
50
25 0
100
200
300
FVAL.FOR

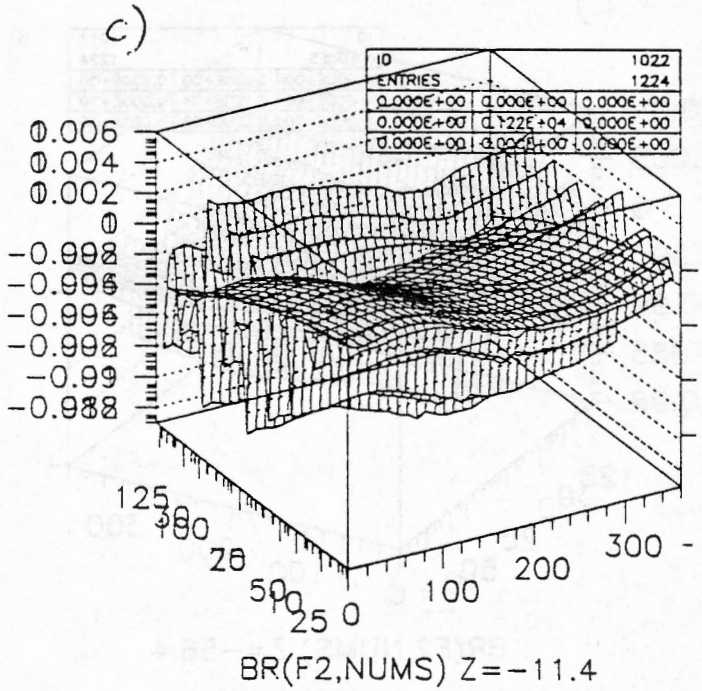
c)
ID 1022
ENTRIES 1224
0.006
0.004
0.002
0
-0.998
-0.996
-0.996
-0.998
-0.99
-0.988
125
100
75
50
25 0
100
200
300
BR(F2,NUMS) Z=-11.4

Fig. 6

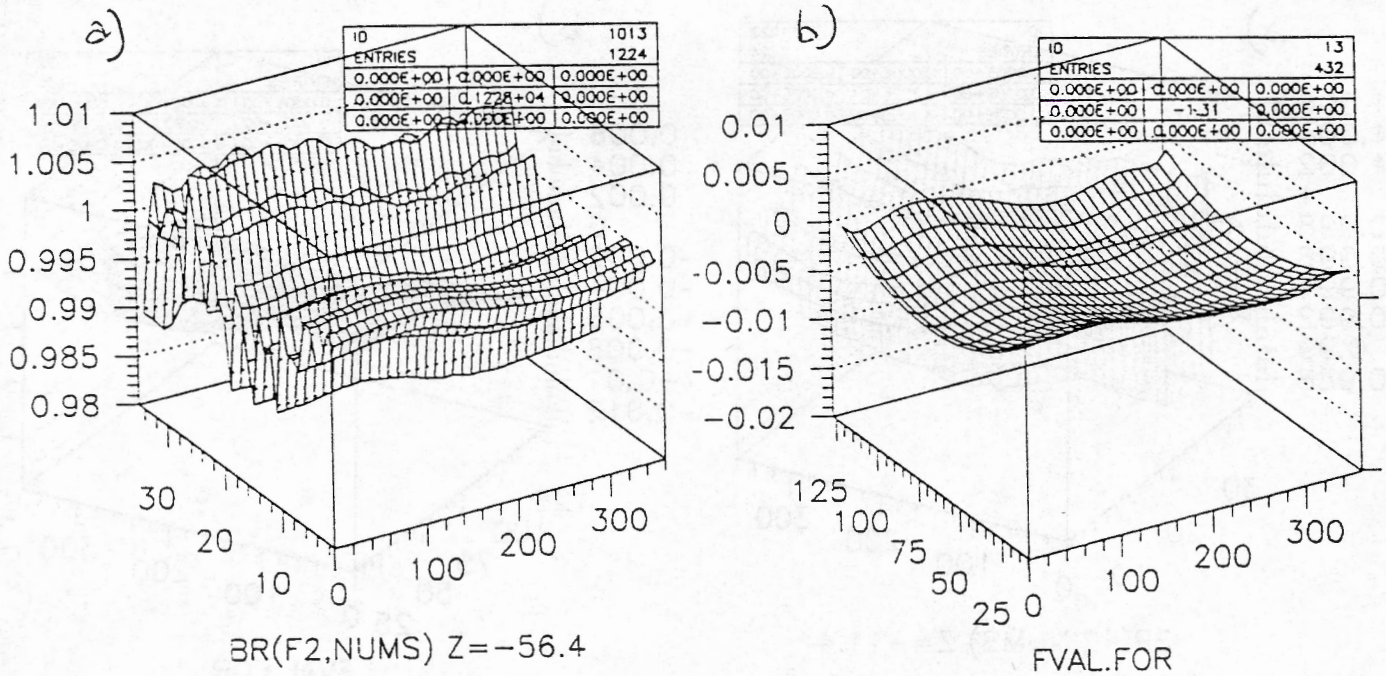
a)
ID 1013
ENTRIES 1224
1.01
1.005
1
0.995
0.99
0.985
0.98
30
20
10
0
100
200
300
BR(F2,NUMS) Z=-56.4
b)
ID 13
ENTRIES 432
0.01
0.005
0
-0.005
-0.01
-0.015
-0.02
125
100
75
50
25
0
100
200
300
FVAL.FOR

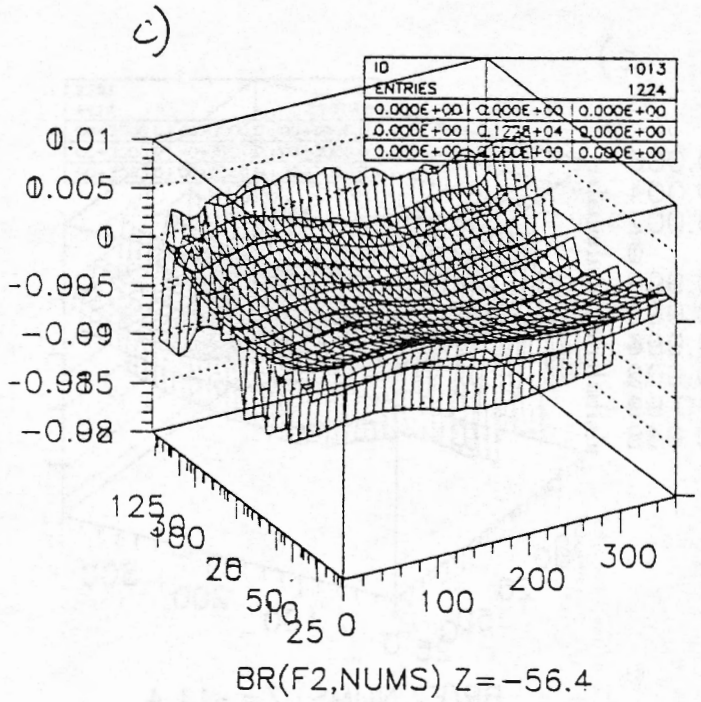
c)
ID 1013
ENTRIES 1224
0.01
0.005
0
-0.995
-0.99
-0.985
-0.98
125
100
75
50
25
0
100
200
300
BR(F2,NUMS) Z=-56.4

Table (1)

	SIM	RIC	MUL	ERR	FWHM/p (E-03)	FWHM/p (E-03) teta cut
1A	Bz=1.1,Br=0	Bz=1.1,Br=0	0	0	0.8	0.6
1B	=	=	1	0	2.3	2.2
2A	Bz=map,Br=0	Bz=1.1,Br=0	0	0	2.8	1.1
	=	=	1	0	3.4	2.4
3A	Bz=map,Br=0	Bz=map,Br=0	0	0	0.8	0.6
3B	=	=	1	0	2.3	2.2
3C	=	=	1	1	2.7	2.5
5A	Bz=map,Br=map	Bz=map,Br=0	0	0	1.4	0.7
5B	=	=	1	0	3.1	2.7
6A	Bz=map,Br=map	Bz=map	0	0	2.3	0.9
6B	=	Br=map+30G	1	0	3.3	2.4
6C			1	1	3.5	2.4
7A	Bz=map,Br=map	Bz=map,Br=map	0	0	0.9	0.6
7B	=	=	1	0	2.5	2.2
7C			1	1	2.7	2.3
8A	Bz=map,Br=map	Bz=map+-10G	0	0	0.9	0.7
8B	=	Br=map+-5G	1	0	2.6	2.2
			1	1	2.8	2.3

Poster 9/6/97 FRASCATI

The FINUDA apparatus

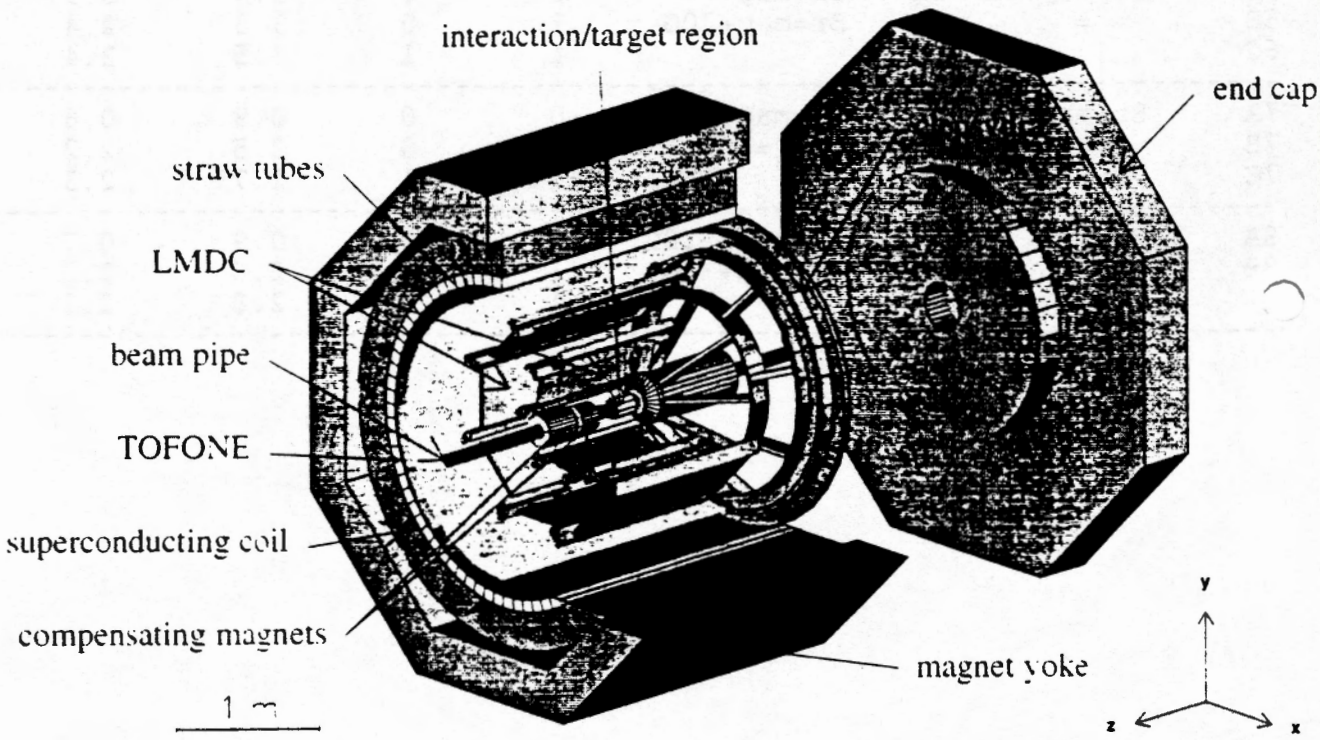

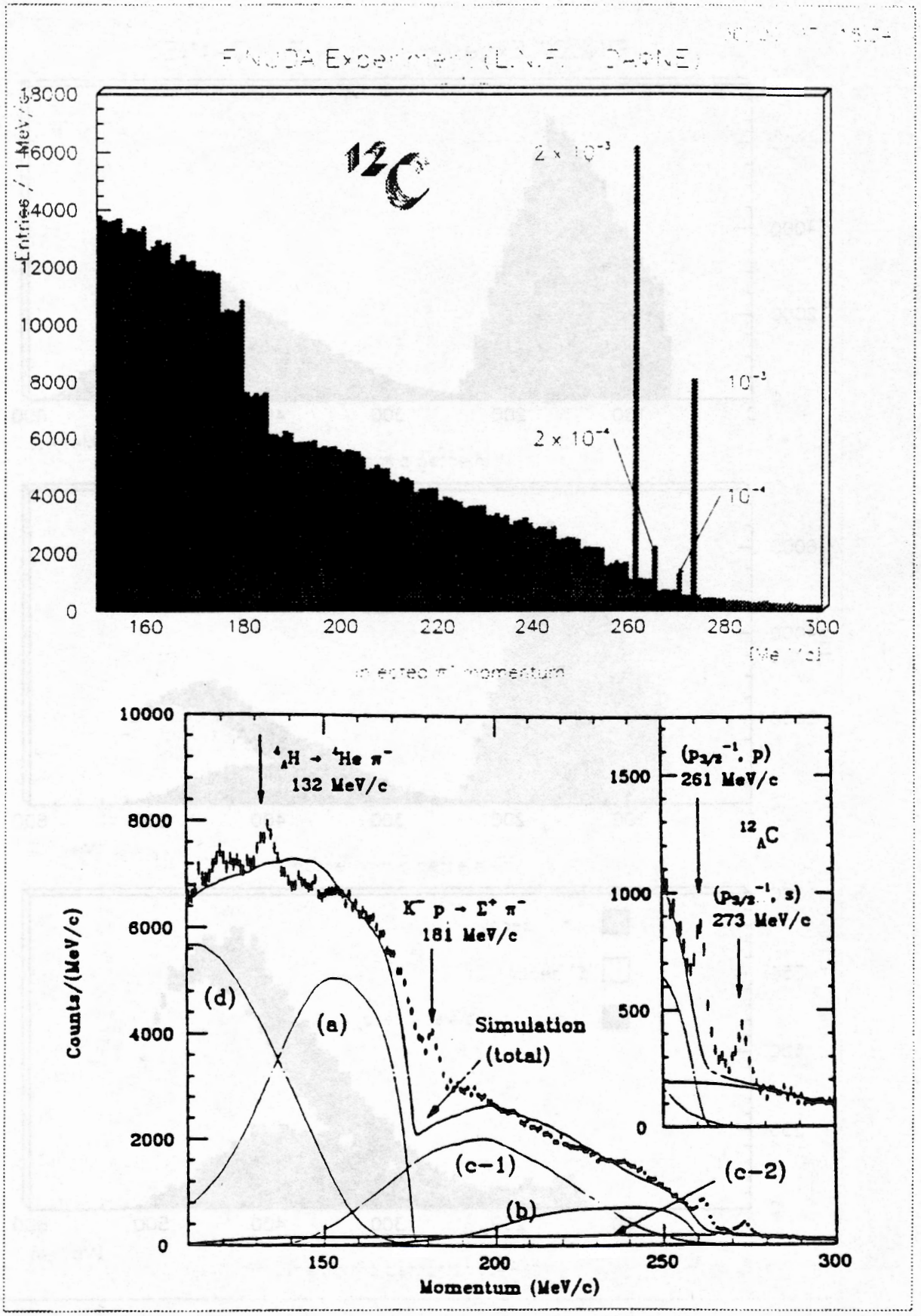
FINUDA Experiment (L.N.F. DAΦNE)
$^{12}_{\Lambda}C$
2×10^{-3}
10^{-3}
2×10^{-4}
10^{-4}
Entries / 1 MeV/c
18000
16000
14000
12000
10000
8000
6000
4000
2000
0
160
180
200
220
240
260
280
300
(MeV/c)
Counts/(MeV/c)
10000
8000
6000
4000
2000
0
$^{4}_{\Lambda}H \rightarrow {}^{4}He\ \pi^-$
132 MeV/c
$K^- p \rightarrow \Sigma^+ \pi^-$
181 MeV/c
(d)
(a)
Simulation
(total)
(c−1)
(c−2)
(b)
150
200
250
300
Momentum (MeV/c)
$(P_{3/2}^{-1}, p)$
261 MeV/c
$^{12}_{\Lambda}C$
$(P_{3/2}^{-1}, s)$
273 MeV/c
1500
1000
500
0

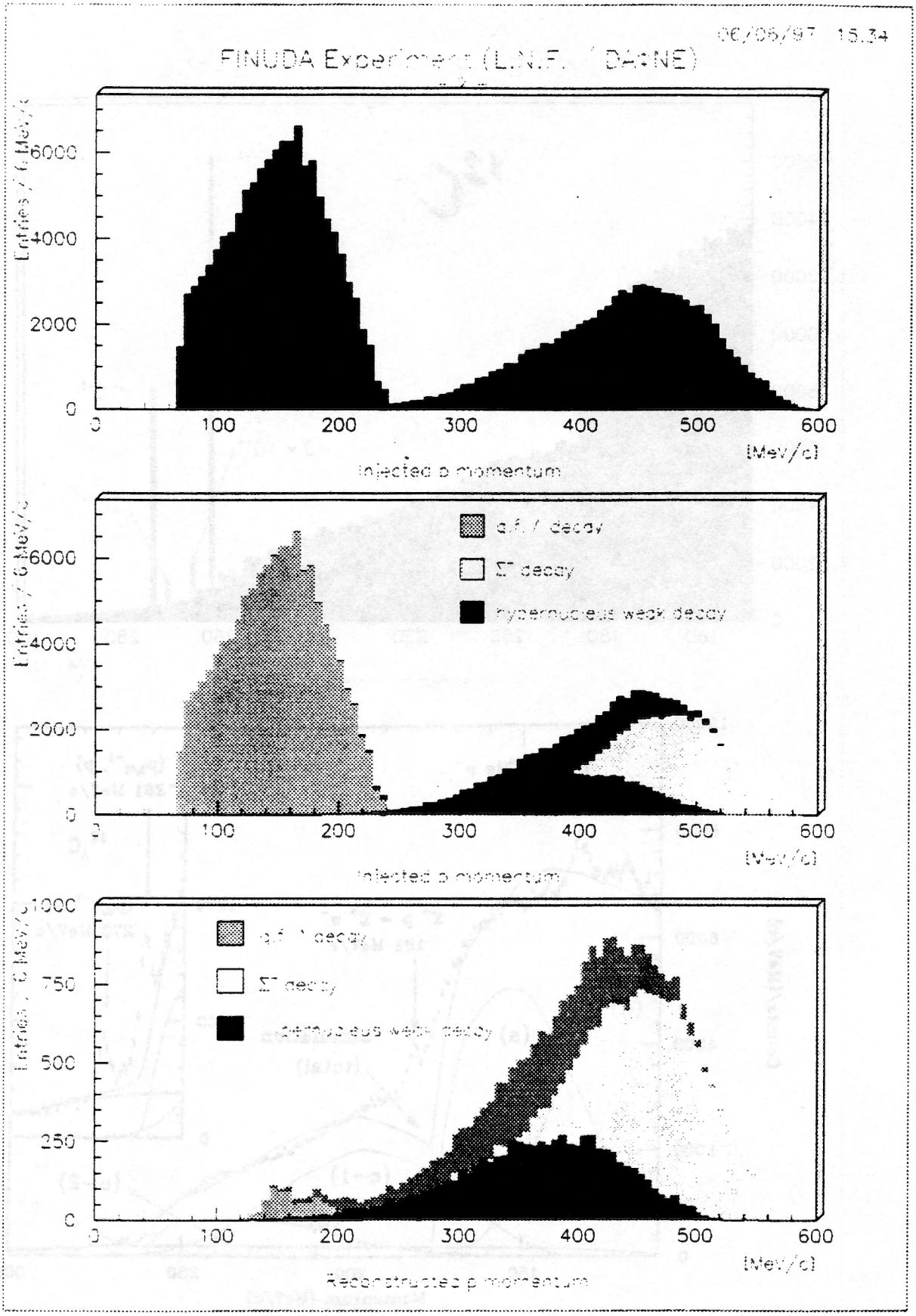
06/06/97 15.34
FINUDA Experiment (L.N.F. - DA:NE)
Entries / 6 MeV/c
6000
4000
2000
0
0
100
200
300
400
500
600
[MeV/c]
Injected p momentum
Entries / 6 MeV/c
6000
4000
2000
0
0
100
200
300
400
500
600
[MeV/c]
Injected p momentum
Σ⁻ decay
hypernucleus weak decay
Entries / 6 MeV/c
1000
750
500
250
0
0
100
200
300
400
500
600
[MeV/c]
Reconstructed p momentum
Σ⁻ decay

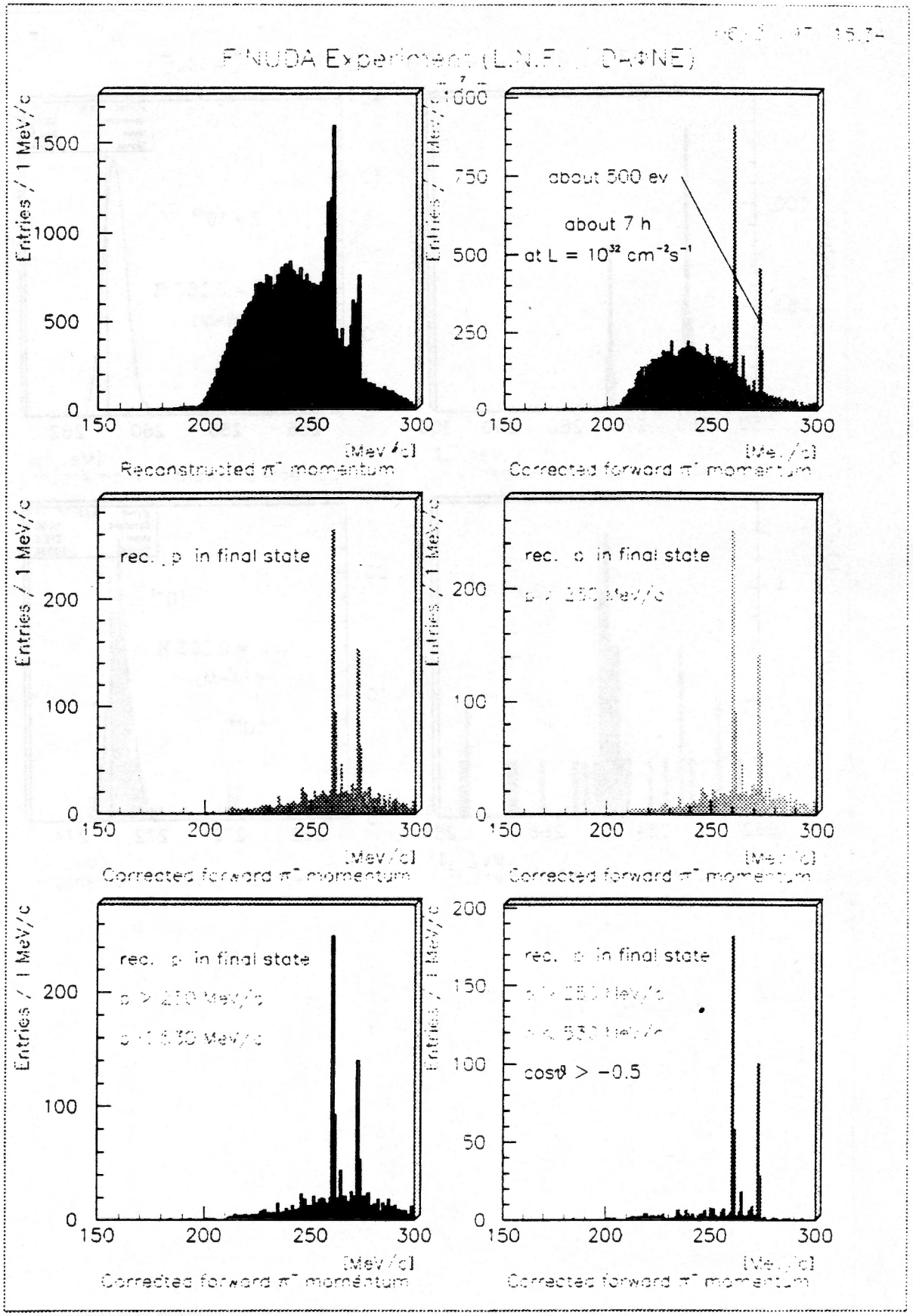
FINUDA Experiment (L.N.F. DAΦNE)
Entries / 1 MeV/c
Reconstructed π⁻ momentum
[MeV/c]
about 500 ev
about 7 h
at L = 10³² cm⁻²s⁻¹
Corrected forward π⁻ momentum
rec. p in final state
rec. d in final state
p > 250 MeV/c
rec. p in final state
p > 270 MeV/c
cosϑ > −0.5

FINUDA Experiment (L.N.F. DAΦNE)

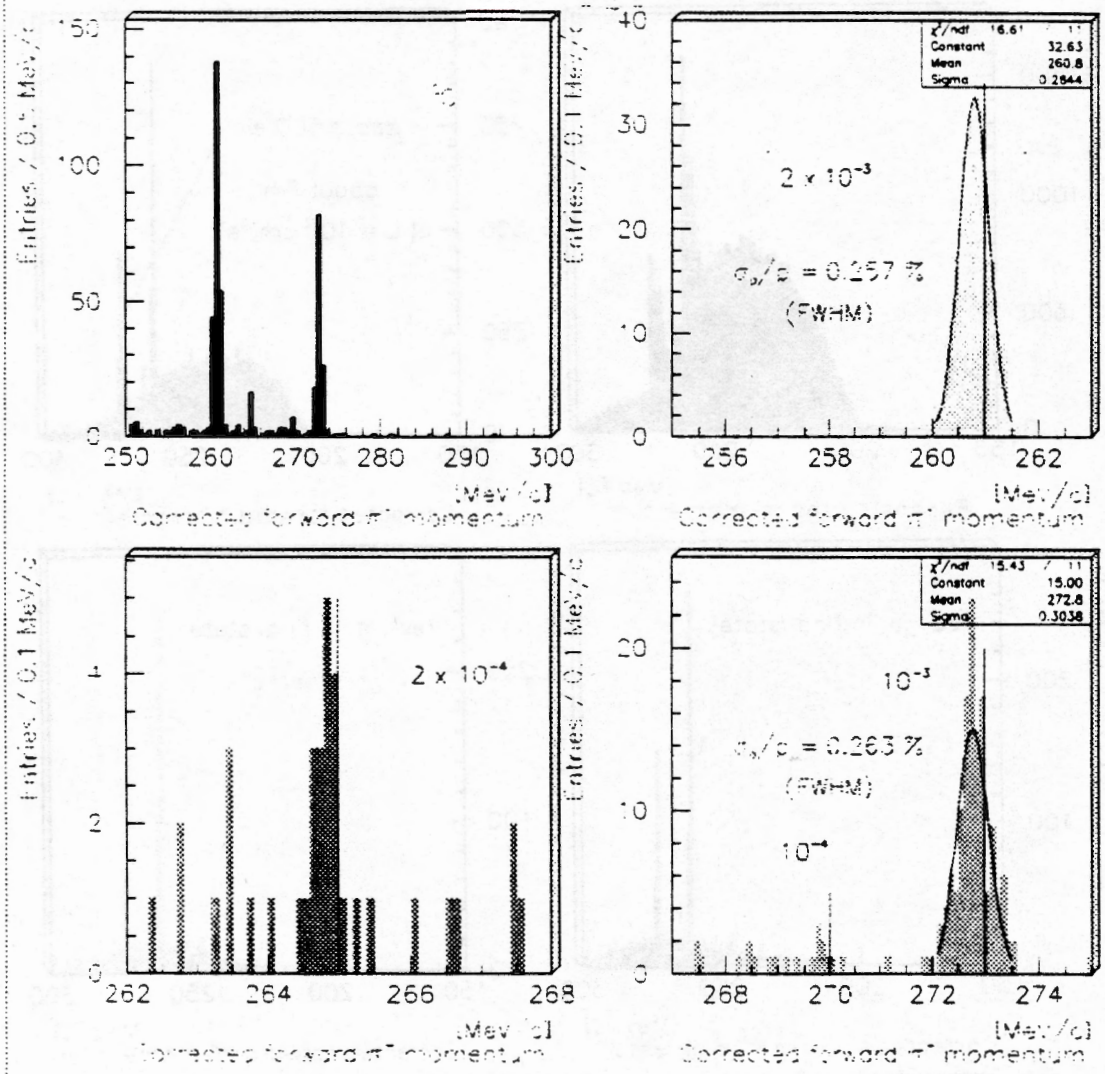

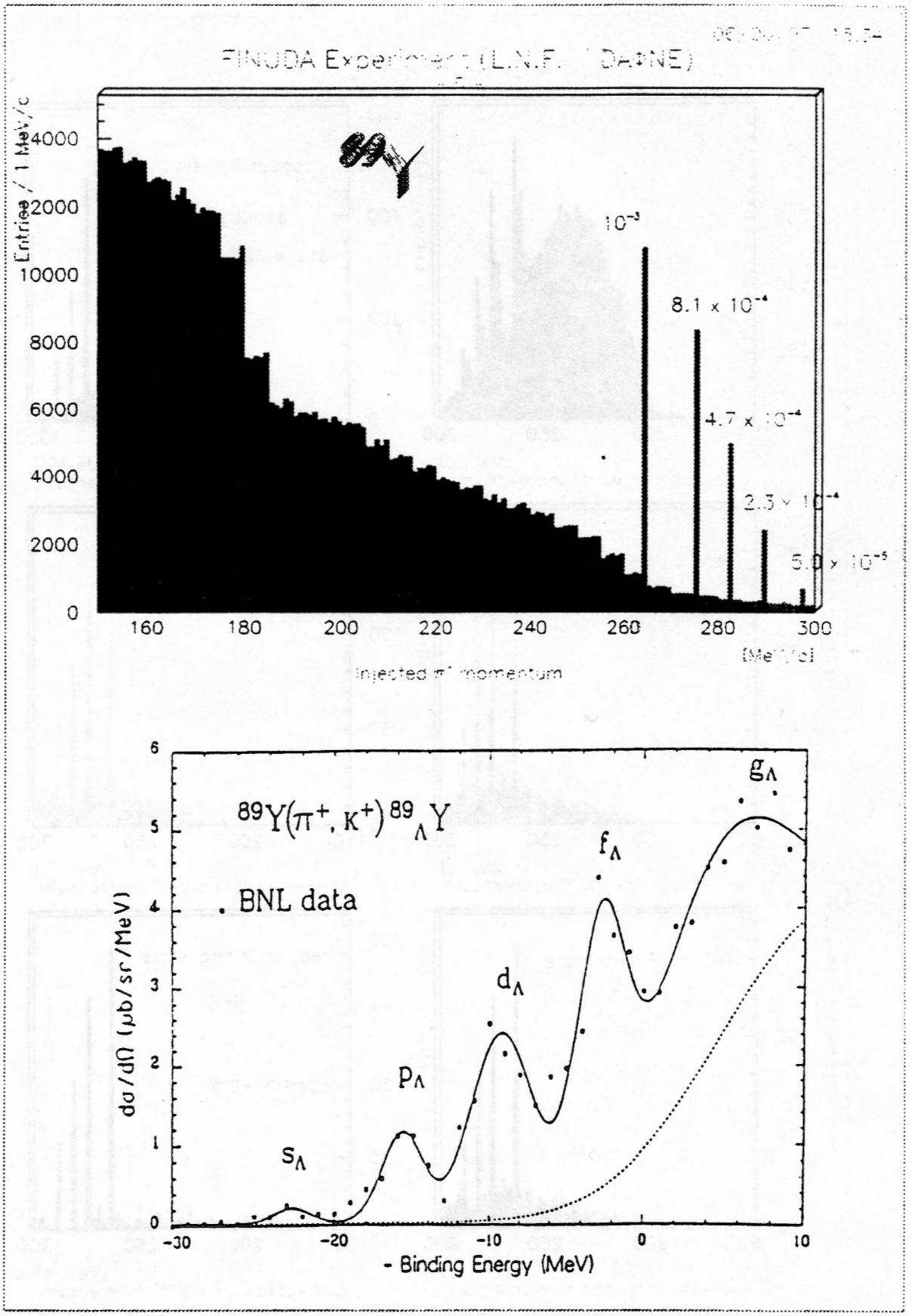
FINUDA Experiment (L.N.F. DAΦNE)
^{89}Y
Entries / 1 MeV/c
14000
12000
10000
8000
6000
4000
2000
0
160
180
200
220
240
260
280
300
10^{-3}
8.1×10^{-4}
4.7×10^{-4}
2.3×10^{-4}
5.0×10^{-5}
Injected π^- momentum
$^{89}Y(\pi^+, K^+)^{89}{}_{\Lambda}Y$
BNL data
s_Λ
p_Λ
d_Λ
f_Λ
g_Λ
$d\sigma/d\Omega$ (μb/sr/MeV)
- Binding Energy (MeV)

FINUDA Experiment (L.N.F. DAΦNE)

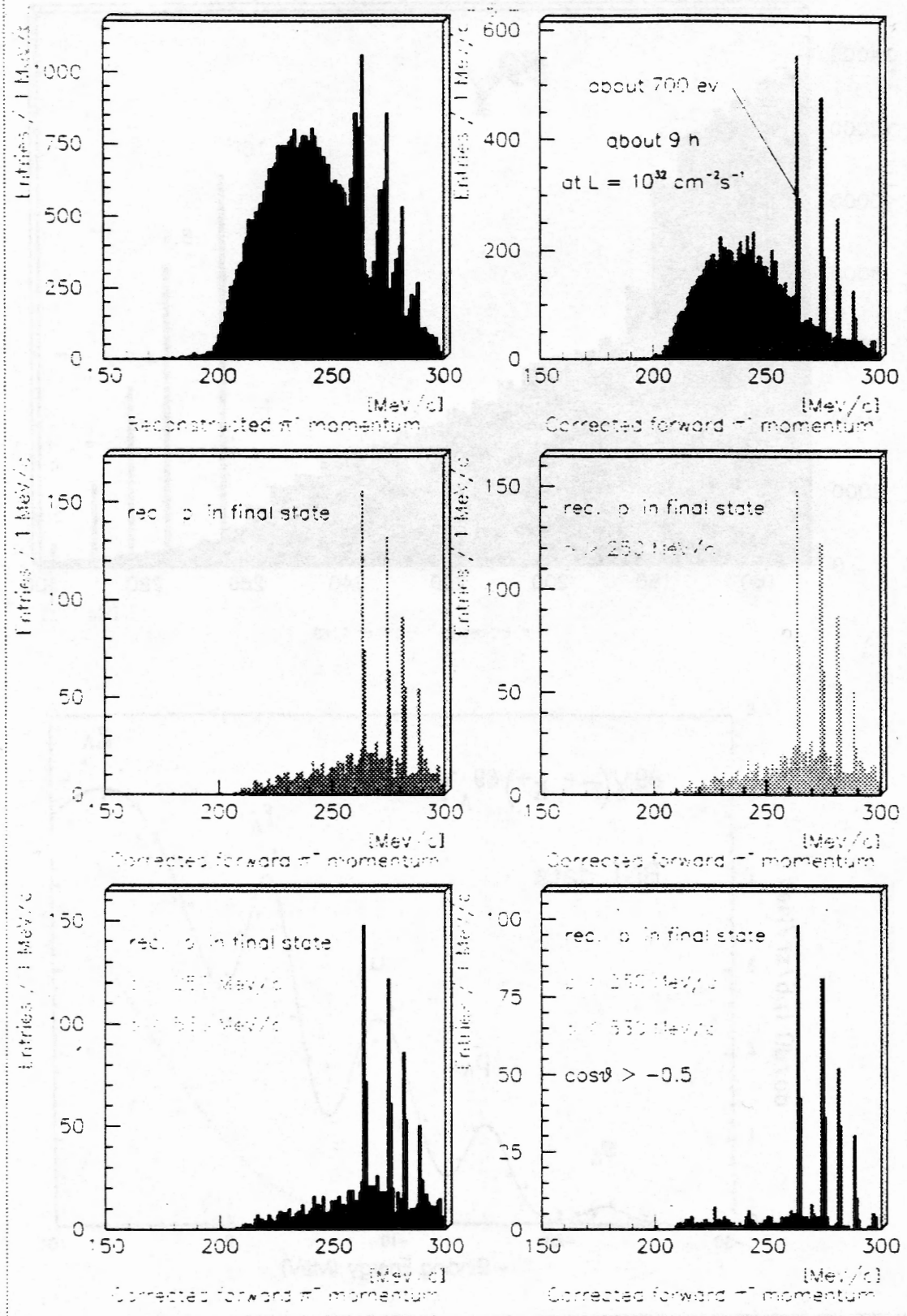

FINUDA Experiment (L.N.F. DAΦNE)

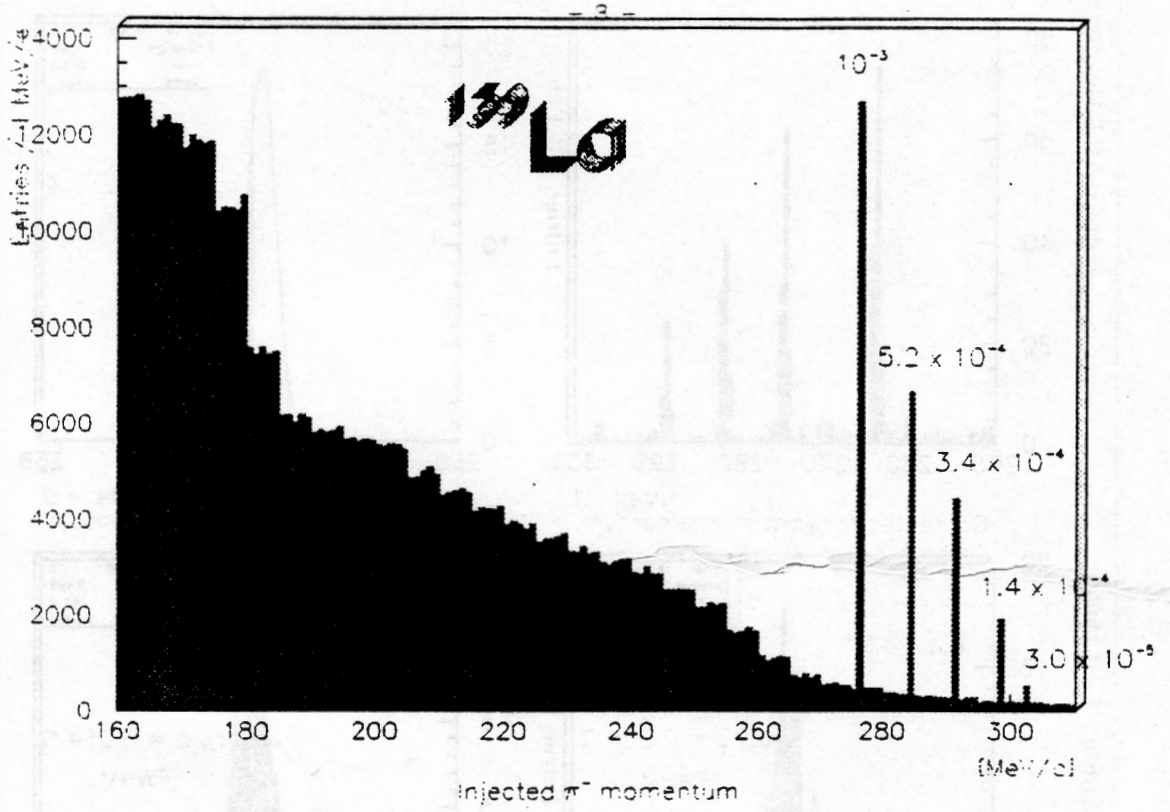

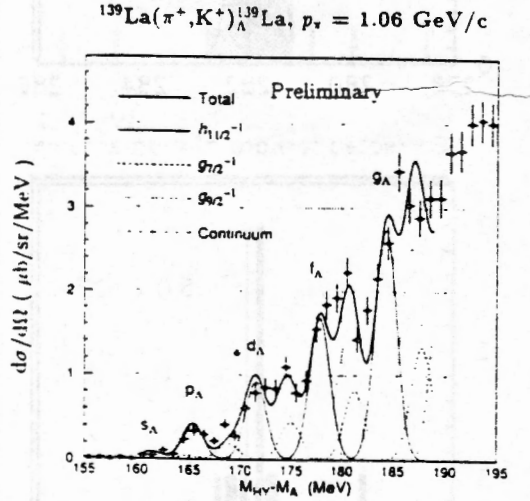

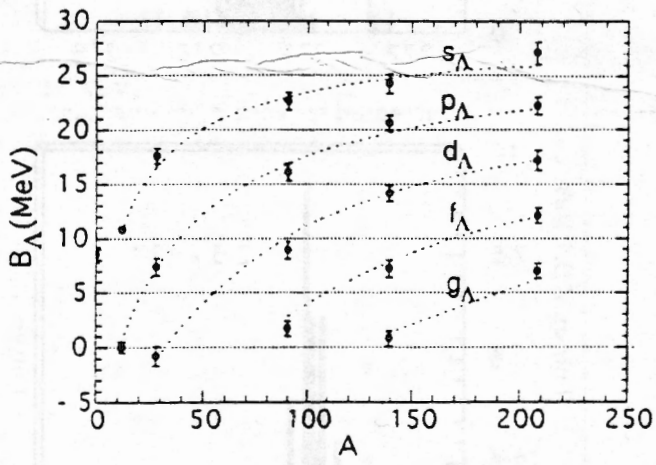

S. Ajimura et al. / Nuclear Physics A585 (1995) 173c-182c

FINUDA Experiment (L.N.F. DAΦNE)

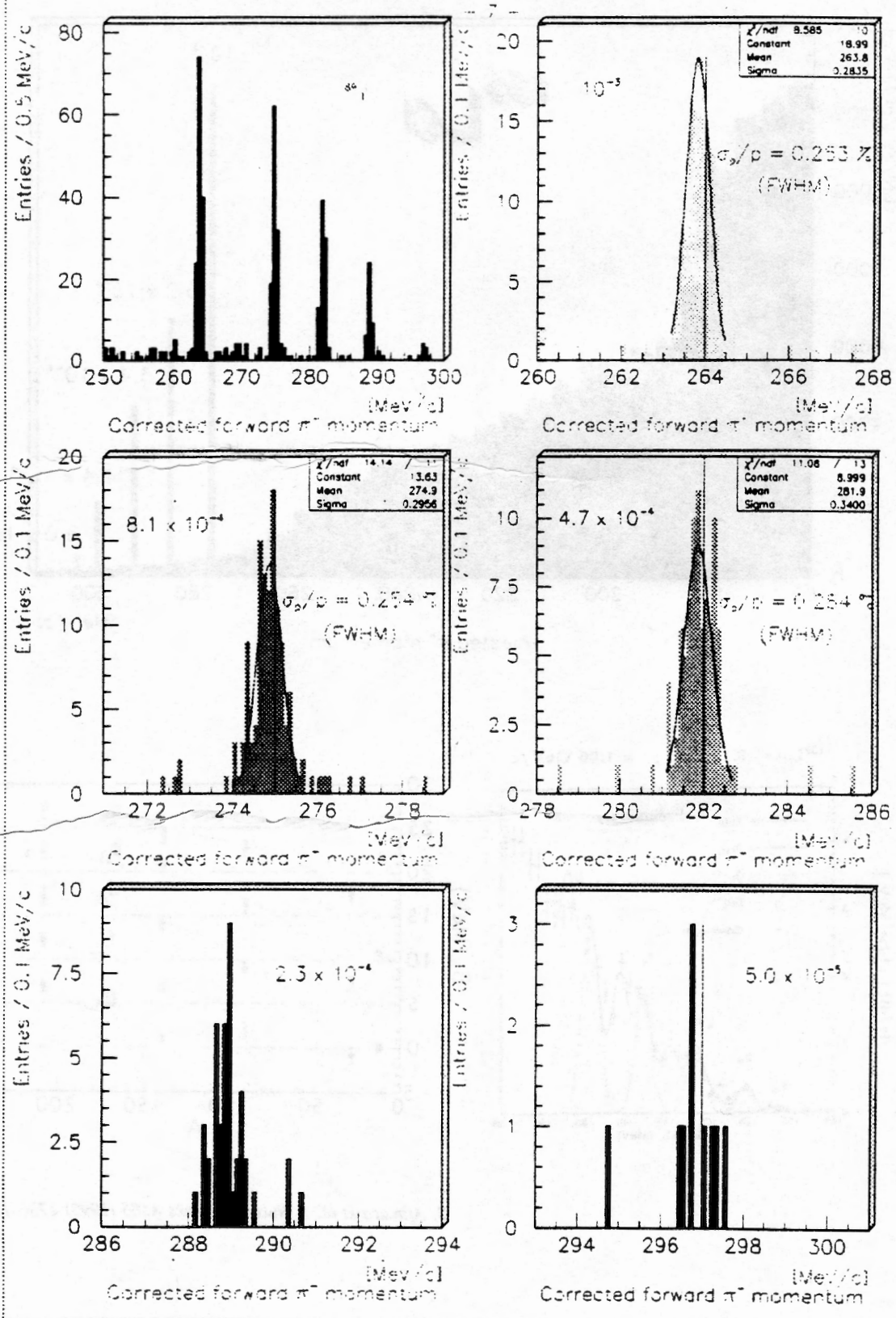

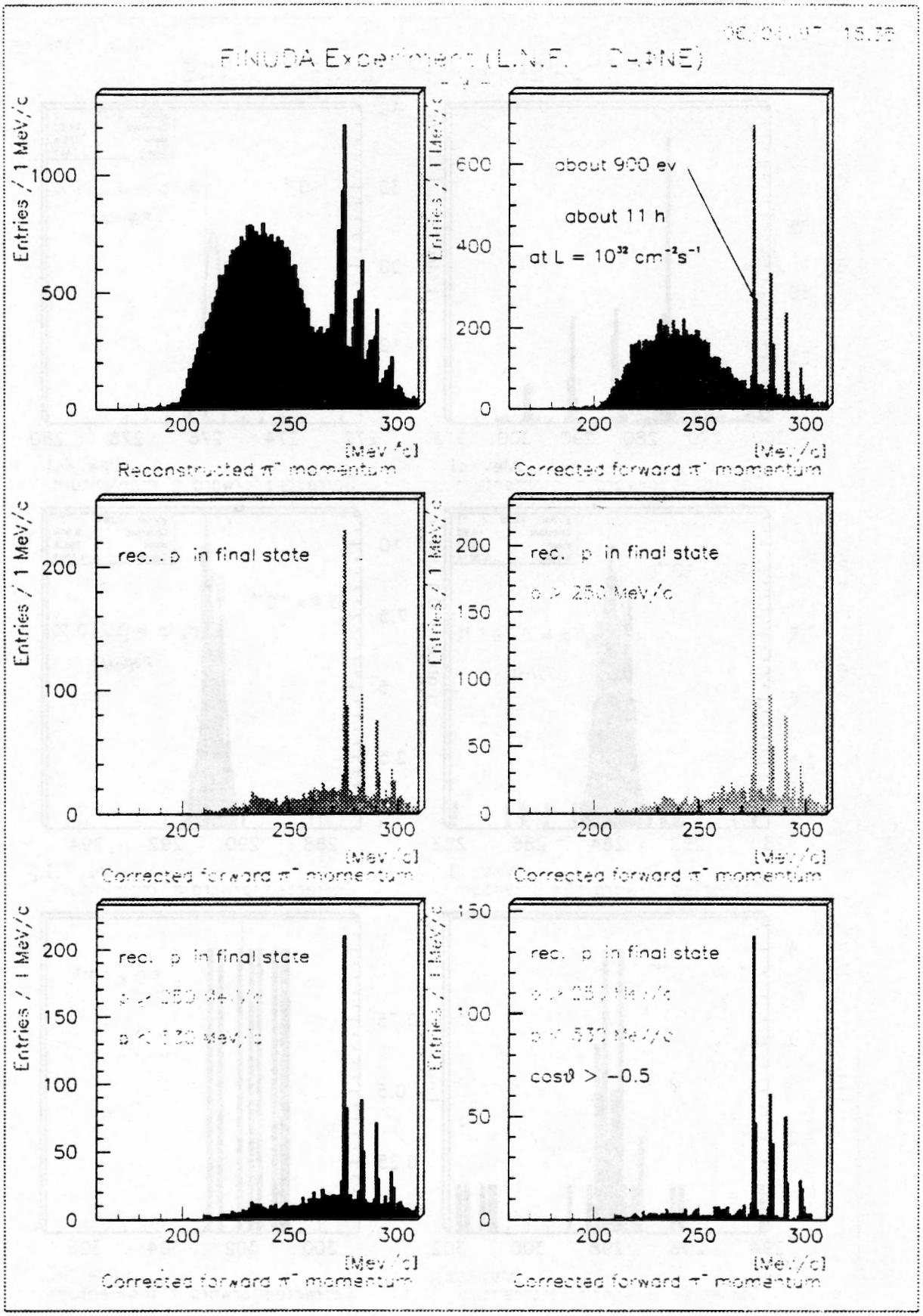
FINUDA Experiment (L.N.F. DAΦNE)
Entries / 1 MeV/c
Reconstructed π⁻ momentum
about 900 ev
about 11 h
at L = 10³² cm⁻²s⁻¹
Corrected forward π⁻ momentum
rec. p in final state
rec. p in final state
p > 250 MeV/c
rec. p in final state
p > 250 MeV/c
p < 530 MeV/c
rec. p in final state
p > 250 MeV/c
p < 530 MeV/c
cosϑ > −0.5
[Mev/c]

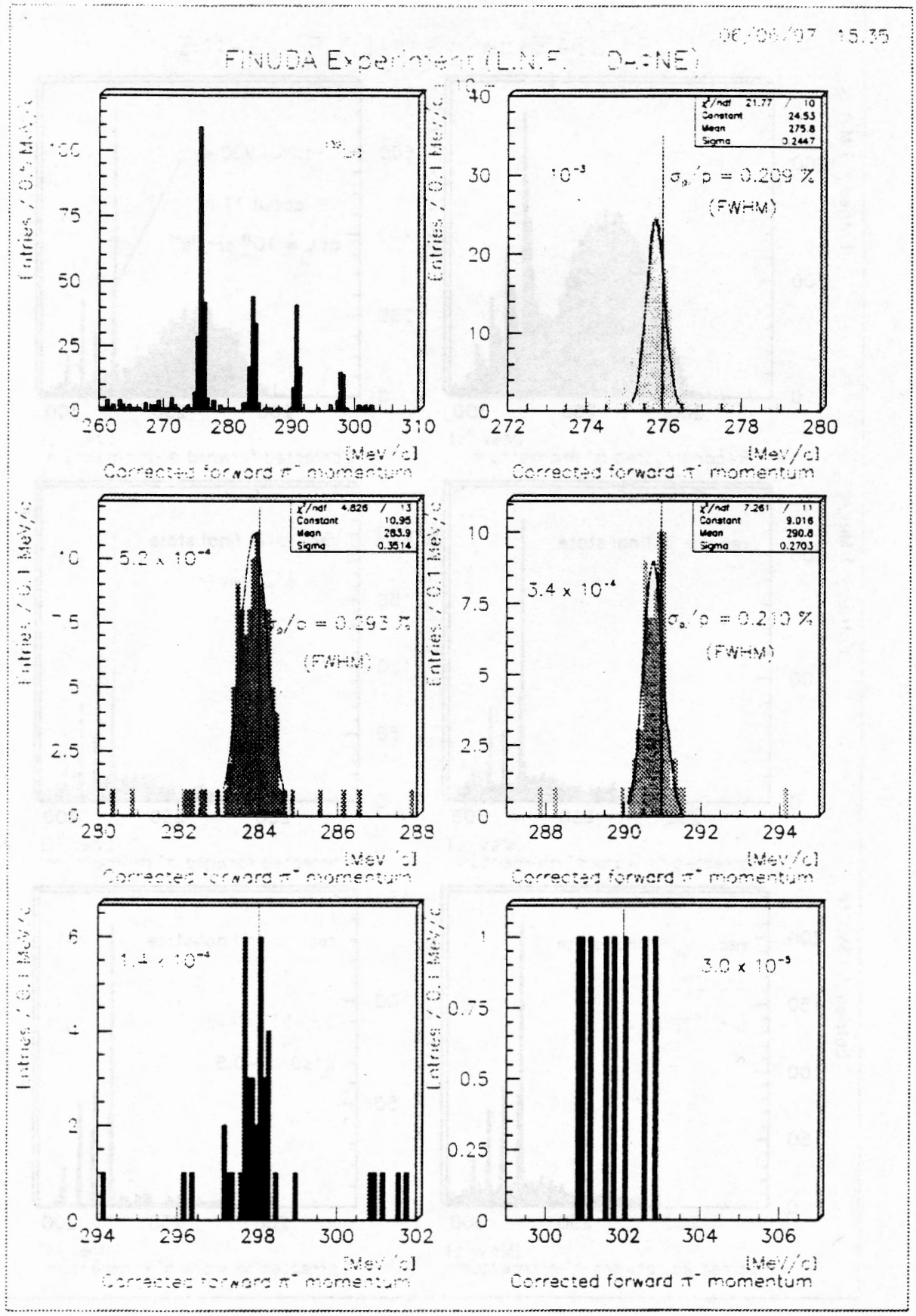
06/06/07 15.35
FINUDA Experiment (L.N.F. DAΦNE)
Entries / 0.5 MeV/c
Entries / 0.1 MeV/c
[MeV/c]
Corrected forward π⁻ momentum
10⁻³
σp/p = 0.209 %
(FWHM)
χ²/ndf 21.77 / 10
Constant 24.53
Mean 275.8
Sigma 0.2447
5.2 x 10⁻⁴
σp/p = 0.293 %
(FWHM)
χ²/ndf 4.826 / 13
Constant 10.95
Mean 283.9
Sigma 0.3514
3.4 x 10⁻⁴
σp/p = 0.210 %
(FWHM)
χ²/ndf 7.261 / 11
Constant 9.016
Mean 290.8
Sigma 0.2703
1.4 x 10⁻⁴
3.0 x 10⁻⁵

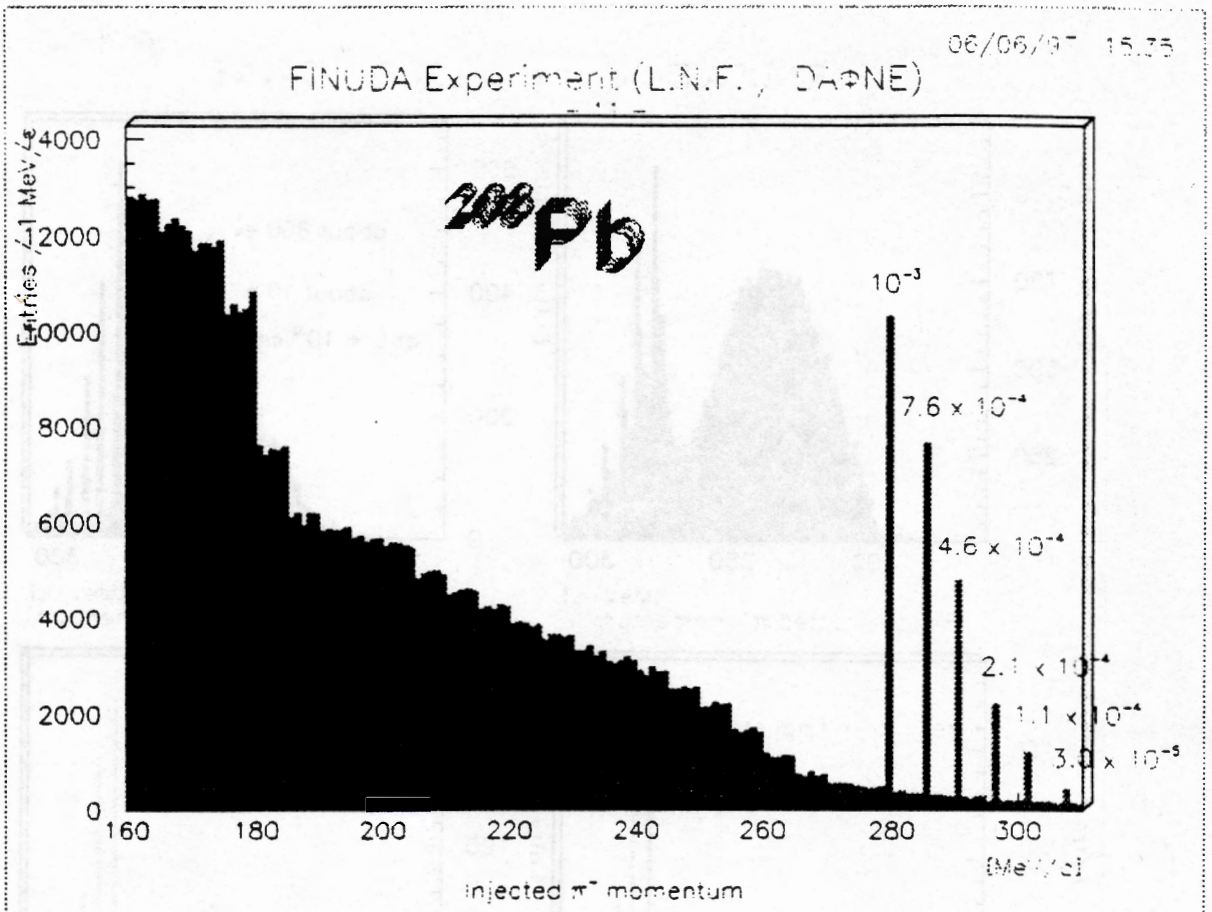

$^{208}Pb(\pi^+,K^+)^{208}_{\Lambda}Pb$, $p_\pi = 1.06$ GeV/c

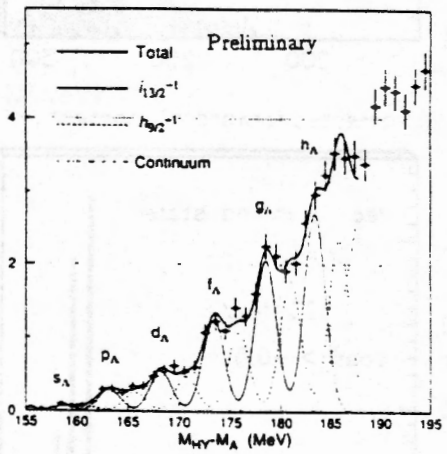

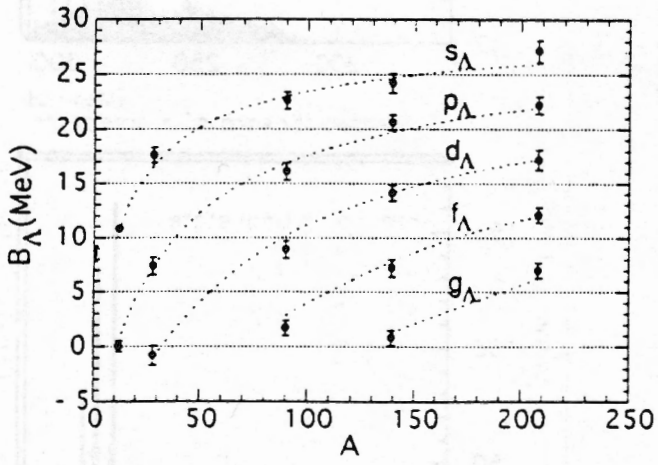

S. Ajimura et al. / Nuclear Physics A585 (1995) 173c-182c

FINUDA Experiment (L.N.F. DAΦNE)

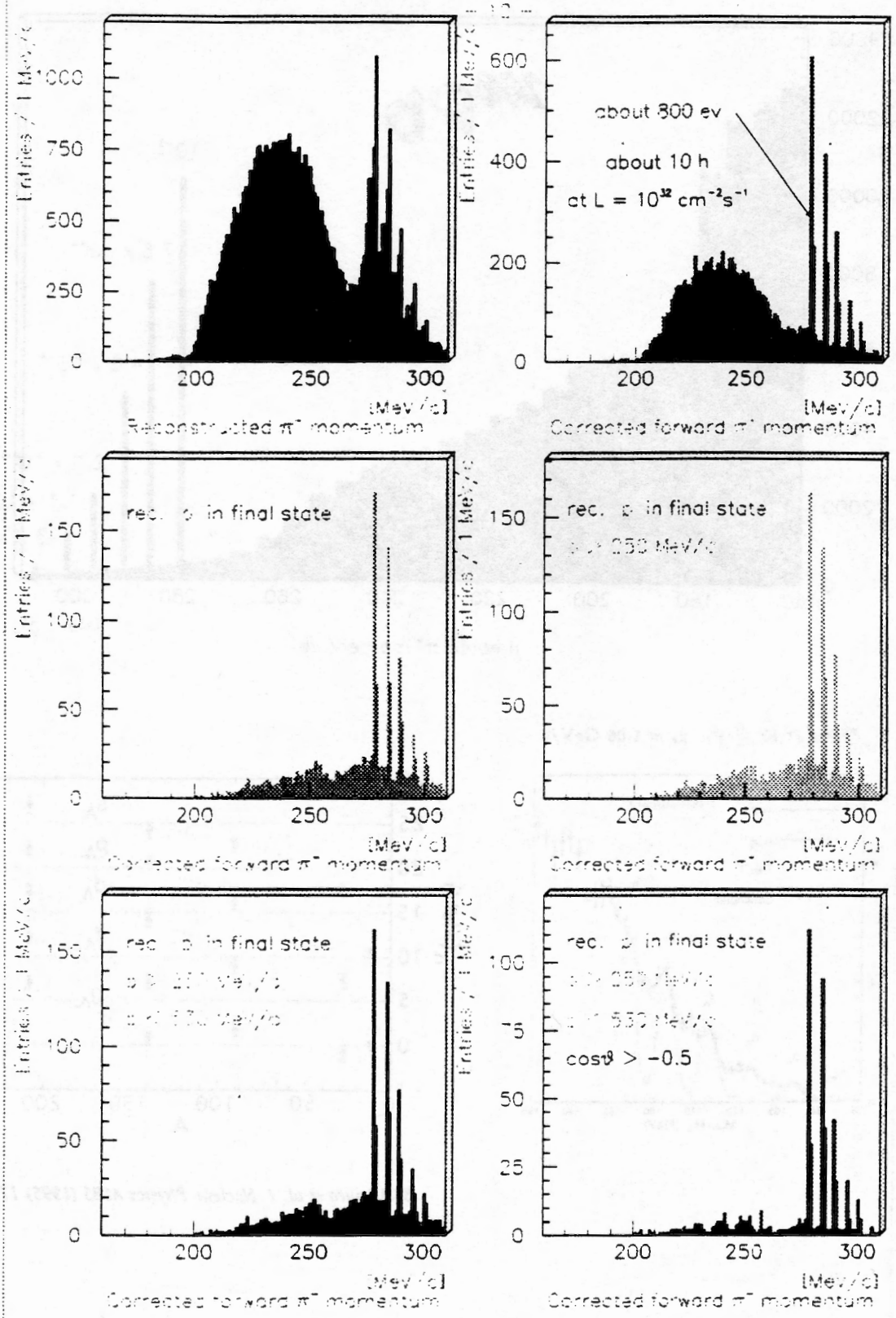

FINUDA Experiment (L.N.F. DAΦNE)

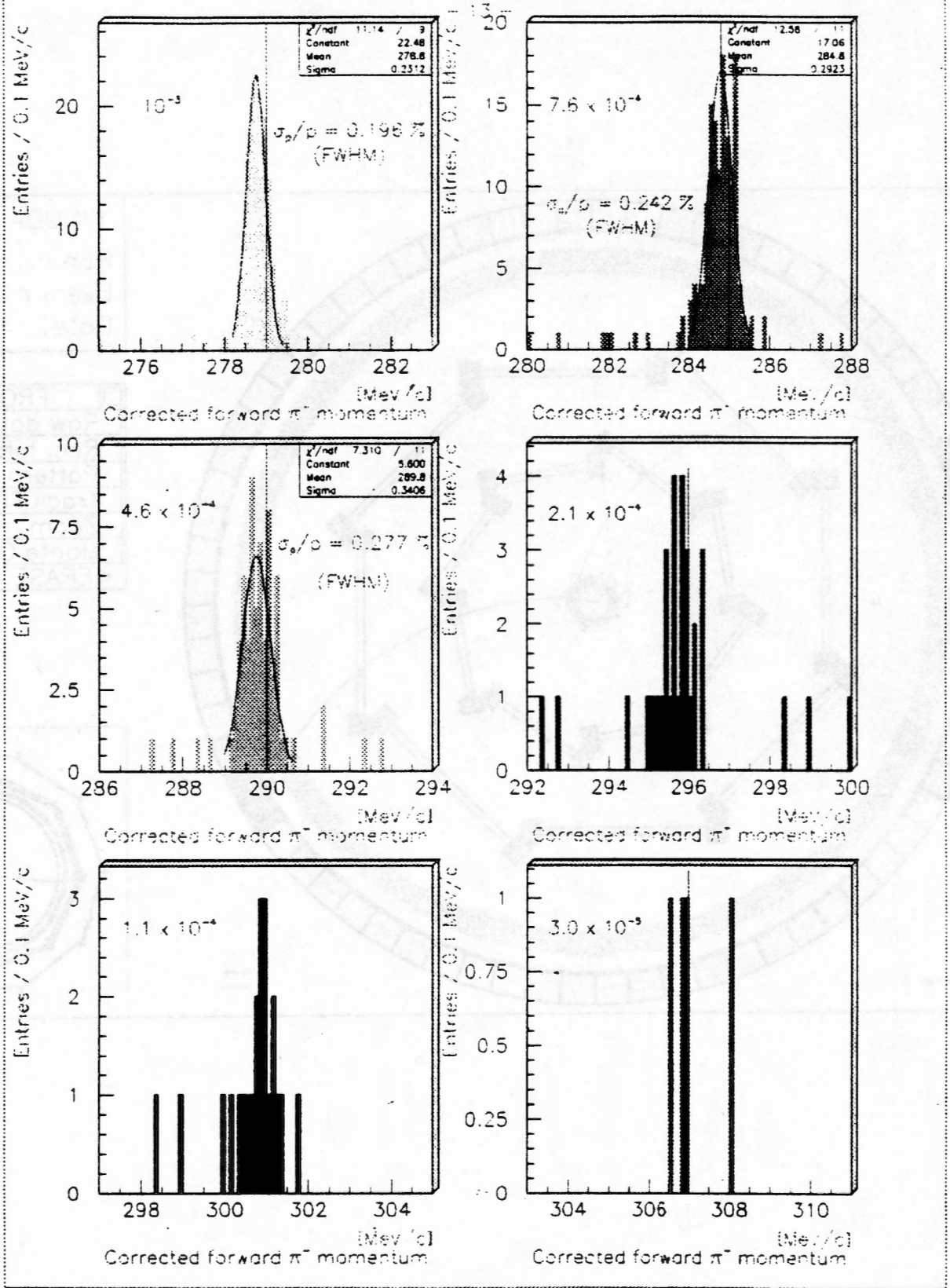

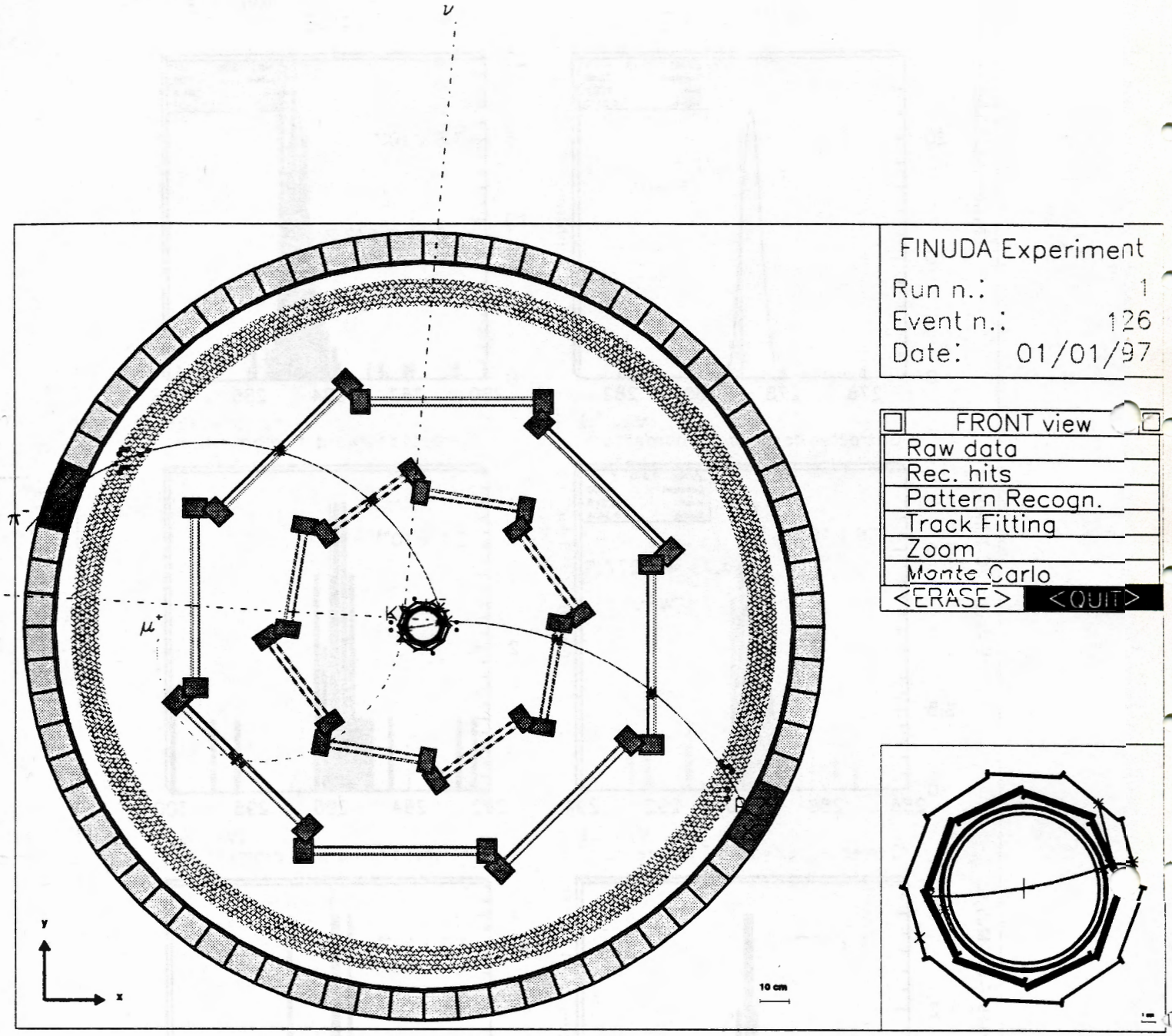
ν
π⁻
μ⁺
K⁻
p
y
x
10 cm
FINUDA Experiment
Run n.: 1
Event n.: 126
Date: 01/01/97
FRONT view
Raw data
Rec. hits
Pattern Recogn.
Track Fitting
Zoom
Monte Carlo
<ERASE>
<QUIT>

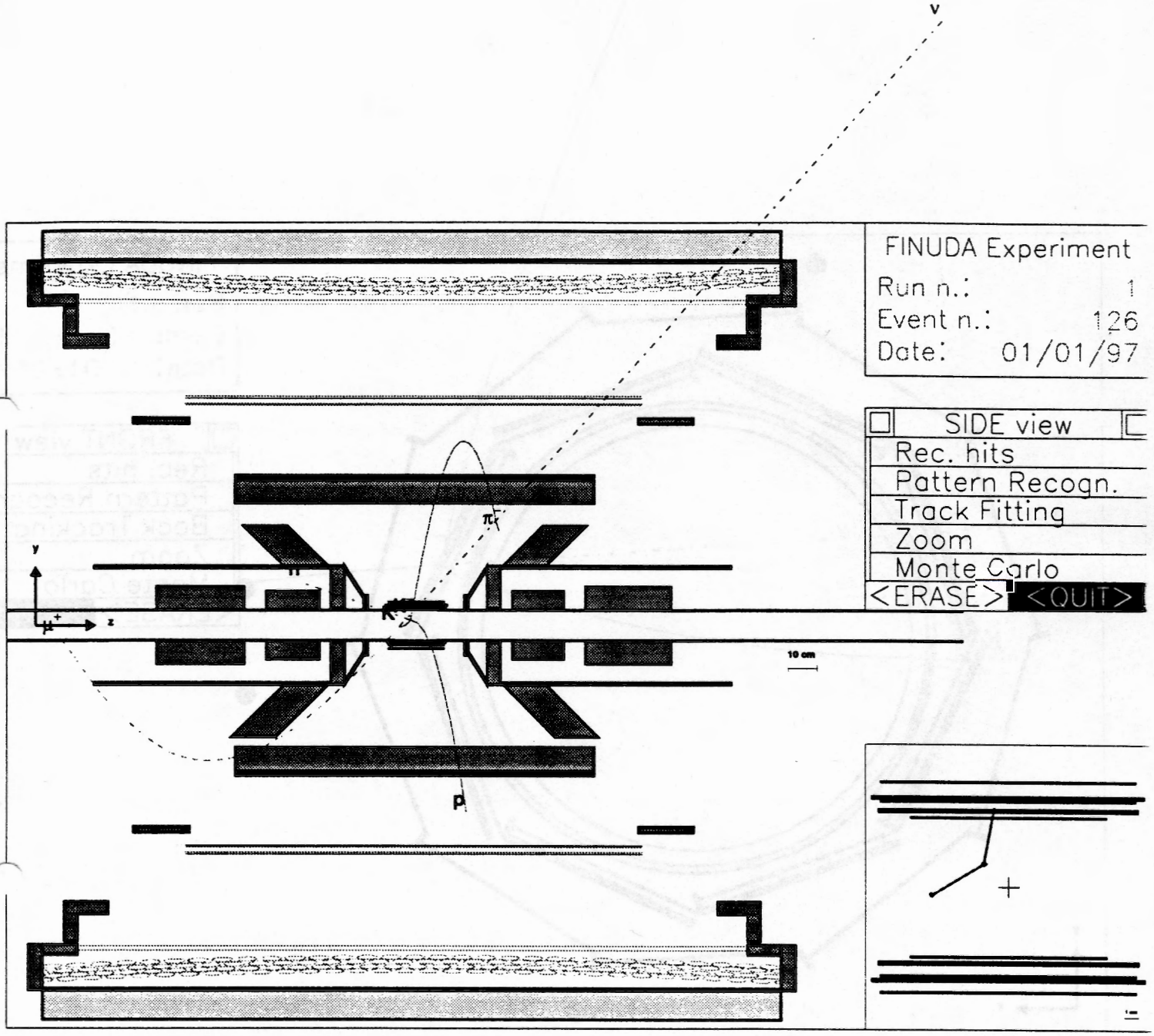
FINUDA Experiment
Run n.: 1
Event n.: 126
Date: 01/01/97
SIDE view
Rec. hits
Pattern Recogn.
Track Fitting
Zoom
Monte Carlo
<ERASE>
<QUIT>
10 cm
y
z

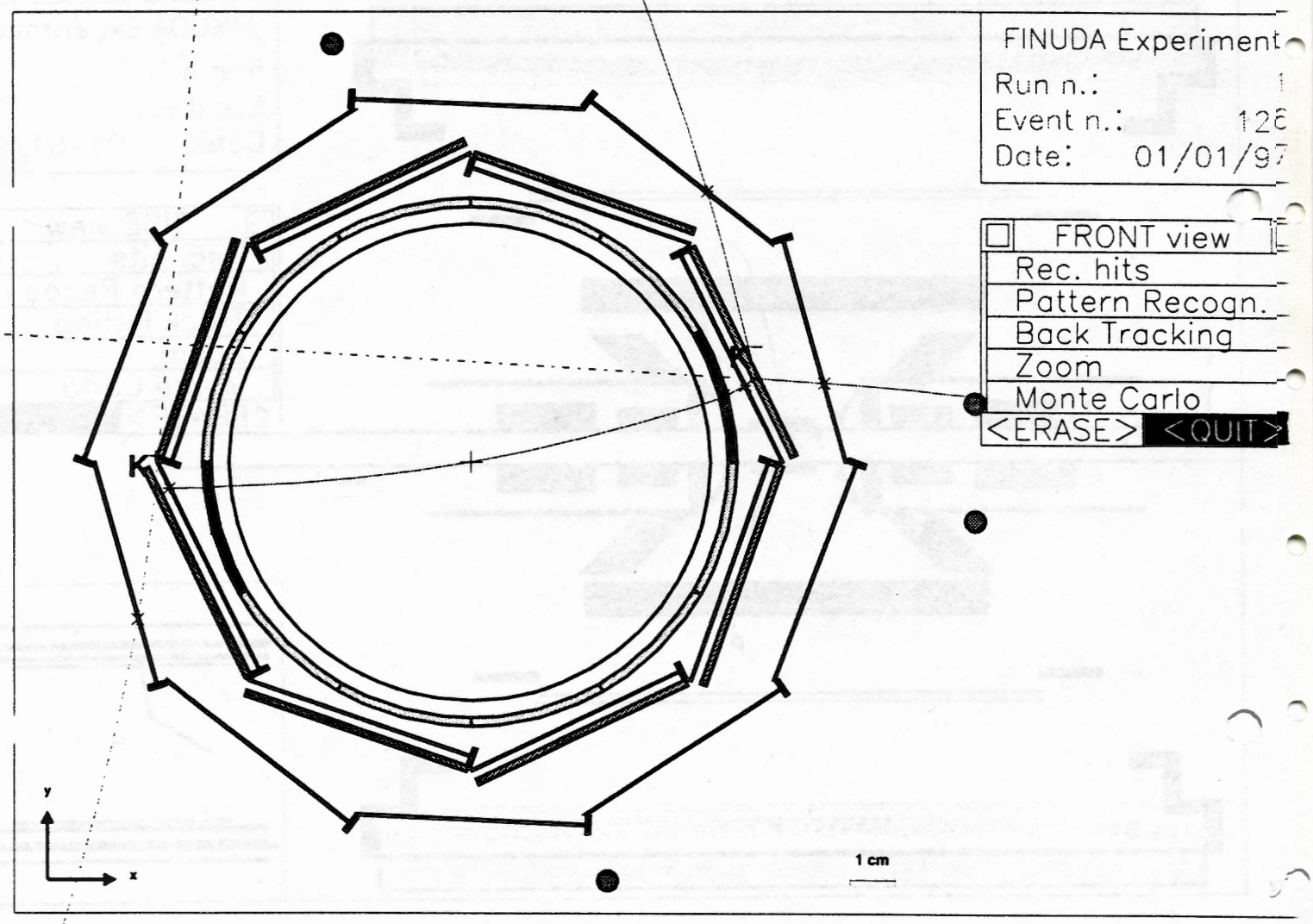
FINUDA Experiment
Run n.: 1
Event n.: 126
Date: 01/01/97
FRONT view
Rec. hits
Pattern Recogn.
Back Tracking
Zoom
Monte Carlo
<ERASE>
<QUIT>
y
x
1 cm

Calcolo di spettri con sottrazione di fondo

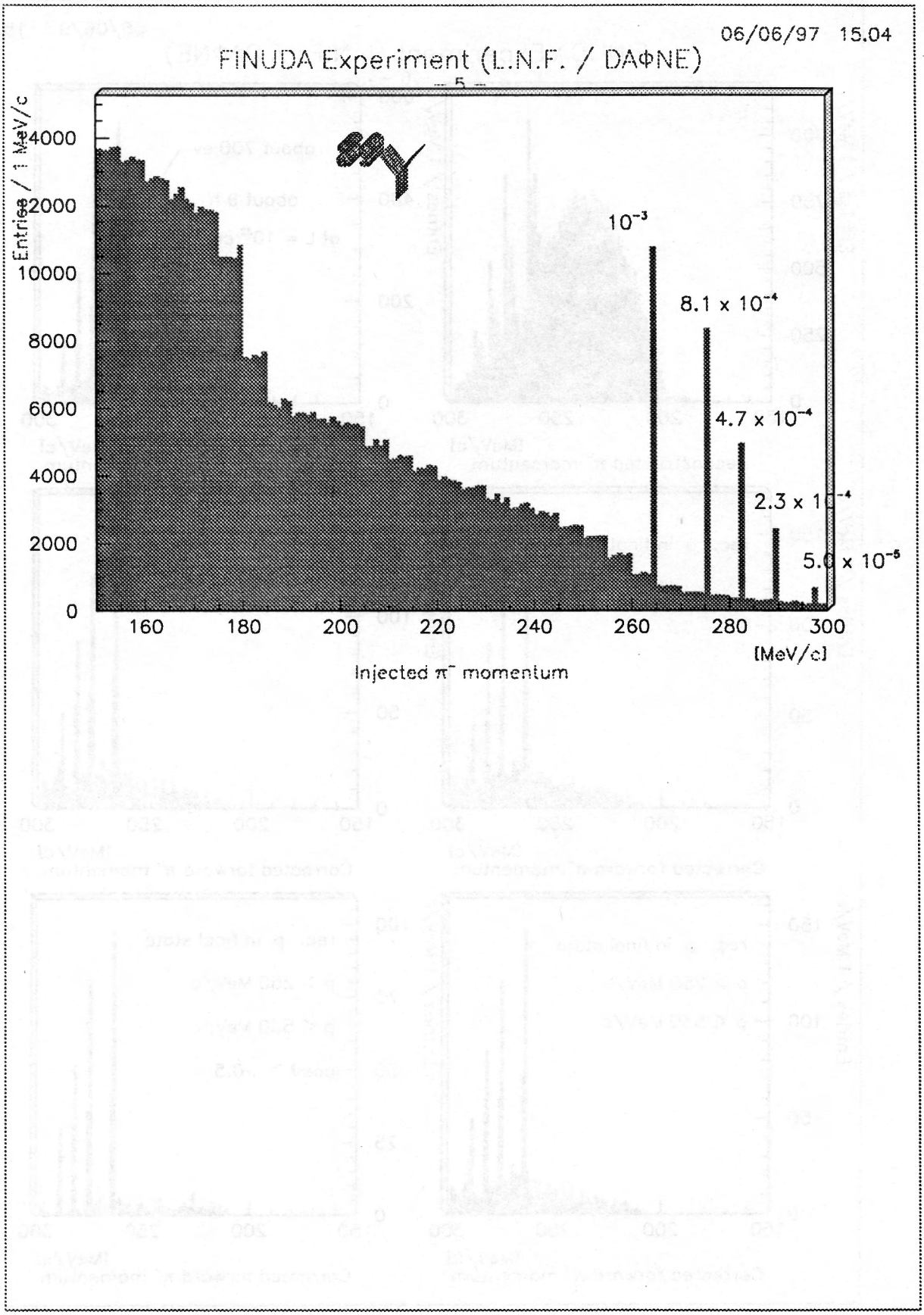

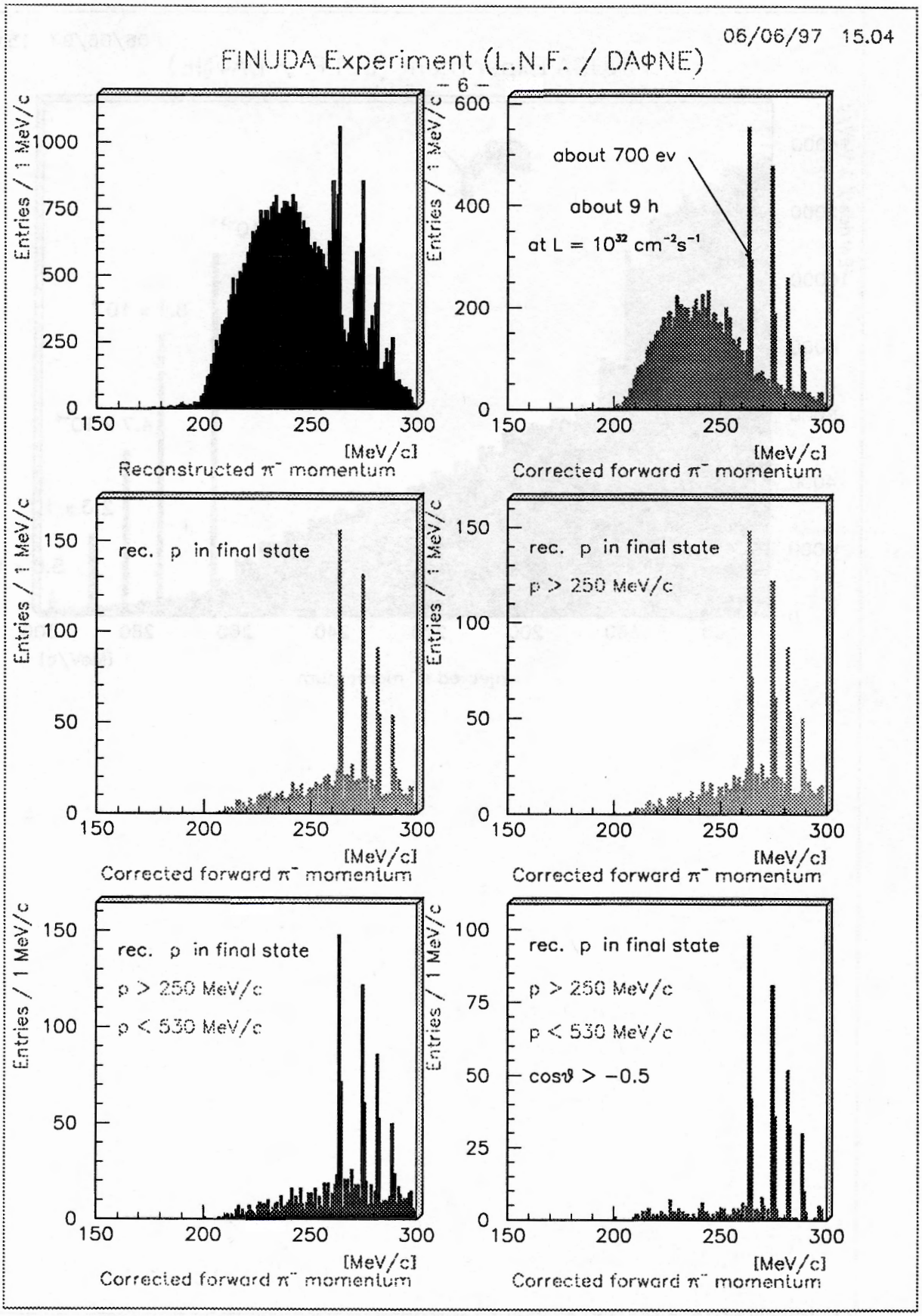
06/06/97 15.04
FINUDA Experiment (L.N.F. / DAΦNE)
Entries / 1 MeV/c
[MeV/c]
Reconstructed π⁻ momentum
about 700 ev
about 9 h
at L = 10³² cm⁻²s⁻¹
Corrected forward π⁻ momentum
rec. p in final state
p > 250 MeV/c
p < 530 MeV/c
cosϑ > −0.5

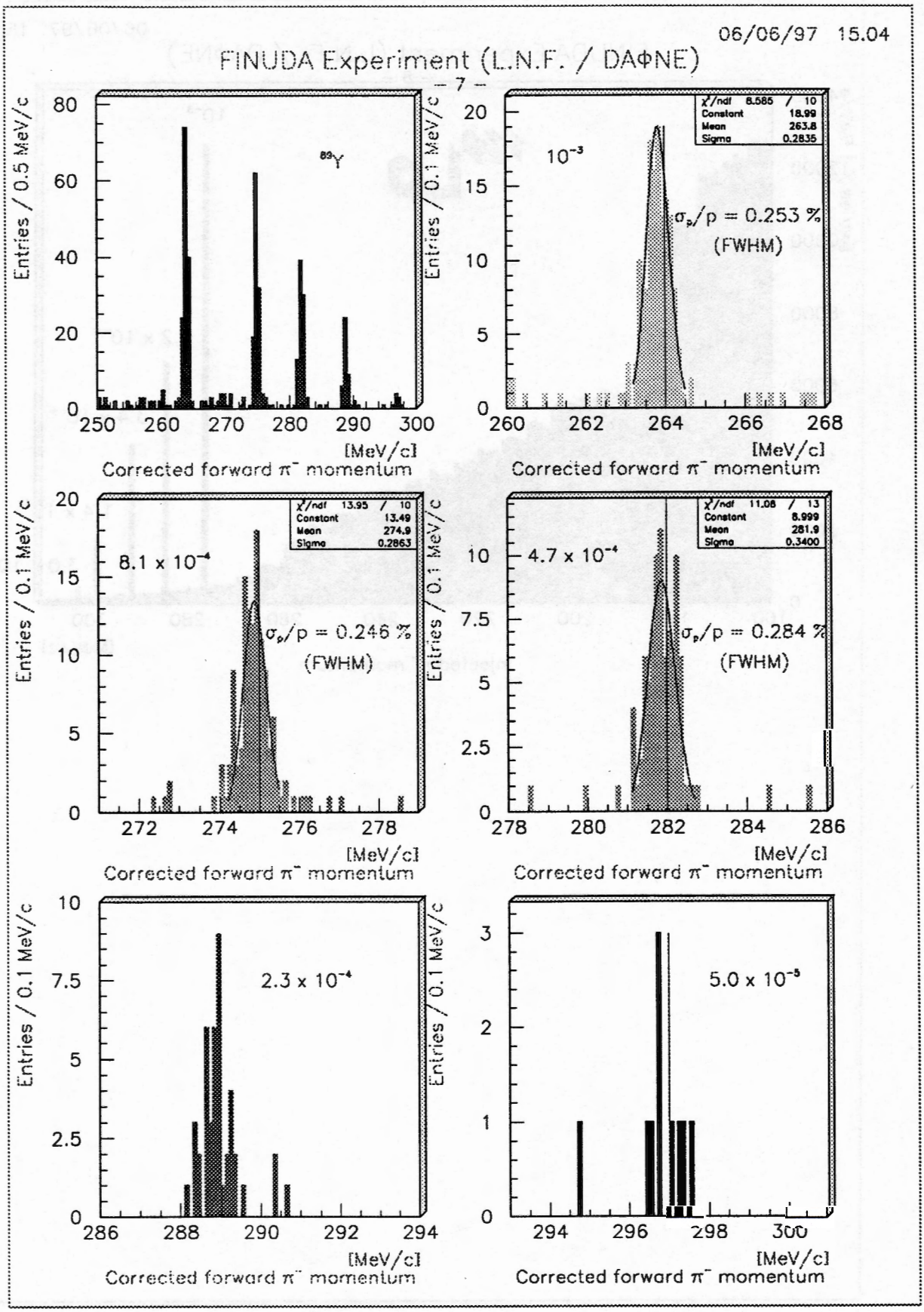
06/06/97 15.04
FINUDA Experiment (L.N.F. / DAΦNE)
Entries / 0.5 MeV/c
89Y
Entries / 0.1 MeV/c
χ²/ndf 8.585 / 10
Constant 18.99
Mean 263.8
Sigma 0.2835
10⁻³
σp/p = 0.253 %
(FWHM)
[MeV/c]
Corrected forward π⁻ momentum
Entries / 0.1 MeV/c
χ²/ndf 13.95 / 10
Constant 13.49
Mean 274.9
Sigma 0.2863
8.1 x 10⁻⁴
σp/p = 0.246 %
(FWHM)
χ²/ndf 11.08 / 13
Constant 8.999
Mean 281.9
Sigma 0.3400
4.7 x 10⁻⁴
σp/p = 0.284 %
(FWHM)
2.3 x 10⁻⁴
5.0 x 10⁻⁵

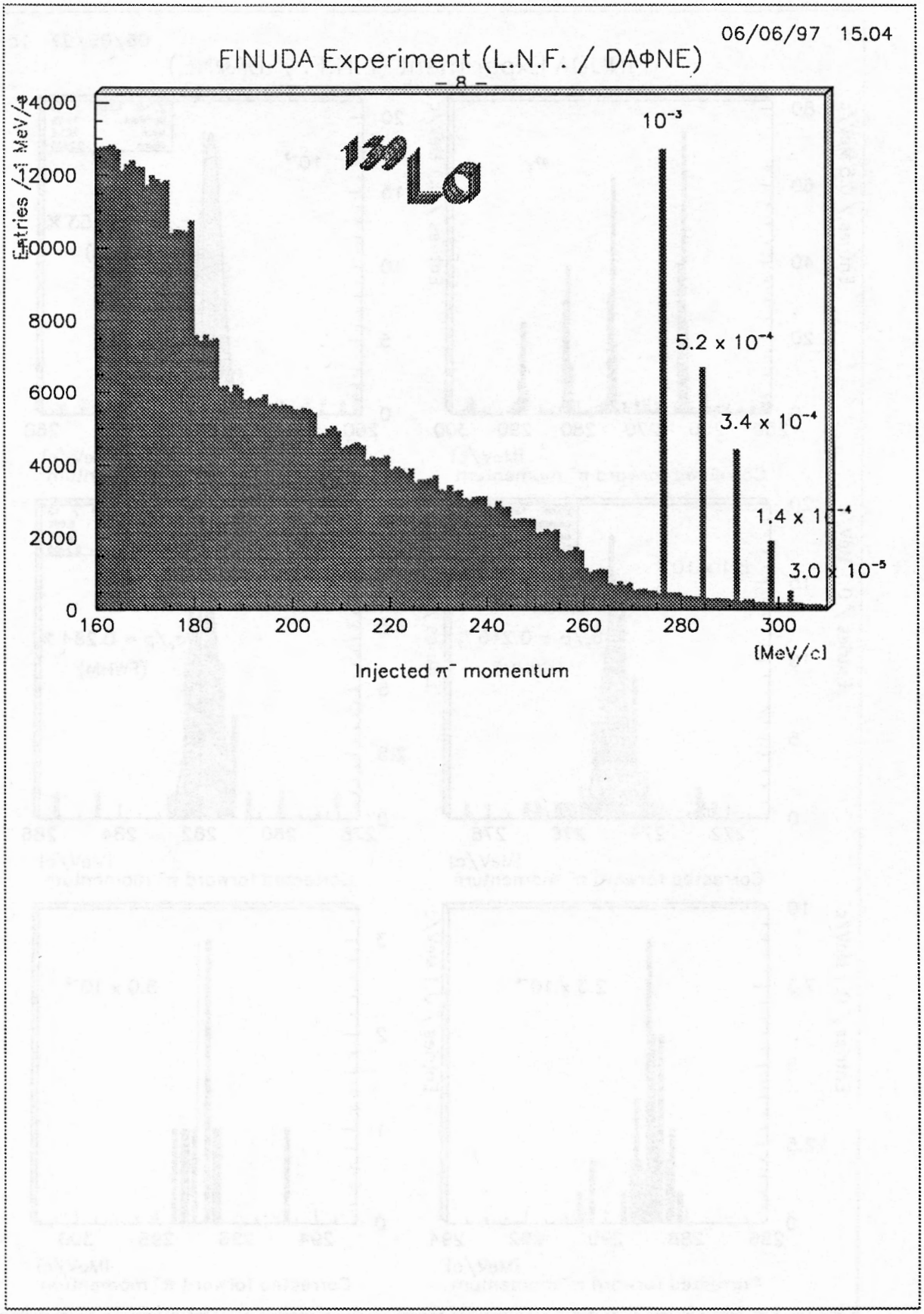
06/06/97 15.04
FINUDA Experiment (L.N.F. / DAΦNE)
- 8 -
^{139}La
10^{-3}
5.2×10^{-4}
3.4×10^{-4}
1.4×10^{-4}
3.0×10^{-5}
Entries / 1 MeV/c
4000
2000
0
8000
6000
4000
2000
0
160
180
200
220
240
260
280
300
[MeV/c]
Injected π^- momentum

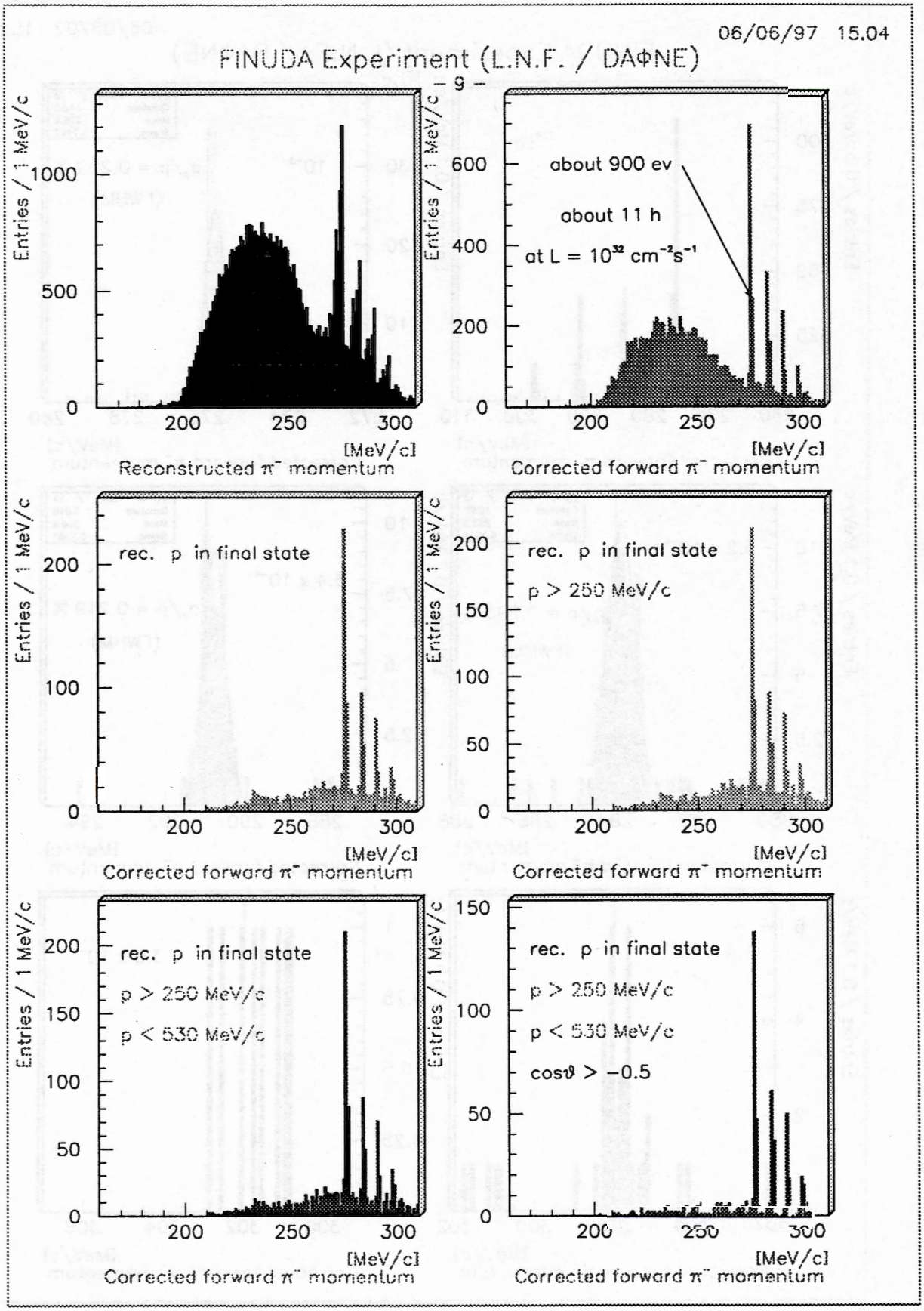
FINUDA Experiment (L.N.F. / DAΦNE)
Entries / 1 MeV/c
Reconstructed π⁻ momentum
[MeV/c]
about 900 ev
about 11 h
at L = 10³² cm⁻²s⁻¹
Corrected forward π⁻ momentum
rec. p in final state
p > 250 MeV/c
p < 530 MeV/c
cosϑ > −0.5

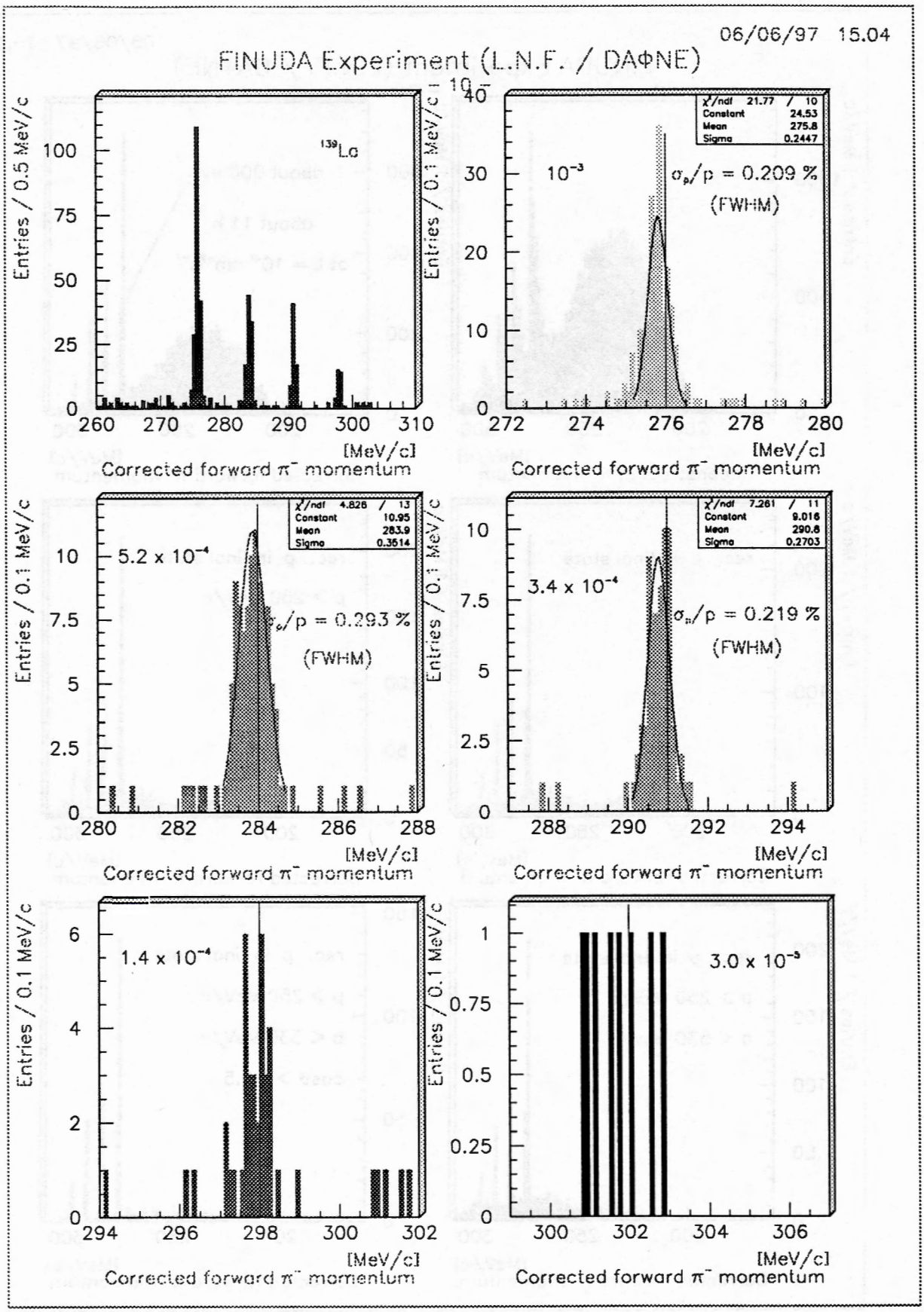
06/06/97 15.04
FINUDA Experiment (L.N.F. / DAΦNE)
Entries / 0.5 MeV/c
^{139}La
Corrected forward π^- momentum [MeV/c]
Entries / 0.1 MeV/c
10^{-3}
σ_p/p = 0.209 %
(FWHM)
χ²/ndf 21.77 / 10
Constant 24.53
Mean 275.8
Sigma 0.2447
Corrected forward π^- momentum [MeV/c]
Entries / 0.1 MeV/c
5.2×10^{-4}
σ_p/p = 0.293 %
(FWHM)
χ²/ndf 4.826 / 13
Constant 10.95
Mean 283.9
Sigma 0.3614
Corrected forward π^- momentum [MeV/c]
Entries / 0.1 MeV/c
3.4×10^{-4}
σ_p/p = 0.219 %
(FWHM)
χ²/ndf 7.261 / 11
Constant 9.016
Mean 290.8
Sigma 0.2703
Corrected forward π^- momentum [MeV/c]
Entries / 0.1 MeV/c
1.4×10^{-4}
Corrected forward π^- momentum [MeV/c]
Entries / 0.1 MeV/c
3.0×10^{-5}
Corrected forward π^- momentum [MeV/c]

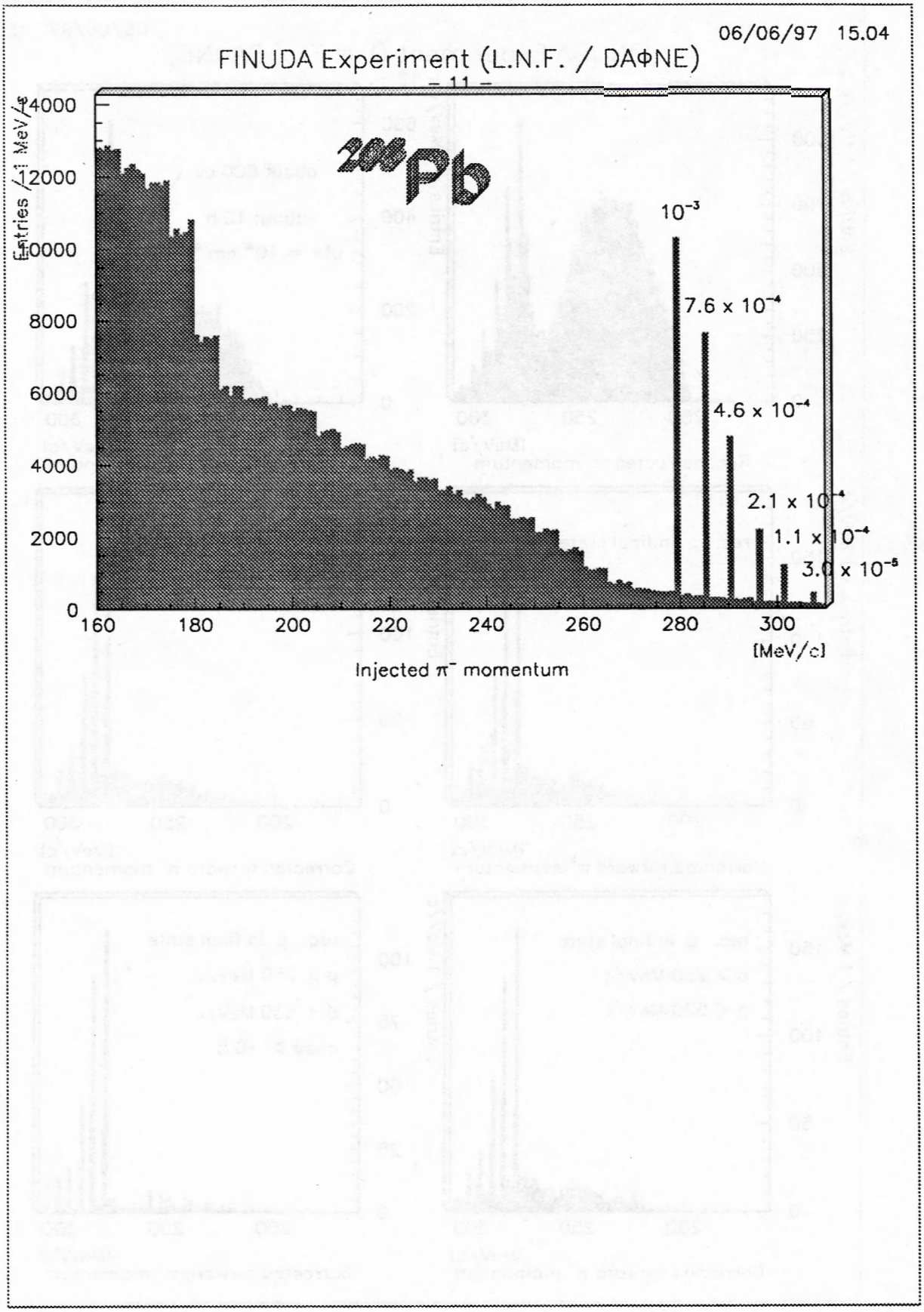
06/06/97 15.04
FINUDA Experiment (L.N.F. / DAΦNE)
- 11 -
Entries / 1 MeV/c
14000
12000
10000
8000
6000
4000
2000
0
208Pb
10-3
7.6 x 10-4
4.6 x 10-4
2.1 x 10-4
1.1 x 10-4
3.0 x 10-5
160
180
200
220
240
260
280
300
[MeV/c]
Injected π- momentum

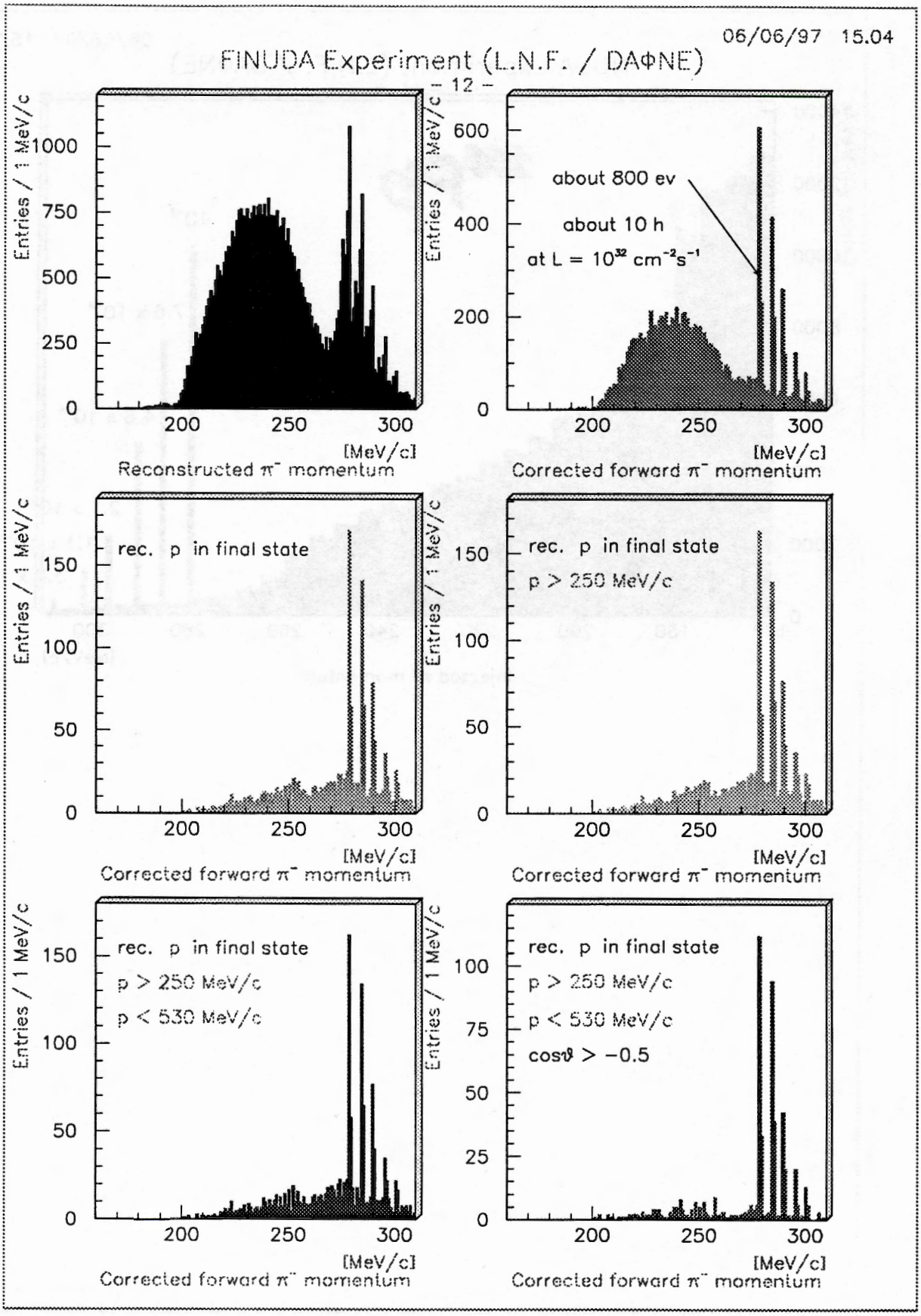
06/06/97 15.04
FINUDA Experiment (L.N.F. / DAΦNE)
Entries / 1 MeV/c
[MeV/c]
Reconstructed π⁻ momentum
about 800 ev
about 10 h
at L = 10³² cm⁻²s⁻¹
Corrected forward π⁻ momentum
rec. p in final state
p > 250 MeV/c
p < 530 MeV/c
cosϑ > −0.5

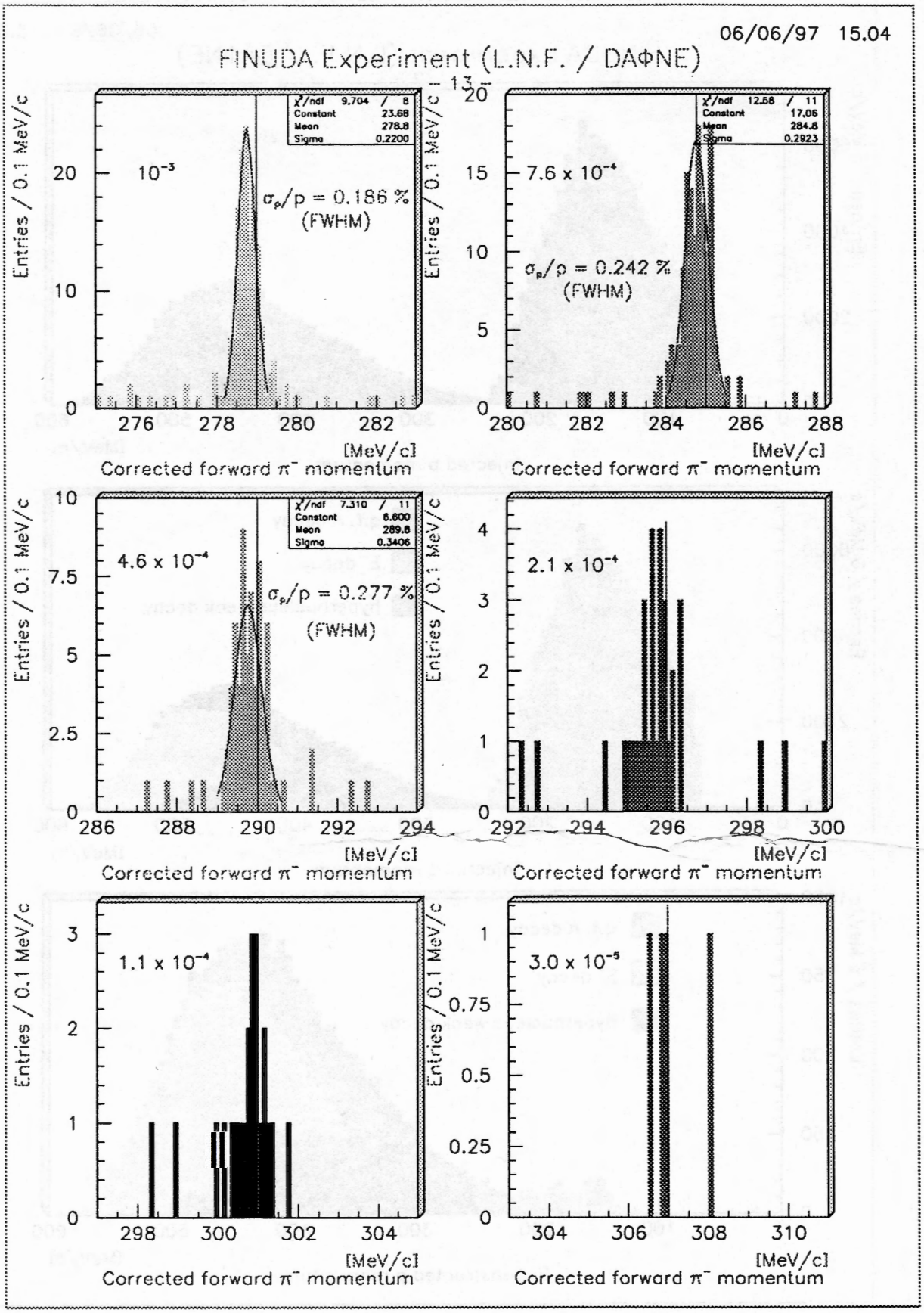
FINUDA Experiment (L.N.F. / DAΦNE)
$^{13}_{\Lambda}$C
χ²/ndf 9.704 / 8
Constant 23.68
Mean 278.8
Sigma 0.2200
10^{-3}
σ_p/p = 0.186 %
(FWHM)
χ²/ndf 12.58 / 11
Constant 17.06
Mean 284.8
Sigma 0.2923
7.6×10^{-4}
σ_p/p = 0.242 %
(FWHM)
χ²/ndf 7.310 / 11
Constant 6.600
Mean 289.8
Sigma 0.3406
4.6×10^{-4}
σ_p/p = 0.277 %
(FWHM)
2.1×10^{-4}
1.1×10^{-4}
3.0×10^{-5}
Entries / 0.1 MeV/c
[MeV/c]
Corrected forward π^- momentum

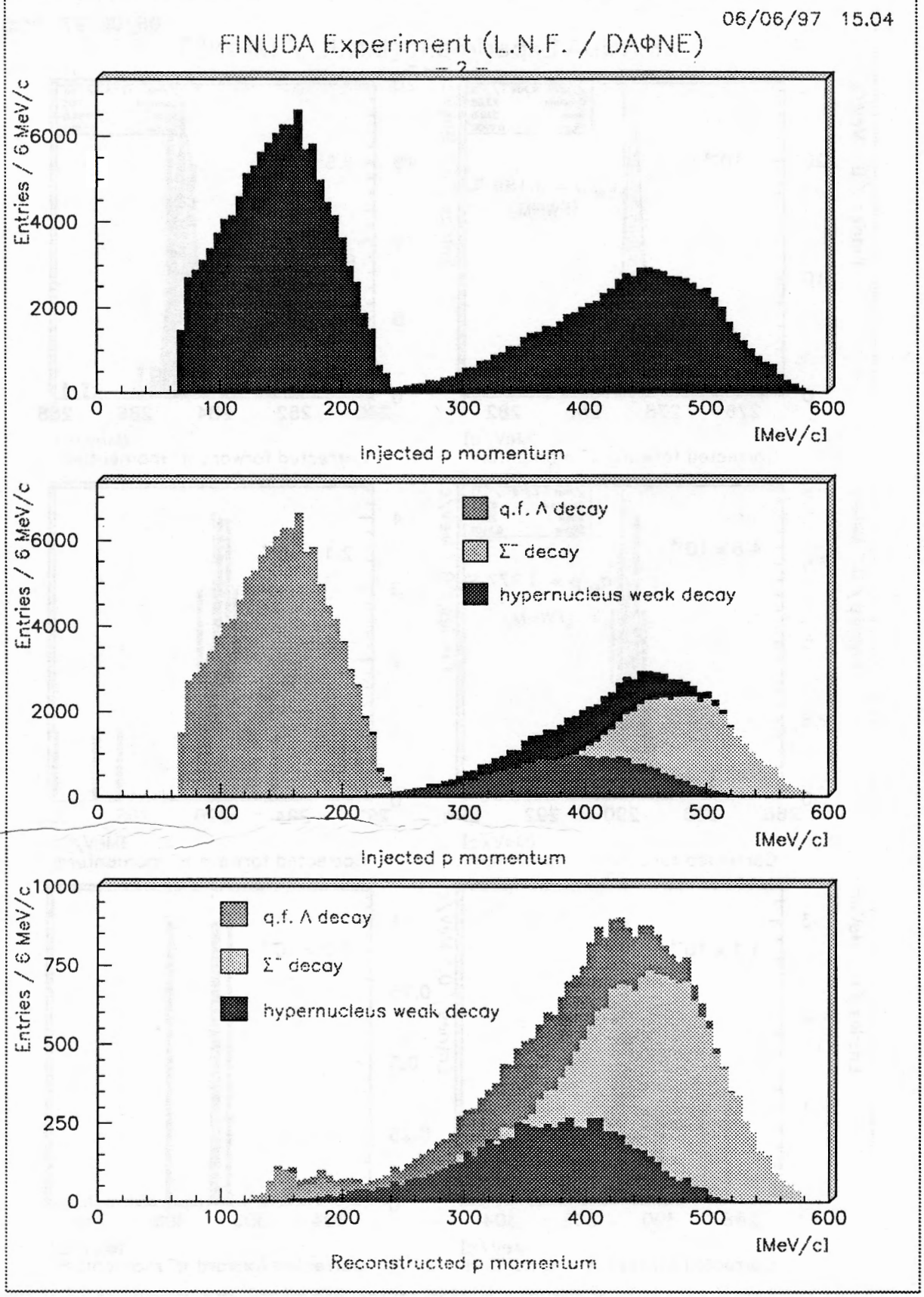
06/06/97 15.04
FINUDA Experiment (L.N.F. / DAΦNE)
Entries / 6 MeV/c
6000
4000
2000
0
0
100
200
300
400
500
600
[MeV/c]
Injected p momentum
Entries / 6 MeV/c
6000
4000
2000
0
q.f. Λ decay
Σ⁻ decay
hypernucleus weak decay
0
100
200
300
400
500
600
[MeV/c]
Injected p momentum
Entries / 6 MeV/c
1000
750
500
250
0
q.f. Λ decay
Σ⁻ decay
hypernucleus weak decay
0
100
200
300
400
500
600
[MeV/c]
Reconstructed p momentum

06/06/97 15.04

FINUDA Experiment (L.N.F. / DAΦNE)

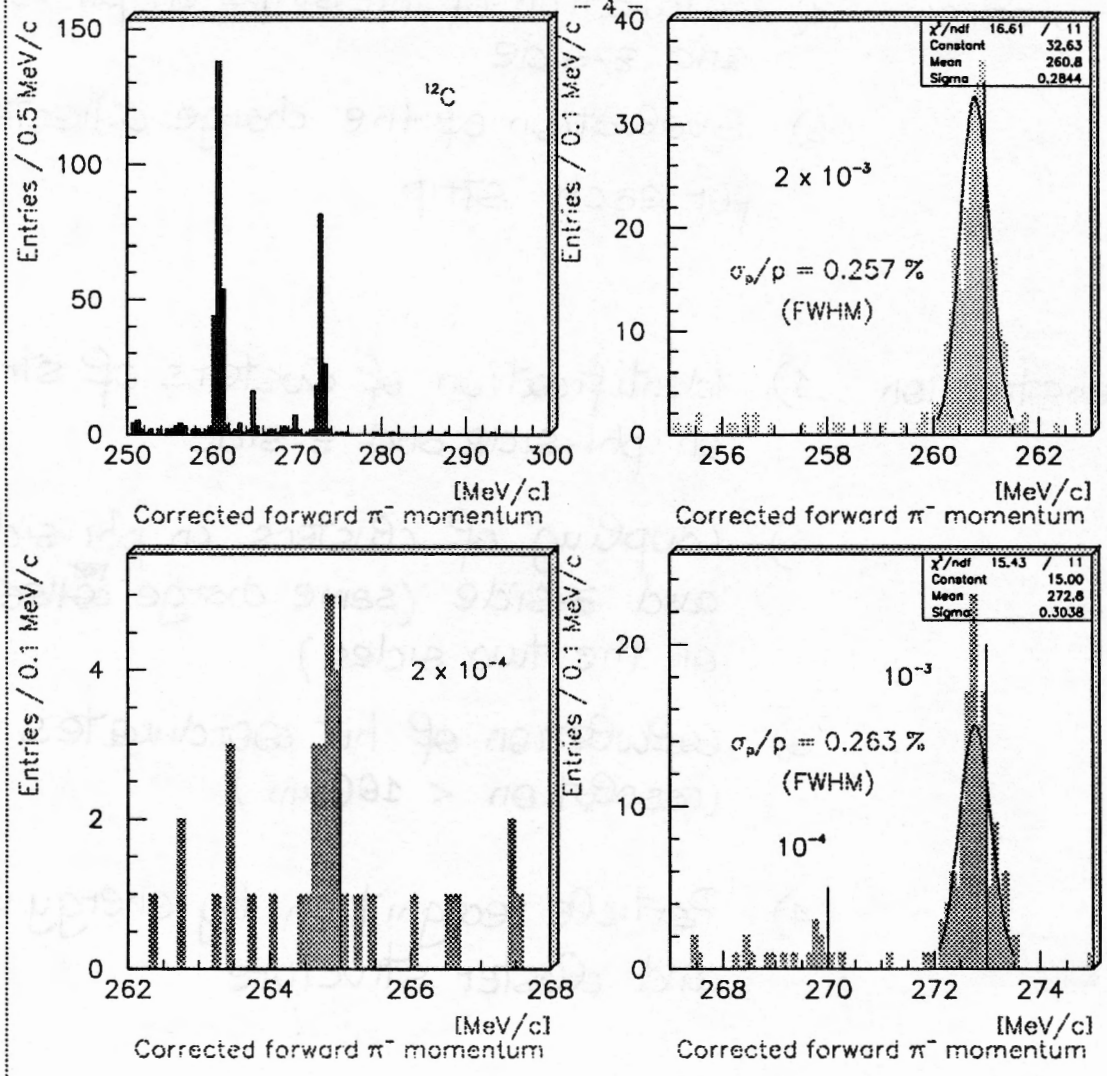

Simulation/Reconstruction of silicon μstrips

Simulation
1) Calculation of hit strips on phi-side and z-side
2) Evaluation of the charge collected for each strip

Reconstruction:
1) Identification of clusters of strips on phi-side and z-side
2) Coupling of clusters on phi-side and z-side (same charge ~~collected~~ recollected on the two sides)
3) Calculation of hit coordinates (resolution < 100μm)
4) Particle recognition by energy loss and cluster structure

FIRUDA

The first version of the reconstruction program is completed and working

2ND WORKSHOP ON PHYSICS AND DETECTORS
FOR **DAΦNE**

Frascati, April 4-7, 1995

FI.NU.DA. Status Report

(**FI**sica **NU**cleare a **DAΦNE**)

Aldo Zenoni (Brescia University)

The FINUDA Collaboration

M.Agnello[a], P.Amaudruz[l], G.Beer[l], M.Bertani[b], S.Bianco[b], E.Botta[c], T.Bressani[c], L.Busso[d], D.Calvo[c], P.Camerini[e], C.Cattaneo[f], N.Colonna[g], M.Corradini[h], G.D'Erasmo[g], A.Donzella[h], F.L.Fabbri[b], A.Feliciello[c], A.Filippi[i], V.Filippini[f], E.M.Fiore[g], L.Fiore[g], P.Gianotti[b], D.R.Gill[l], N.Grion[e], C.Guaraldo[b], F.Iazzi[a], A.Lanaro[b], L.Lee[l], E.Lodi Rizzini[h], V.Lucherini[b], S.Marcello[c], G.M.Marshall[l], B.Minetti[a], N.Mirfakhrai[n], P.Montagna[f], A.A.Nozdrin[l], A.Olin[l], A.Pantaleo[g], V.Paticchio[g], E.Rossetto[c], A.Rotondi[f], R.Rui[e], P.Salvini[f], S.Sarwar[b], A.Sharma[c], G.Smith[l], S.Tessaro[e], L.Venturelli[h], S.Yen[l], A.Zenoni[m].

[a] *Dipartimento di Fisica del Politecnico di Torino and INFN, Sezione di Torino, I-10125 Torino, Italy*
[b] *INFN, Laboratori Nazionali di Frascati, I-00044 Frascati, Italy*
[c] *Dipartimento di Fisica Sperimentale, Università di Torino and INFN, Sezione di Torino, I-10125 Torino, Italy*
[d] *Istituto di Fisica Generale, Università di Torino and INFN, Sezione di Torino, I-10125 Torino, Italy*
[e] *Dipartimento di Fisica, Università di Trieste and INFN, Sezione di Trieste, I-34127 Trieste, Italy*
[f] *Dipartimento di Fisica Nucleare e Teorica, Università di Pavia and INFN, Sezione di Pavia, I-27100 Pavia, Italy*
[g] *Dipartimento di Fisica, Università di Bari and INFN, Sezione di Bari, I-70126 Bari, Italy*
[h] *Dipartimento di Elettronica per l'Automazione, Università di Brescia and INFN, Sezione di Torino, I-25060 Brescia, Italy*
[i] *Dipartimento di Fisica Nucleare e Teorica, Università di Pavia and INFN, Sezione di Torino, I-27100 Pavia, Italy*
[l] *TRIUMF, 4004 Wesbrok Mall, Vancouver, BC, V6T 2A3, Canada*
[m] *Dipartimento di Elettronica per l'Automazione, Università di Brescia and INFN, Sezione di Pavia, I-25060 Brescia, Italy*
[n] *Shahid Beheshty University, Dept of Phys, 19834 Tehran, Iran*

DAΦNE the FRASCATI Φ factory

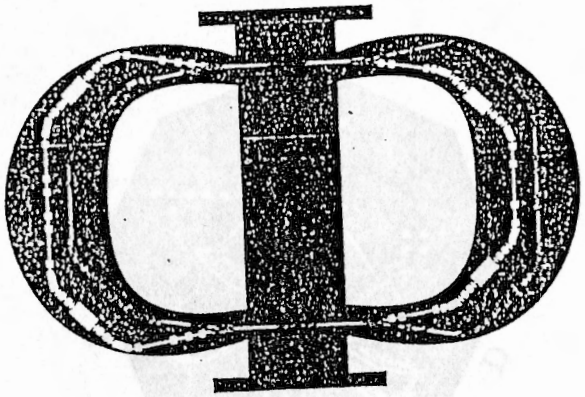

at $L \approx 10^{33}\, cm^{-2} s^{-1}$ $\approx$ 5000 Φ per second

$e^+(510) \longrightarrow \Phi(1020) \longleftarrow e^-(510)$

⇓

Mode	B.R.(%)	P_{max}(MeV/c)
K^+K^-	49	127
$K^0_S K^0_L$	34	110
3π	13	182
$\pi^+\pi^-\pi^0$	2	462
$\eta\gamma$	1.3	362
others	~ 1	–

⇒ $K^\pm$ beam for FINUDA

⇐ KLOE

$Re(\varepsilon'/\varepsilon) \sim 10^{-4}$

CP, CPT violation

... and more

FI.NU.DA. → A **fixed** target experiment carried out at a **collider**

Main physics **Idea**

Use the **low energy** (16 MeV), tagged K^- beam from Φ decay, for **high resolution** studies of **Hypernucleus** formation and **non-mesonic** decay.

$K^-_{stop} + {}^A Z \rightarrow {}^A_\Lambda Z + \pi^-$ → high resolution spectroscopy

$P_{\pi^-} \approx 240\text{-}270$ MeV/c forall ${}^A Z$

Non-mesonic decays:

- ${}^A_\Lambda Z \rightarrow {}^{(A-2)} Z + n + n$
- ${}^A_\Lambda Z \rightarrow {}^{(A-2)}(Z-1) + n + p$

Merits of the Idea → **A lot !**

Inconvenience → **Less flexibility** for :
maintenance
nuclear target handling
variation of magnetic field
etc.

How can a hypernucleus ($^{A}_{\Lambda}Z$) be produced ?

- By collisions of particles which carry **strangeness** (s quark) inside the nucleus.
  " K^- beams"

$$K^- + {}^{A}Z \rightarrow {}^{A}_{\Lambda}Z + \pi^-$$

strangeness exchange

$$K^- + n \rightarrow \Lambda + \pi^-$$

exothermic reaction
Q = 178 MeV

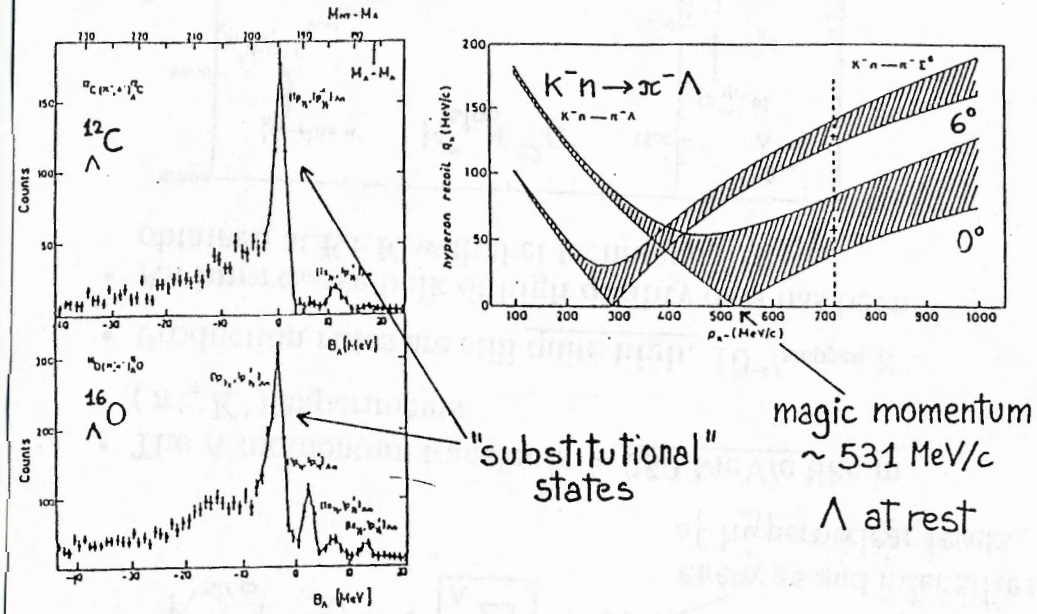

"substitutional" states

magic momentum
~ 531 MeV/c
Λ at rest

- Very **small** momentum transfer.
- One neutron is **replaced** by a Λ, **without** changing the **spatial** and **spin** wave function.
  "**substitutional** excited states"
- Momentum transfer can be **changed** by changing **incident** momentum and **angle** of π^- emission.

- By collisions of particles which create **strangeness** ($\bar{s}s$ quark pairs) **inside** the nucleus.
  " **Associated** production"

$$\pi^+ + {}^{A}Z \rightarrow {}^{A}_{\Lambda}Z + K^+$$

$$\pi^+ + n \rightarrow K^+ + \Lambda$$

endothermic reaction
Q = - 530 MeV

nuclear shells

Λ single particle ground state

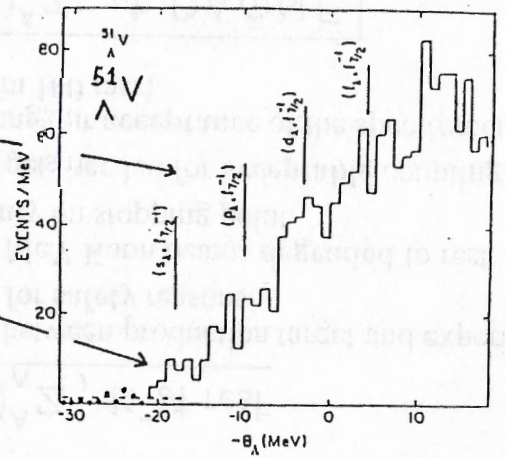

- No "**magic** momentum"; the Λ is produced with momentum transfer ≈ **350** MeV/c.
- Hypernuclei **are not** produced in "substitutional states", but in high spin **excited** states.
- The **high** momentum transfer makes the process more **appropriate** for exciting **low lying** Λ hypernuclear states.
  Complementary process to "strangeness exchange".
- The cross sections are **two orders** of magnitude **lower** but the beam **intensities** overcompensate the drawback.

- **High** production rates and **many** hypernuclear final states can be obtained using K^- **at rest**.

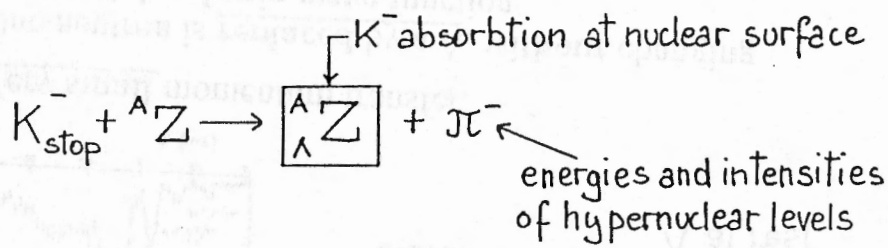

- The Λ momentum transfer is $\approx$ **250** MeV/c like in (π^+, K^+) experiments.
- Production **rates** are still **quite high**; 10^{-3}/stopped K^-.
- An **impressive** bulk of **high quality** data has been obtained at **KEK** with that technique.

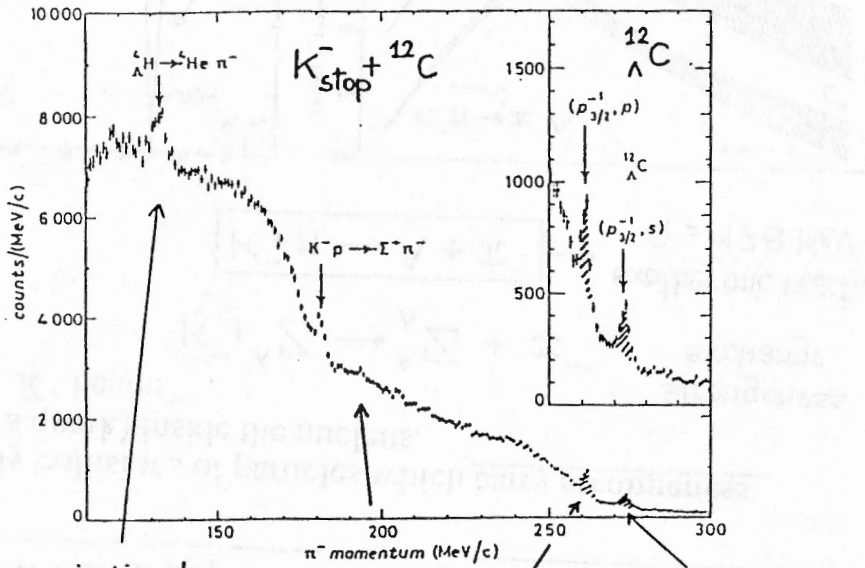

Advantages of K^-_{stop} hypernucleus production at DAΦNE

${}^A_{\Lambda}Z(K^-, \pi^-){}^A_{\Lambda}Z$ and ${}^A_{\Lambda}Z(\pi^+, K^+){}^A_{\Lambda}Z$ reactions

- **Thick** targets needed : **several** g/cm² for **acceptable** counting rates.
- Momentum **resolution** on π^-, K^+ limited by target **thickness**.
- Limited **acceptance** for hypernucleus decay **products**.

${}^A_{\Lambda}Z(K^-_{stop}, \pi^-){}^A_{\Lambda}Z$, K^- at rest

- Distance between production target and experiment **10÷15** m for **safety** reasons.
- **500÷600** MeV Kaon beams **degraded** to rest. Large **uncertainty** on stopping point.
- **Thick** targets needed for **acceptable** counting rates.
- Limited angular **acceptance** of the spectrometers (maximum **100** msr).

${}^A_{\Lambda}Z(K^-_{stop}, \pi^-){}^A_{\Lambda}Z$ at DAΦNE

- **Low** energy (**16** MeV) **monochromatic** K^- beam.
- Very **thin** target (≈**100** mg/cm²).
- K^+ **tagging** of the K^- beam.
- Large **acceptance** (typical of **collider** experiments) **both** for π^- and hypernucleus decay **products**

Inconvenience → **Low** K^- intensity : **216** K^-/s at $L = 10^{32}\ cm^{-2} s^{-1}$. Non **collimated** beam.

FINUDA expected performances. Comparison with other experiments

	Resolution (FWHM)	Rate (event/hour)	Non-mesonic decays
BNL $(K^-,\pi^-)(\pi^+,K^+)$	≃ 1 MeV	1÷5	YES
KEK (π^+,K^+)	≃ 2 MeV	1÷5	?
CEBAF (proposed) (e,e',K^+)	≃ 200 KeV	5	No
BNL (proposed) (K^-_{stop},π^0)	< 1 MeV	60	?? thick target
FINUDA $(L=10^{32}\,cm^{-2}s^{-1})$	≃ 700 KeV	80 per state at 10^{-3}	6 (n+p) 1 (n+n)

Machine **time** (hours) for hypernuclear state production

Production rates

Expected: Signal / Backg.	10^{-3} 10%st.	10^{-4} 10%st.	10^{-5} 10%st.	10^{-5} 20%st.
$\frac{4}{1}$ at 10^{-3}	2.4 h	96 h	8000 h	2000 h
$\frac{8}{1}$ at 10^{-3}	1.8 h	56 h	4000 h	1000 h

Suppression of background from Σ^- decay in flight

A factor 10 increase at $\mathcal{L} = 10^{33} cm^{-2}s^{-1}$

FINUDA internal detector region

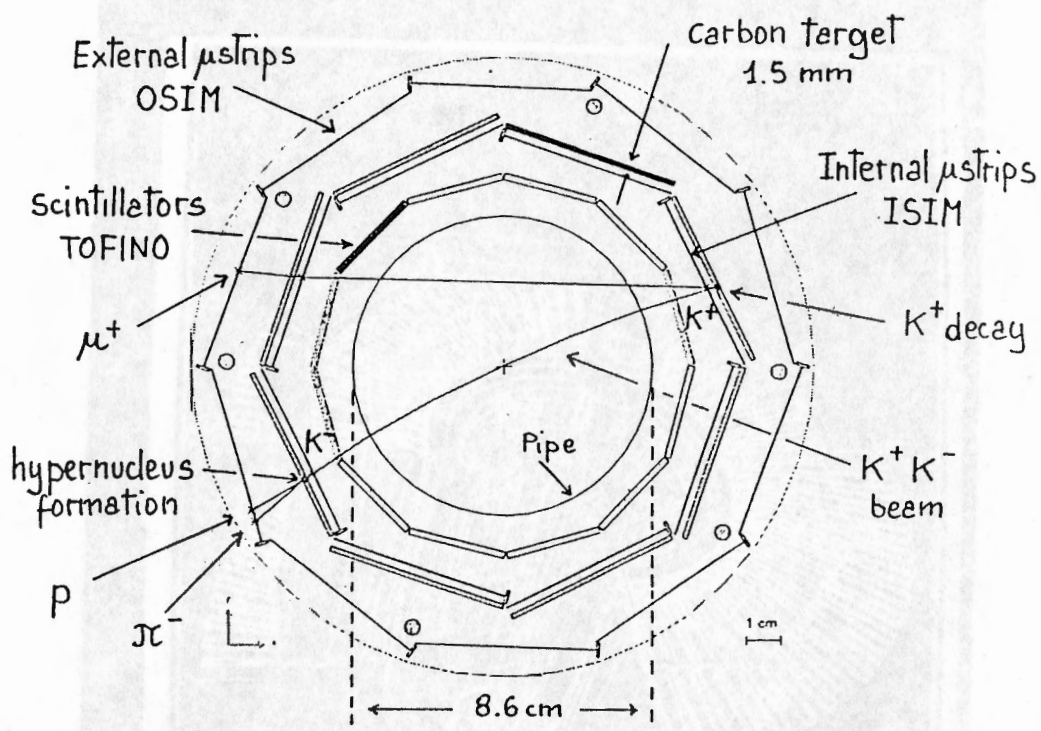

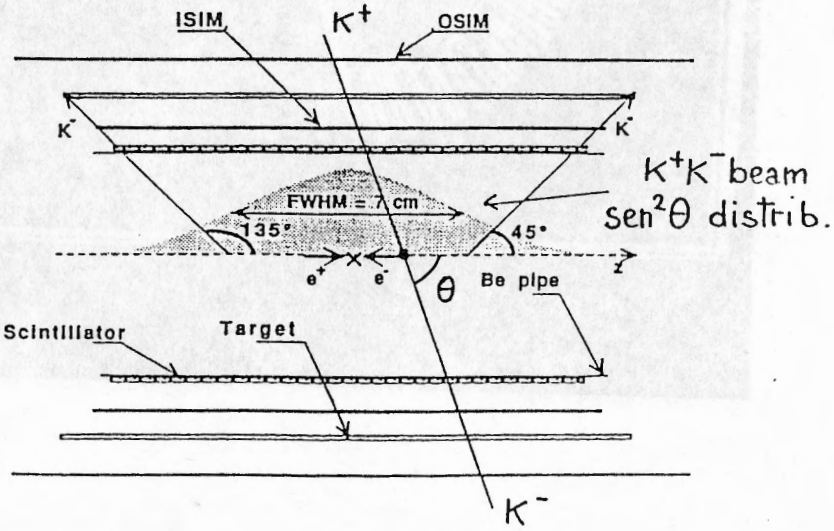

FINUDA spectrometer and scintillators

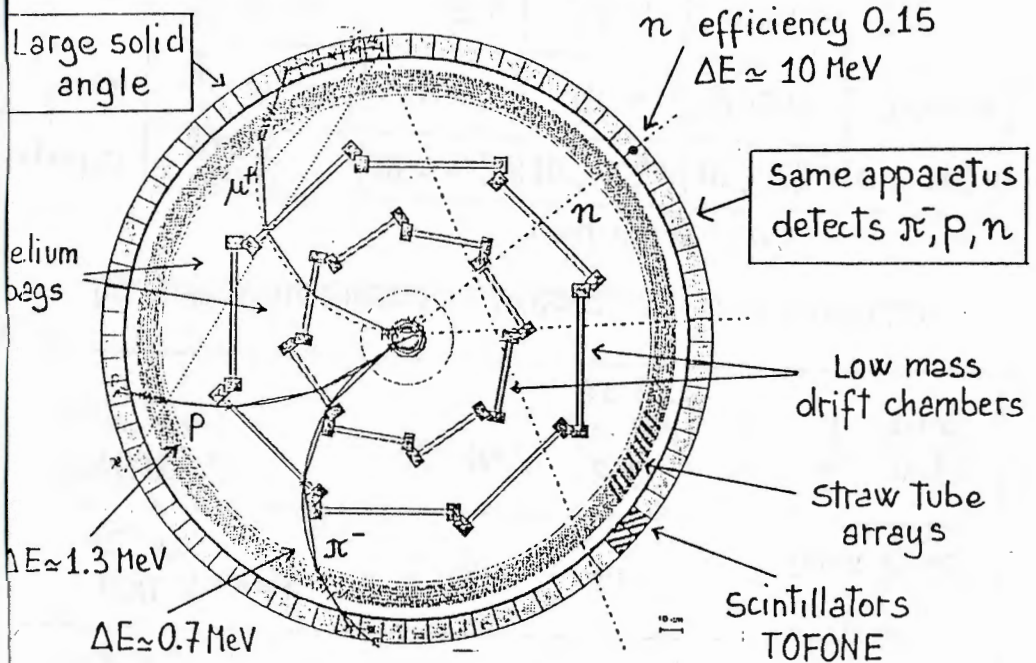

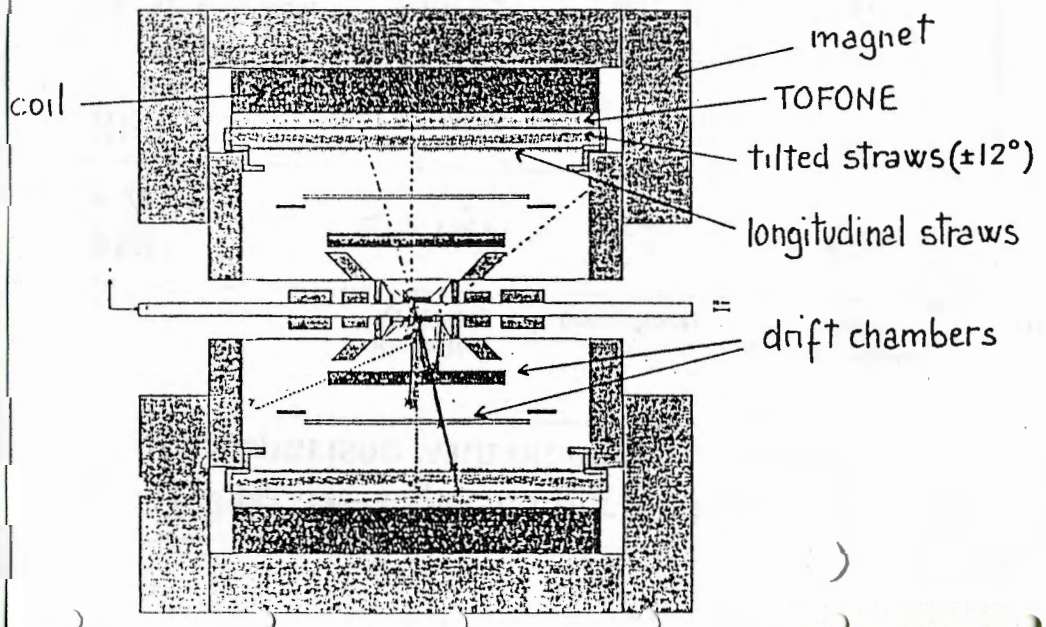

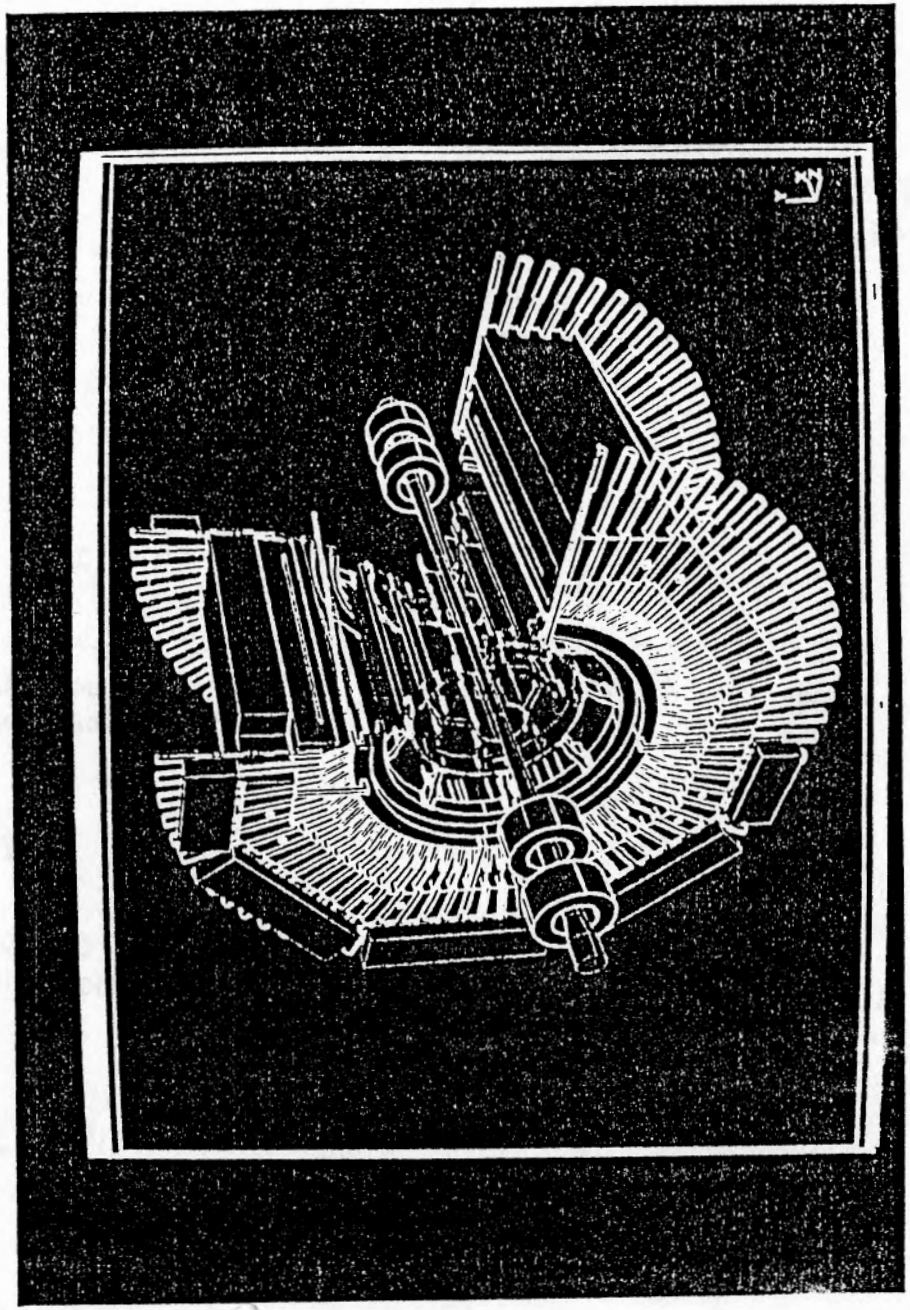

Main physics goals of FINUDA

Main physics goals of FINUDA

1) Λ - hypernucleus **spectroscopy.**

- A **new** dimension added to the evolving picture of **nuclear** physics (p, n, Λ).

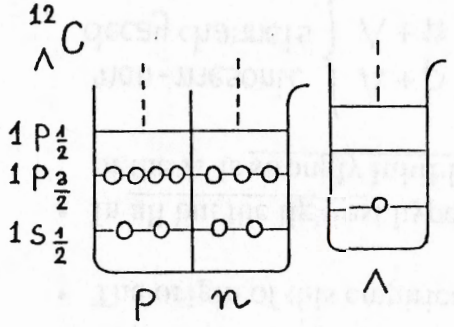

The Λ inside a nucleus

- A **distinguishable** baryon.
- Not Pauli-blocked.
- It experiences a potential well **weaker** than the one of **nucleons**, with small **spin-orbit** contribution.

All single particle states are **allowed** to the Λ.
A **textbook** example of the **shell model.**

Never seen in ordinary nuclei

deep single particle states

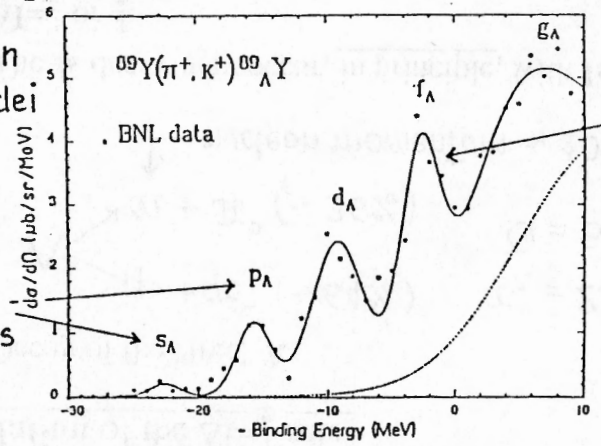

resolution 2.6 MeV

FINUDA expected resolution **0.7** MeV
May spin **splitting** appear ?

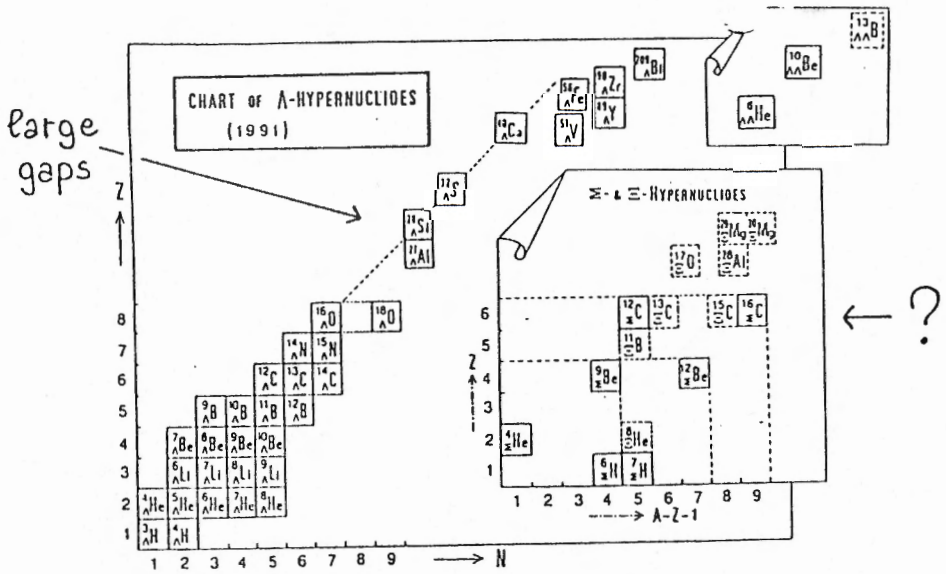

- **FINUDA** can perform a **large** scientific program of **high** resolution **hypernuclear** spectroscopy on **all** nuclides that can be machined in **solid** targets.

- The **completion** of this program could constitute an important **step forward** in the **understanding** of the main hypernuclear physics problems :

  - Possible new **symmetries** in many body spectroscopy, **forbidden** in ordinary nuclei by Pauli principle.

  - **Hyperon-nucleon** interaction which may be investigated **only** inside the nuclear medium.

  - Dynamical aspects of the **strangeness** degree of freedom in the nuclear system and its **role** in strong interaction.

  - Possibile **modifications** of the baryon properties in the **nuclear** environment.

2) **Non-mesonic** decay of hypernuclei and possible **violation** of the $\Delta I=\frac{1}{2}$ rule

- Decay of the "free" Λ

$$\Lambda \to p + \pi^- \ (\sim 64\%) \qquad \tau_\Lambda = 2.63\times10^{-10}\ s$$
$$\Lambda \to n + \pi^0 \ (\sim 36\%) \qquad Q = 37\ MeV$$
$$\uparrow \text{ nucleon momentum} \sim 100\ MeV/c$$

- The Λ decay may occur, in principle, with **Isospin** change $\Delta I=\frac{1}{2}$ or $\frac{3}{2}$.

- The **experimental** B.R.s of the Λ (and other **hyperons**) imply a $\Delta I=\frac{1}{2}$ **dominance** over $\Delta I=\frac{3}{2}$ of at least **20**.

- The **origin** of this empirical rule is **unknown.**

- In **all** but the **lightest** hypernuclei the mesonic decay mode of the Λ is strongly **inhibited** by Pauli principle.

non-mesonic decay channels:
$\Lambda + p \to n + p$ (nucleon momentum ~ 417 MeV/c)
$\Lambda + n \to n + n$ (nucleon momentum ~ 417 MeV/c)

- It has been **suggested** that the $\Delta I=\frac{1}{2}$ rule may be strongly **violated** in **non-mesonic** decays, which probe the **high** momentum and parity conserving part of the **weak** interaction.

- A measurement of the **relative B.R.'s** of the two channels could provide information about the **structure** of the **weak** hamiltonian.

- In spite of the very **important** physical interest for the **decay** of hypernuclei, the available data are **scarce** and **not precise.**

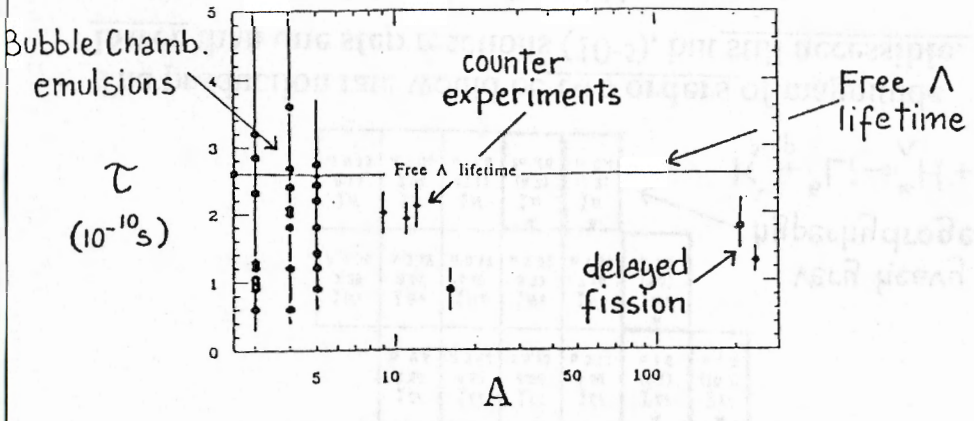

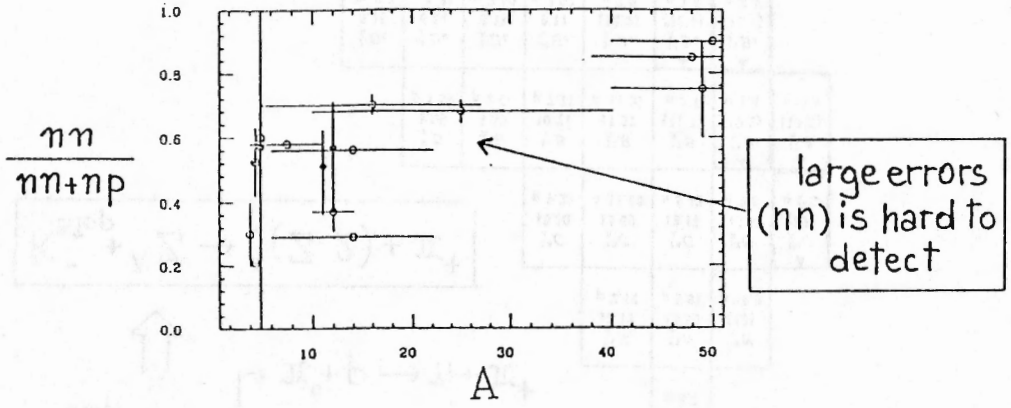

- **Correlated** measurements of Λ-hypernucleus **ground** states and decay **products** (expecially **n + n**) are **very** difficult.

- The **FINUDA** apparatus seems **ideal** for the study of **non-mesonic** decays :
  - It is **very transparent**
  - It provides a large **acceptance**, with the **same** detectors, for both π^- from hypernucleus formation and decay **products**

$\Delta I=\frac{1}{2}$ rule. **Inclusive** measurements

- The possible **violation** of the $\Delta I=\frac{1}{2}$ rule can be investigated by studying the relative **B.R.** :

$$^{A}_{\Lambda}Z \rightarrow {}^{A-2}(Z-1)+n+p \quad \leftarrow \Delta E = 1.3\ \text{MeV}$$

$$^{A}_{\Lambda}Z \rightarrow {}^{A-2}Z+n+n \quad \leftarrow \Delta E = 10\ \text{MeV}$$

in **coincidence** with the measurement of the **ground state** of the hypernucleus.

- The **energy** resolutions on "**n**" and "**p**" **do not** allow the identification of the nuclear **final** states $^{(A-2)}(Z-1)$ and $^{(A-2)}Z$.

- A **systematic** study of the ratio of the **p-n** and **n-n** B.R.'s over the **mass range** A is needed.

An example of **exclusive** measurement with a ^{6}Li target

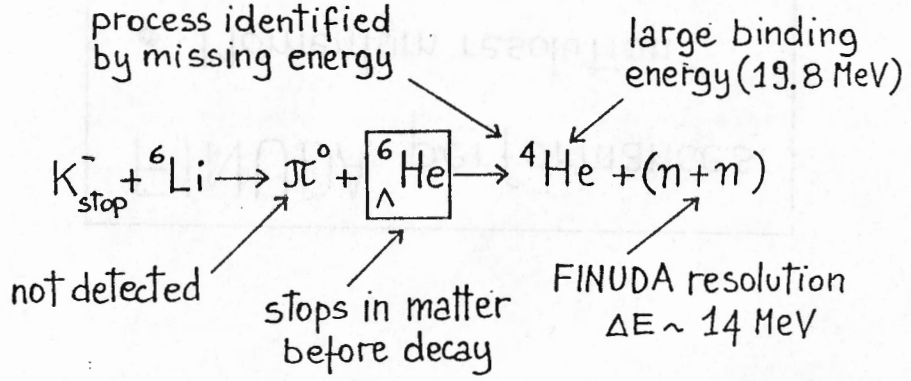

- In FINUDA the process can be triggered requesting Two Back to Back slabs hit in TOFONE

Production of Λ hypernuclei with **large** neutron **excess**

- In **FINUDA**, **two step** reactions with formation of **new**, **neutron rich** hypernuclei are **detectable**.

$$K^-_{stop} + p \rightarrow \pi^0 + \Lambda$$
$$\hookrightarrow \pi^0 + p \rightarrow n + \pi^+$$

$$K^-_{stop} + {}^{A}Z \rightarrow {}^{A}_{\Lambda}(Z-2) + \pi^+$$

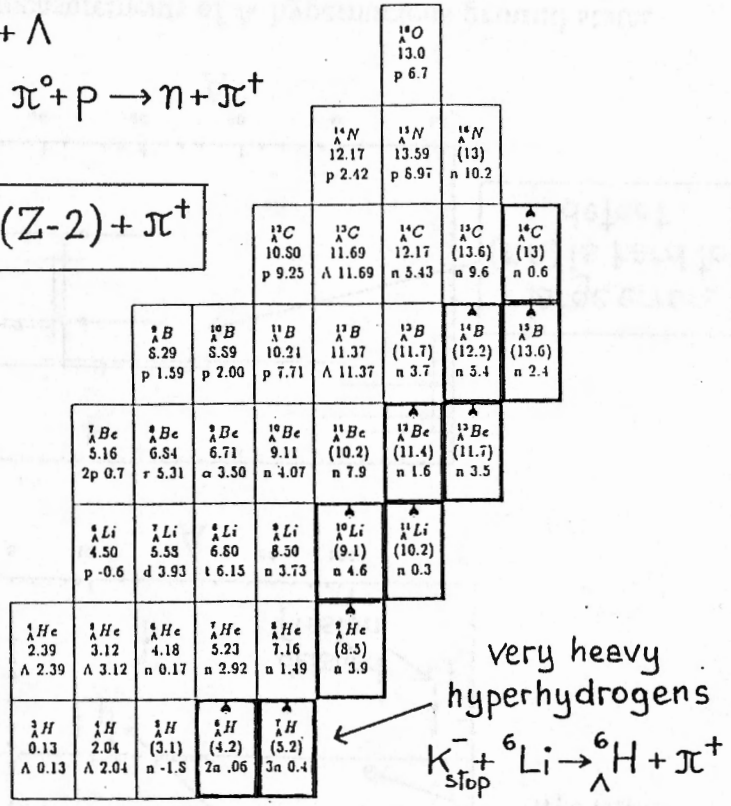

- The production rate would be **two orders** of magnitude **lower** than **one step** reactions (10^{-5}), but **still accessible.**
  - **All** the hypernuclei produced would be **new ones.**
  - Some of them **may be stable.**
  - **Very heavy** hyperhydrogens ${}^{6}_{\Lambda}H$ and ${}^{7}_{\Lambda}H$ might be produced

FINUDA performances

- Momentum resolution
- Trigger and rates
- Pattern Recognition

Apparatus **performances**
Spectrometer momentum **resolution**

- The momentum **resolution** is the most **crucial** feature of the apparatus.

$$\frac{\Delta T_\pi}{T_\pi} = \frac{\sqrt{P_\pi^2 + m_\pi^2} + m_\pi}{\sqrt{P_\pi^2 + m_\pi^2}} \cdot \frac{\Delta P_\pi}{P_\pi}$$

at $P_\pi = 270$ MeV/c

$\frac{\Delta P}{P} \sim 10^{-3}$

$\Delta T \sim 236$ KeV

- The detectors have **high** spatial resolution and **low mass** and are immersed in a **helium** atmosphere to minimize **multiple** scattering.

- Silicon μstrips	R ϕ	**50** μm
	Z	**50** μm
- Drift **chambers**	R ϕ	**150** μm (pessimistic)
	Z	**1%** wire length (1÷2 cm)
- **Straw tube** array	R	**100** μm
	Z	**1.0** mm (pessimistic)

reasonable extrapolations of the **present** technology.

- The tracking volume is **very transparent** :
  - **Total** radiation length ⟶ **170,000** cm
    Pure Helium 540,000 cm
    Air 34,000 cm
  - Spectrometer **size** ⟶ **103** cm
  - **Homogeneous** magnetic field ⟶ **1.1** Tesla

- Using the **standard** formulae for evaluating the **expected** momentum **resolution**. (Gluckstern(1963))

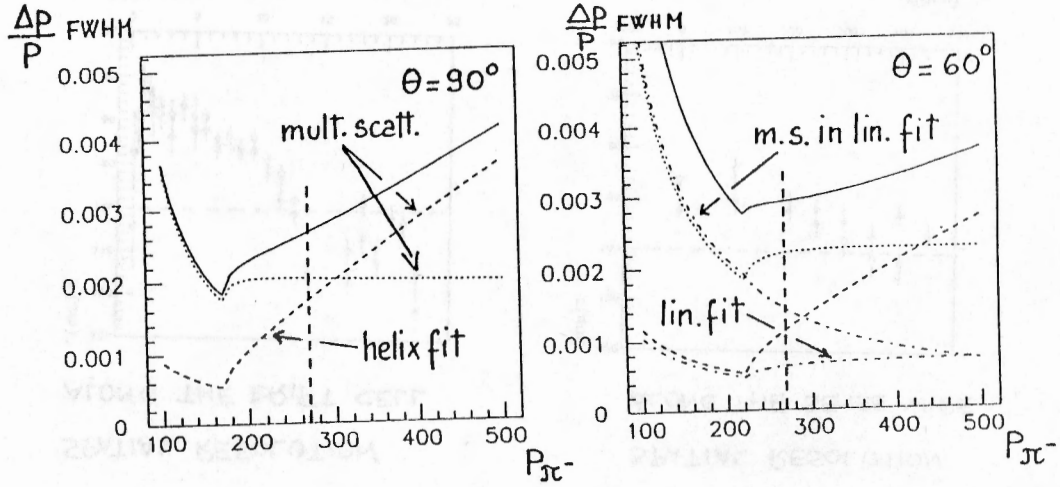

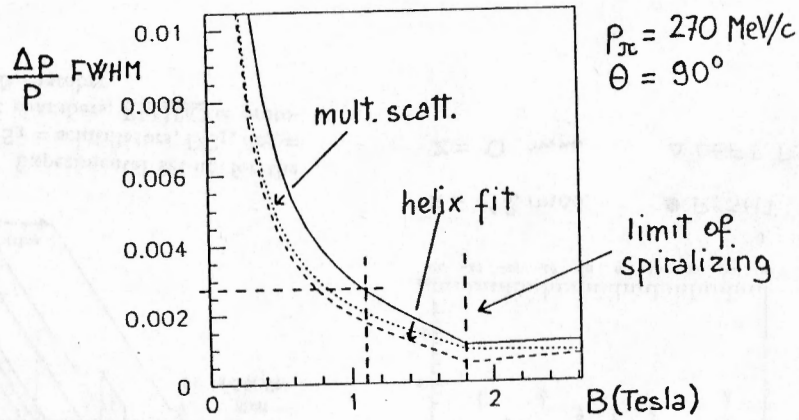

Check with Monte Carlo simulation

Particle	Momentum resolution (FWHM)
π⁻ 270 MeV/c	0.28 %
p 417 MeV/c	0.79%
μ 236 MeV/c	0.24%

Monte Carlo **simulation** of populations of tracks

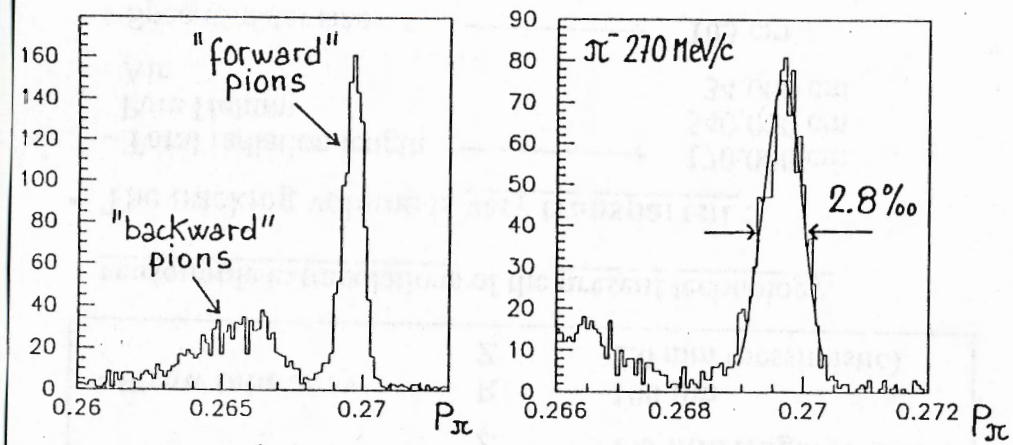

Correction for energy lost inside the target

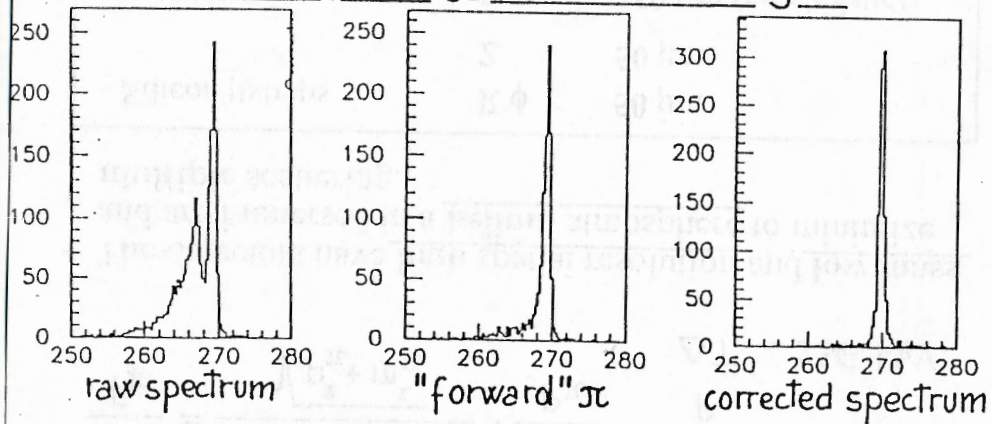

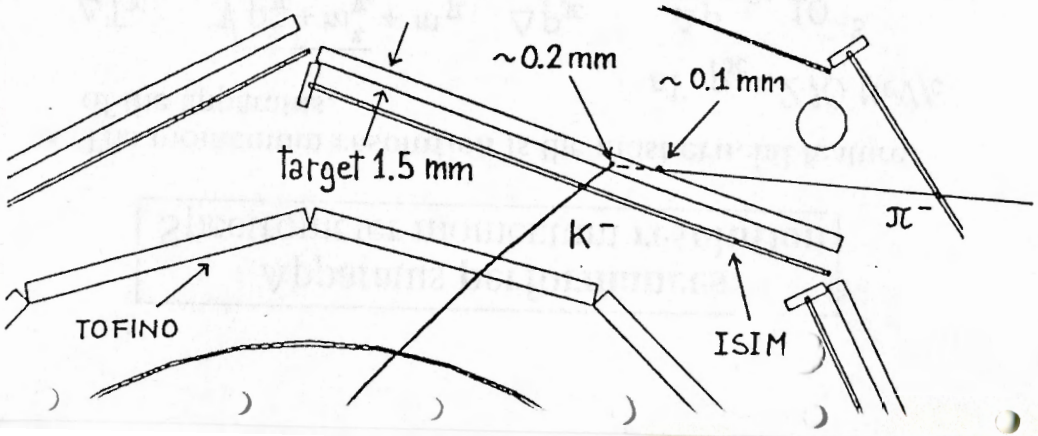

SUMMARY OF MEASUREMENTS AT PS TEST BEAM

EXPERIMENTAL SET-UP

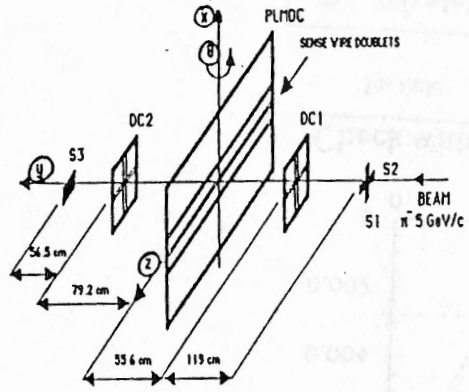

Experimental set-up for the beam test. S_1, S_2 S_3 = scintillators, DC_1, dc_2 = small surface drift chambers, PLMDC = prototype low mass drift chamber.

SPATIAL RESOLUTION AS FUNCTION OF INCIDENCE ANGLE

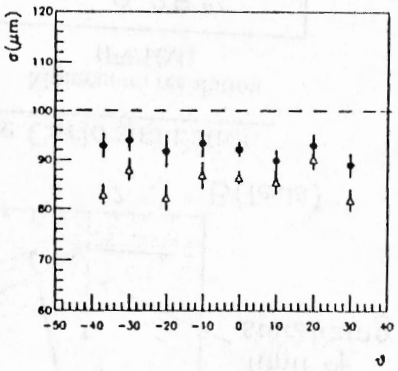

X = 12 mm ● RIGHT TDC

Z = 0 mm Δ LEFT TDC

SPATIAL RESOLUTION ALONG THE DRIFT CELL

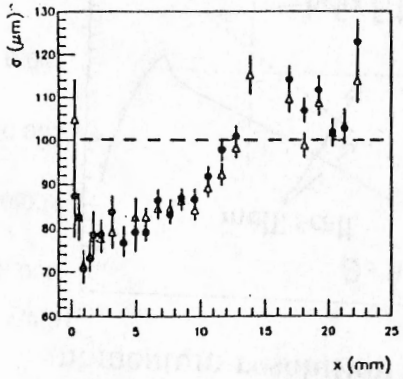

Z = 0 mm ● RIGHT TDC

ϑ = 0° Δ LEFT TDC

SPATIAL RESOLUTION ALONG THE SENSE WIRE

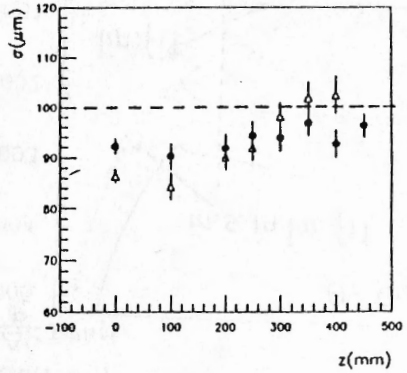

X = 12 mm ● RIGHT TDC

ϑ = 0° Δ LEFT TDC

CORRELATION AMONG the
GEOMETRICAL Z-COORDINATE
and THAT MEASURED BY THE CHARGE
DIVISION METHOD

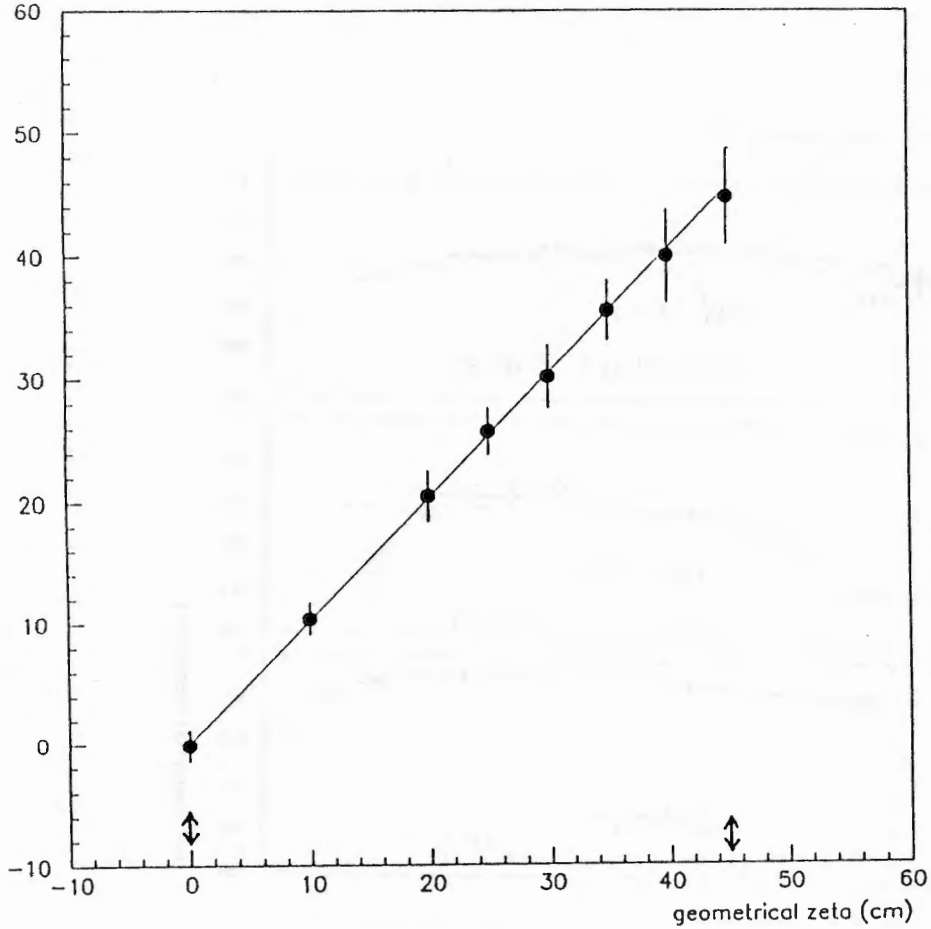

		STANDARD ELECT.	DIFFERENTIAL AMPLIF.
σ %	z = 0	0,95 %	0.61 %
	z = 45	2,7 %	1.3 %

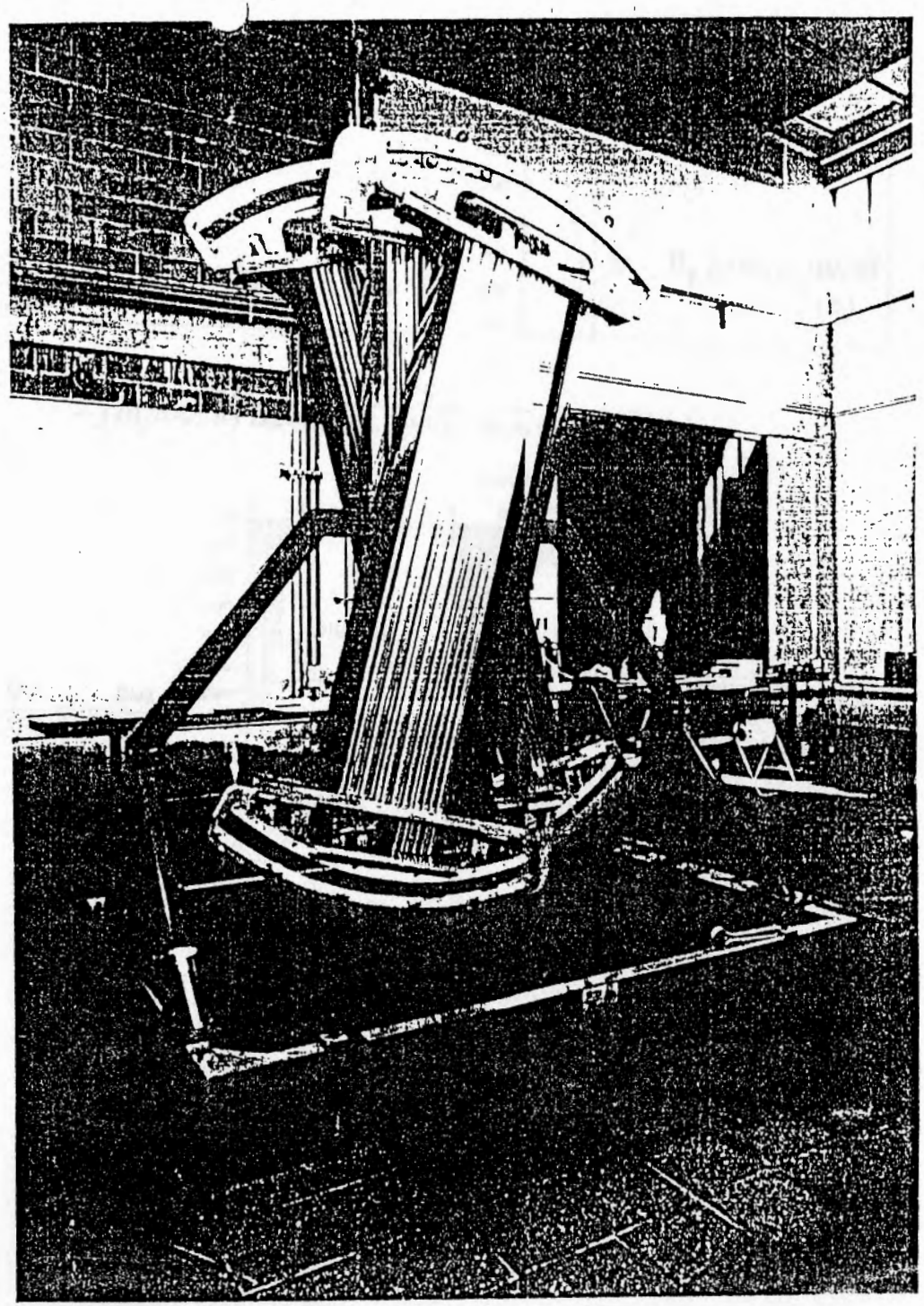

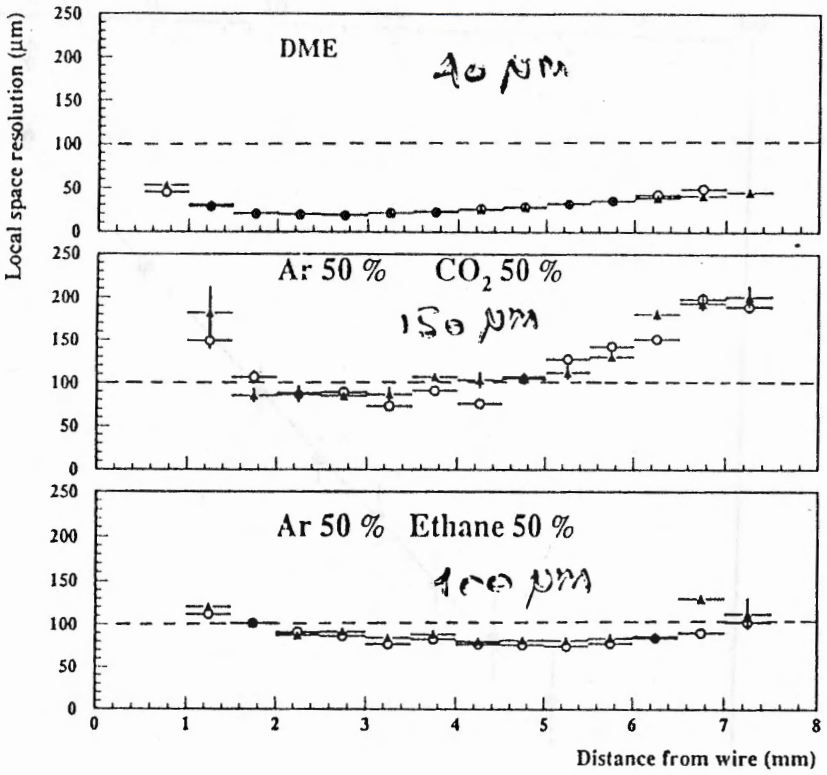

Trigger strategy

- The **aim** of the trigger logic is to **select**, against the background, events where :
  - The Φ decays into K^+K^-.
  - The K^- stops **inside** the target.
  - It forms a **hypernucleus** emitting a **prompt** π^- which crosses the **full** spectrometer.

- Trigger requests :
  - Tofino: a) "extended" **Back to Back** topology.
    b) **threshold** discrimination on **both** B.to B. slabs.

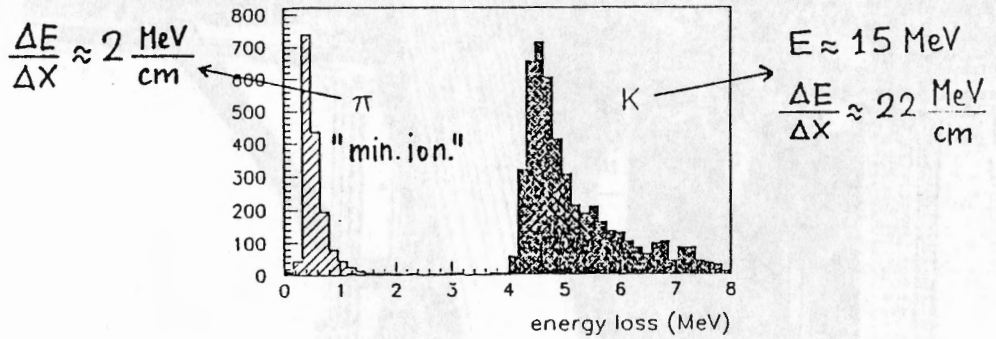

  - Tofone: a) **prompt** coincidence (<10 ns)
    b) multiplicity ≥ 1

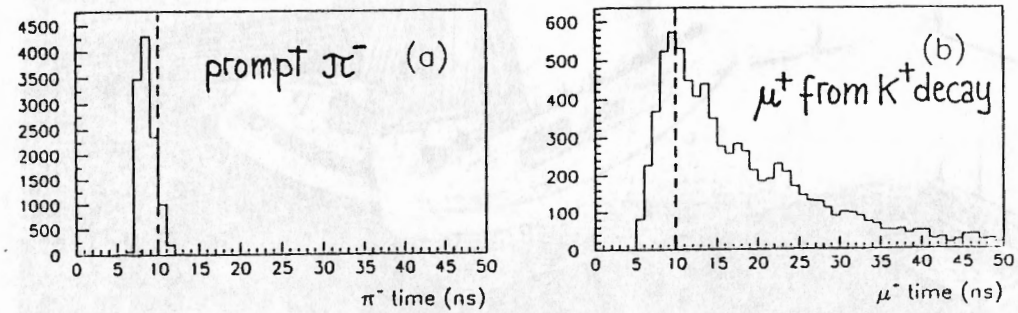

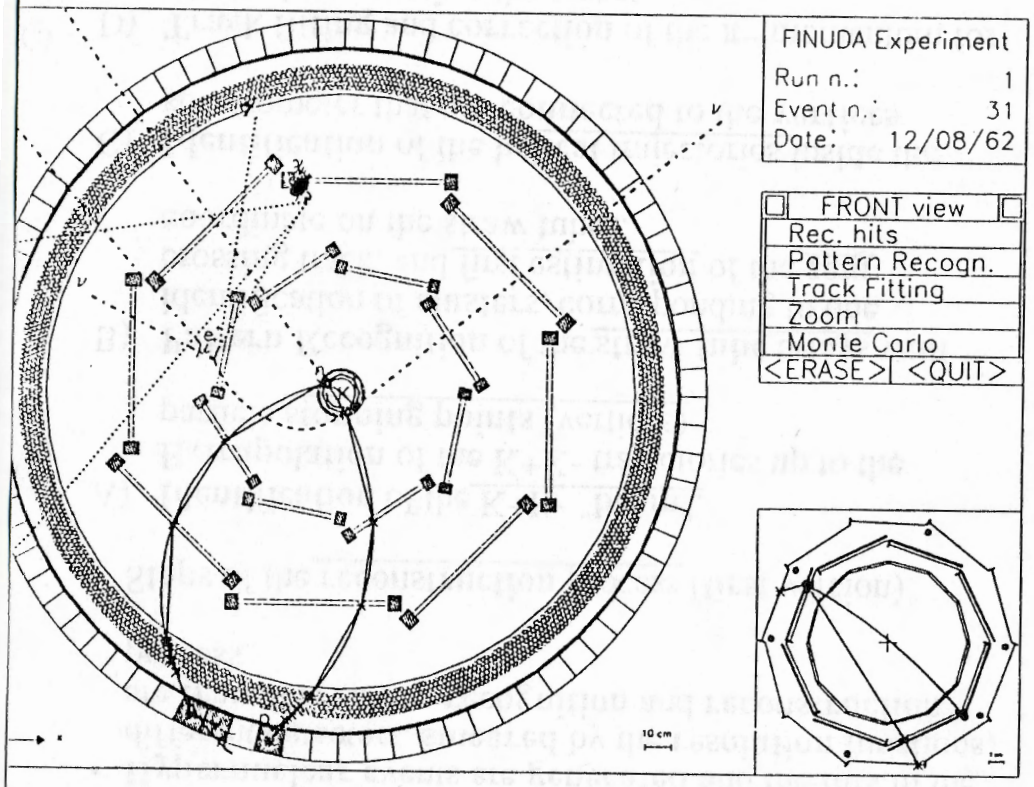

Trigger efficiency and rates

Trigger efficiency for hypernucleus formation events

Extended Back to Back, energy threshold and 10 ns time delay	
Back to Back * Energy Threshold	(80.6±1.3)%
Time coincidence	(46.2±1.0)%
TRIGGER	→ (38.6±1.0)%
TRIGGER + π^- 4 hits	→ (29.4±0.8)%

↑ "useful events" ~ $\frac{1}{2}$ has "forward pions"

Trigger rejection powers for background processes

Bhabha	$< 10^{-2}$ %
$\Phi \rightarrow K_S K_L$	$(3\pm1)\ 10^{-2}$ %
$\Phi \rightarrow \rho\pi$	$(4\pm1)\ 10^{-2}$ %
$\Phi \rightarrow \pi^+\pi^-\pi^\circ$	10^{-2} %
K^- interaction without hypernucleus formation	(7.3±0.5)%

Trigger rates at luminosity : $(L = 10^{32}\ cm^{-2}\ s^{-1})$

Hypernucleus formation (10^{-3} capture rate) →	$8\cdot10^{-2}$ Hz
Bhabha	$< 4\cdot10^{-2}$ Hz
$\Phi \rightarrow K_S K_L$	$\approx 5\cdot10^{-2}$ Hz
$\Phi \rightarrow \rho\pi$	$\approx 2\cdot10^{-2}$ Hz
$\Phi \rightarrow \pi^+\pi^-\pi^\circ$	$\approx 10^{-3}$ Hz
K^- interaction without hypernucleus formation	15 Hz

useful events · forward pions

$$8\cdot10^{-2}\ \text{Hz} \times \frac{29.4}{38.6} \times 0.80 \times 0.45 \times 3600 \approx 80\ \frac{\text{event}}{\text{hour}}$$

Trigger rate · chamber transparency · for high resolution spectroscopy

PATTERN RECOGNITION AND EVENT RECONSTRUCTION STRATEGY

- **Hypernuclear** events are **generated** and the **hits** in the different detectors, **smeared** by the **resolution** functions, are **transferred** to a **recognition** and **reconstruction** process

- Steps of the **reconstruction** process (**first** version)

A) **Identification** of the K+K- **"beam".**
Extrapolation of the K+K- trajectories up to the particle **stopping points** (vertices)

B) **Pattern Recognition** of the **straw tube** arrays with identification of **clusters**, corresponding to one crossing track, and **first estimation** of the **zeta** coordinate on the straw tubes.

C) **Identification** of the **helical** trajectories inside the spectrometer that are **connected** to the **vertices**

D) **Track fitting** and **correction** of the π^- momentum for energy lost **crossing** the target

- Tracks with only **three** points are **recognized** and **reconstructed** with **lower** quality and resolution

Low momentum π^-

"minimum ionizing"

$\Delta E \approx 0.12$ MeV, $\frac{\Delta E}{\Delta X} \approx 3.9 \frac{MeV}{cm}$

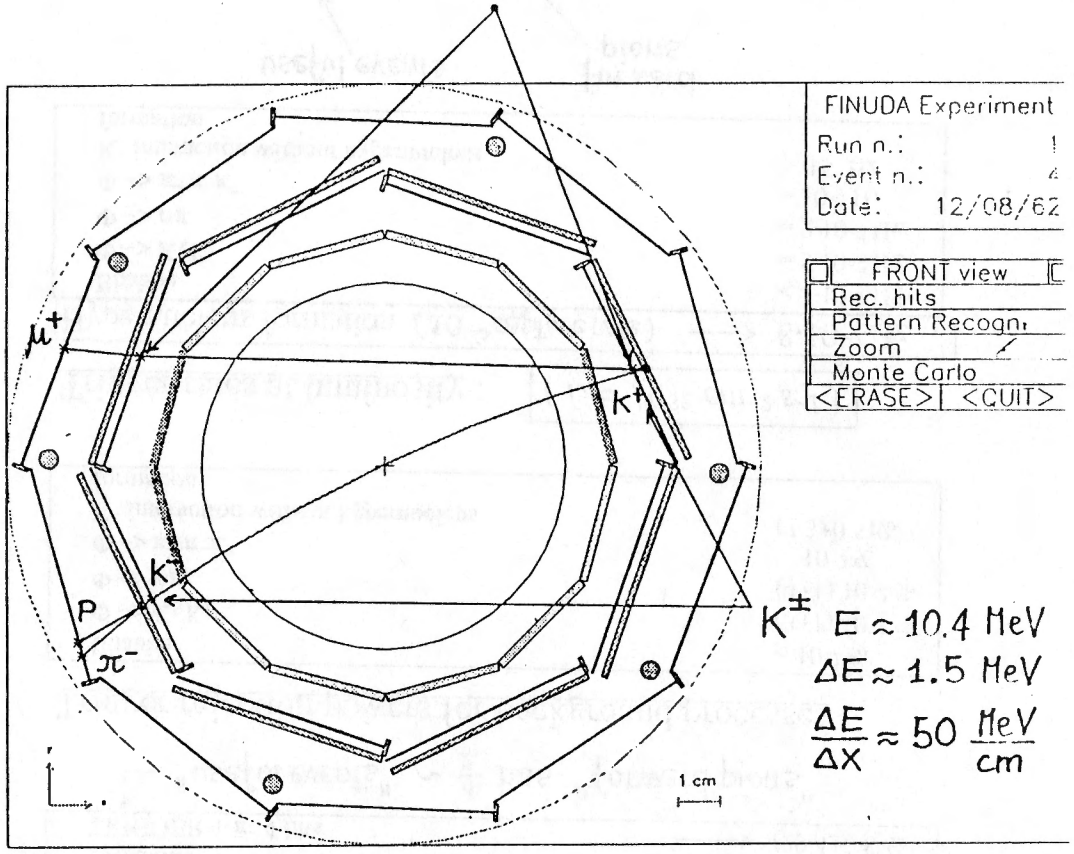

$K^\pm$ $E \approx 10.4$ MeV
$\Delta E \approx 1.5$ MeV
$\frac{\Delta E}{\Delta X} \approx 50 \frac{MeV}{cm}$

Pattern Recognition efficiency > 95%

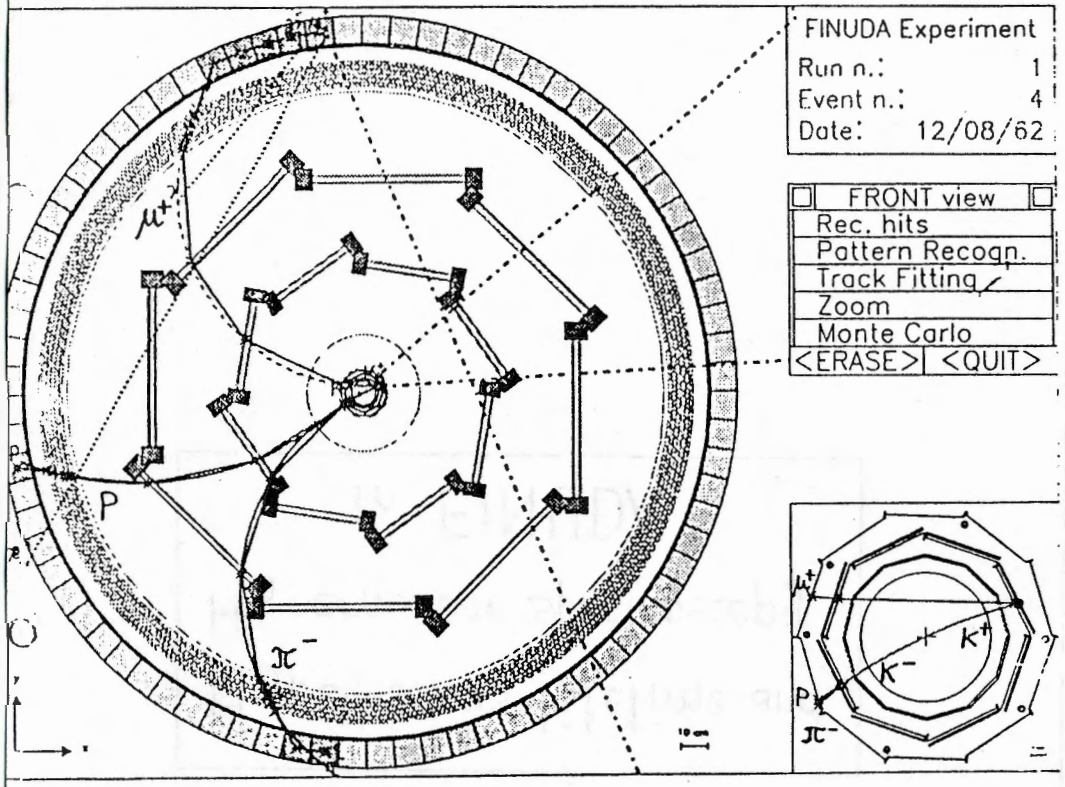

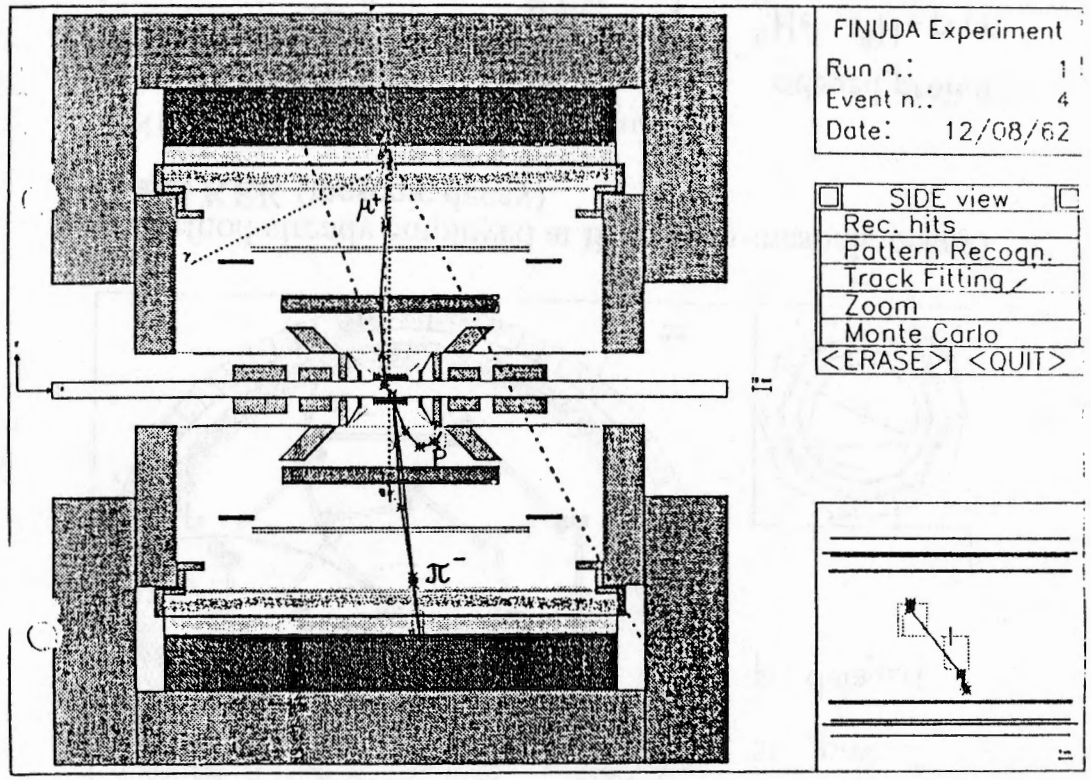

Hypernucleus lifetime and Hypernuclear spectroscopy in FINUDA

Hyp ...ucleus **lifetime** (τ) measurement

- The hypernucleus **lifetime** can be directly measured from the hit of the emitted **proton** in **Tofone**.

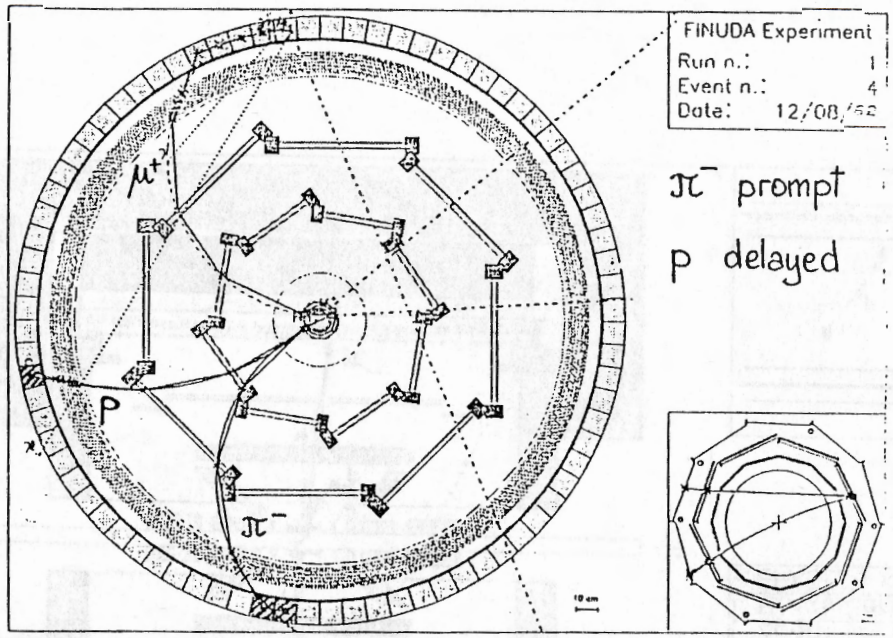

- Method already employed at **BNL** (non-mesonic decay) and **KEK** (mesonic decay).

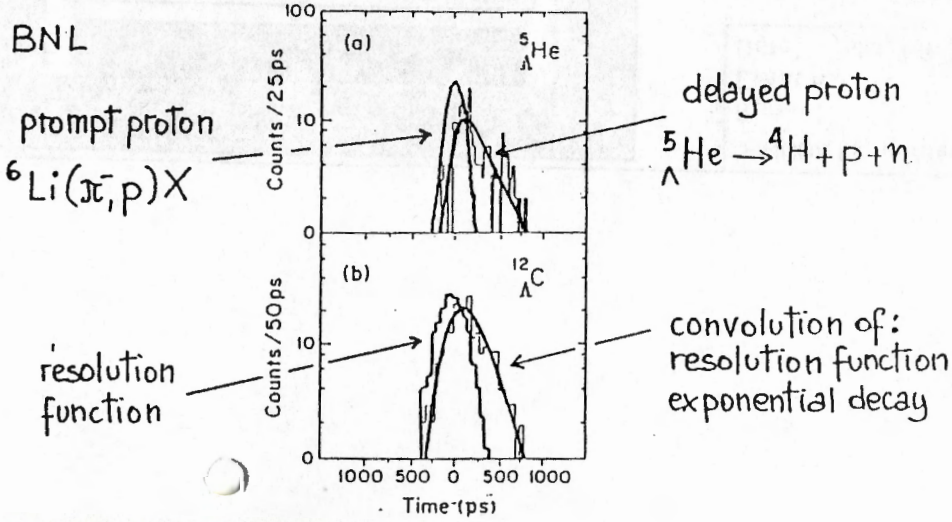

Hypernuclear lifetime measurement

$$time_p = time(tofone) - \frac{\text{proton path length}}{\beta_{proton} \cdot c}$$

$$time_\pi = time(tofone) - \frac{\pi \text{ path length}}{\beta_{pion} \cdot c}$$

$\sigma_t \sim 210$ ps (for $time_p$) ; $\sigma_t \sim 20$ ps (for $time_\pi$)

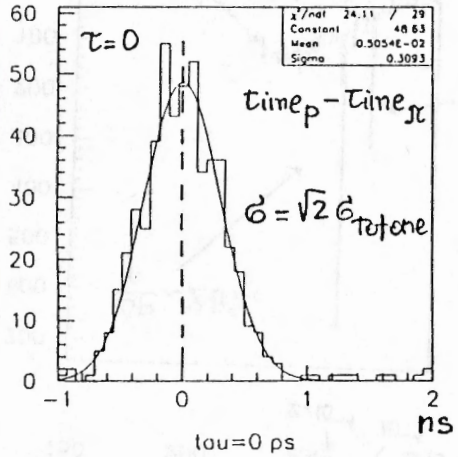

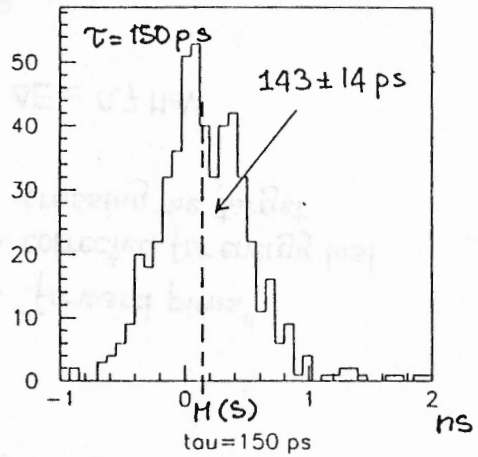

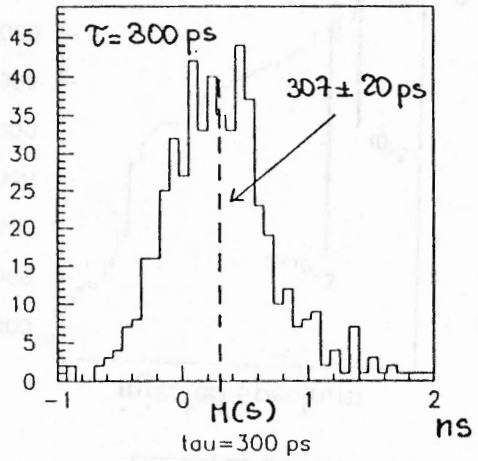

Convolution

$P(t) = \frac{1}{\tau} e^{-\frac{t}{\tau}}$ decay

$R(t)$ = experimental resolution function

$$S(t) = \frac{1}{N} \int R(u)\, P(t-u)\, du$$

$$M(S) = M(R) + M(P)$$

$$\tau = M(P) = M(S) - M(R) = M(S)$$

$M(R) = 0$

Obtained with ~1000 events in the hypernucleus ground state peak

12 hours at $\mathcal{L} = 10^{32} cm^{-2} s^{-1}$

Expected performances of FINUDA in **high** resolution hypernuclear **spectroscopy**

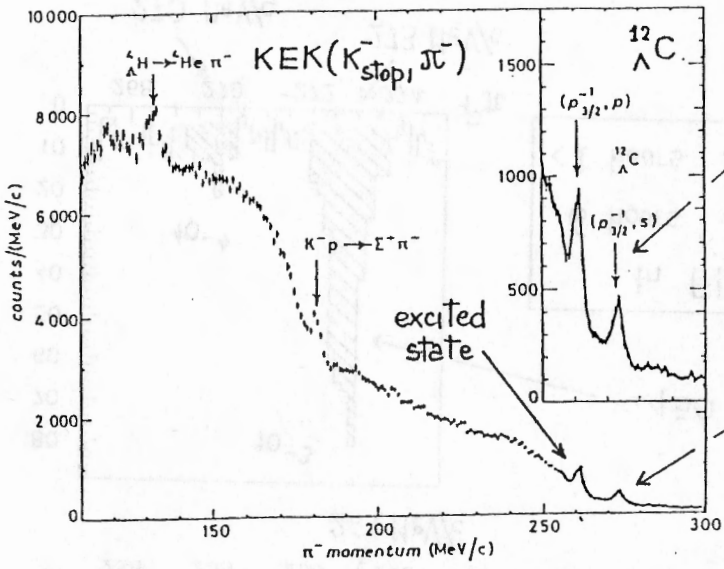

Energy resolution ~ 3 MeV (FWHM)

$\frac{\text{Signal}}{\text{Background}} = \frac{1}{1}$

KEK (π^+, K^+) Excitation Energy (MeV)

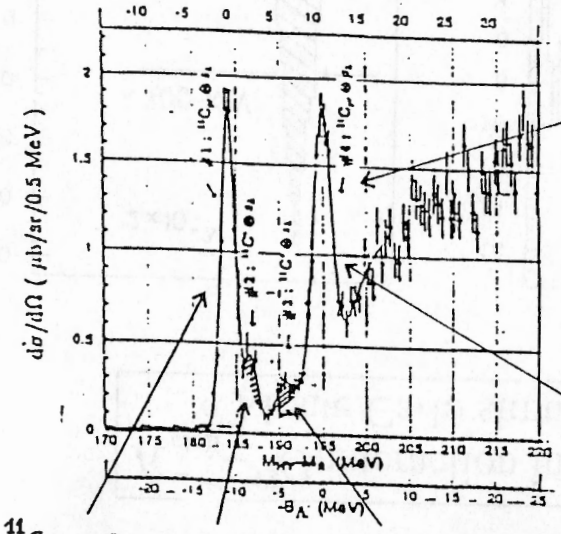

Energy resolution ~ 2 MeV (FWHM)

At least one week of data taking

K^-_{stop} – ^{12}C interaction in FINUDA
Monte Carlo simulation

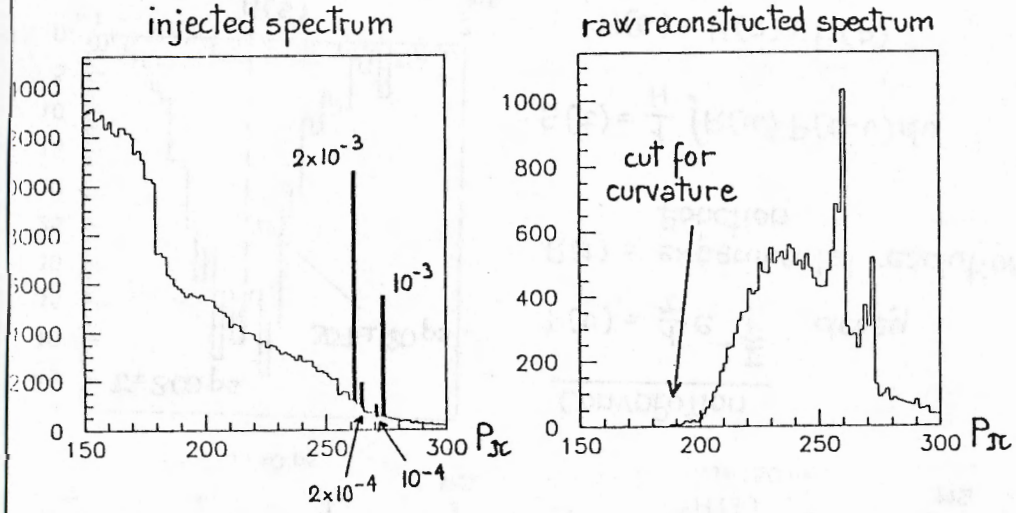

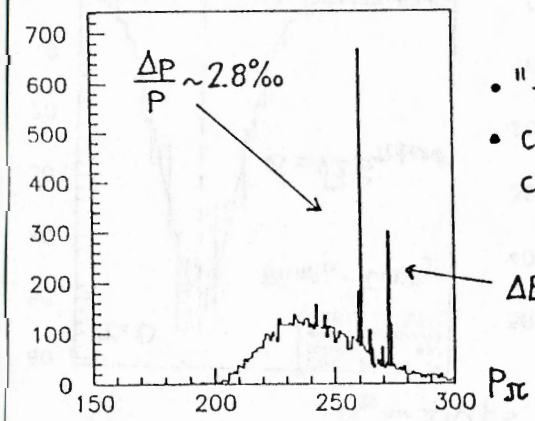

- "forward pions"
- corrected for energy lost crossing the target

ΔE ≈ 0.7 MeV

K^-_{stop} – ^{12}C interaction in FINUDA
Monte Carlo simulation

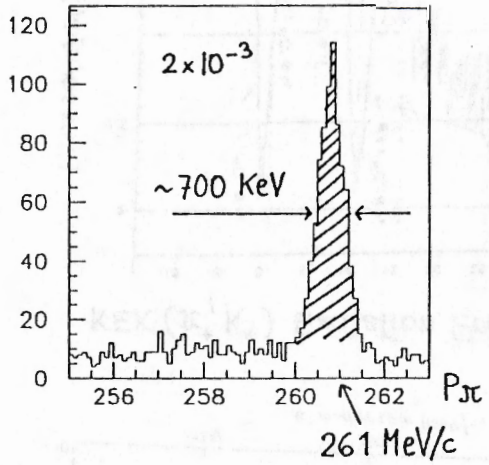

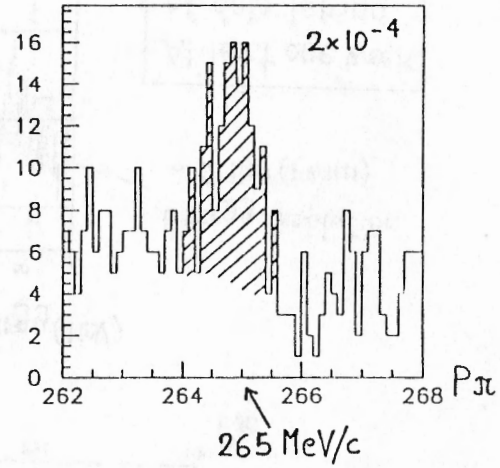

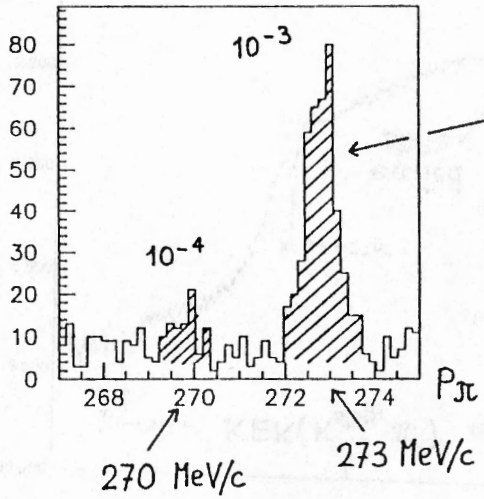

~450 events

In FINUDA
6 hours at 10^{32} cm^{-2}s^{-1}
<1 hours at 10^{33} cm^{-2}s^{-1}

A possible **improvement** for FINUDA
A background **suppression** method

H.Tamura et al. P.L. 160B(1985)32

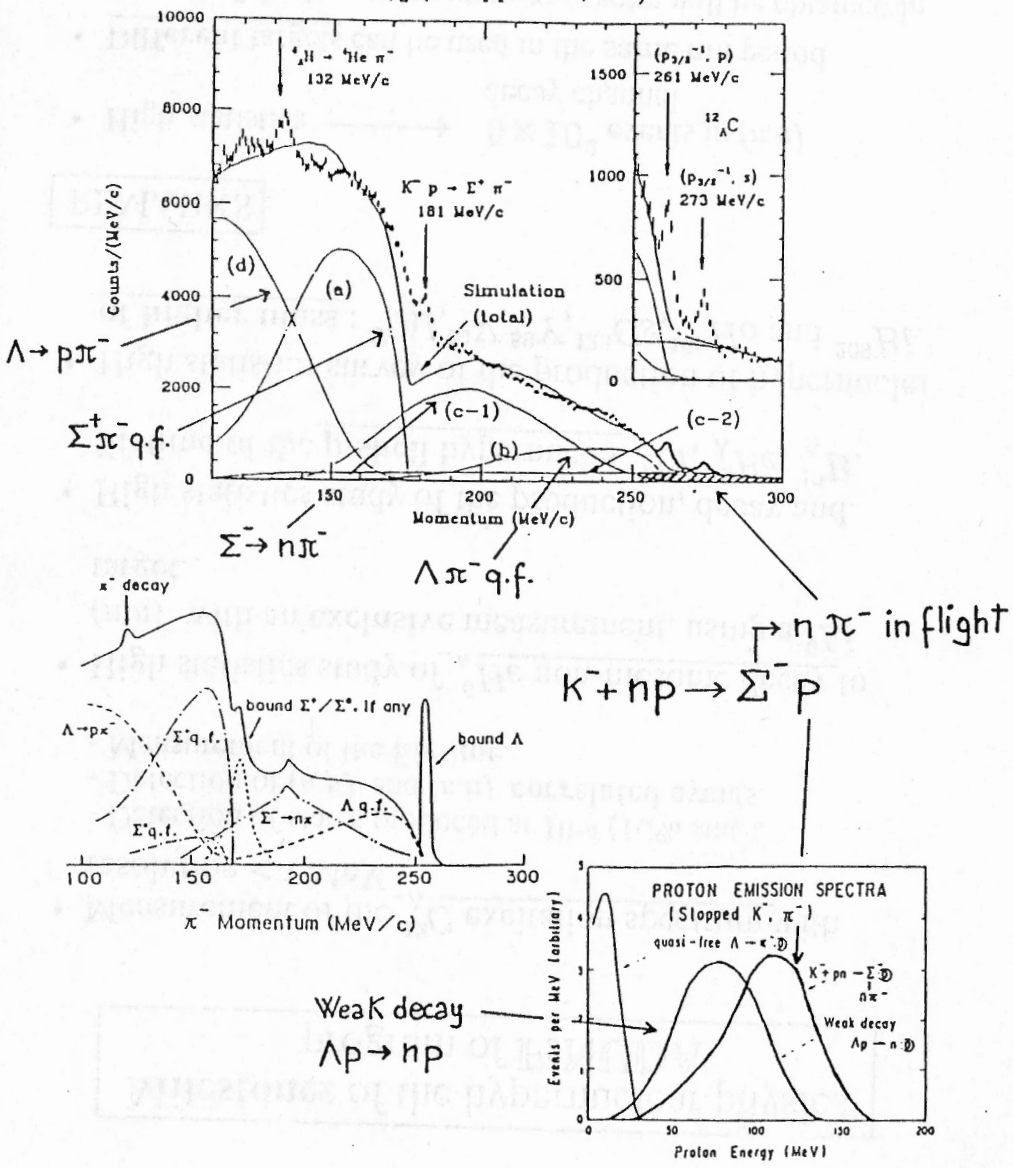

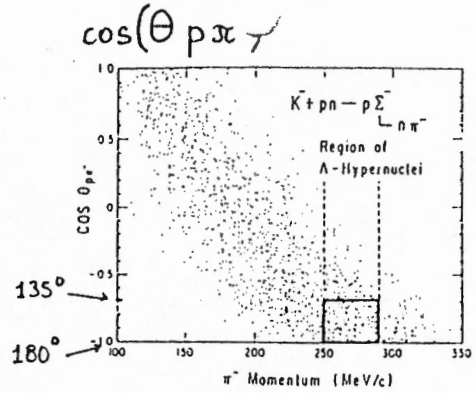

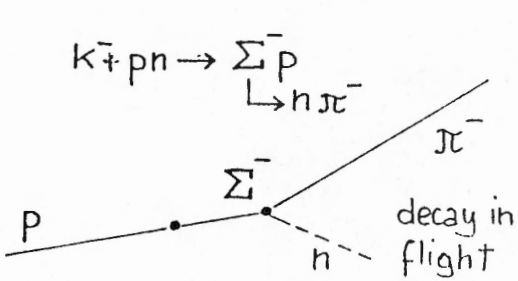

protons from non-mesonic decays are uncorrelated

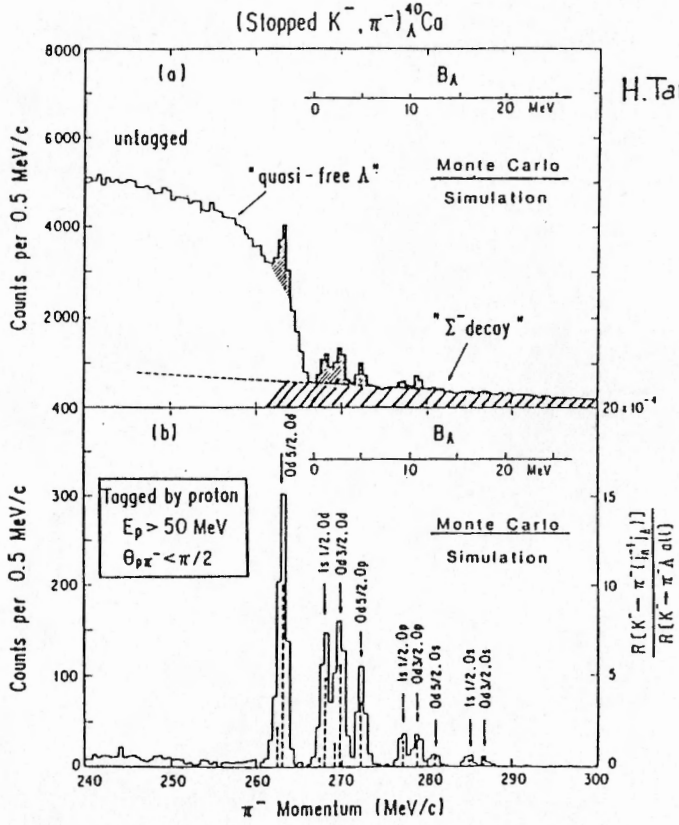

H.Tamura (1985)

- The **transparency** of **FINUDA** and the **thin** target allow the background **suppression** method to be applied **successfully**.

Milestones of the hypernuclear physics program of FINUDA

- Measurement of the ${}^{12}_{\Lambda}C$ excitation spectrum with resolution < 1 MeV.
  - Detection of states produced at 10^{-4} (10% stat.).
  - Detection of *(n,p)* and *(n,n)* **correlated** events.
  - Measurement of the **lifetime**.
- High statistics study of ${}^{6}_{\Lambda}He$ non-mesonic decay to *(n,n)* with an **exclusive** measurement, using a ${}^{6}Li$ target.
- High statistics study of the production, decay and lifetime of the **p-shell** hypernuclei ${}^{7}_{\Lambda}Li$, ${}^{9}_{\Lambda}Be$, ${}^{10}_{\Lambda}B$.
- High statistics survey of the production of hypernuclei of **higher mass** : ${}^{27}Al$, ${}^{51}V$, ${}^{89}Y$, ${}^{133}Cs$, ${}^{165}Ho$ and ${}^{209}Bi$.

REMARKS

- **High** statistics $\longrightarrow$ 5×10^2 events in *(n,n)* decay channel
- **Different** targets can be used in the **same** run period
- Survey of the **low momentum** π^- spectra will be obtained in **parasitic** way in parallel with the data taking.

April '95

Monte Carlo simulation of the performance of the realistic detector configuration.

- Final FINUDA geometry
- Spectrometer acceptance
- Spectrometer momentum resolution
- Trigger efficiency and rates

Rotation by $\frac{\pi}{8}$ of the internal chamber layer.

Improvement of 30% acceptance for curved tracks. (π of 270 MeV/c)

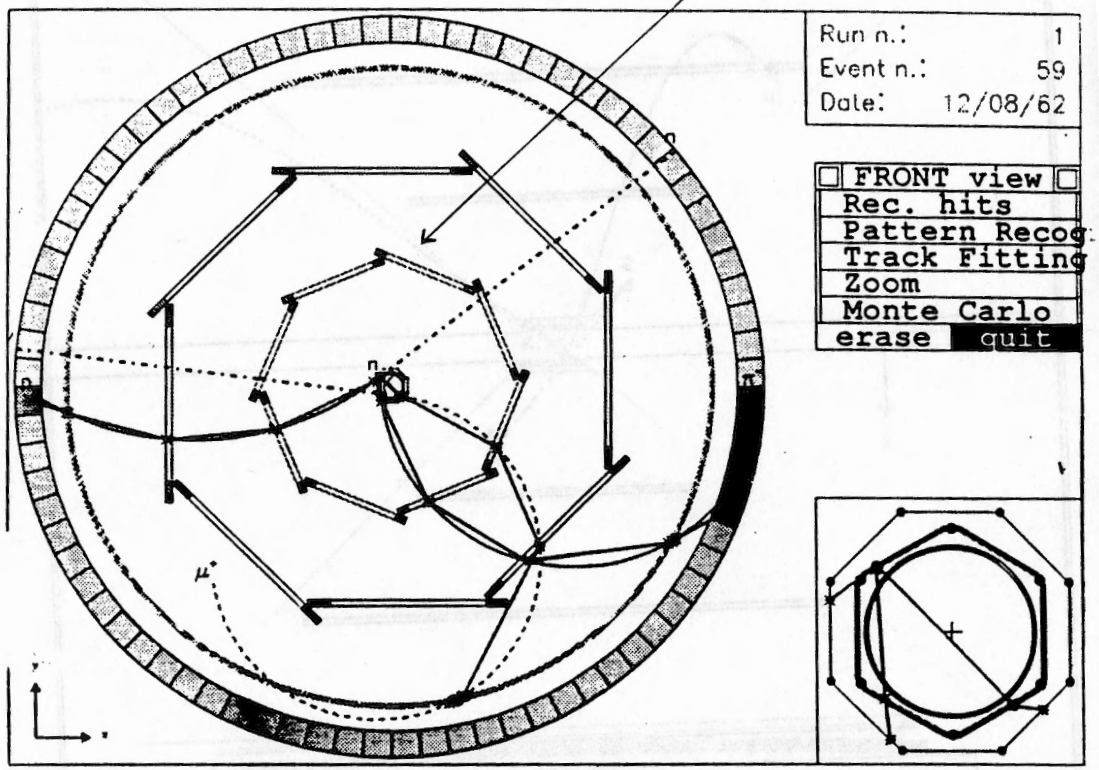

Hexagonal target geometry
better determination of K^- and K^+
stopping points

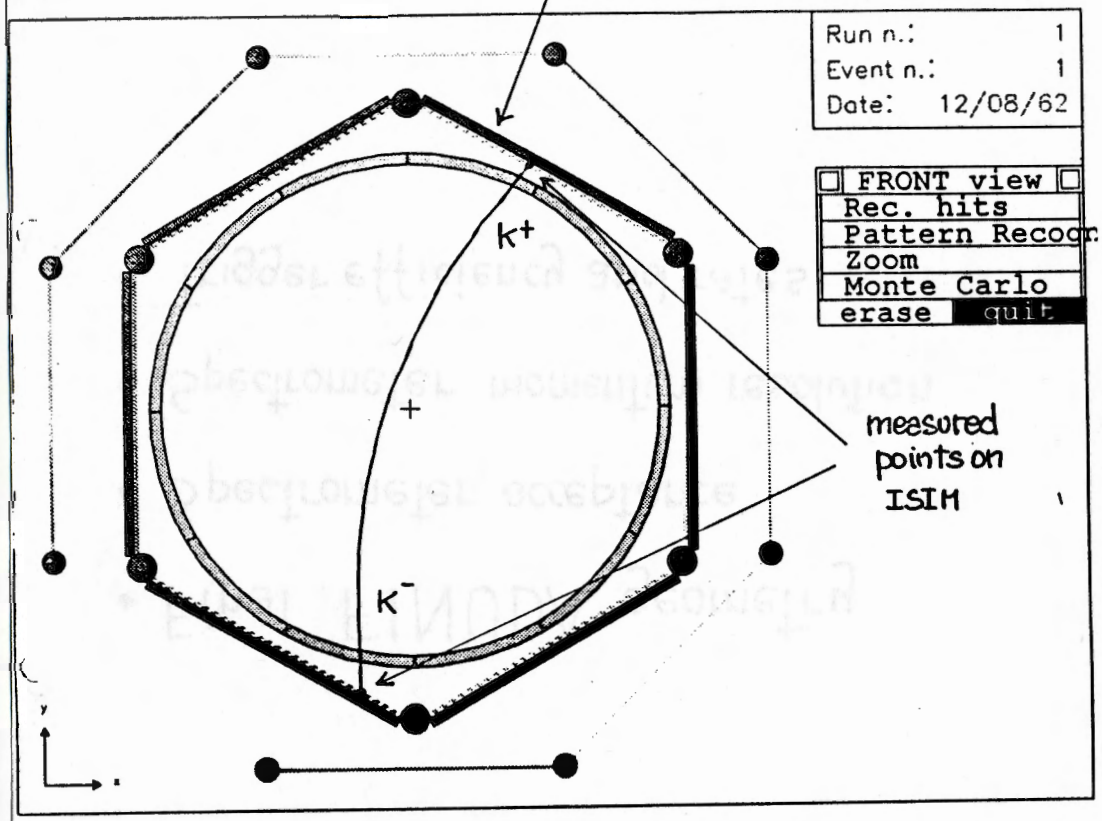

FINUDA Experiment (L.N.F. / DAΦNE)

SIDE view

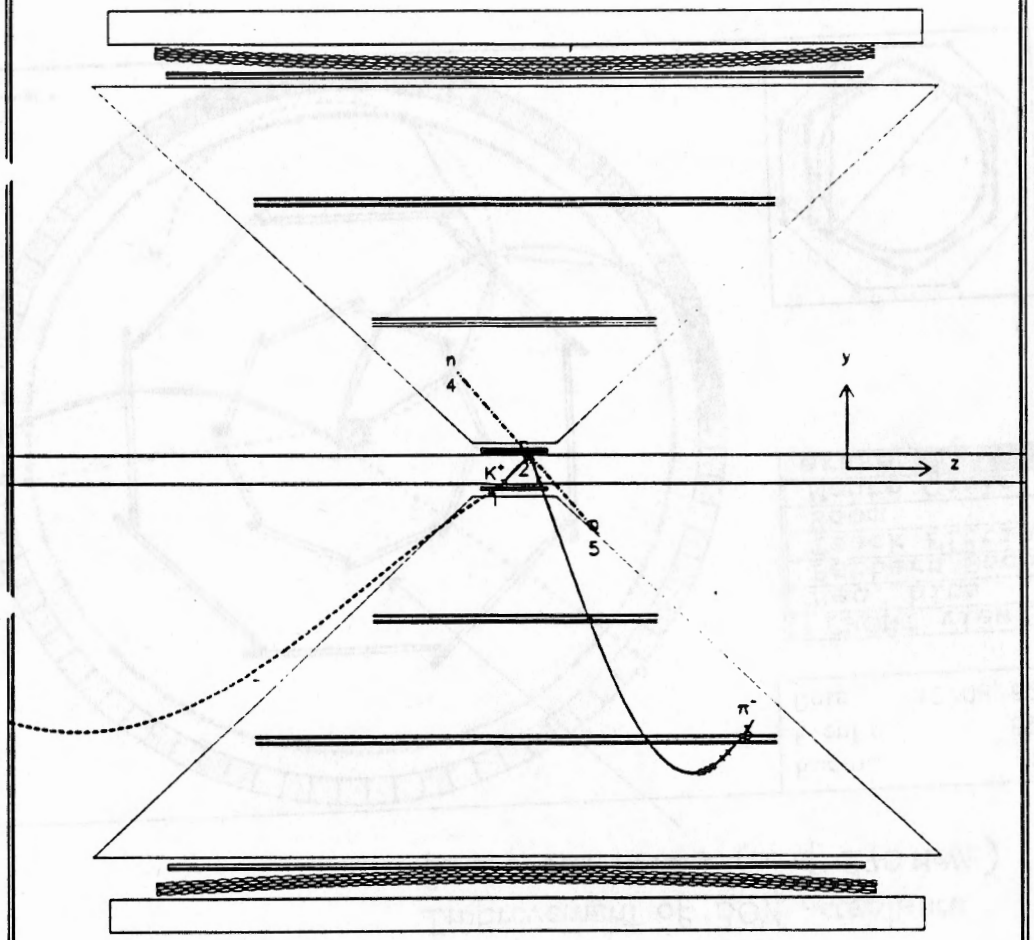

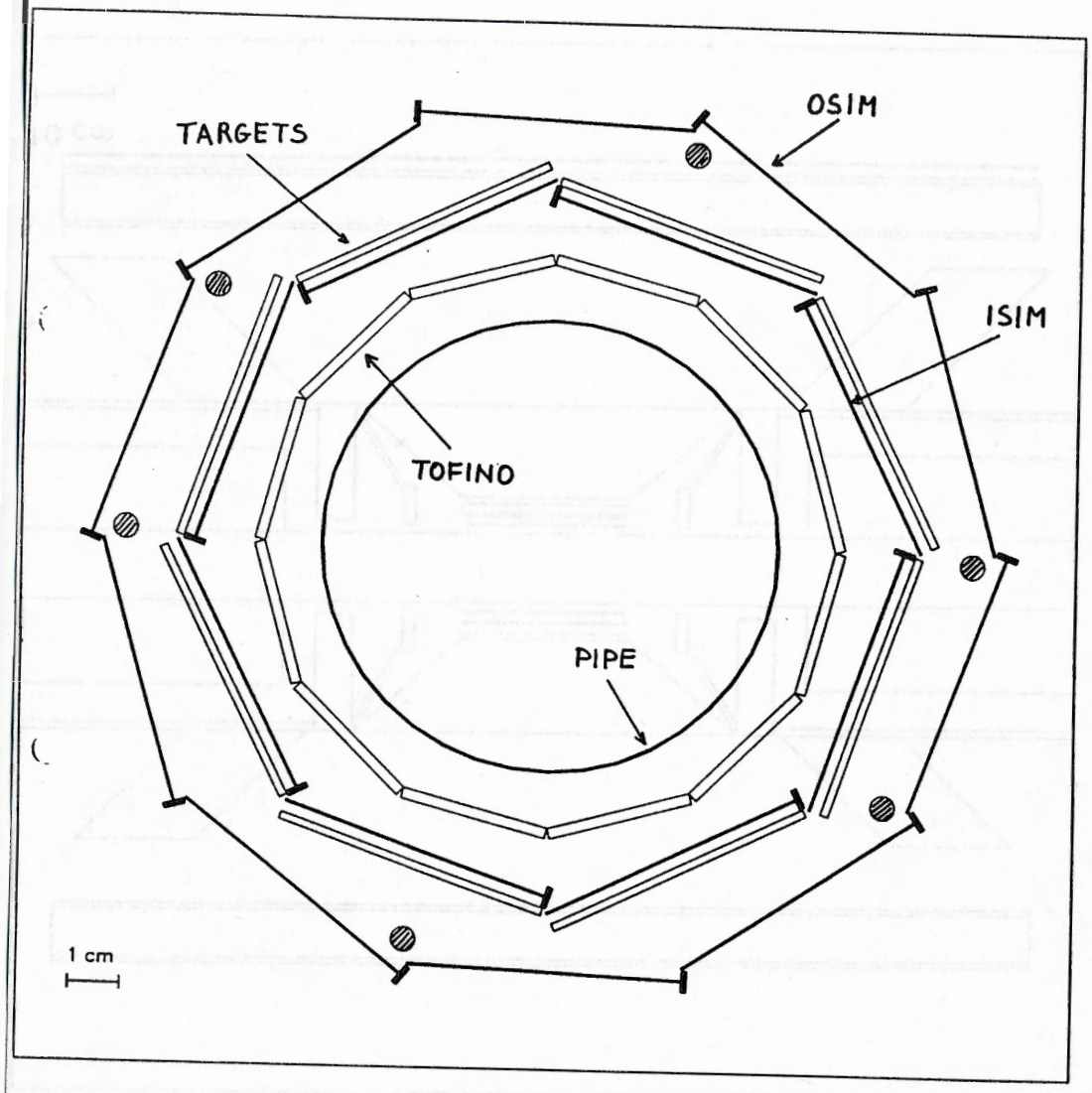
TARGETS
OSIM
ISIM
TOFINO
PIPE
1 cm

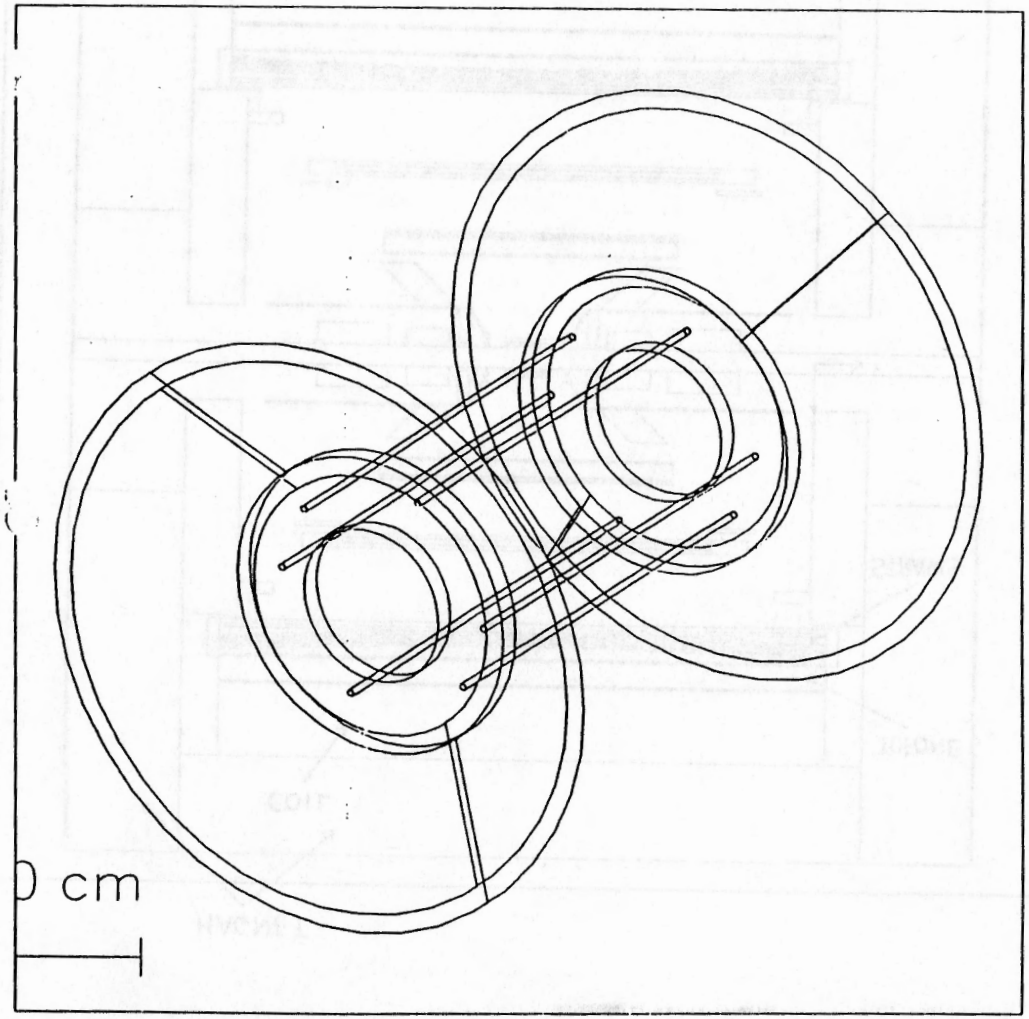
cm

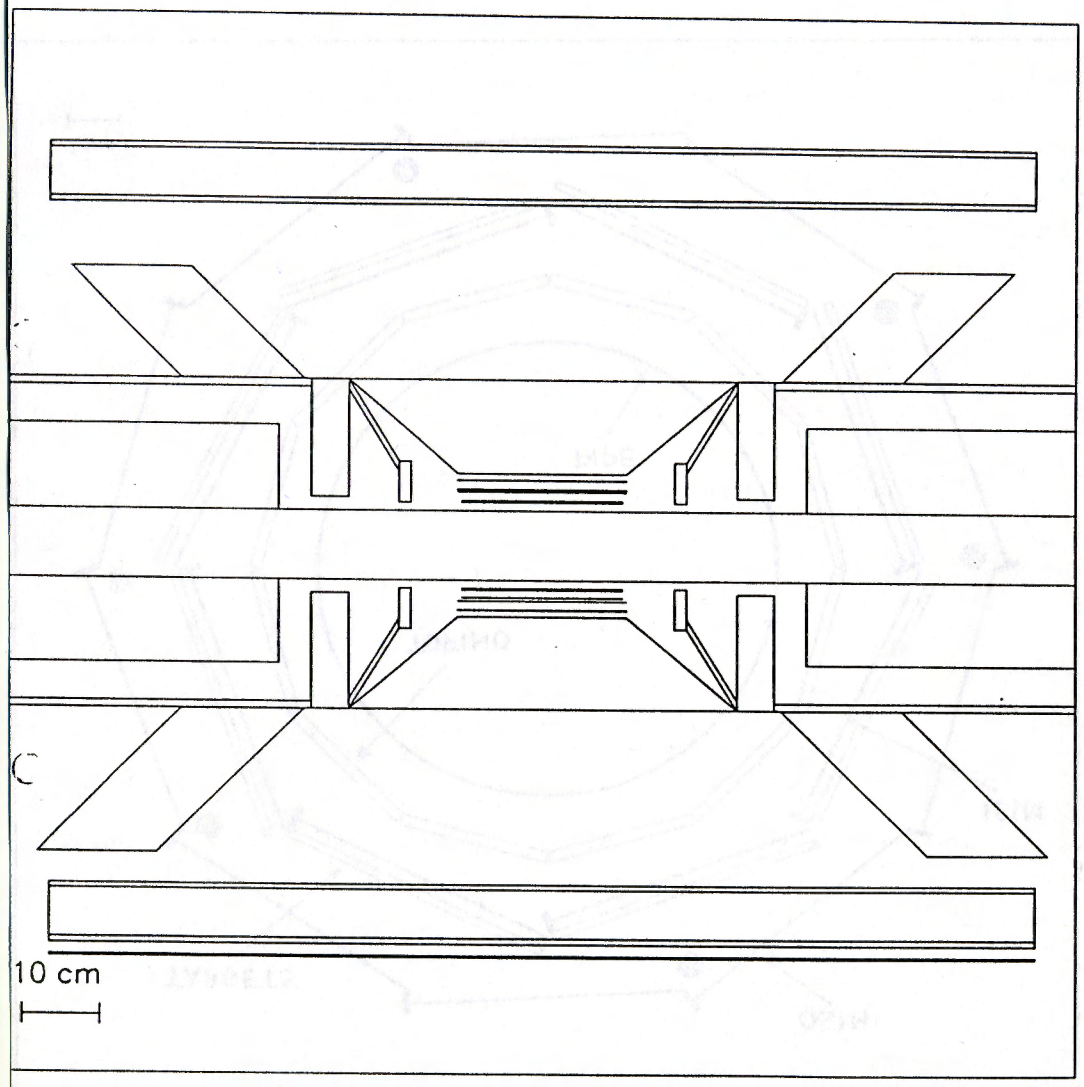
10 cm

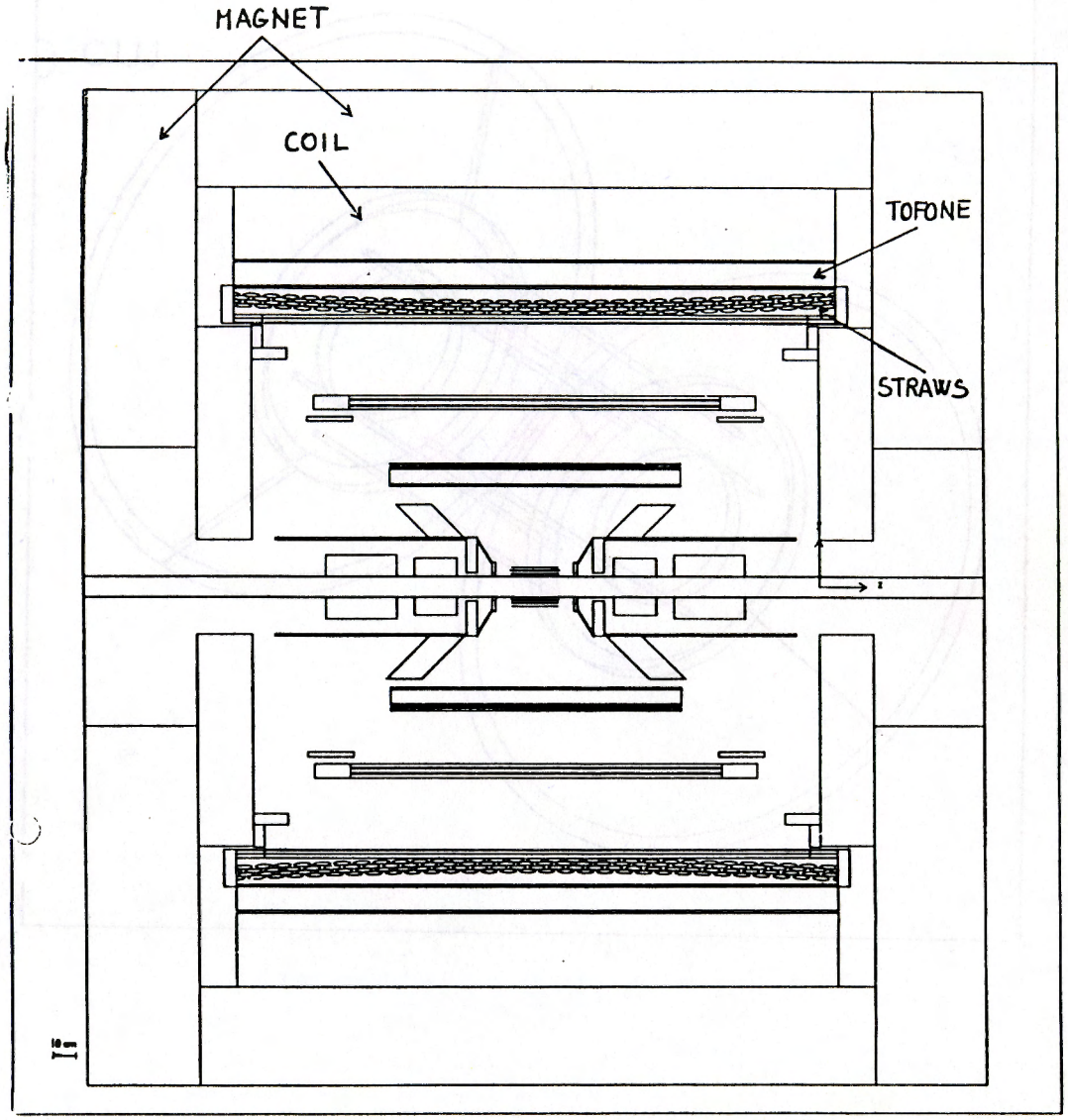
MAGNET
COIL
TOFONE
STRAWS

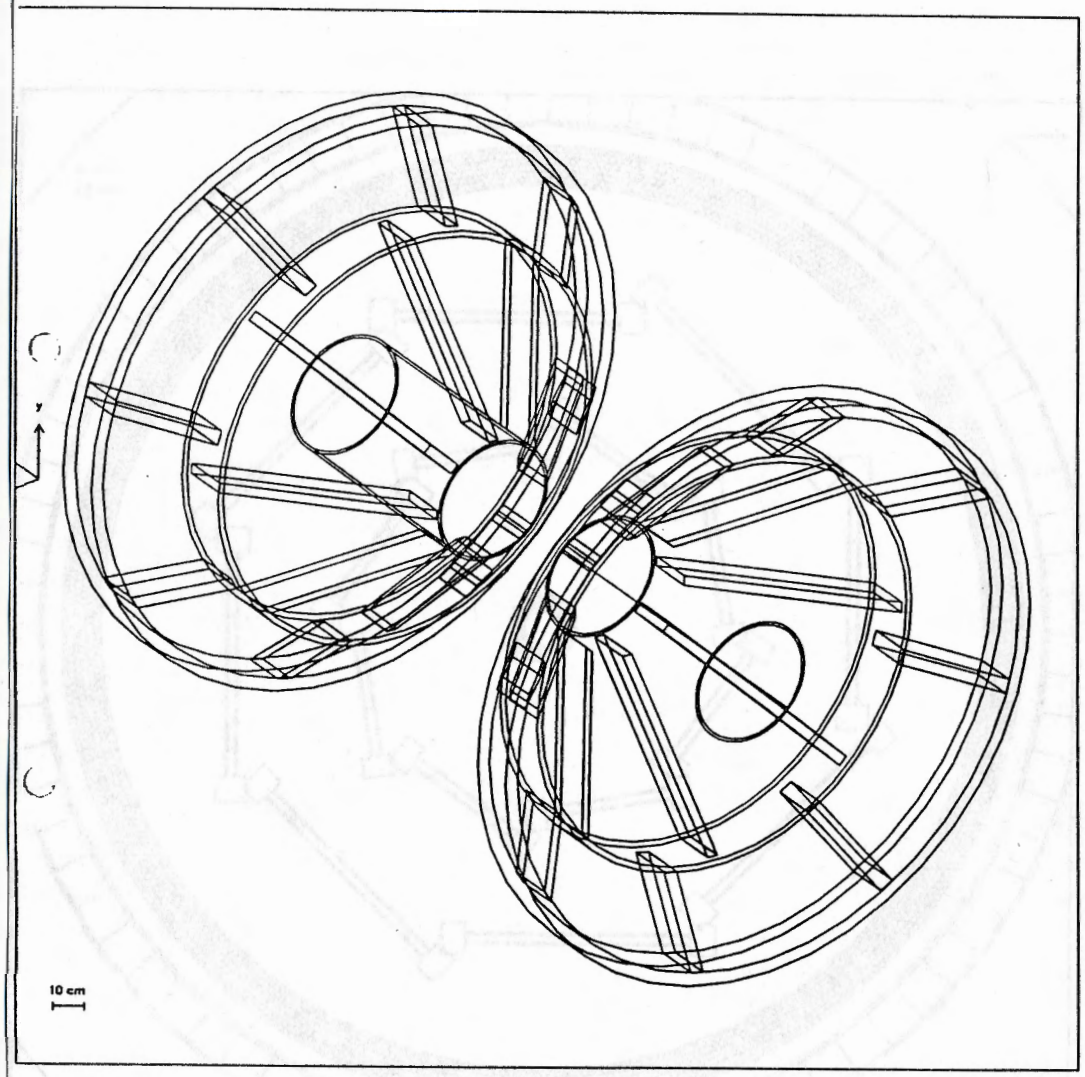
10 cm

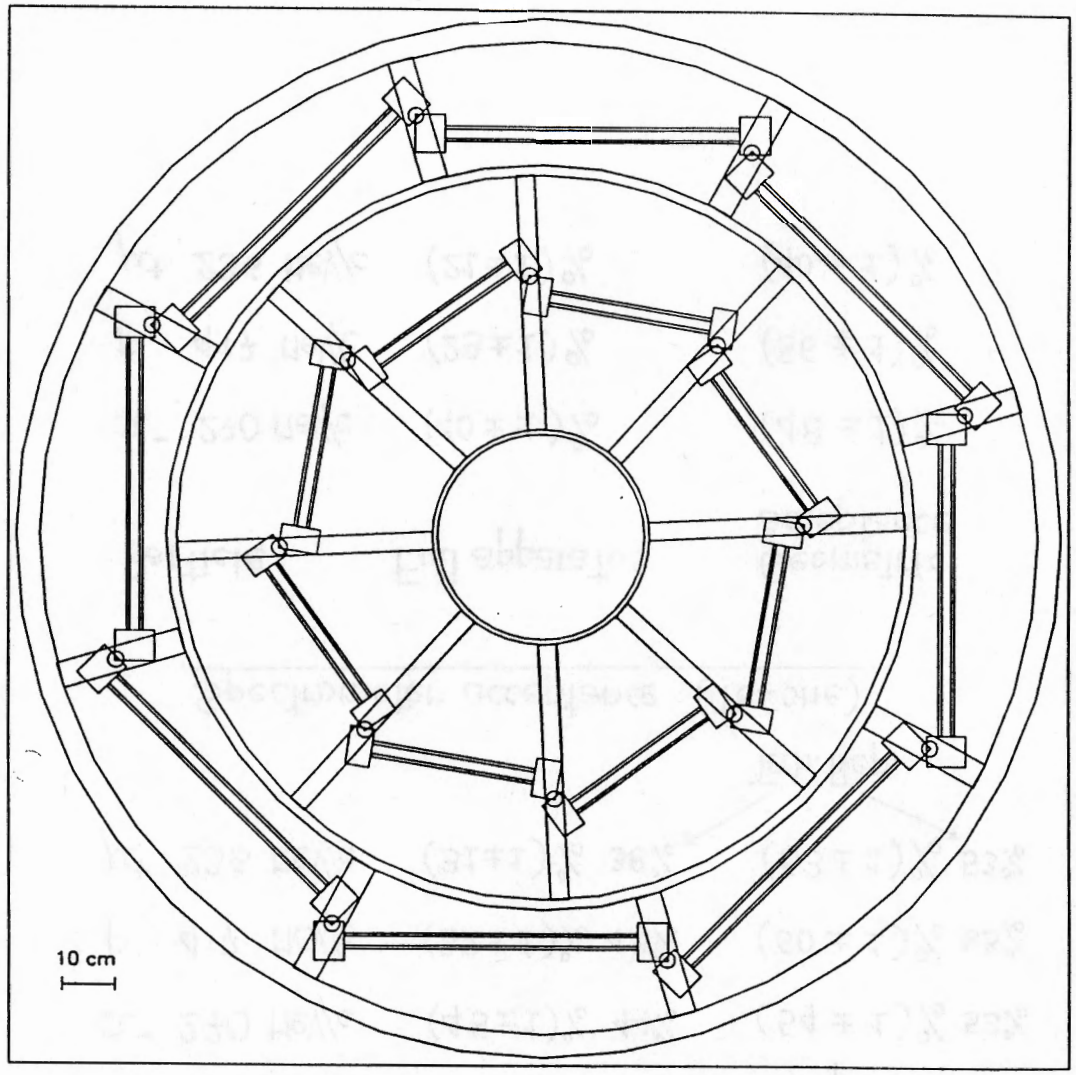
10 cm

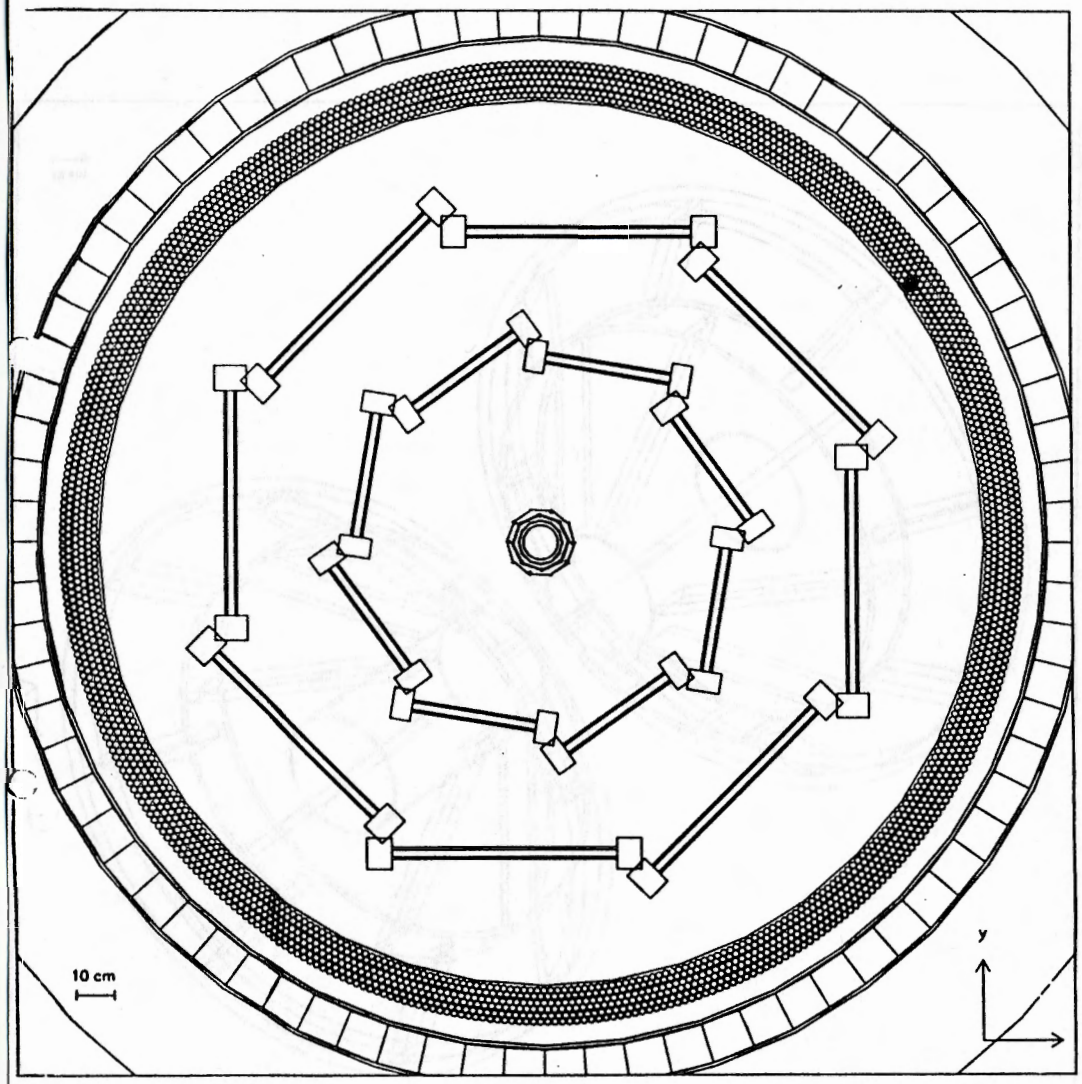

Spectrometer acceptance (straw Tubes)

Particle	Full apparatus	Geometric acceptance
π^- 270 MeV/c	(45±1)% 44%	(54 ± 1)% 53%
P 417 MeV/c	(32±1)% 43%	(60 ± 1)% 63%
μ^+ 236 MeV/c	(31±1)% 38%	(53 ± 1)% 53%

Tech. Rep.

Spectrometer acceptance (Tofone)

Particle	Full apparatus	Geometric acceptance
π^- 270 MeV/c	(40 ± 1)%	(48 ± 1)%
P 417 MeV/c	(29±1)%	(56 ± 1)%
μ^+ 236 MeV/c	(21±1)%	(40 ± 1)%

Momentum resolution of the Spectrometer

Detector resolutions

			σ	
μstrips	Rφ		50 μm	
	z		50 μm	
chambers	Rφ	(100)	150 μm	(pessimistic)
	z		1 % wire (1-2 cm)	
Straws	r		100 μm	
	z	(500)	1,0 mm	(pessimistic)

Particle	Momentum resolution (FWHM)	
π^- 270 MeV/c	0.28 %	0.25%
p 417 MeV/c	0.79 %	0.70%
μ^+ 236 MeV/c	0.24%	

Total radiation length	170,000 cm
Helium	540,000 cm
Air	30,400 cm
Spectrometer size	102 cm (110 cm)

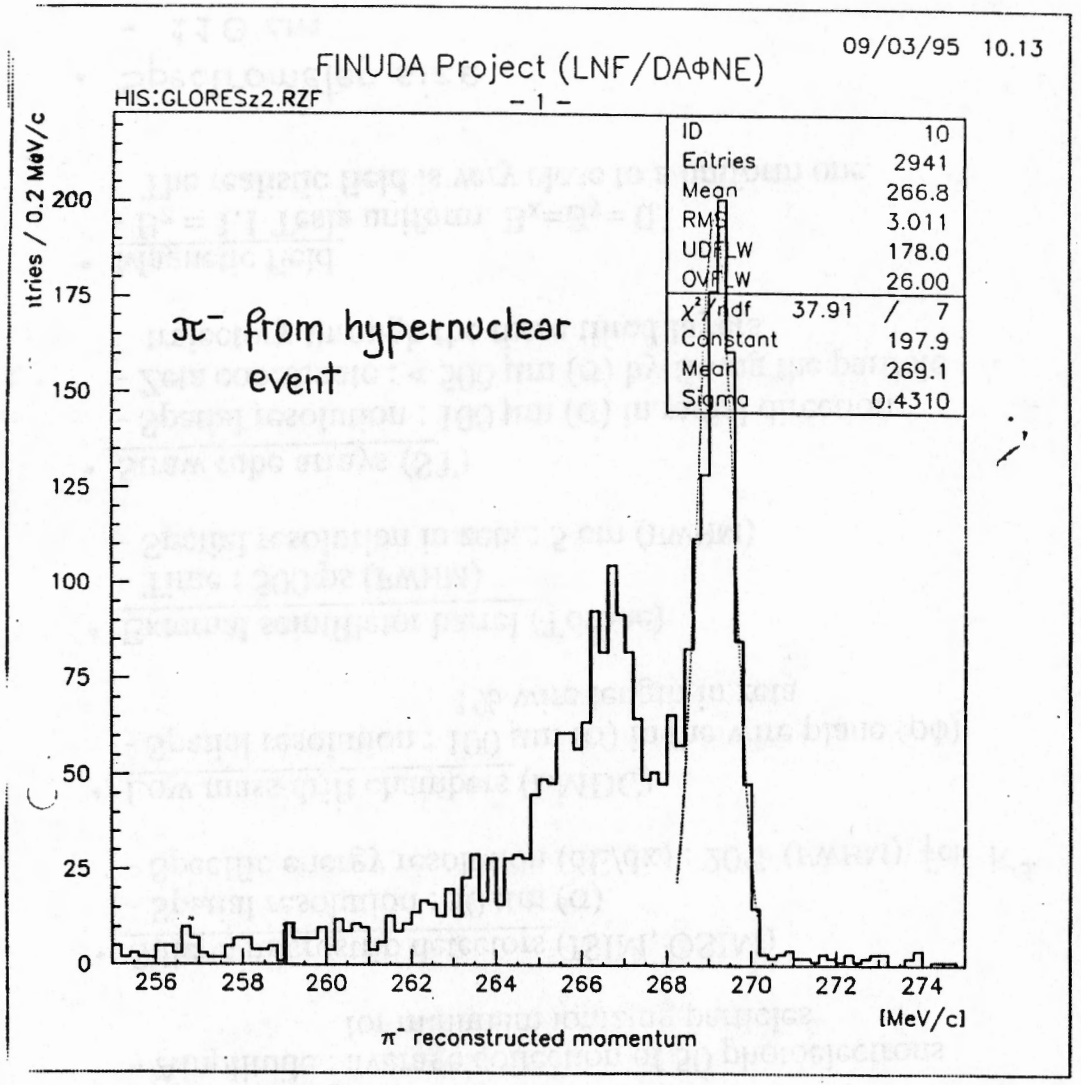

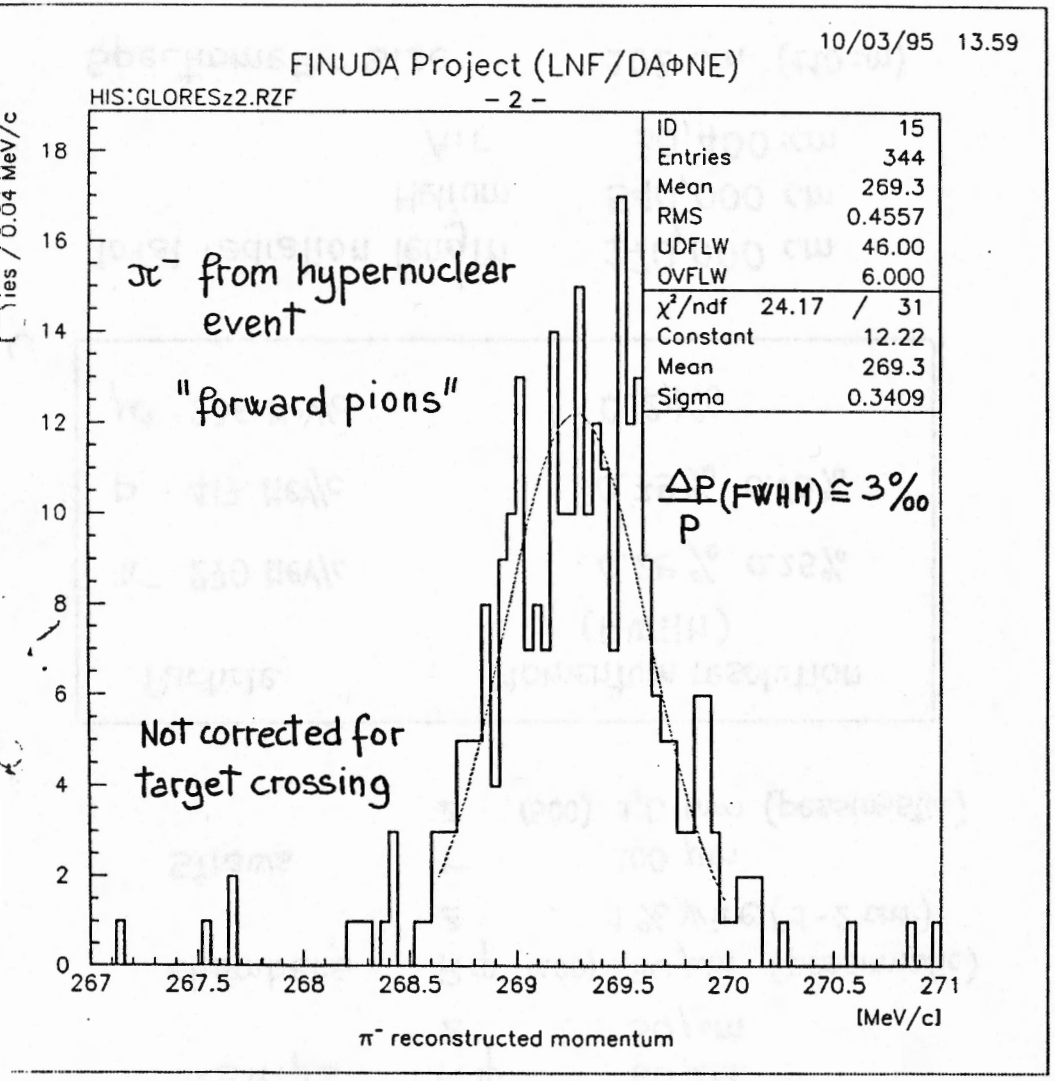

Previous configuration

Spatial, energy and time resolution of the detectors

- Internal scintillator barrel (Tofino) :
  - Time : 500 ps (FWHM)
  - Amplitude : average collection of 50 photoelectrons for minimum ionizing particles
- Silicon microstrip detectors (ISIM, OSIM)
  - Spatial resolution : 50 μm (σ)
  - Specific energy resolution (dE/dx) : 20% (FWHM) for $K^{\pm}$
- Low mass drift chambers (LMDC)
  - Spatial resolution : 100 μm (σ) in the wire plane (ρφ)
    1% wire length in zeta
- External scintillator barrel (Tofone)
  - Time : 500 ps (FWHM)
  - Spatial resolution in zeta : 5 cm (FWHM)
- Straw tube arrays (ST)
  - Spatial resolution : 100 μm (σ) in radial direction
  - Zeta coordinate : < 500 μm (σ) by fitting the particle trajectory through the three tilted layers
- Magnetic field
  - B_z = 1.1 Tesla uniform. $B_x = B_y = 0$.
    The realistic field is very close to a uniform one.
- Spectrometer size
  - 110 cm

FACTORS AFFECTING THE RESOLUTION IN MOMENTUM

① Intrinsic resolution of a spectrometer

$$p = \frac{p_T}{\sin\theta} \longrightarrow \left(\frac{\sigma_p}{p}\right)^2 = \left(\frac{\sigma_{p_T}}{p_T}\right)^2 + \left(\frac{\sigma_\theta}{\mathrm{tg}\theta}\right)^2$$

Resolution on p_T

$$\left(\frac{\sigma_{p_T}}{p_T}\right) \begin{cases} \text{helix fit} & \propto \dfrac{\varepsilon\, p_T}{B L^2} \dfrac{1}{\sqrt{N}} \\ \text{M.S.} & \propto \dfrac{1}{BL\beta} \sqrt{\dfrac{L}{L_0}} \end{cases}$$

Resolution on θ

$$\left(\frac{\sigma_\theta}{\mathrm{tg}\theta}\right) \begin{cases} \text{linear fit} & \propto \dfrac{1}{\mathrm{tg}\theta} \dfrac{\varepsilon}{L} \dfrac{1}{\sqrt{N}} \\ \text{M.S.} & \propto \dfrac{1}{\mathrm{tg}\theta} \dfrac{1}{\beta p} \sqrt{\dfrac{L}{L_0}} \end{cases}$$

② Energy straggling in materials before entering the spectrometer

$$\sigma_E^{\text{straggling}} \sim \sqrt{\frac{Z}{A} \cdot \frac{1}{1-\beta^2}\, \rho\, \Delta x} \quad \text{MeV}$$

③ Errors in evaluating energy lost before entering the spectrometer

Standard formulae

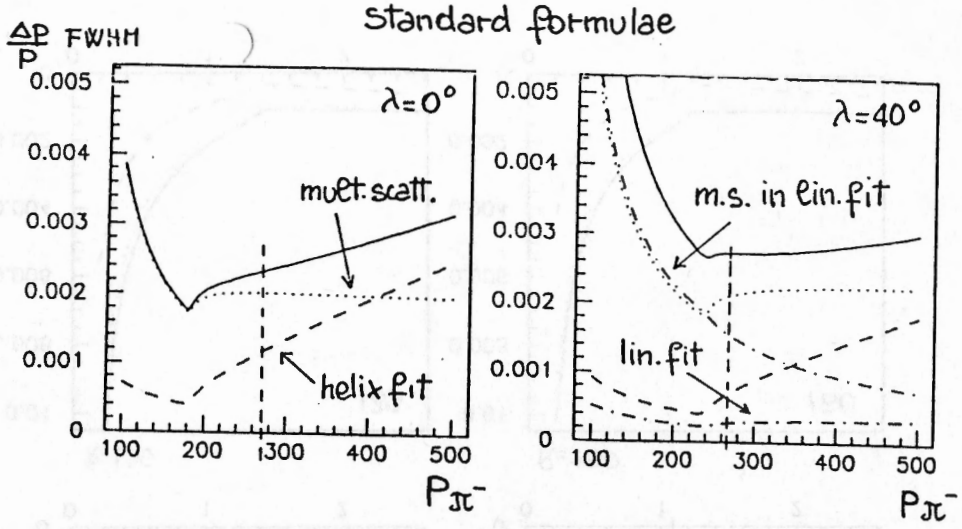

Check with Monte Carlo

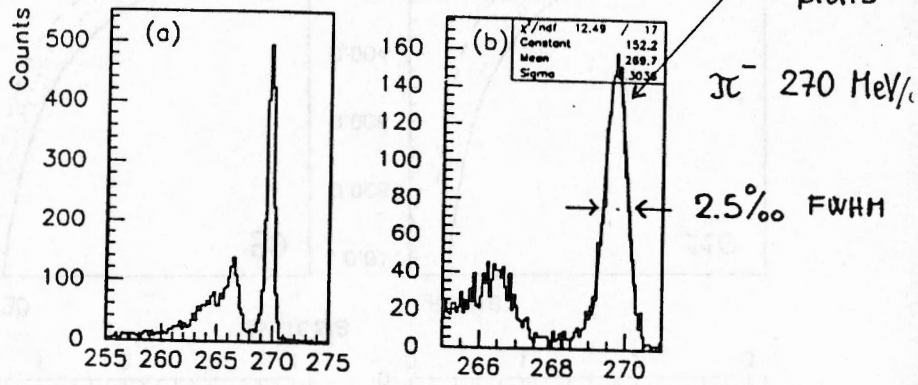

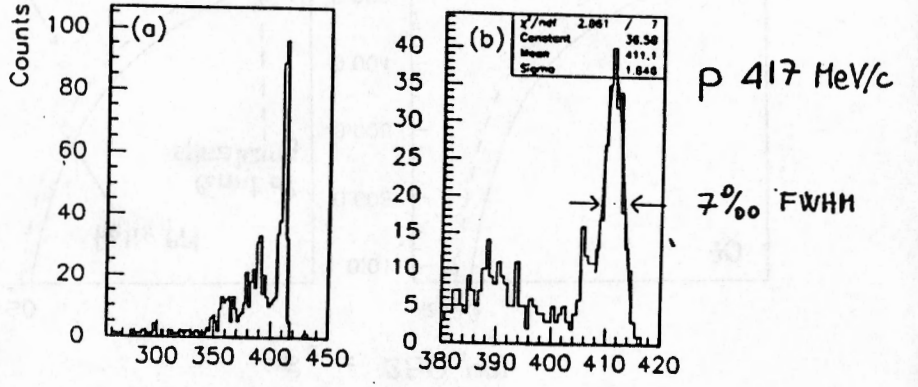

Resolution vs Magnetic Field at R= 110 cm.

π^- of 270 MeV/c σ_{xy} = 100 μm

$\lambda = 0$ σ_z = 250 μm

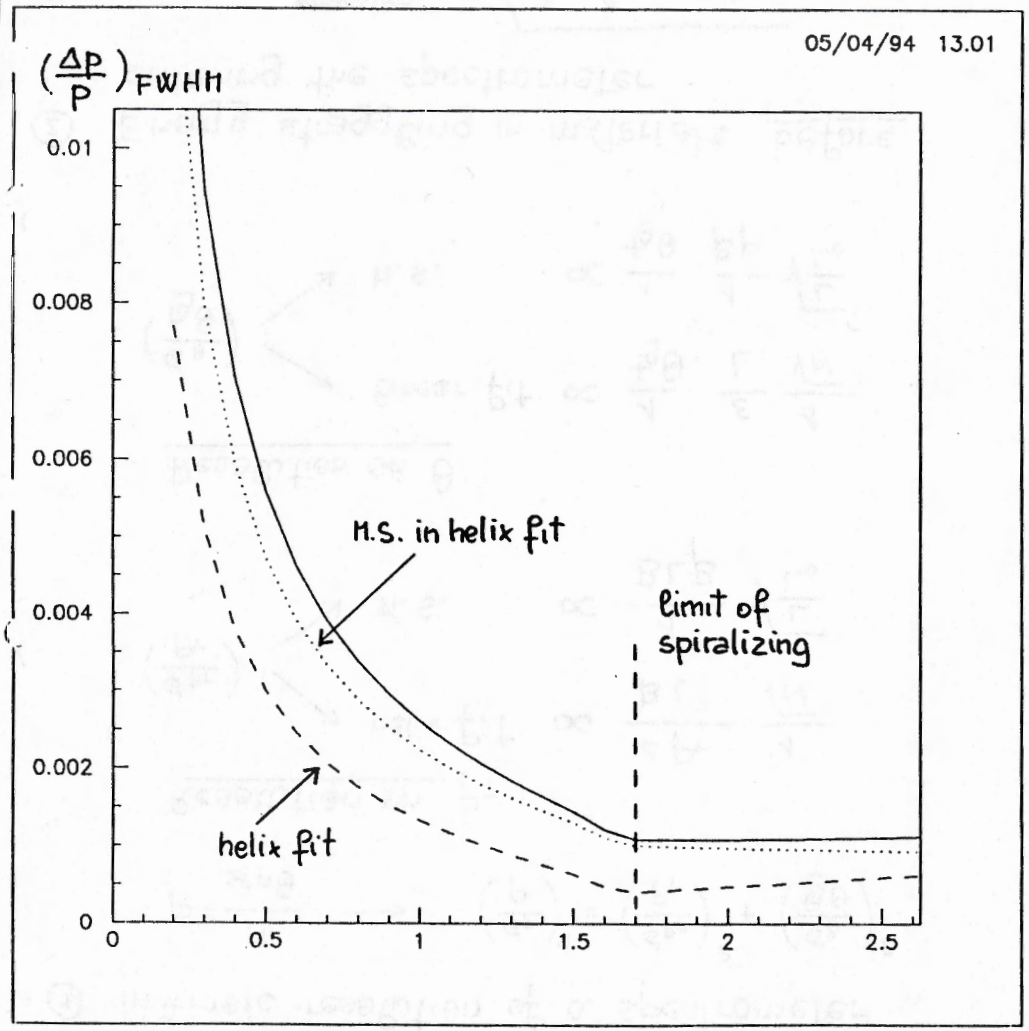

π^- of 270 .leV/c σ_{xy} = 100 μm

$\lambda = 0$ σ_z = 250 μm

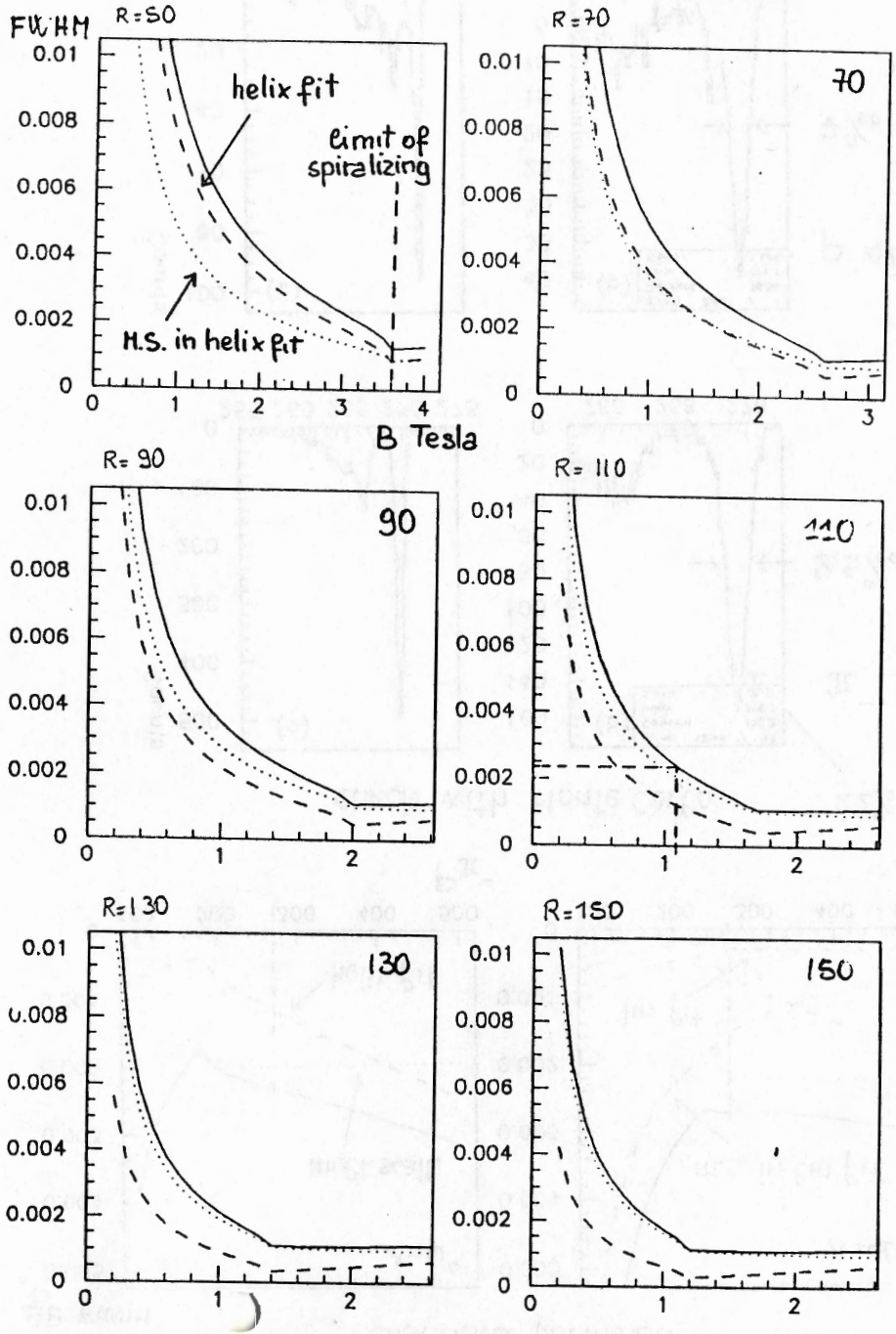

TRIGGER STRATEGY

- The **aim** of the trigger logic is to **select**, against the background, events where :
  - The Φ decays to K+ K−
  - the K− stops **inside** the target and forms an hypernucleus emitting a **prompt** π− which crosses the **full** spectrometer.
- Trigger **requests** :
  - Tofino : a) "extended" **Back to Back** topology
    b) **threshold** discrimination on both B.toB. slabs (threshold fluctuation 5% (FWHM))
  - Tofone : a) **prompt** coincidence (< 10 ns)
    b) multiplicity ≥ 1

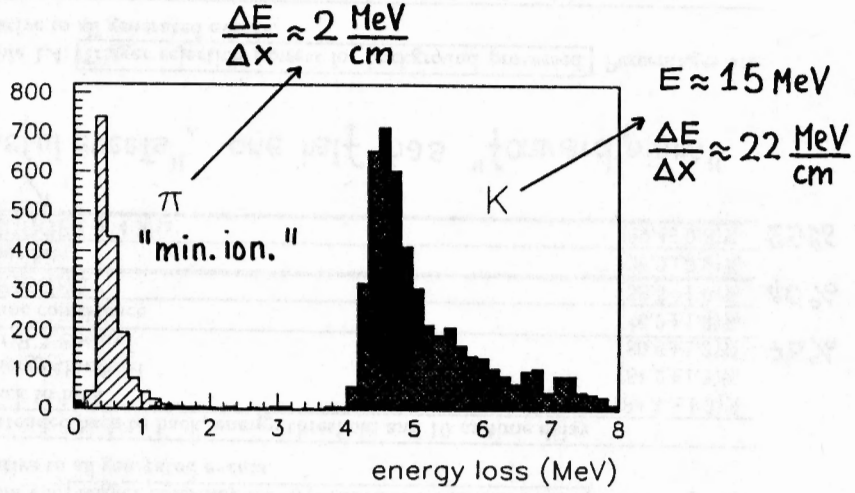

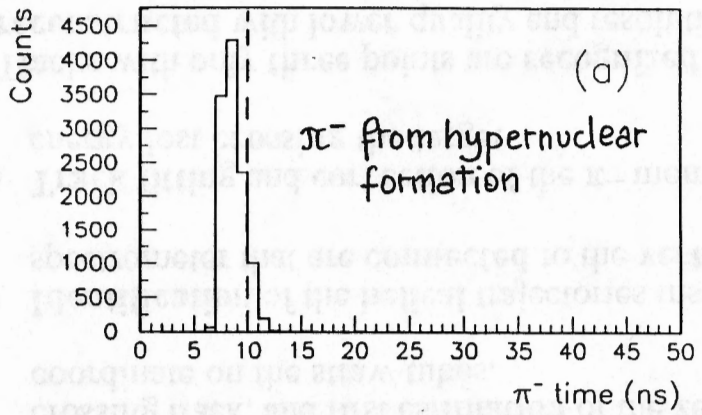

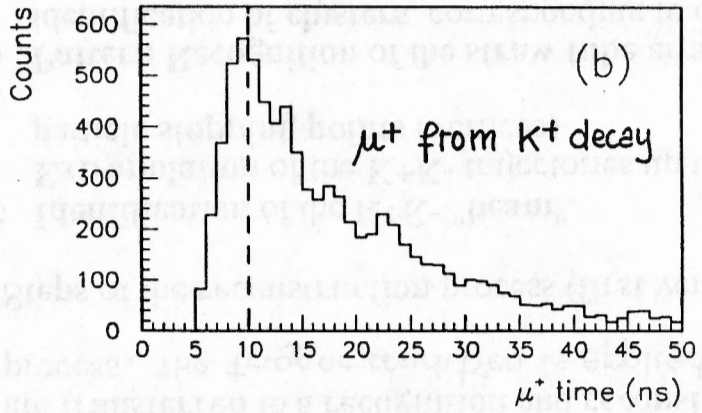

TRIGGER efficiency and rates

Table 1.3: Trigger efficiency for hypernucleus formation events. Percentages are relative to all generated events.

Extended back to back, energy threshold and 10 ns time delay	
Back to back	(89.3.±1.3)%
Energy threshold	(81.2±1.3)%
B.t.B * Energy	(80.6±1.3)% 75%
Time coincidence	(46.2±1.0)%
TRIGGER	(38.6±1.0)% 40%
Four hits	(36.0±0.9)%
TRIGGER + 4 hits	(29.4±0.8)% 25%

"useful events", one half has "forward pions"

Table 1.4: Trigger rejection powers for background processed. Percentages are relative to all generated events.

Extended back to back, energy threshold and 10 ns time delay	
Bhabha scattering	$< 10^{-2}$%
$\phi \to K_S K_L$	$(3 \pm 1)10^{-2}$%
$\phi \to \rho\pi$	$(4 \pm 1)10^{-2}$%
$\phi \to \pi^+\pi^-\pi^o$	10^{-2}%
K^- interaction without hypernucleus formation	(7.3±0.5)%

Table 1.5: Trigger rates at luminosity $L = 10^{32} cm^{-2} s^{-1}$.

Extended back to back, energy threshold and 10 ns time delay	
Hypernucleus formation	$8 \cdot 10^{-2}$Hz
Bhabha scattering	$< 4 \cdot 10^{-2}$Hz
$\phi \to K_S K_L$	$\approx 5 \cdot 10^{-2}$Hz
$\phi \to \rho\pi$	$\approx 2 \cdot 10^{-2}$Hz
$\phi \to \pi^+\pi^-\pi^o$	$\approx 10^{-3}$Hz
K^- interaction without hypernucleus formation	15 Hz

$8{,}3 \times 10^{-2}$ Hz ⟶ 86 ev/h (75 ev/h) for high resolution hypernuclear spectroscopy

PATTERN RECOGNITION AND EVENT RECONSTRUCTION STRATEGY

- **Hypernuclear** events are **generated** and the **hits** in the different detectors, **smeared** by the **resolution** functions, are **transferred** to a **recognition** and **reconstruction** process. The trigger condition is applied.
- **Steps** of the **reconstruction** process (**first** version)

A) **Identification** of the K+K- "**beam**".
Extrapolation of the K+K- trajectories up to the particle **stopping points** (vertices)

B) **Pattern Recognition** of the **straw tube** arrays with identification of **clusters**, corresponding to one crossing track, and first **estimation** of the **zeta** coordinate on the straw tubes.

C) **Identification** of the **helical** trajectories inside the spectrometer that are **connected** to the **vertices**

D) **Track fitting** and **correction** of the $\pi-$ momentum for energy lost **crossing** the target

- Tracks with only **three** points are **recognized** and **reconstructed** with **lower** quality and resolution

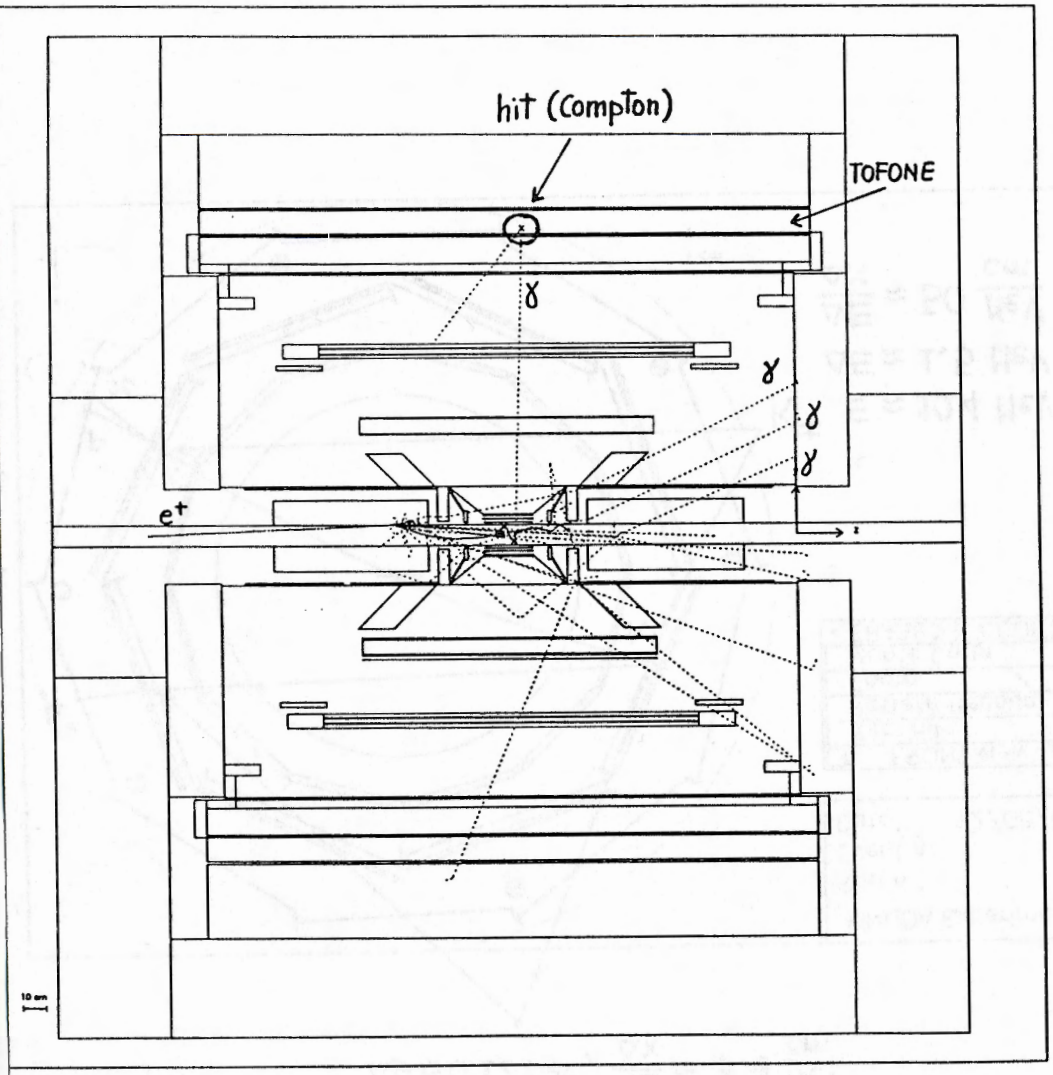
hit (Compton)
TOFONE
γ
γ
γ
γ
e+
z

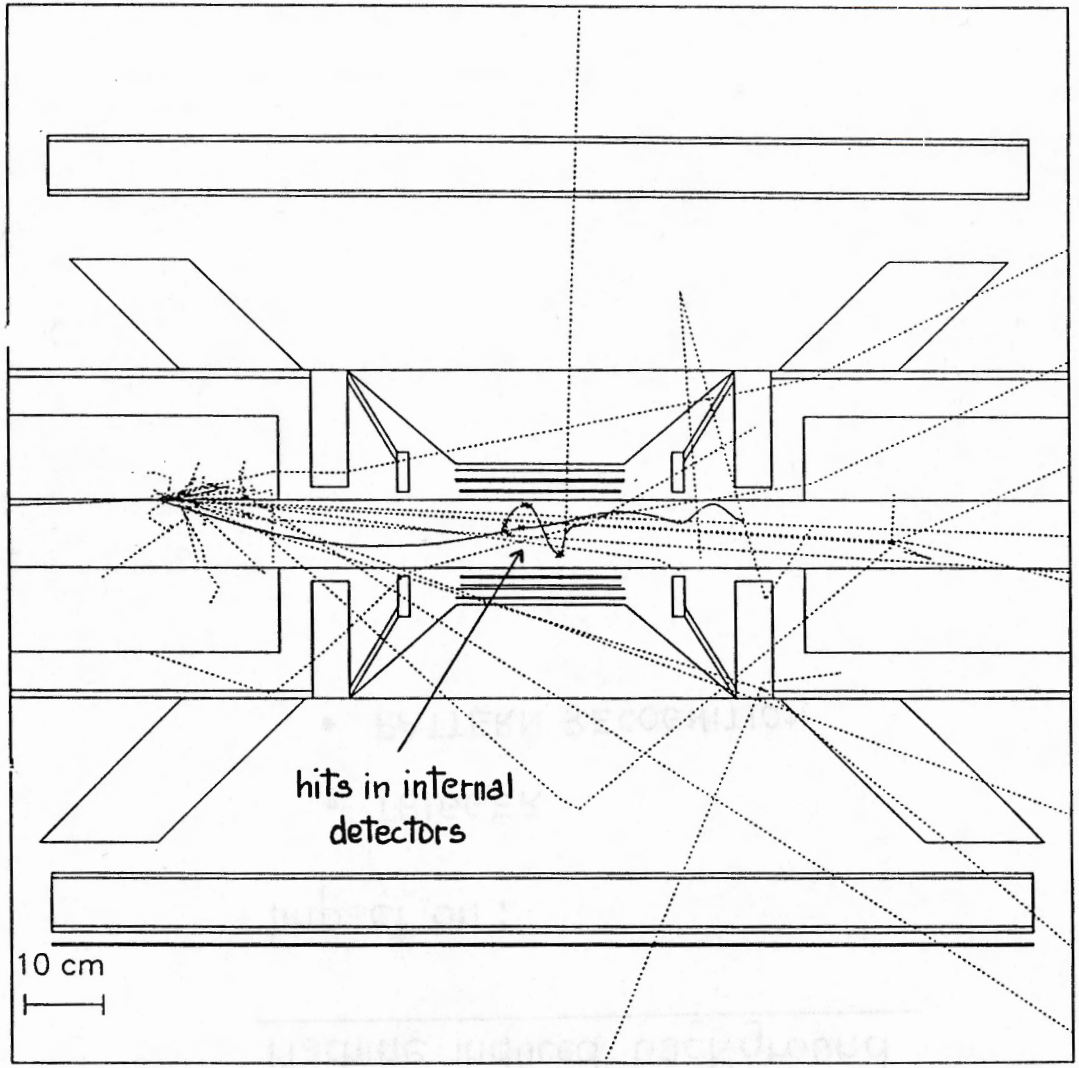
hits in internal
detectors
10 cm

"minimum ionizing"

$\Delta E \approx 0.12$ MeV, $\frac{\Delta E}{\Delta X} \approx 3.9 \frac{MeV}{cm}$

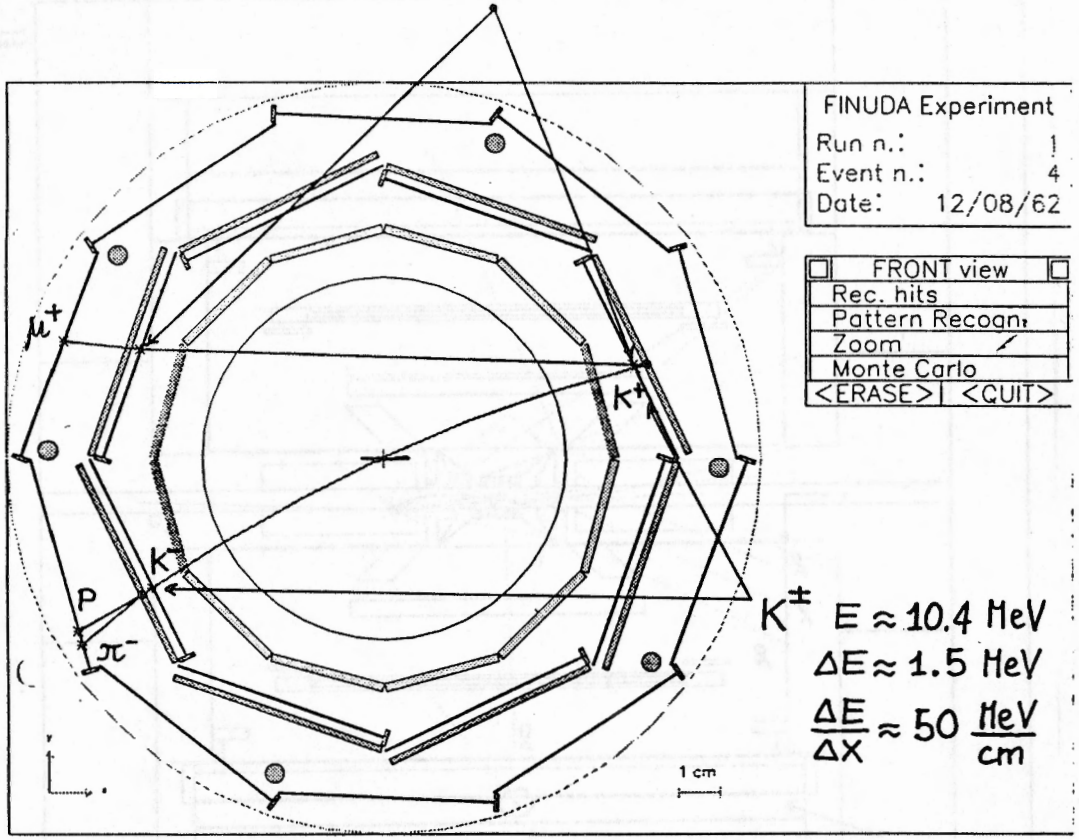

$K^\pm$ $E \approx 10.4$ MeV

$\Delta E \approx 1.5$ MeV

$\frac{\Delta E}{\Delta X} \approx 50 \frac{MeV}{cm}$

Machine induced background

Impact on :

- TRIGGER
- PATTERN RECOGNITION

TRIGGER rejection for machine induced background

TRIGGER conditions:

- Extended Back to Back
- Energy threshold on BtoB slabs $\Delta E > 3.5$ MeV
- Time coincidence on Tofone $\Delta T < 10$ ns, $\Delta E > 5.0$ MeV

TRIGGER rejection $\longrightarrow$ $3{,}3 \times 10^{-5}$

at $6 \times 10^6 \frac{\text{lost } e^+(e^-)}{\text{sec}} \longrightarrow$ 200 trigger/sec

- Asking 2 Tofone slabs over threshold

$\Delta E > 5.0$ MeV $\longrightarrow$ 7 trigger/sec

$\Delta E > 7.5$ MeV $\longrightarrow$ 2 trigger/sec

Impact of machine background on PATTERN RECOGNITION

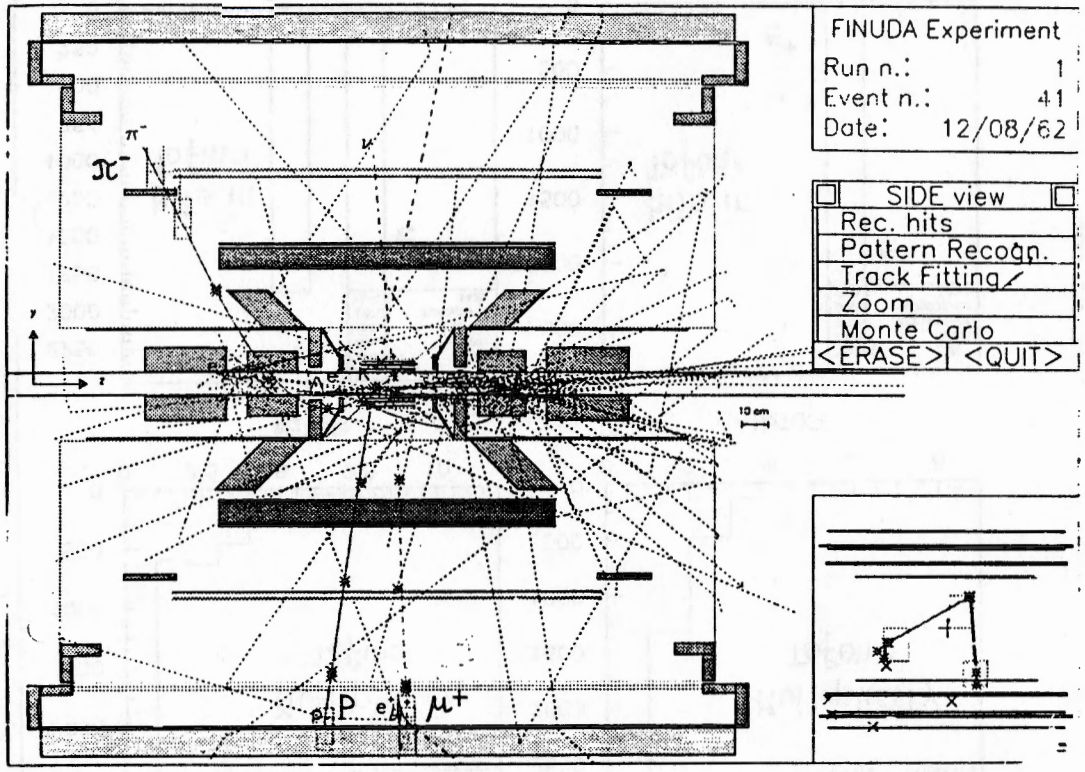

$\sim 6 \times 10^6 \frac{\text{lost } e^+(e^-)}{\text{sec}} \longrightarrow 6\ e^+(e^-)/\mu\text{sec}$ around inter. zone

at $\mathcal{L} = 10^{33}\ \text{cm}^{-2}\,\text{s}^{-1}$

5000 showers around interaction zone

$Z = -30, +30$ cm – incidence angle $< 1°$

17/03/95 10.55

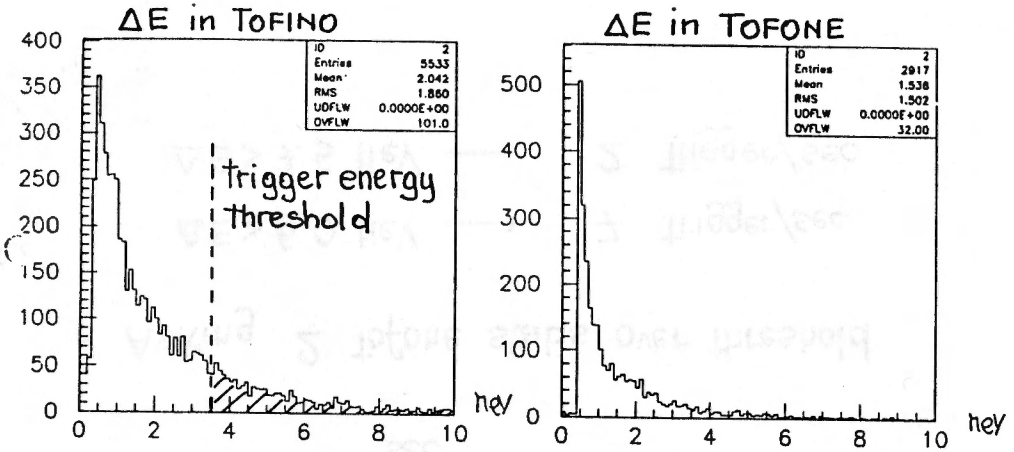

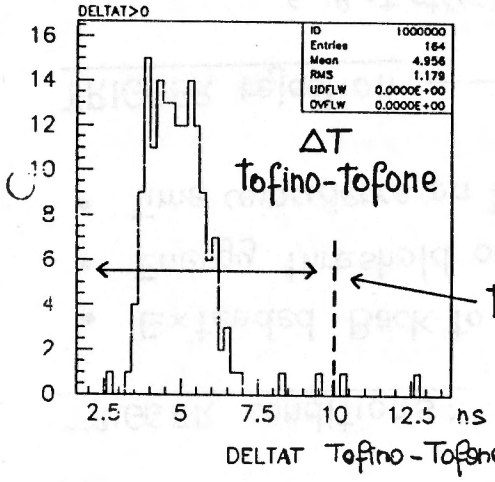

e.m. showers from machine background

e.m. showers from machine background

17/03/95 10.55

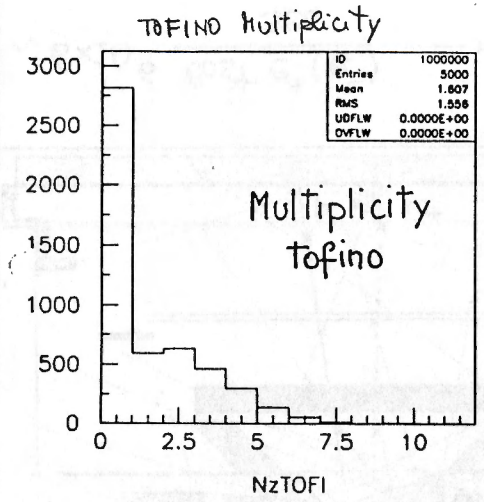

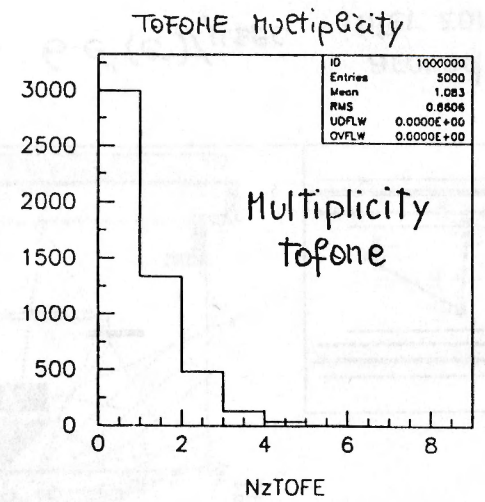

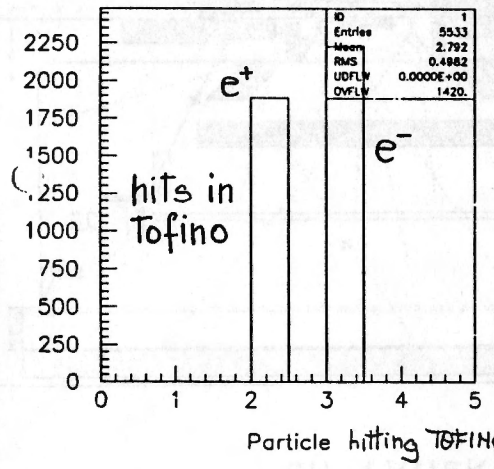

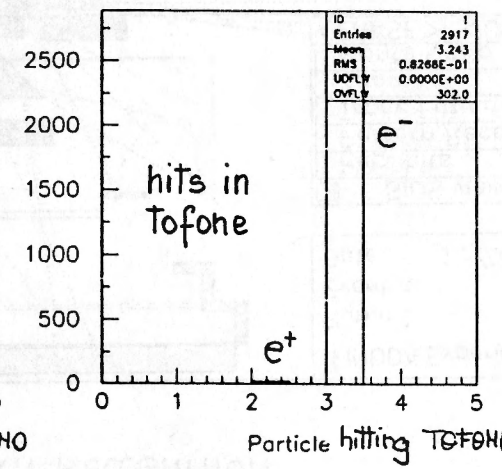

Pattern Recognition efficiency > 95%

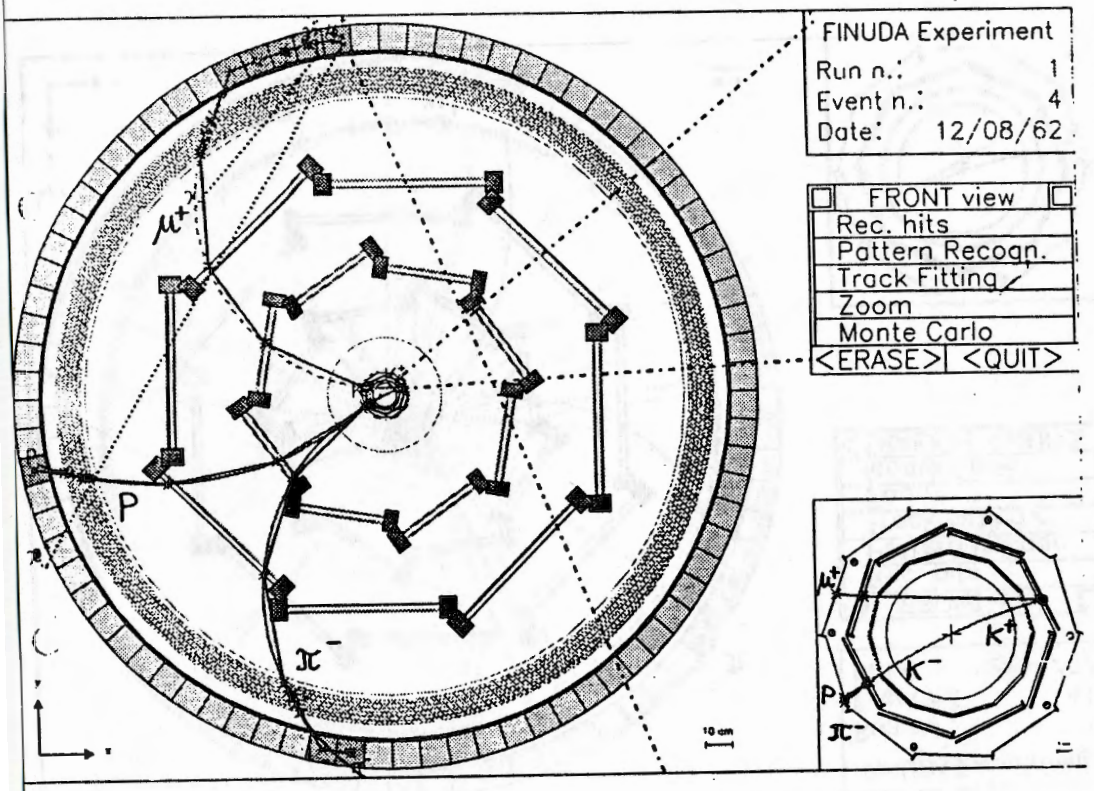

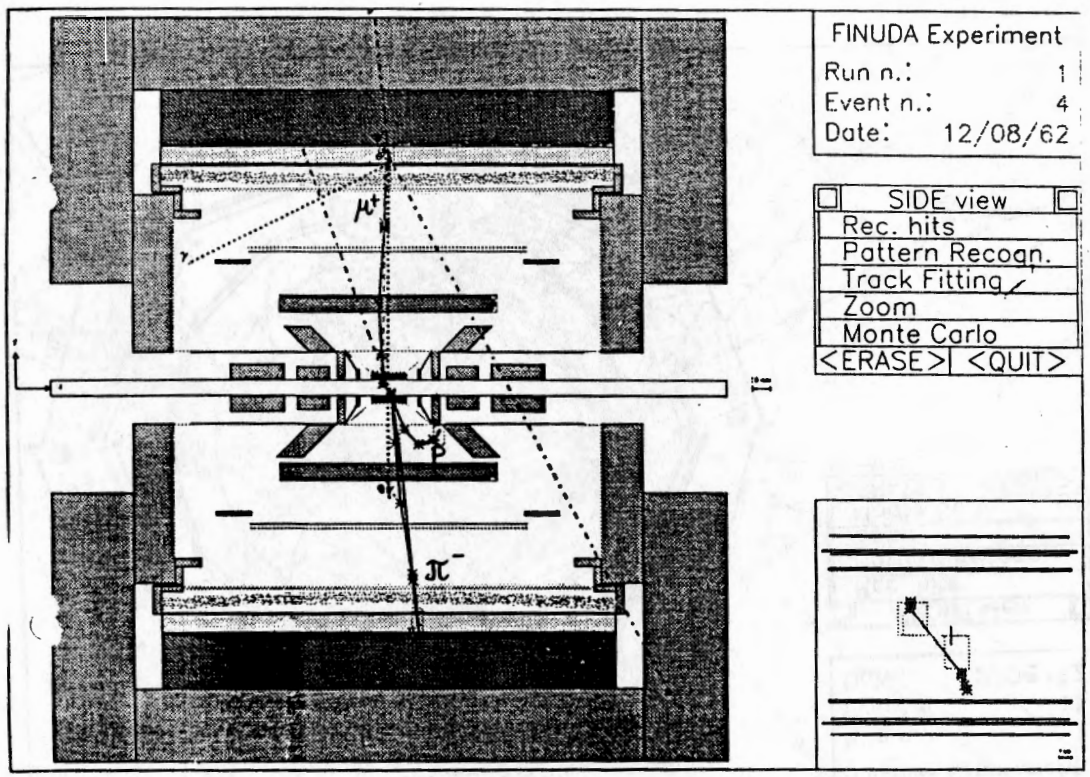

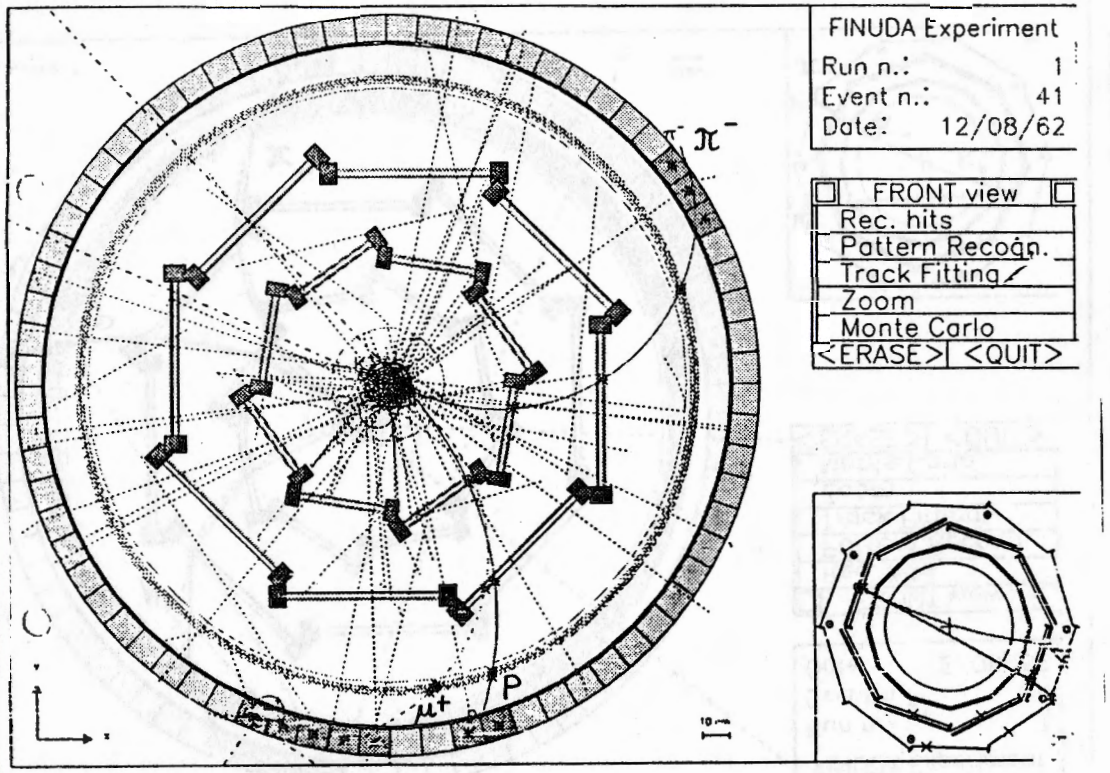
FINUDA Experiment
Run n.: 1
Event n.: 41
Date: 12/08/62
FRONT view
Rec. hits
Pattern Recogn.
Track Fitting
Zoom
Monte Carlo
<ERASE>
<QUIT>
π⁻
μ+
P

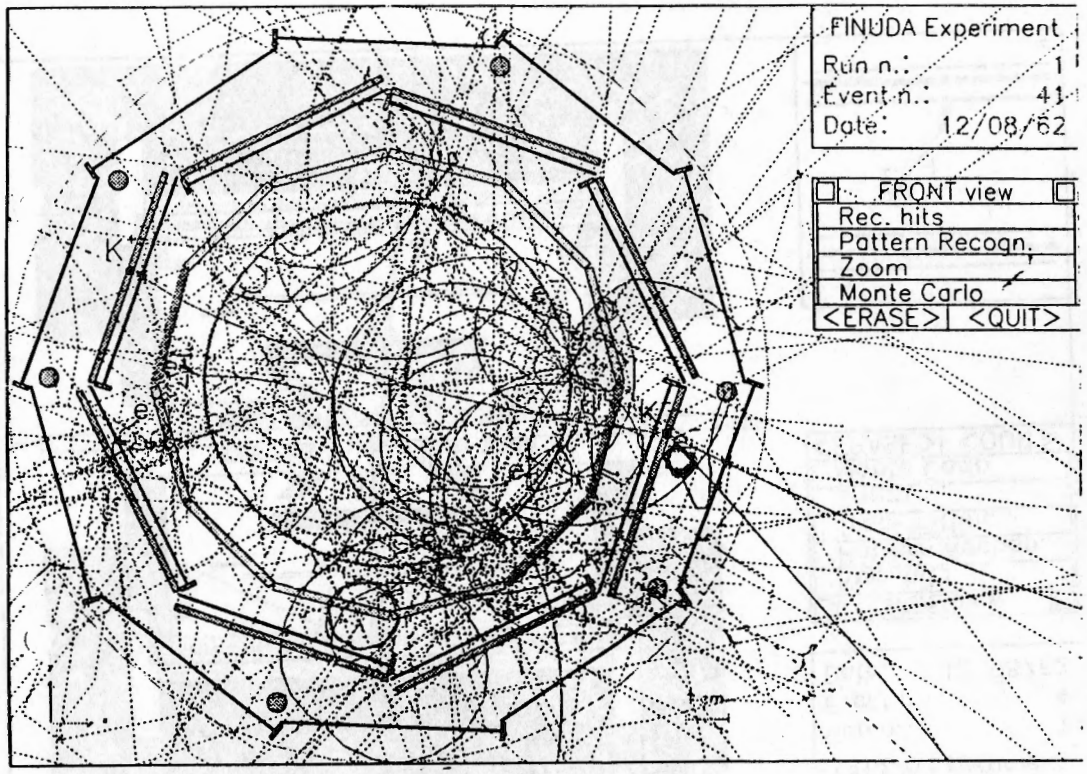
FINUDA Experiment
Run n.: 1
Event n.: 41
Date: 12/08/62
FRONT view
Rec. hits
Pattern Recogn.
Zoom
Monte Carlo
<ERASE>
<QUIT>
K⁺
e⁻
e⁺

RECONSTRUCTION

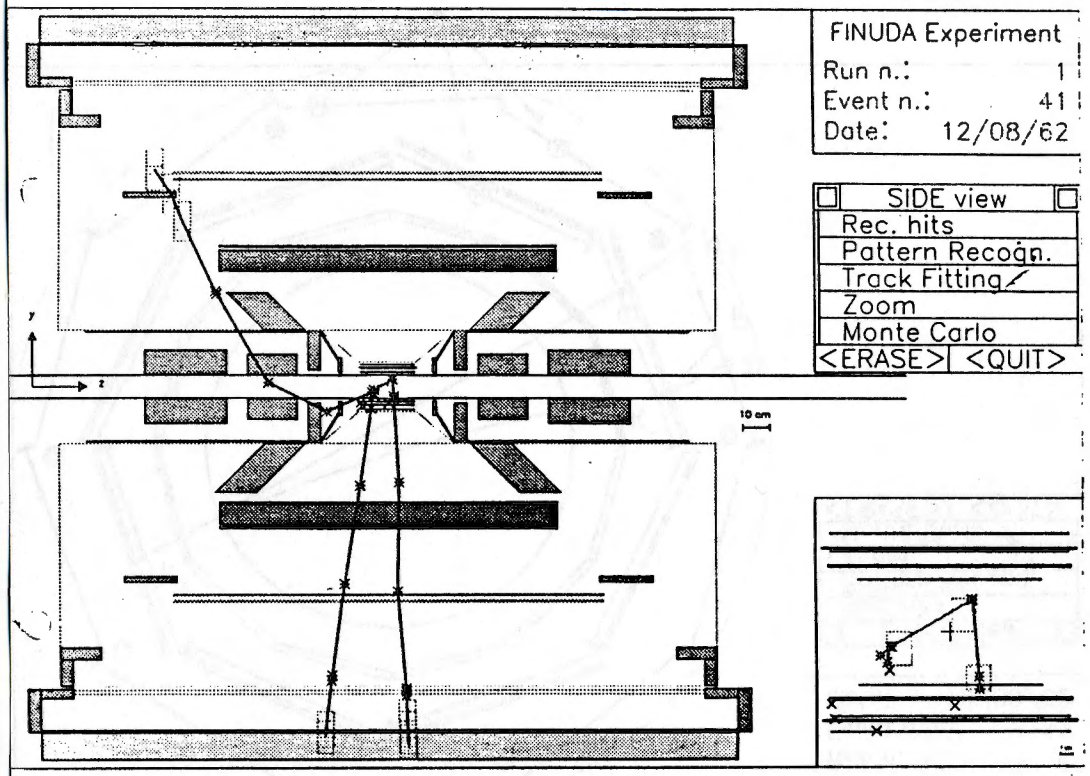

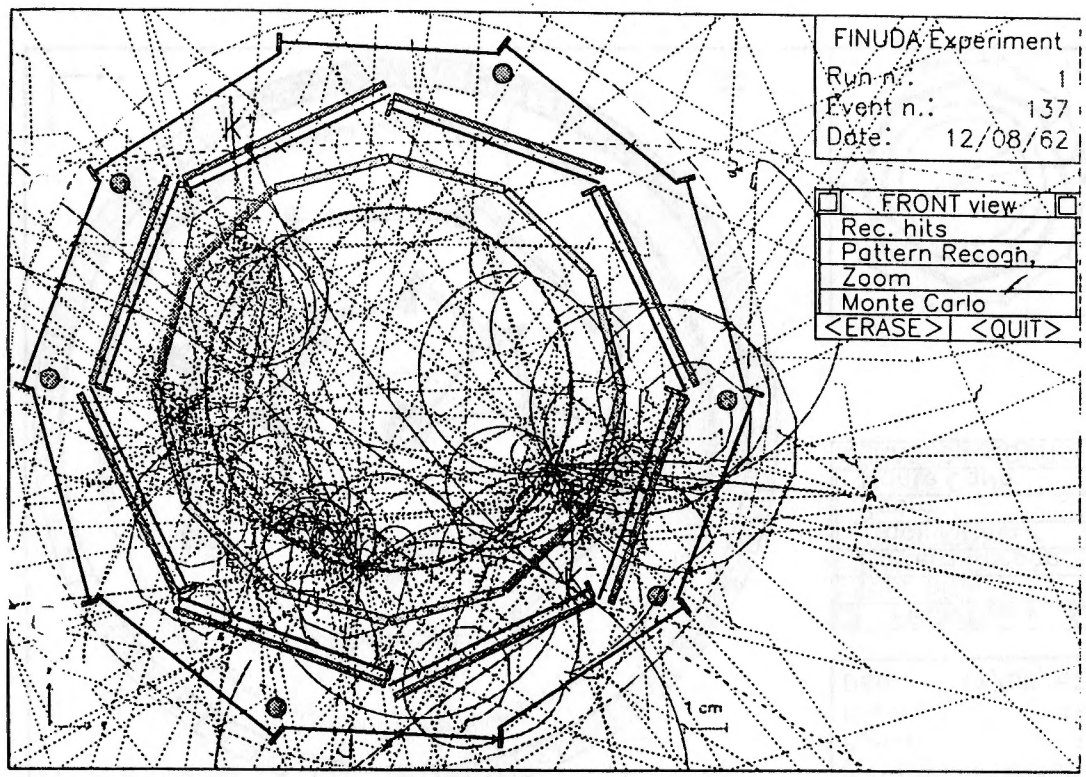

RECONSTRUCTION

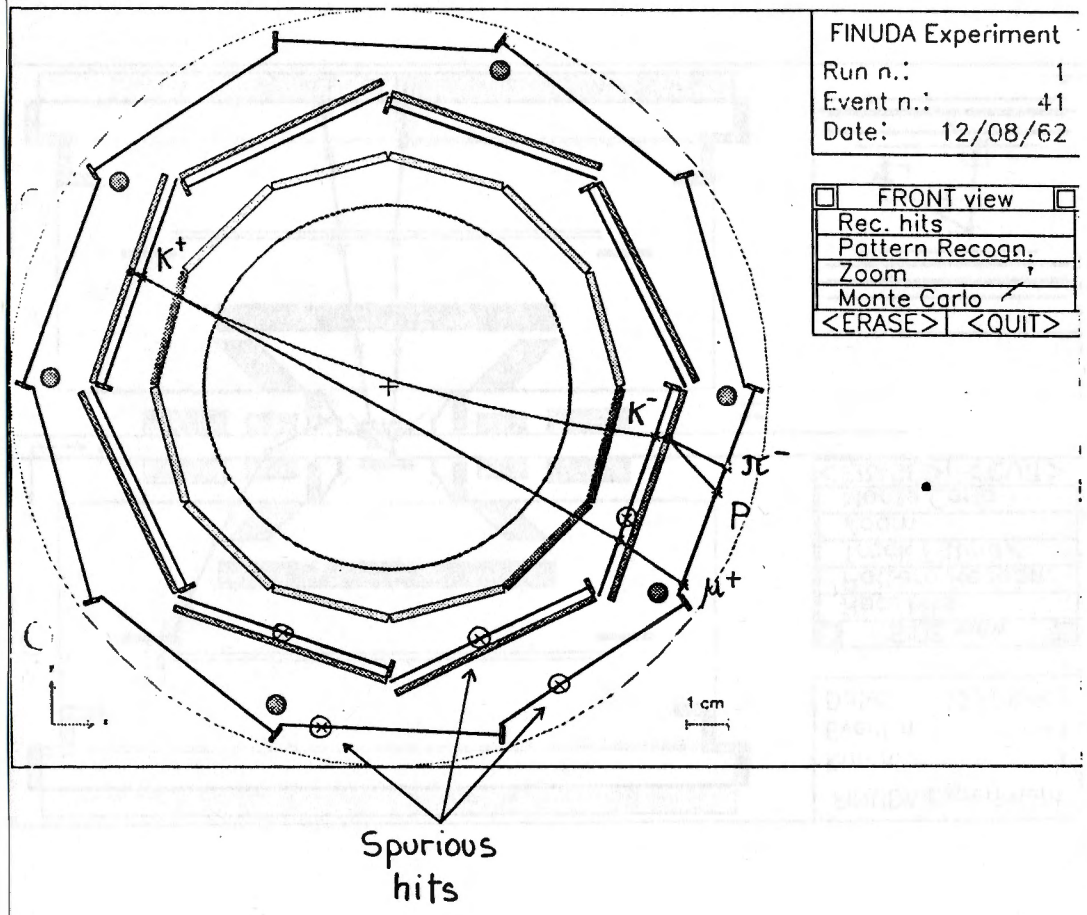

Spurious hits

RECONSTRUCTION

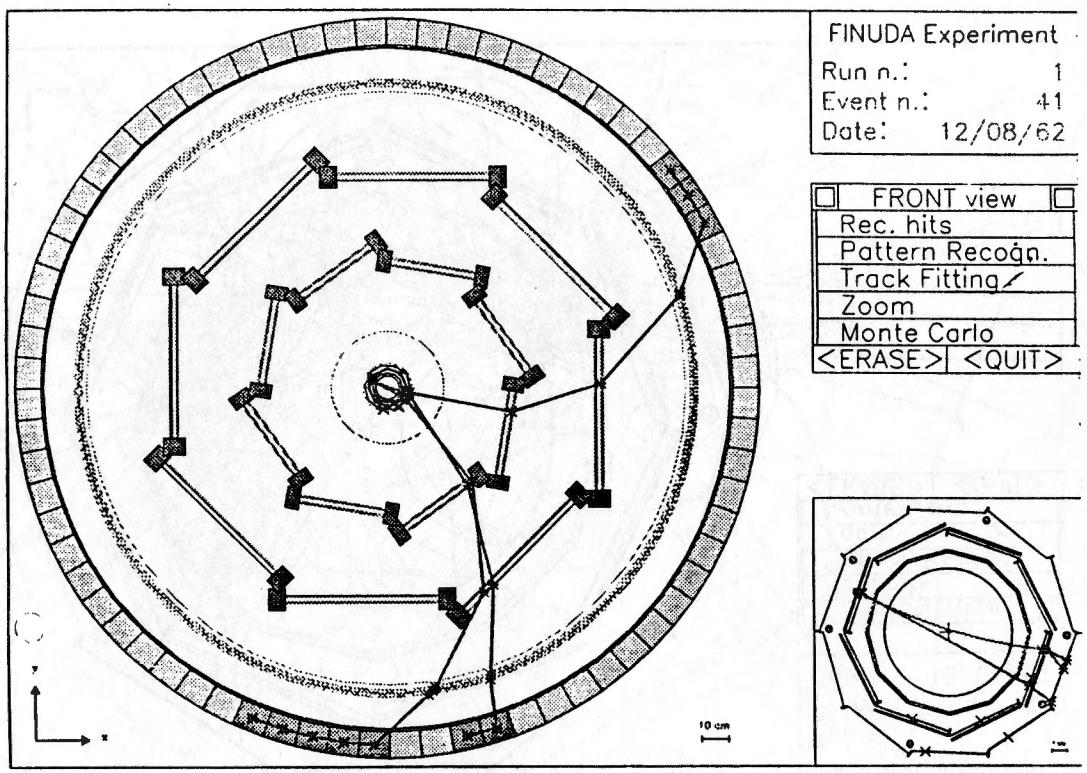

e.m. showers from machine background

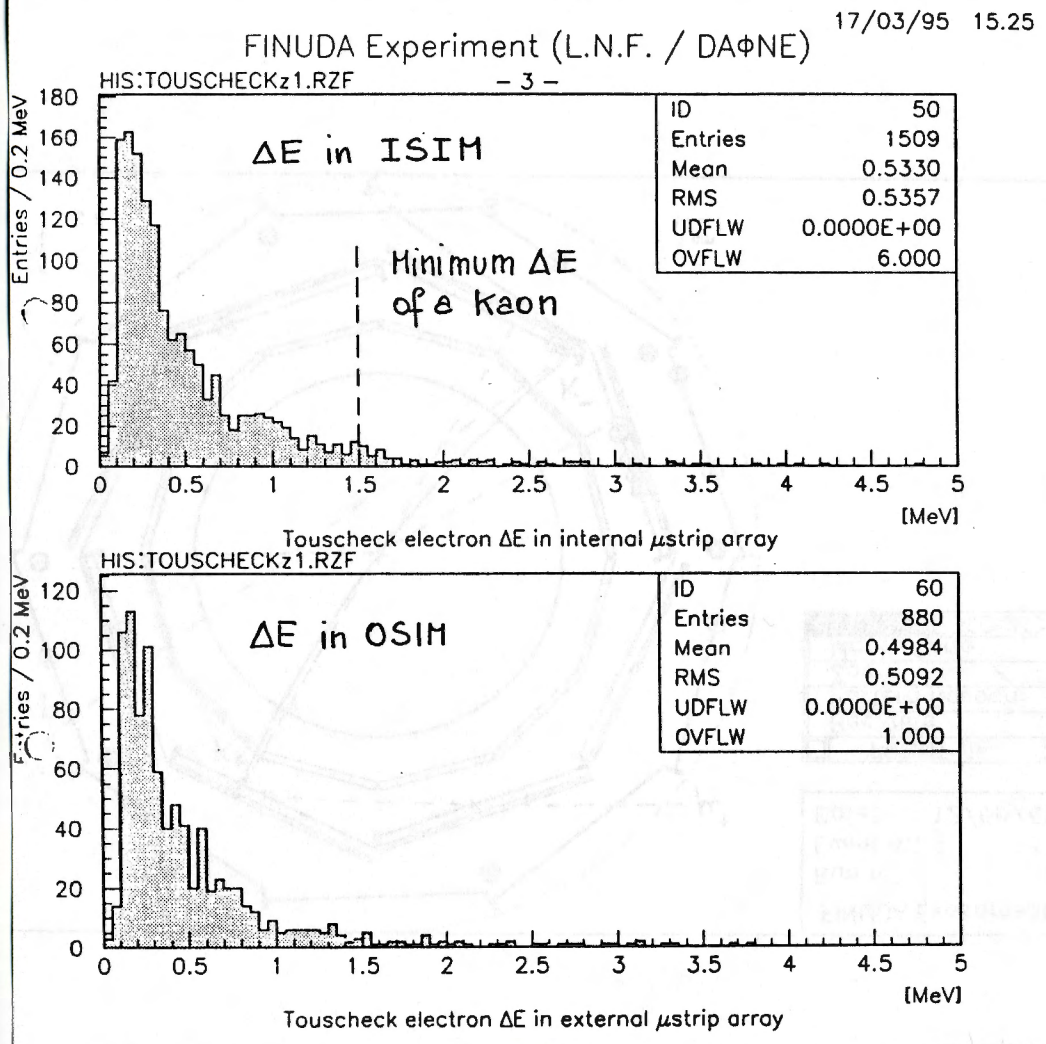

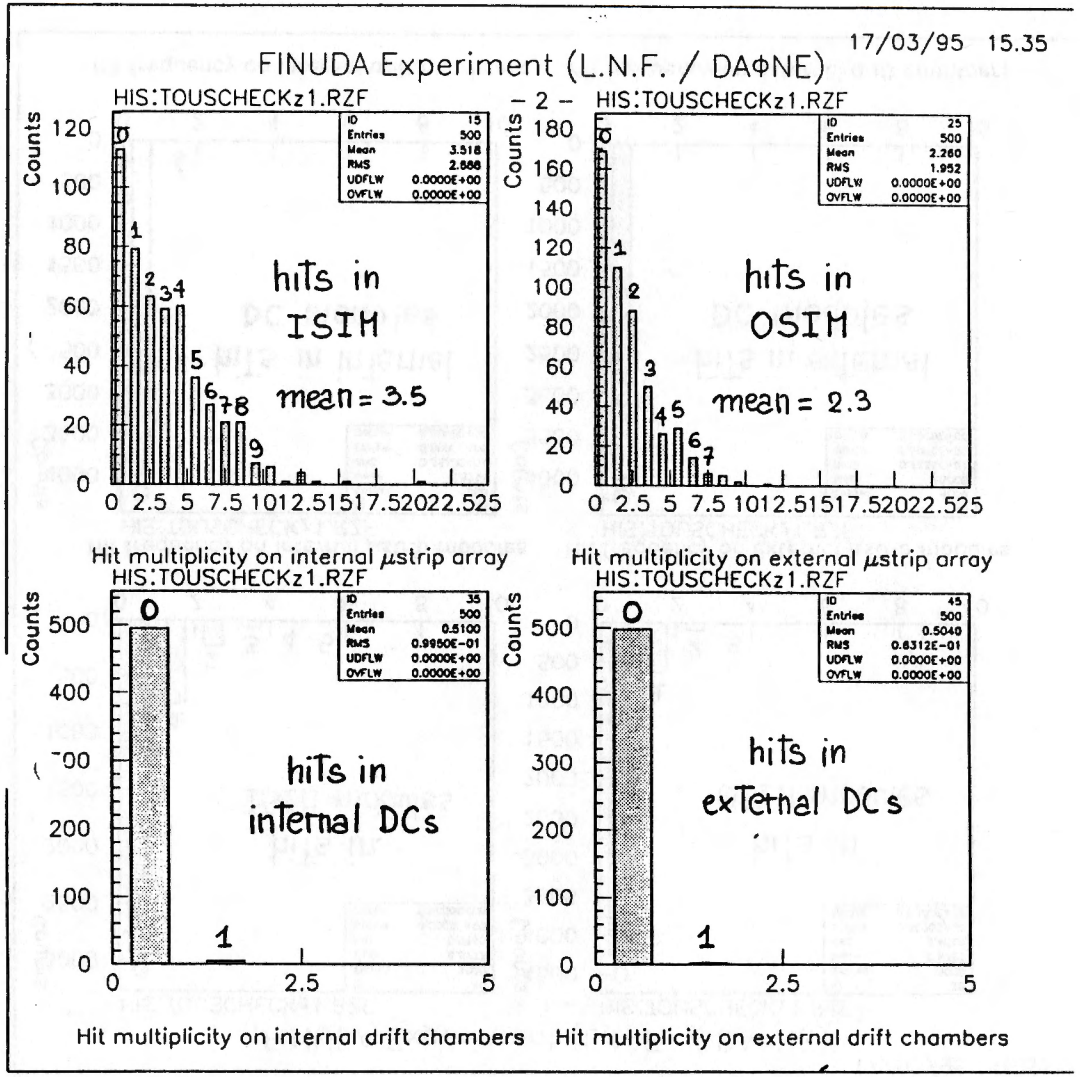

RECONSTRUCTION

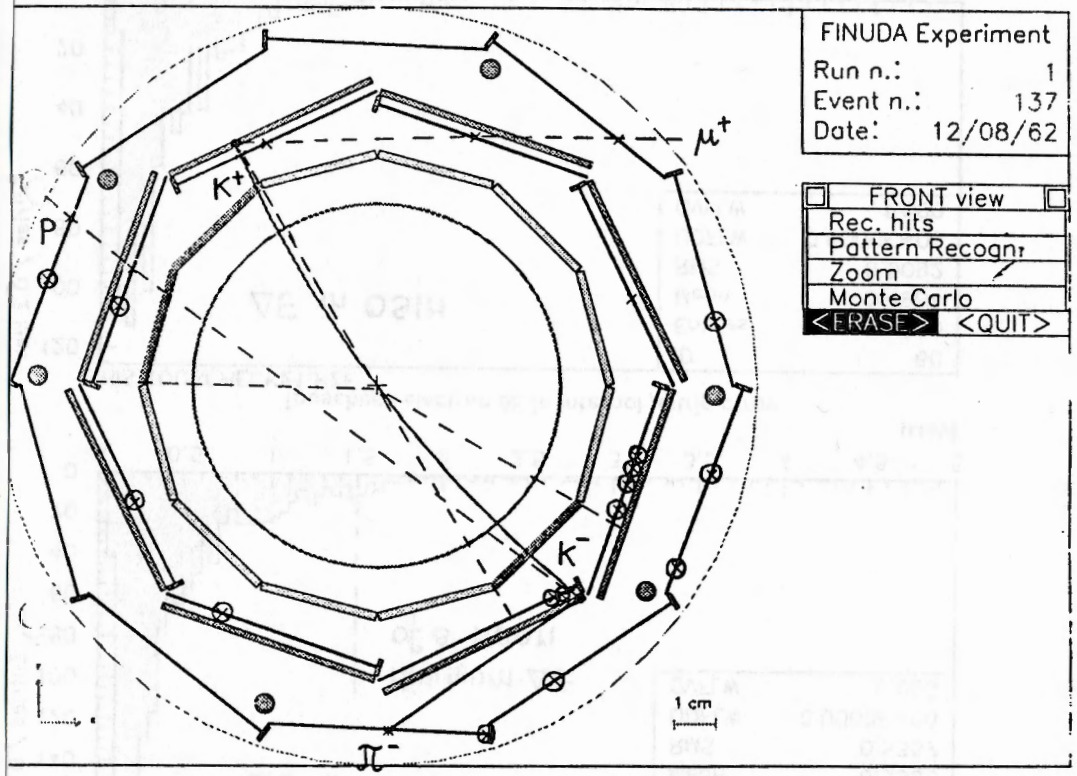

e.m. showers from machine background

500 x 6 showers

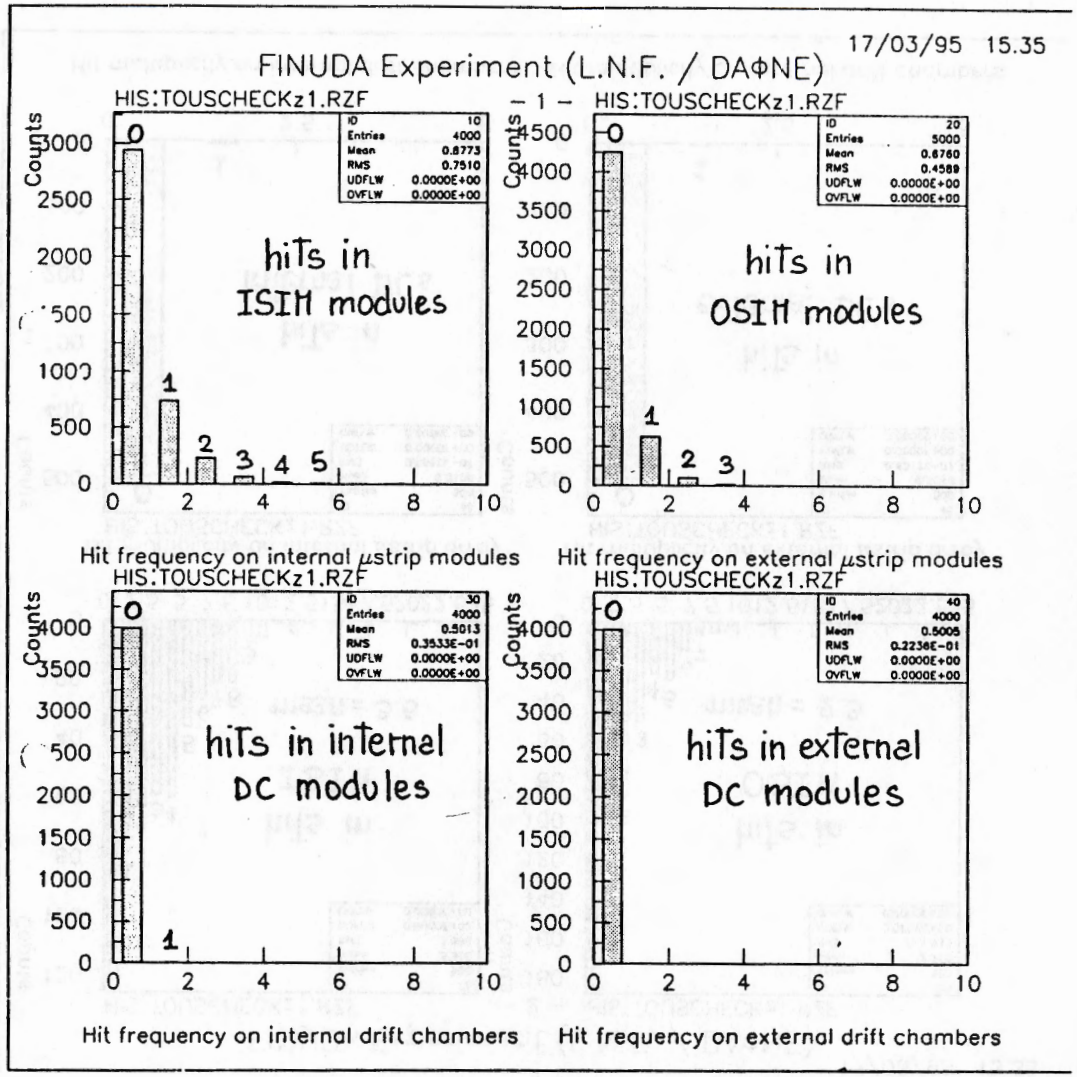

Apparatus **performance**
Spectrometer momentum **resolution**

- The momentum **resolution** is the most **crucial** feature of the apparatus.

$$\frac{\Delta T_\pi}{T_\pi} = \frac{\sqrt{P_\pi^2 + m_\pi^2} + m_\pi}{\sqrt{P_\pi^2 + m_\pi^2}} \cdot \frac{\Delta P_\pi}{P_\pi}$$

at $P_\pi = 270$ MeV/c

$\frac{\Delta P}{P} \sim 10^{-3}$

$\Delta T \sim 236$ KeV

- The detectors have **high** spatial resolution and **low mass** and are immersed in a **helium** atmosphere to minimize **multiple** scattering.

- Silicon **μstrips**	R ϕ	**50** μm
	Z	**50** μm
- Drift **chambers**	R ϕ	**150** μm (pessimistic)
	Z	**1%** wire length (**1÷2** cm)
- **Straw tube** array	R	**100** μm
	Z	**1.0** mm (pessimistic)

reasonable extrapolations of the **present** technology.

- The tracking volume is very **transparent** :
  - **Total** radiation length ⟶ **170,000** cm
    Pure Helium 540,000 cm
    Air 34,000 cm
  - Spectrometer **size** ⟶ **103** cm
  - **Homogeneous** magnetic field ⟶ **1.1** Tesla

momem m **resolution**. (Gluckstern(1963))

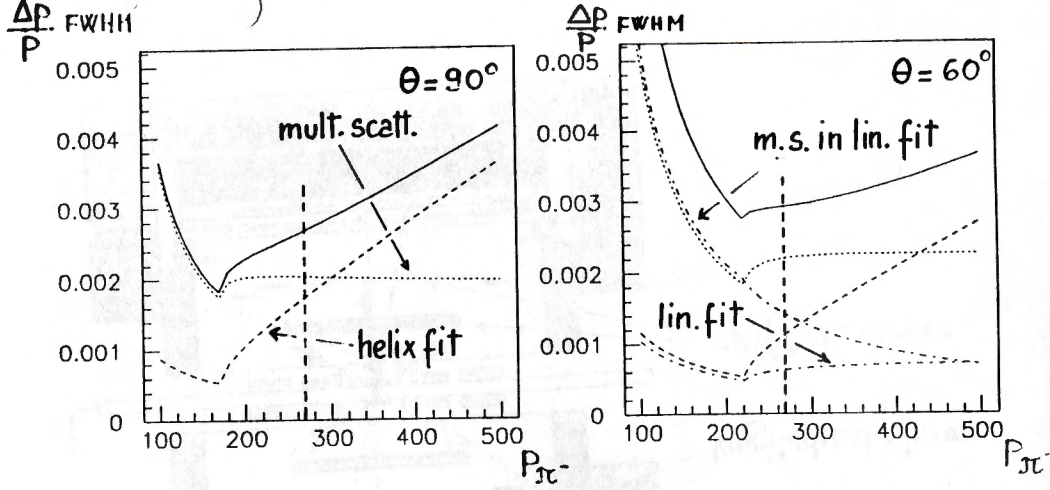

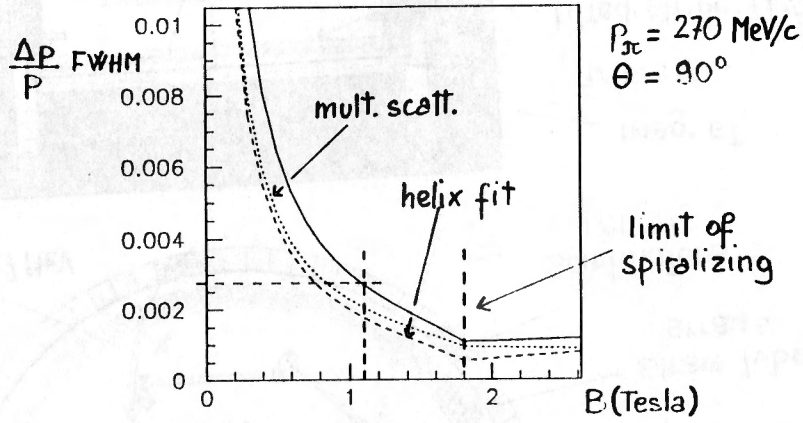

Check with **Monte Carlo** simulation

Particle	Momentum resolution (FWHM)
π^- 270 MeV/c	0.28 %
p 417 MeV/c	0.79 %
μ 236 MeV/c	0.24 %

PROGRESS REPORT ON FINUDA OFFL .E SOFTWARE

- Optimization of apparatus design for event acceptance, trigger efficiency and background rejection.
- Vertex reconstruction algorithm and momentum correction for target crossing.
- Simulation of the response of detectors and detector reconstruction.
- Global track fitting procedure.

FIN DA spectrometer and scintillators

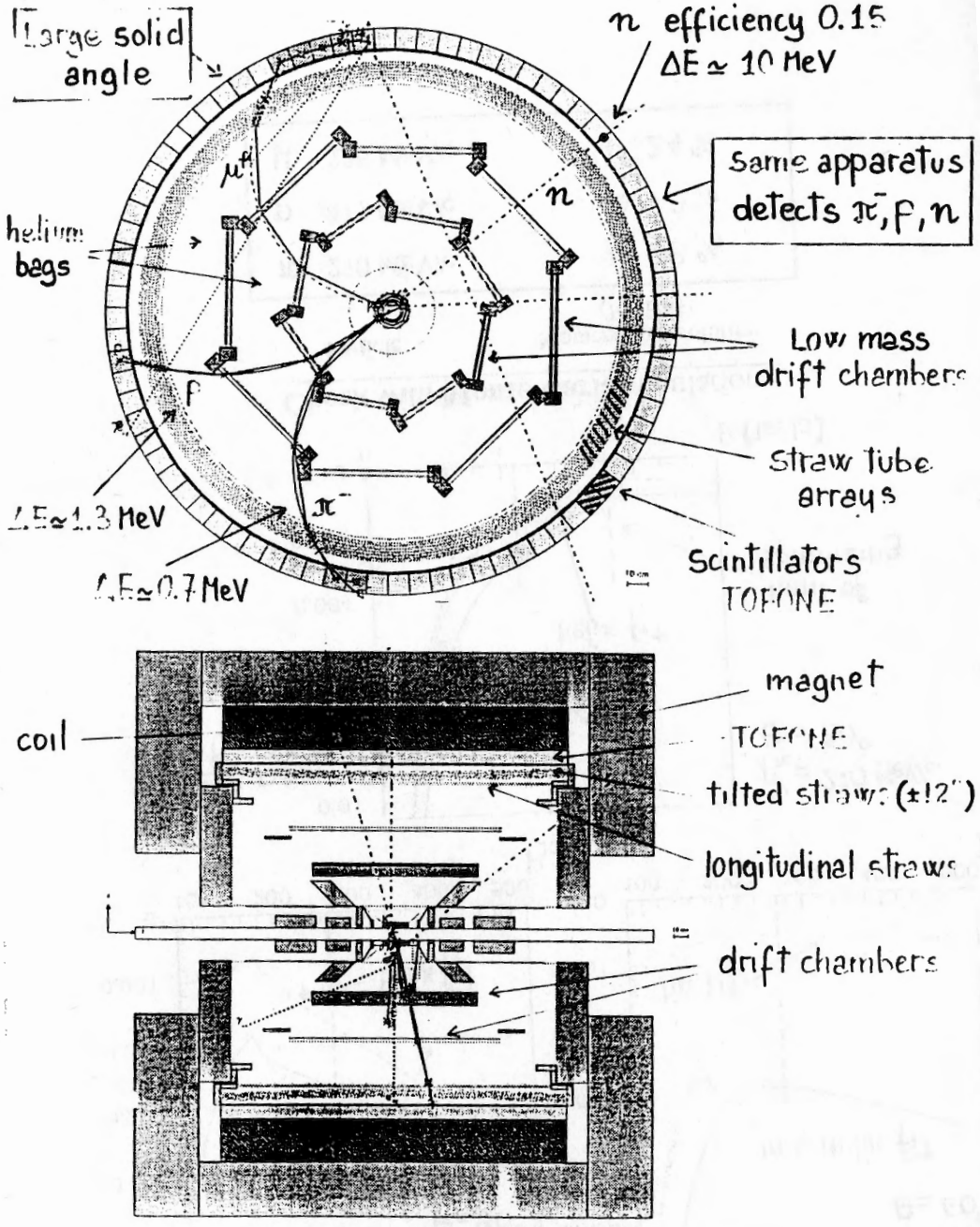

Touschek events

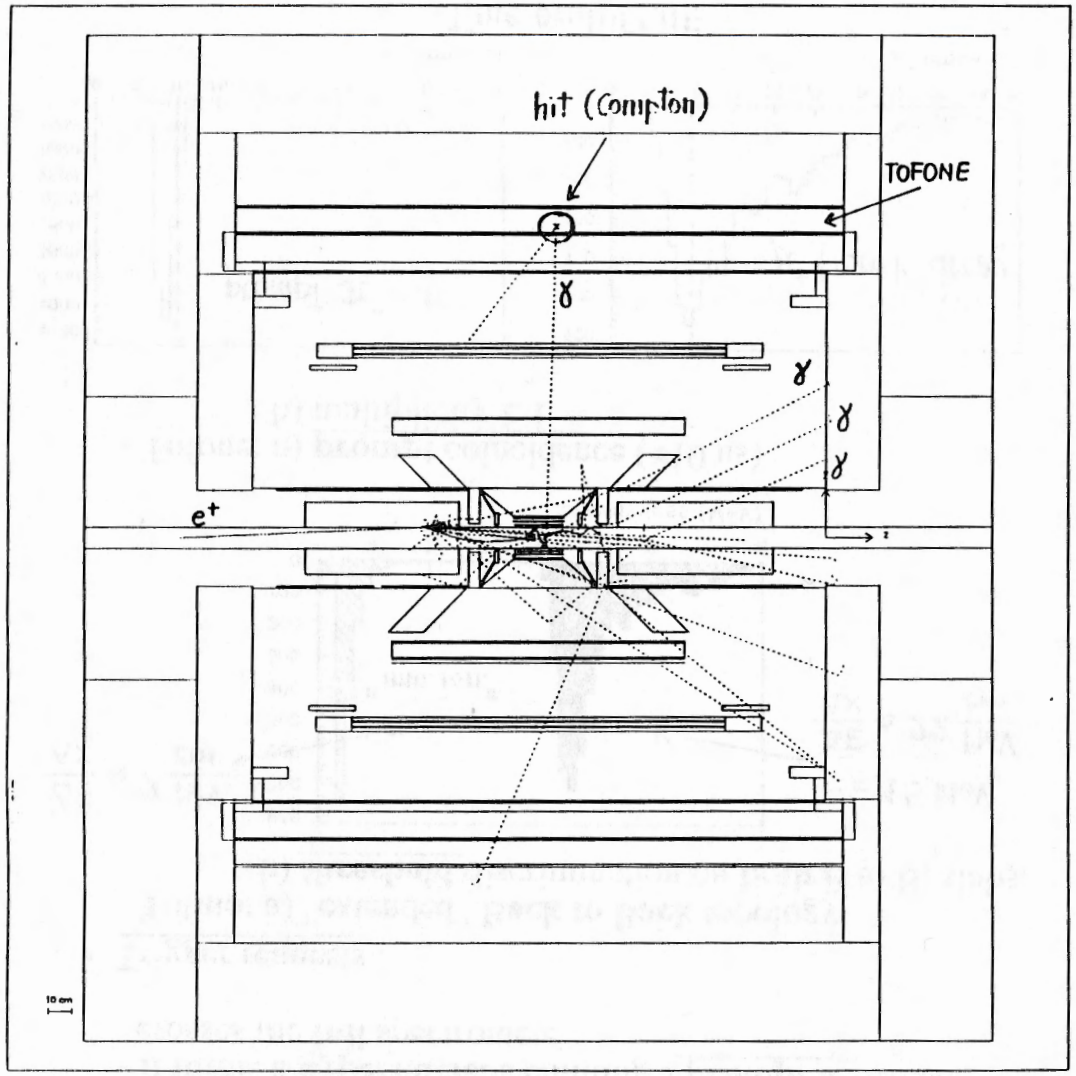

5000 showers around interaction zone

$z = -30, +30$ cm – incidence angle $< 1°$

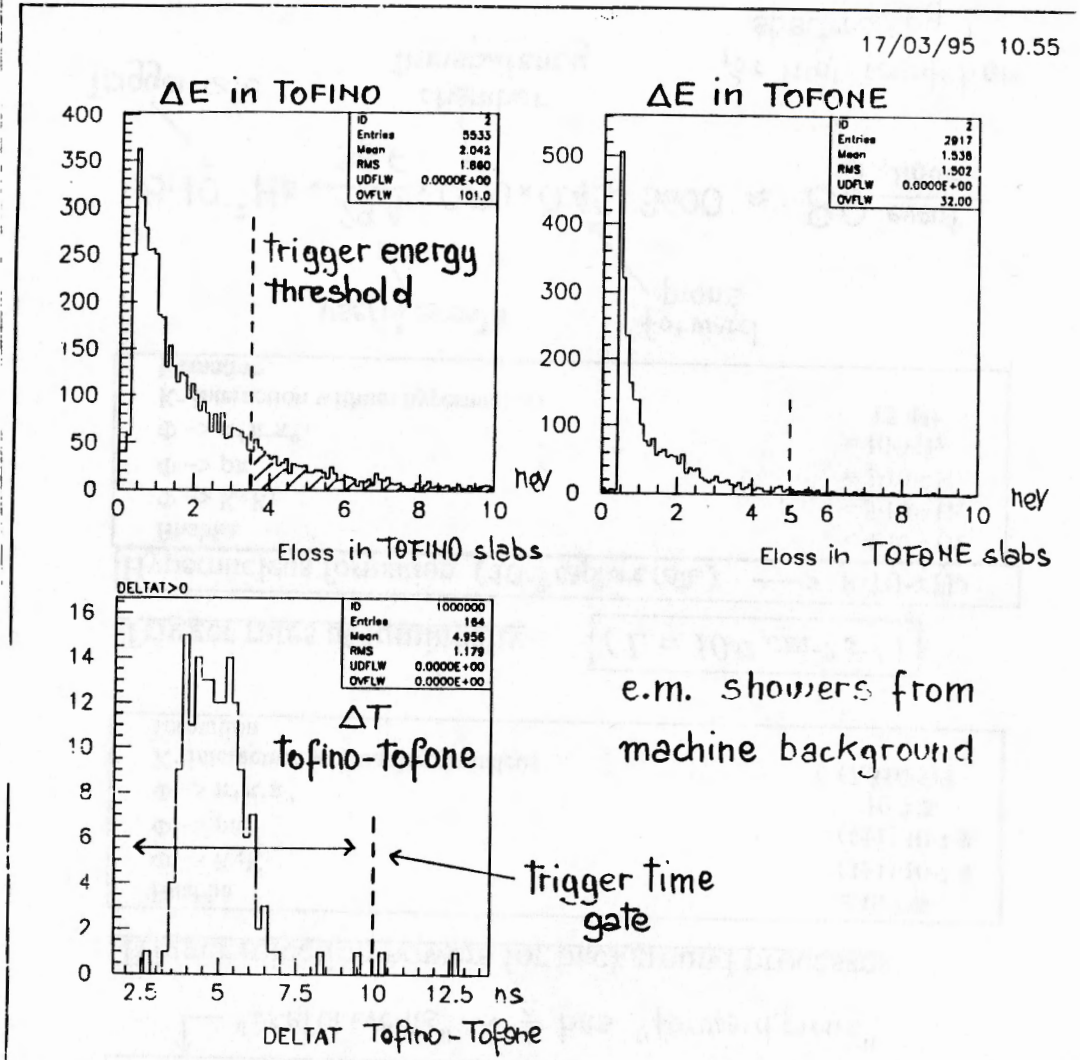

e.m. showers from machine background

Trigger strategy

- The **aim** of the trigger logic is to **select**, against the background, events where :
  - The Φ decays into K^+K^-.
  - The K^- stops **inside** the target.
  - It forms a **hypernucleus** emitting a **prompt** π^- which crosses the **full** spectrometer.

- Trigger requests :
  - Tofino: a) "extended" **Back to Back** topology.
    b) **threshold** discrimination on **both** B.to B. slabs.

$\frac{\Delta E}{\Delta X} \approx 2 \frac{MeV}{cm}$

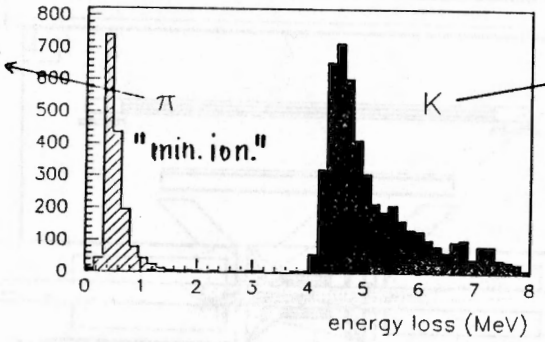

$E \approx 15$ MeV

$\frac{\Delta E}{\Delta X} \approx 22 \frac{MeV}{cm}$

  - Tofone: a) **prompt** coincidence (<10 ns)
    b) multiplicity ≥ 1

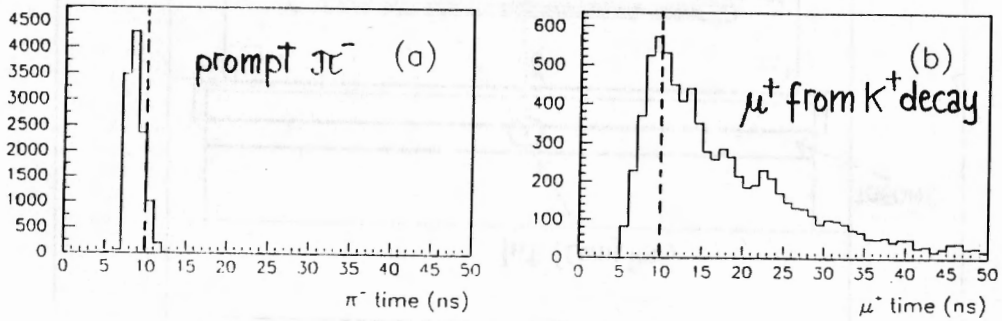

Time on TOFONE

Trigger efficiency for hypernucleus formation events

Extended Back to Back, energy threshold and 10 ns time delay	
Back to Back * Energy Threshold	(80.6±1.3)%
Time coincidence	(46.2±1.0)%
TRIGGER	⟶ (38.6±1.0)%
TRIGGER + π^- 4 hits	⟶ (29.4±0.8)%

↑ "useful events" ~ $\frac{1}{2}$ has "forward pions"

Trigger rejection powers for background processes

Bhabha	$< 10^{-2}$ %
$\Phi \to K_S K_L$	$(3\pm1)\ 10^{-2}$ %
$\Phi \to \rho\pi$	$(4\pm1)\ 10^{-2}$ %
$\Phi \to \pi^+\pi^-\pi^\circ$	10^{-2} %
K^- interaction without hypernucleus formation	(7.3±0.5)%

Trigger rates at luminosity : $(L = 10^{32}\ cm^{-2}\ s^{-1})$

Hypernucleus formation (10^{-3} capture rate) ⟶	$8\cdot10^{-2}$ Hz
Bhabha	$< 4\cdot10^{-2}$ Hz
$\Phi \to K_S K_L$	$\approx 5\cdot10^{-2}$ Hz
$\Phi \to \rho\pi$	$\approx 2\cdot10^{-2}$ Hz
$\Phi \to \pi^+\pi^-\pi^\circ$	$\approx 10^{-3}$ Hz
K^- interaction without hypernucleus formation	15 Hz

useful events — forward pions

$$8\cdot10^{-2}\ Hz \times \frac{29.4}{38.6} \times 0.80 \times 0.45 \times 3600 \approx 80 \frac{event}{hour}$$

Trigger rate — chamber transparency — for high resolution spectroscopy

IMPROVEMENT OF TRIGGER REJECTION FOR TOUSCHEK EVENTS

- Stronger Trigger conditions:
  - TOFINO : a) "extended" Back to Back
    b) threshold discrimination on both B. To B. slabs
  - TOFONE : a) Prompt coincidence (< 10 ns)
    b) Energy threshold ($\Delta E > 5$ MeV)
    c) Multiplicity ≥ 1 or ≥ 2

— o —

		PREVIOUS TRIGGER	NEW TRIGGER ≥ 1	NEW TRIGGER ≥ 2
Hypernuclear events (π^- with 4 hits)	Efficiency	29.0%	27.7%	26.4%
	rate of useful events $\mathcal{L} = 10^{32} cm^{-2} s^{-1}$	~ 0.02 Hz	~ 0.02 Hz	~ 0.02 Hz
Touschek events	Rejection	2×10^{-4}	2×10^{-5}	7×10^{-7}
	Event rate at $\mathcal{L} = 10^{32} cm^{-2} s^{-1}$	4×10^2 Hz	40 Hz	1.5 Hz

$2.2 \times 10^6 \frac{\text{lost } e^+e^-}{s}$ at $\mathcal{L} = 10^{32} cm^{-2} s^{-1}$

TOFINO threshold on any two slabs

- Modification of the beam pipe geometry
  - Larger beam pipe diameter 86 mm → 108 mm
  - Larger TOFINO diameter

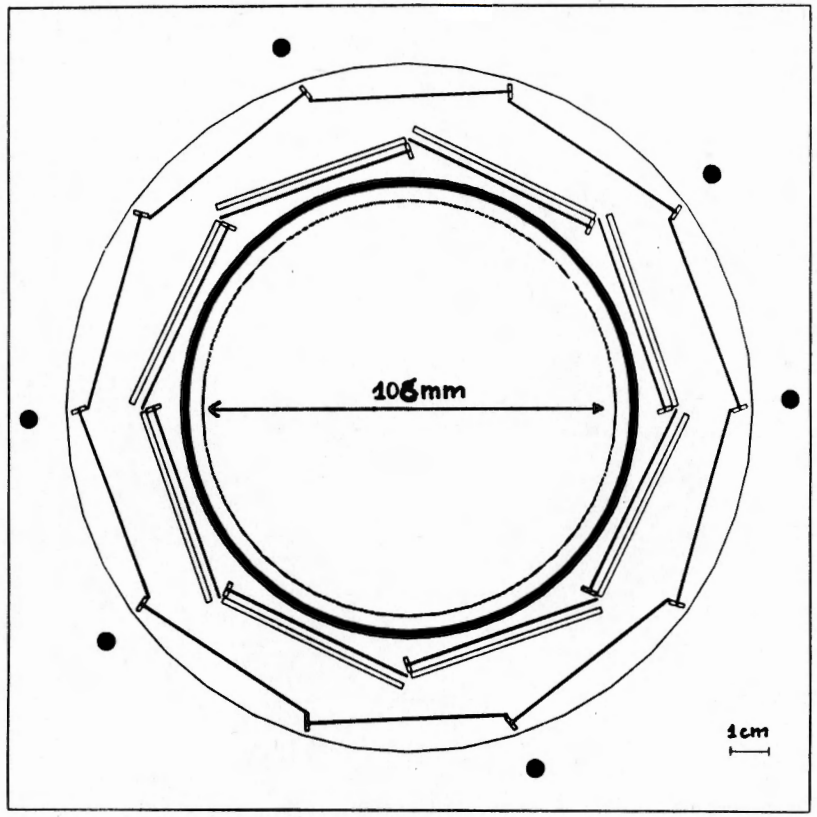

		Multiplicity ≥ 1	Multiplicity ≥ 2
Touschek events	Rejection	$< 1.3 \times 10^{-6}$	$< 4 \times 10^{-8}$
	event rate at $\mathcal{L} = 10^{32} cm^{-2} s^{-1}$	< 0.3 Hz	< 0.01 Hz

$2 \times 10^5 \frac{\text{lost } e^+e^-}{s}$ at $\mathcal{L} = 10^{32} cm^{-2} s^{-1}$

Bhabha differential cross section (valid for $\theta \gg 0$)

$$\frac{d\sigma}{d\Omega} = \left(\frac{\alpha^2}{4s}\right)\left[(1+z^2) - 2\frac{(1+z)^2}{1-z} + 2\frac{4+(1+z)^2}{(1-z)^2}\right] = \left(\frac{\alpha^2}{4s}\right)\left(\frac{3+z^2}{z-1}\right)^2$$

$z = \cos\theta$, $s = 1.0404\ \text{GeV}^2$, $\left(\frac{\alpha^2}{4s}\right) = 4.98\ \text{nbarn}$

Bhabha total cross section

$$\int_0^{2\pi} d\phi \int_0^{0.985=\cos 10^\circ} dz\ \frac{d\sigma}{d\Omega} = 2\pi\left(\frac{\alpha^2}{4s}\right)\left[\frac{16}{1-z} + 9z + z^2 + \frac{z^3}{3} + 16\log(1-z)\right]_0^{0.985} =$$

$= 30.7\ \mu\text{barn} = 30.7\times10^{-30}\text{cm}^2$

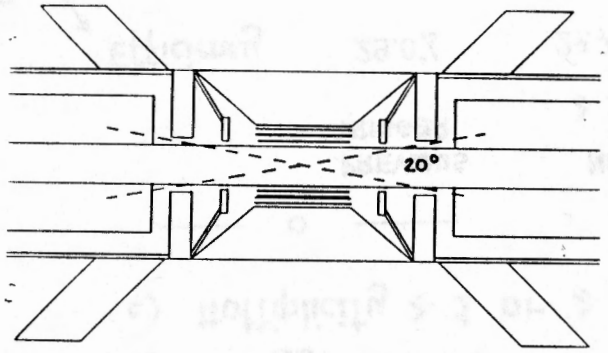

Bhabha events		Multiplicity ≥ 1	Multiplicity ≥ 2
	Rejection	$< 1.7\times10^{-6}$	$< 1.2\times10^{-6}$
	event rate at $\mathcal{L} = 10^{32}\text{cm}^{-2}\text{s}^{-1}$	$< 5\times10^{-3}$ Hz	$< 4\times10^{-3}$ Hz

The strongest trigger condition is the threshold on B. To B. TOFINO slabs

Uncertainties in VERTEX Reconstruction

(old geometry)

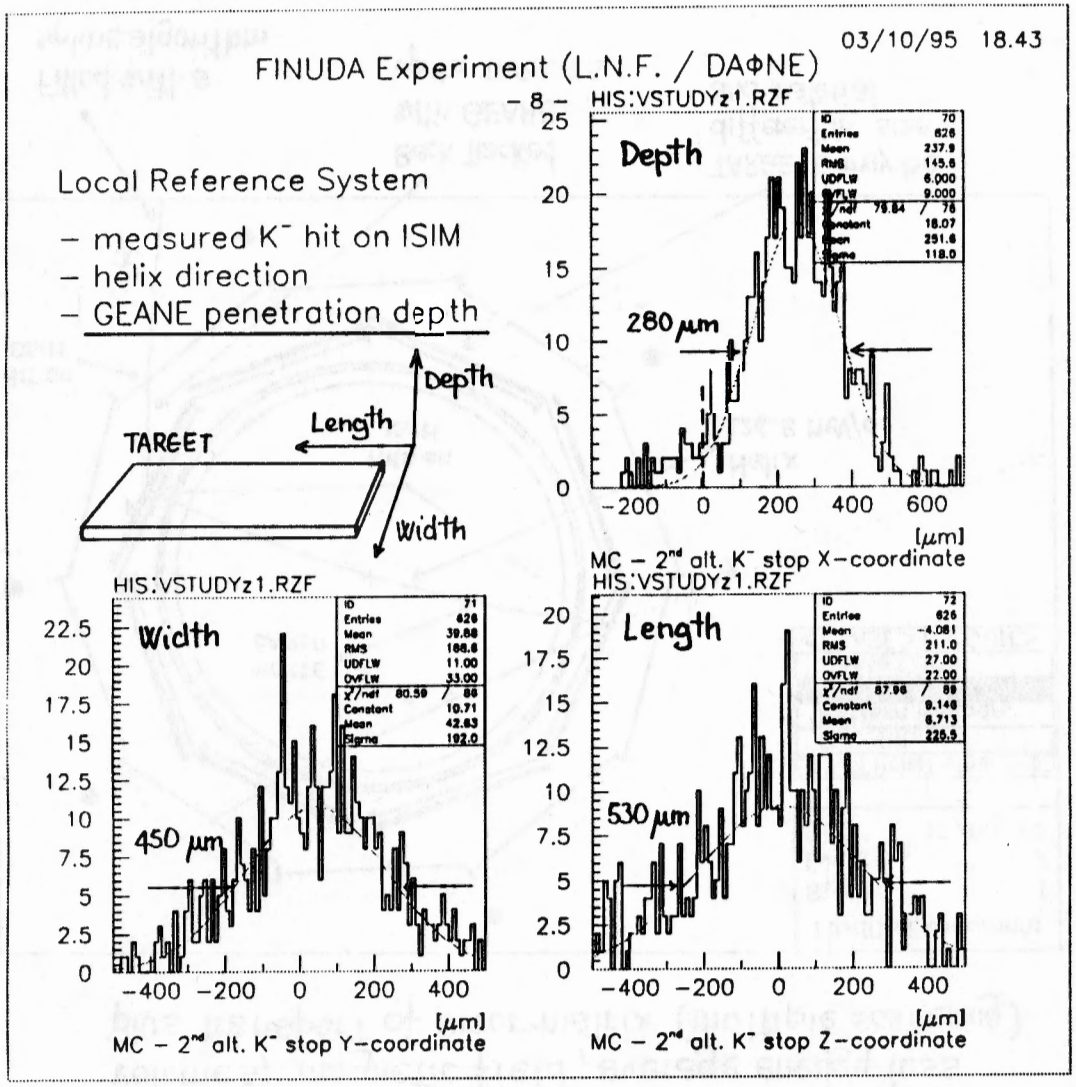

π^- momentum correction for target crossing

(final algorithm)

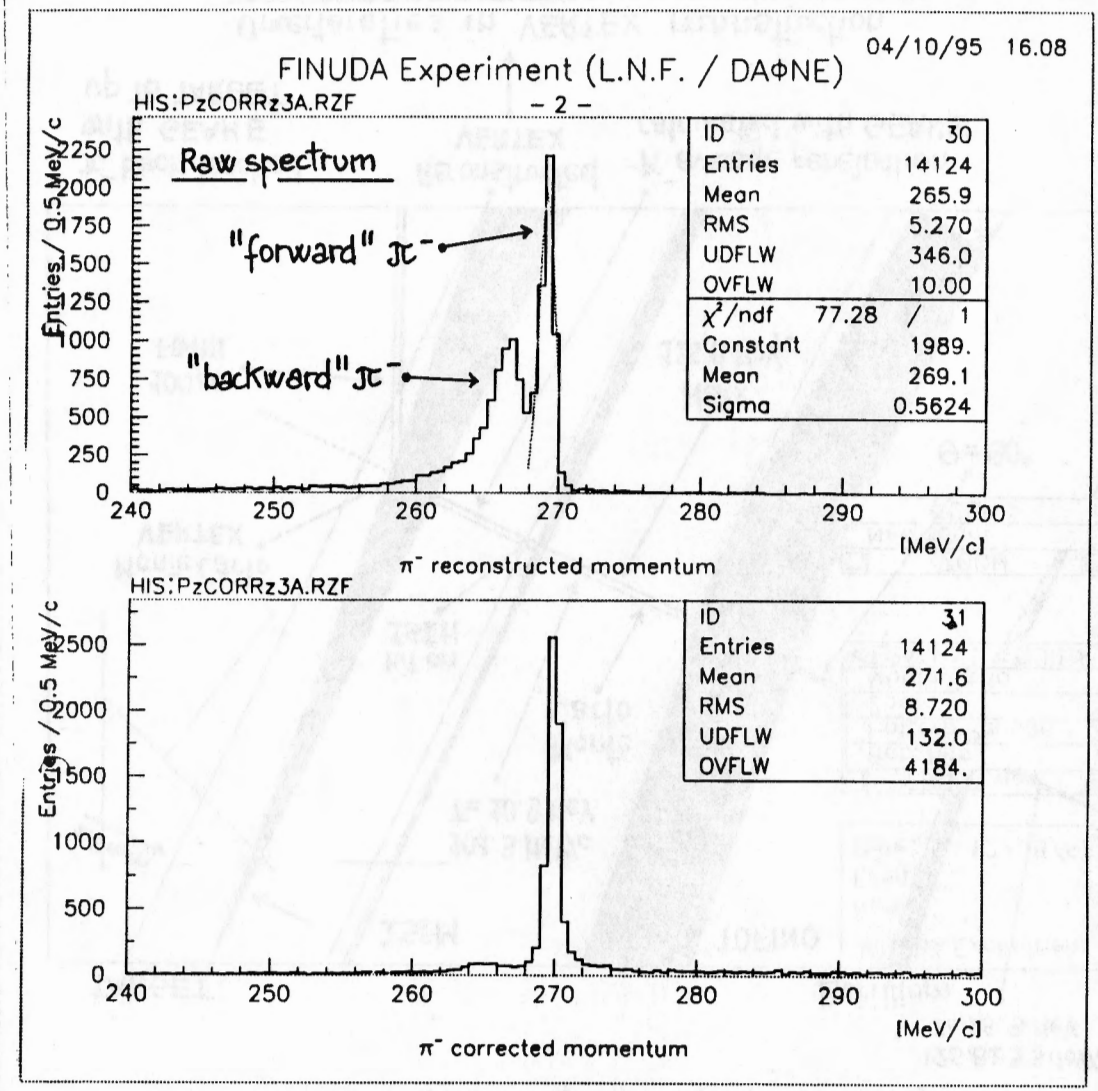

VERTEX RECONSTRUCTION

Use of GEANE package:
tracking of particles with account for geometrical volumes, magnetic field, average energy loss plus transport of error matrix (multiple scattering)

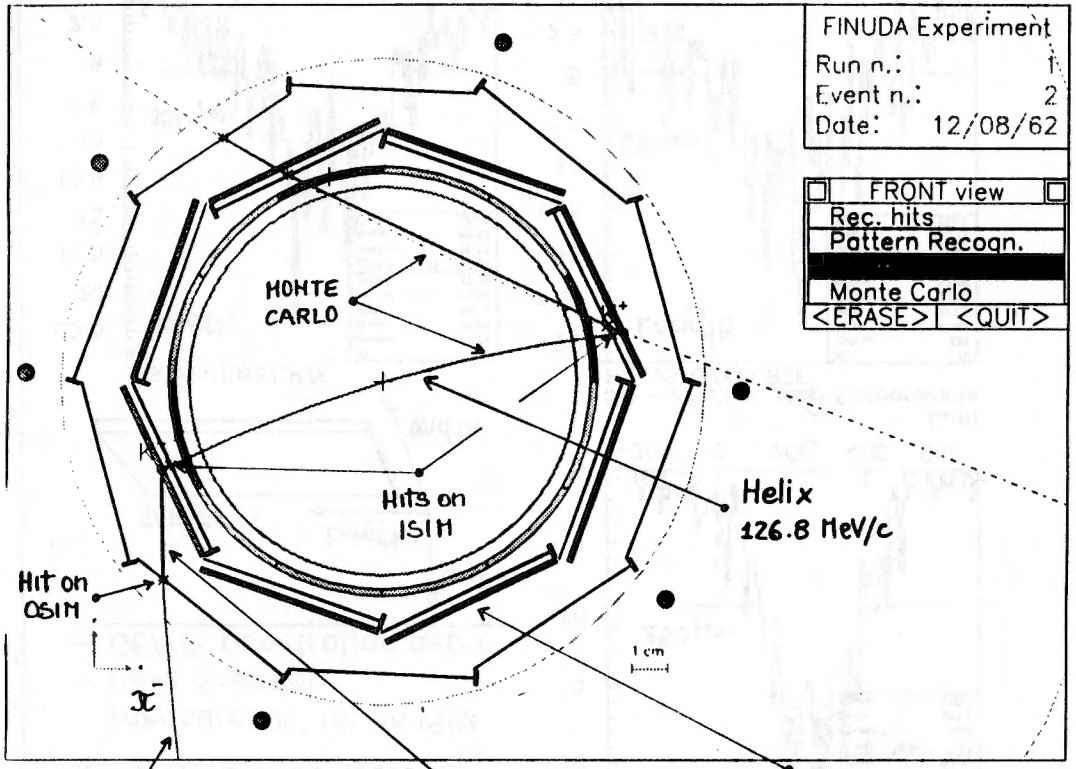

Closeness of TOFINO and ISIM to the target improves the efficacy of the algorithm since reduces the effect of multiple scattering.

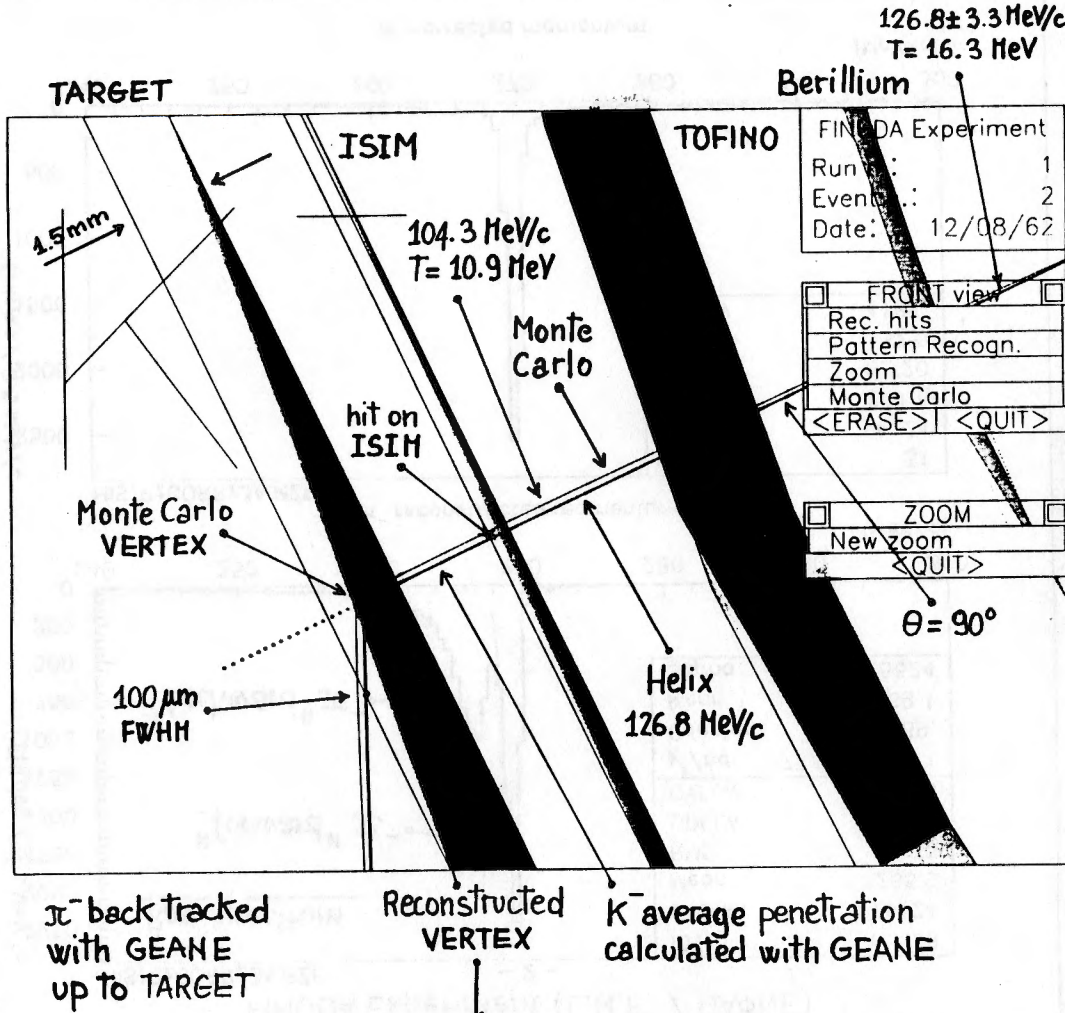

Uncertainties in VERTEX reconstruction

Target depth ~ 280 μm FWHM due mainly to the width of ∅
Target length ~ 530 " " } can be reduced by approaching
Target width ~ 450 " " } the TARGET to ISIM.

ISIM/OSIM Simulation/Reconstruction

RECONSTRUCTION

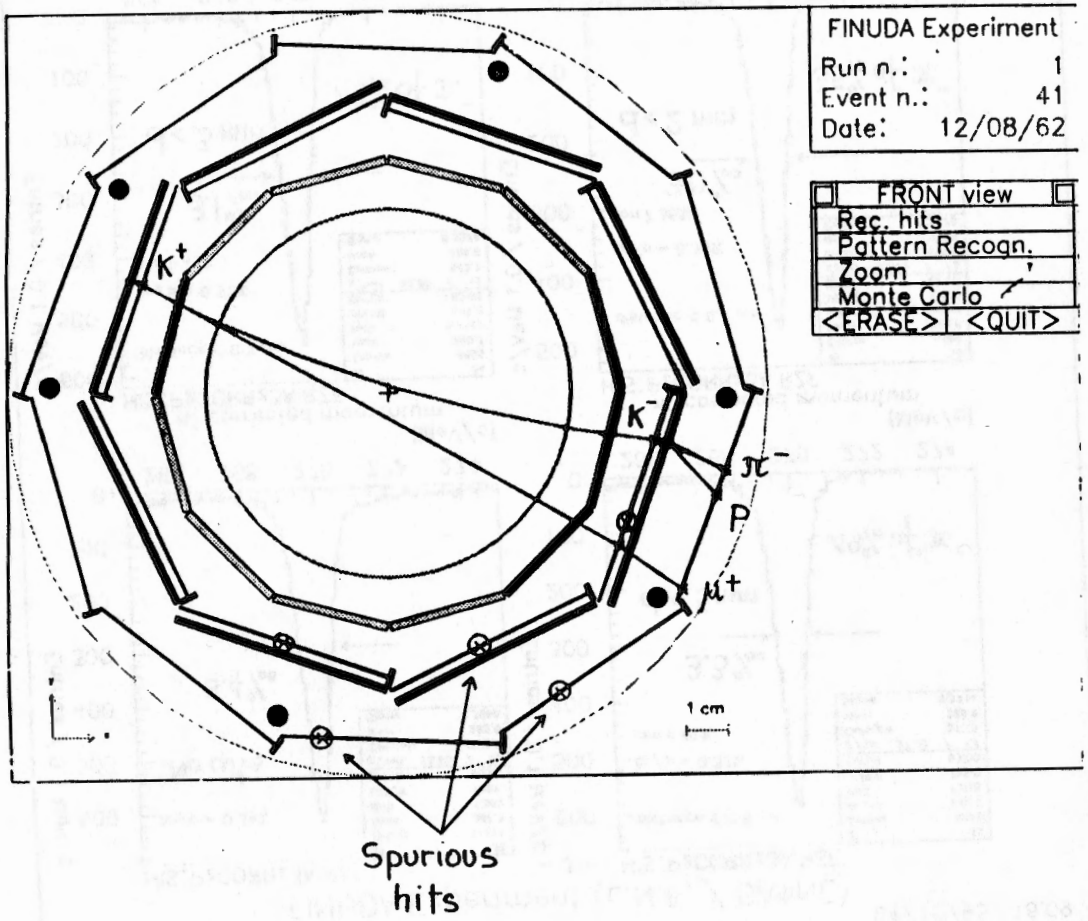

Energy lost in μstrip modules
(hypernuclear events)

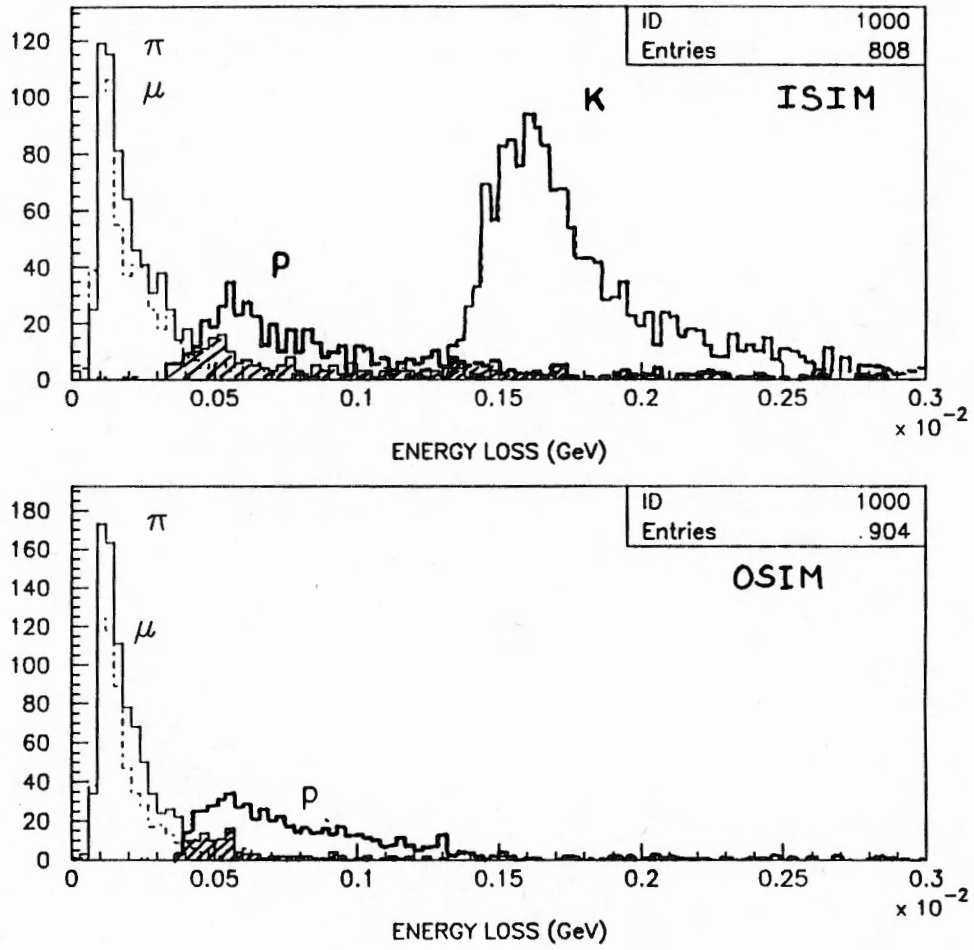

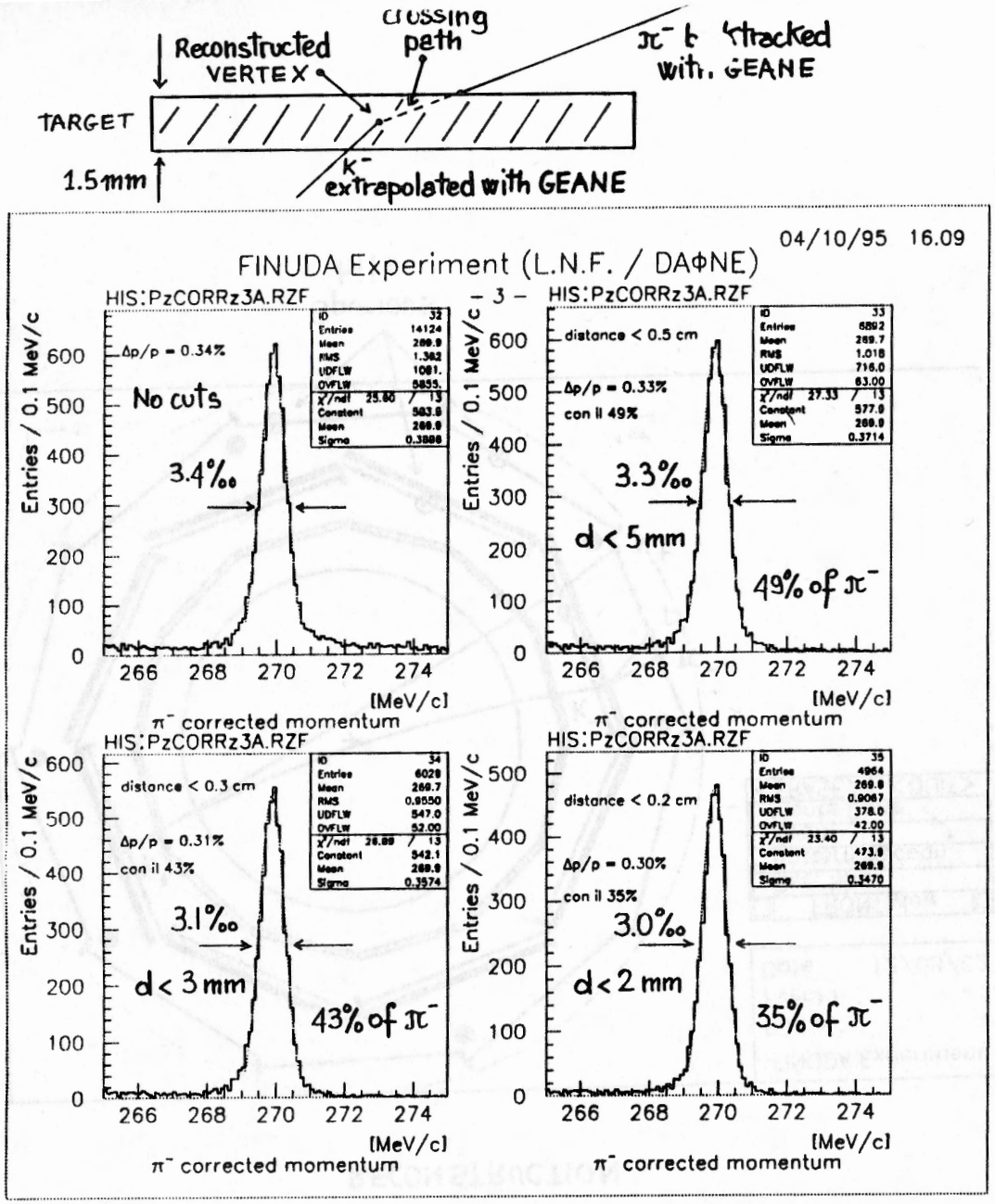
Reconstructed VERTEX
Crossing path
π⁻ tracked with GEANE
TARGET
1.5 mm
K⁻ extrapolated with GEANE
04/10/95 16.09
FINUDA Experiment (L.N.F. / DAΦNE)
HIS:PzCORRz3A.RZF
Δp/p = 0.34%
No cuts
3.4‰
Entries / 0.1 MeV/c
π⁻ corrected momentum [MeV/c]
HIS:PzCORRz3A.RZF
distance < 0.5 cm
Δp/p = 0.33%
con il 49%
3.3‰
d < 5 mm
49% of π⁻
HIS:PzCORRz3A.RZF
distance < 0.3 cm
Δp/p = 0.31%
con il 43%
3.1‰
d < 3 mm
43% of π⁻
HIS:PzCORRz3A.RZF
distance < 0.2 cm
Δp/p = 0.30%
con il 35%
3.0‰
d < 2 mm
35% of π⁻

K^- : number of strips in clusters on ISIM

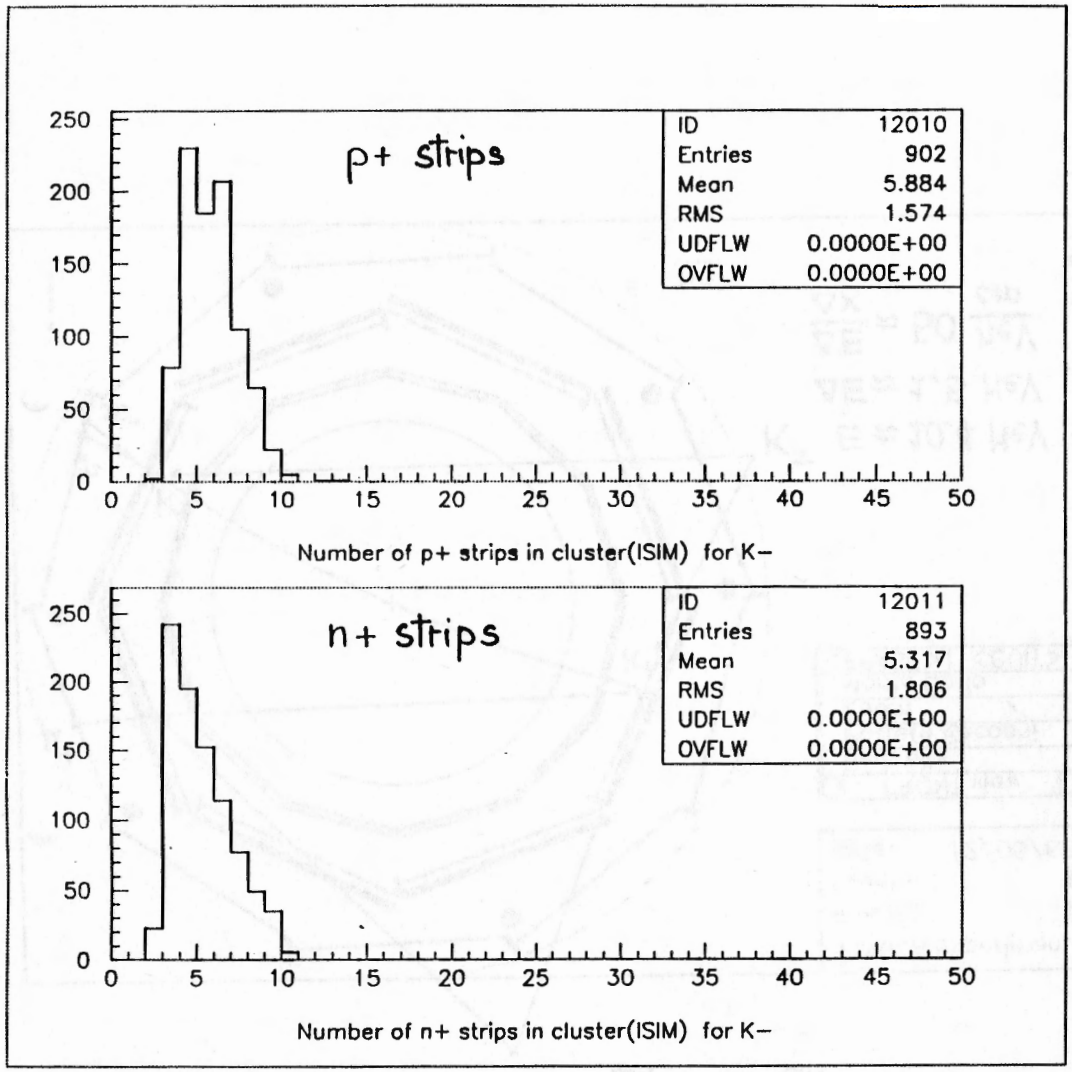

p : number of strips in clusters on ISIM

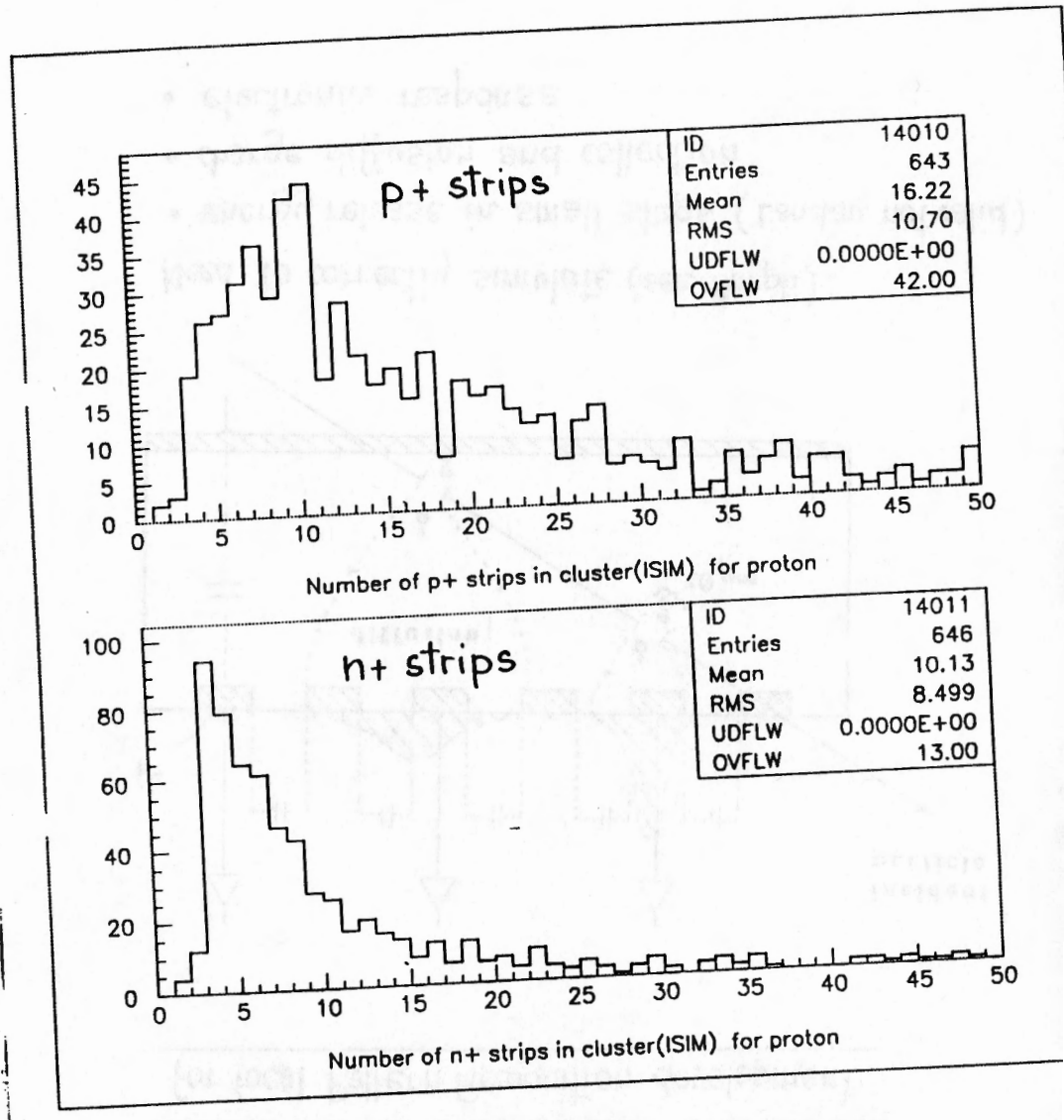

"minimum ionizing"

$\Delta E \approx 0.12$ MeV, $\frac{\Delta E}{\Delta x} \approx 3.9 \frac{MeV}{cm}$

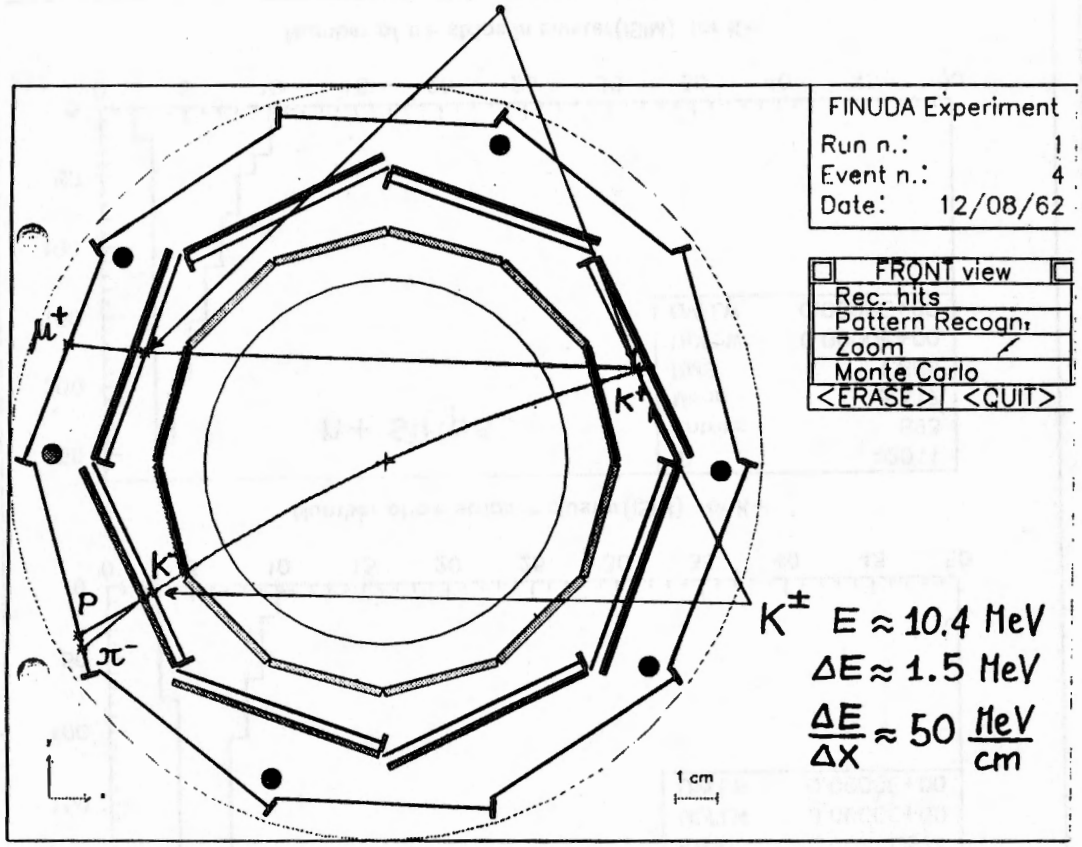

$K^{\pm}$ $E \approx 10.4$ MeV

$\Delta E \approx 1.5$ MeV

$\frac{\Delta E}{\Delta x} \approx 50 \frac{MeV}{cm}$

Simulation of Silicon μstrip response for local Pattern Recognition development

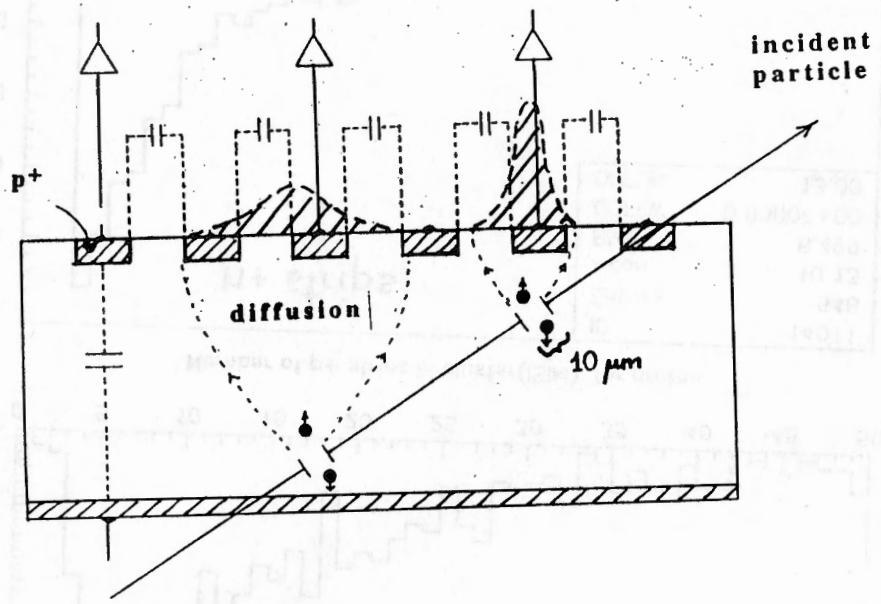

Need to correctly simulate (see Aleph):

- energy release in small steps (Landau not valid)
- charge diffusion and collection
- electronic response

Drift velocity

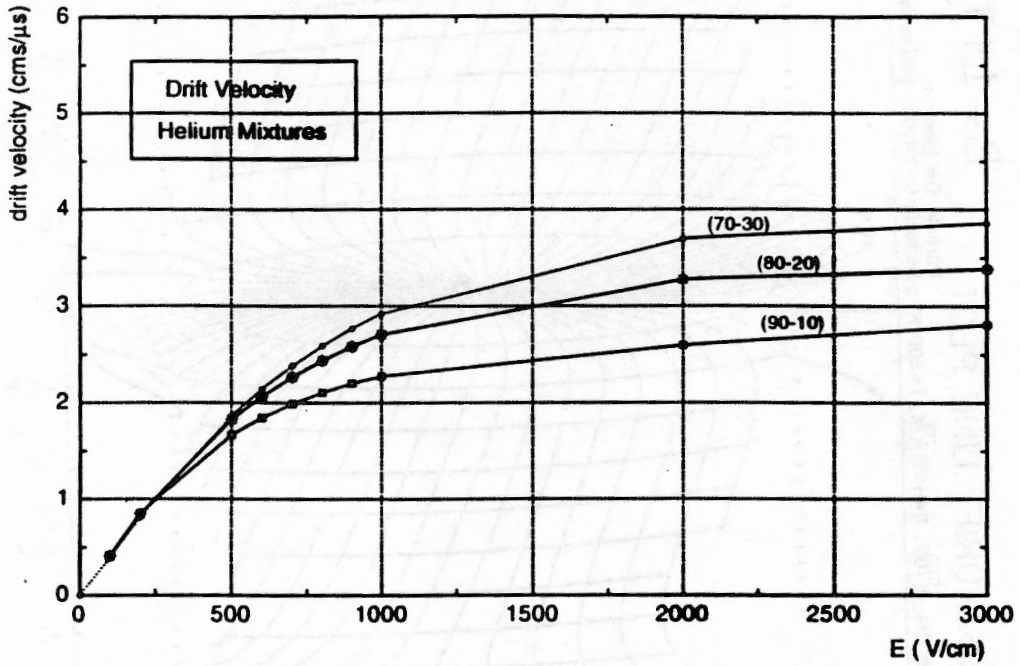

Fig. 2

$He\text{-}iC_4H_{10}$

Calculations with

MAGBOLTZ

Lorentz Angle B=1.1 T

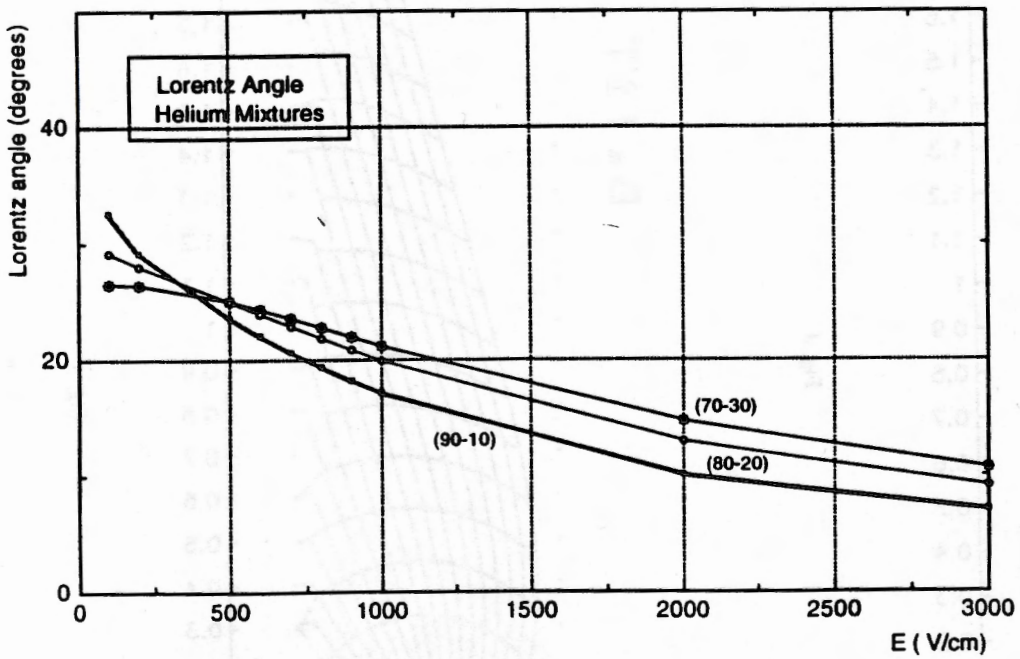

Fig. 6

$He\text{-}iC_4H_{10}$

Calculations with

MAGBOLTZ

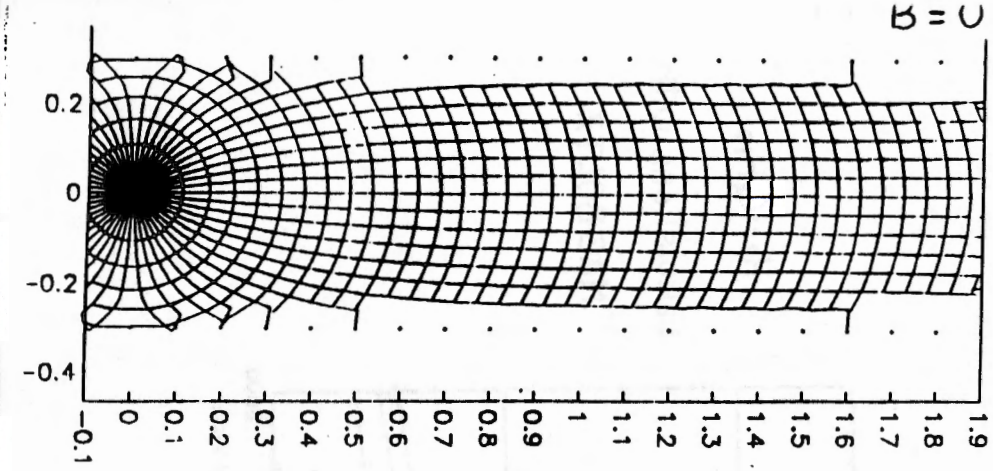

Fig. 4

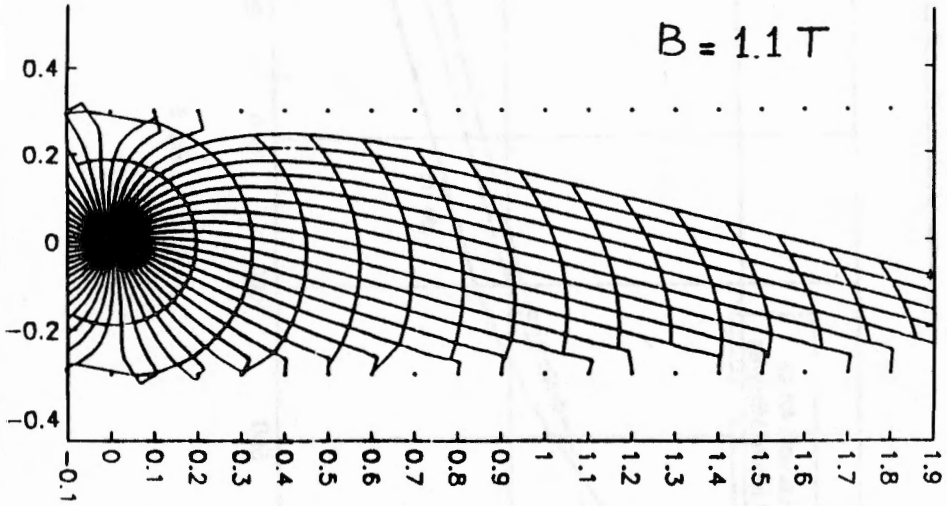

Fig. 5

Calculations with GARFIELD

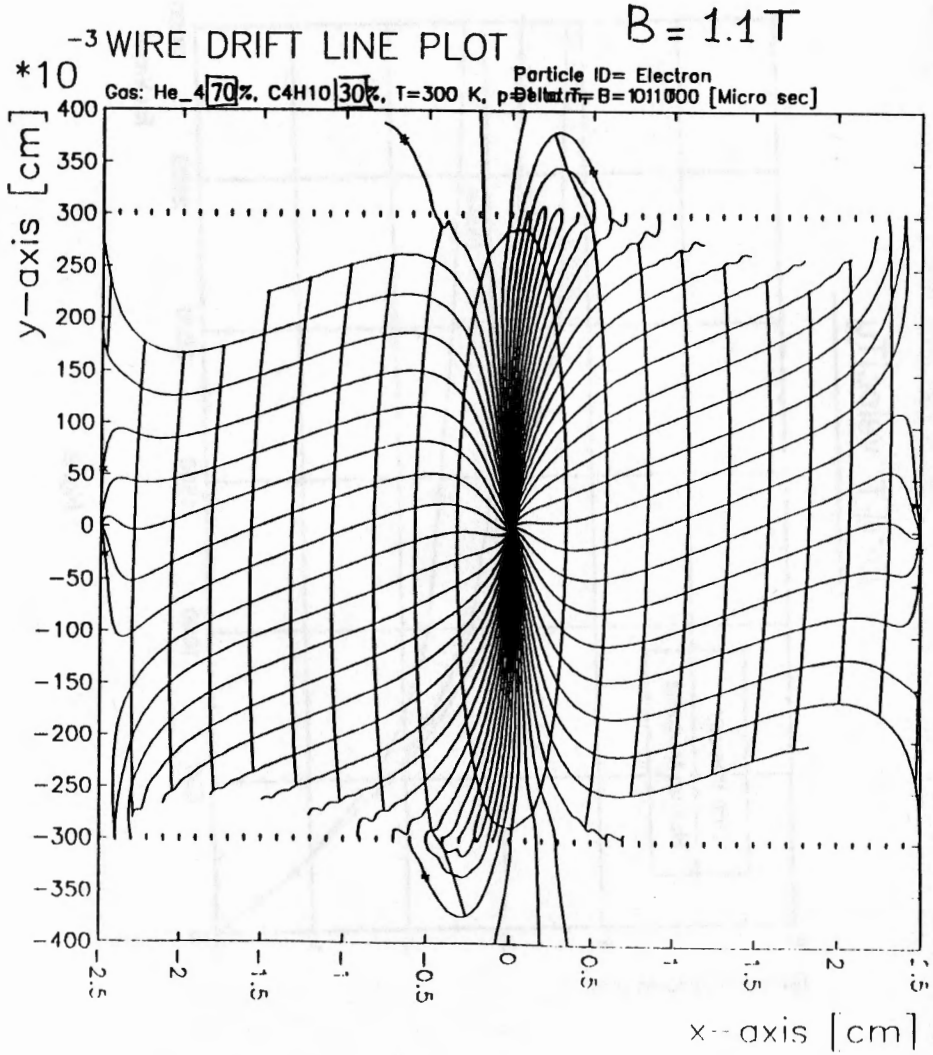

Present track fitting method

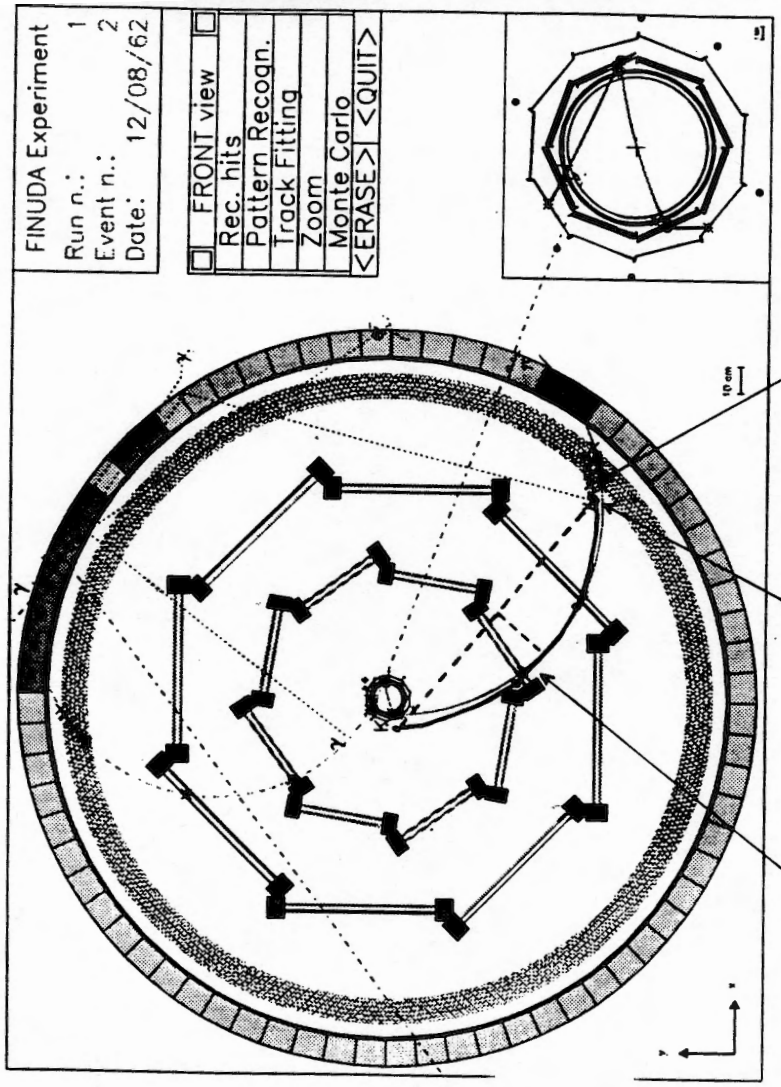

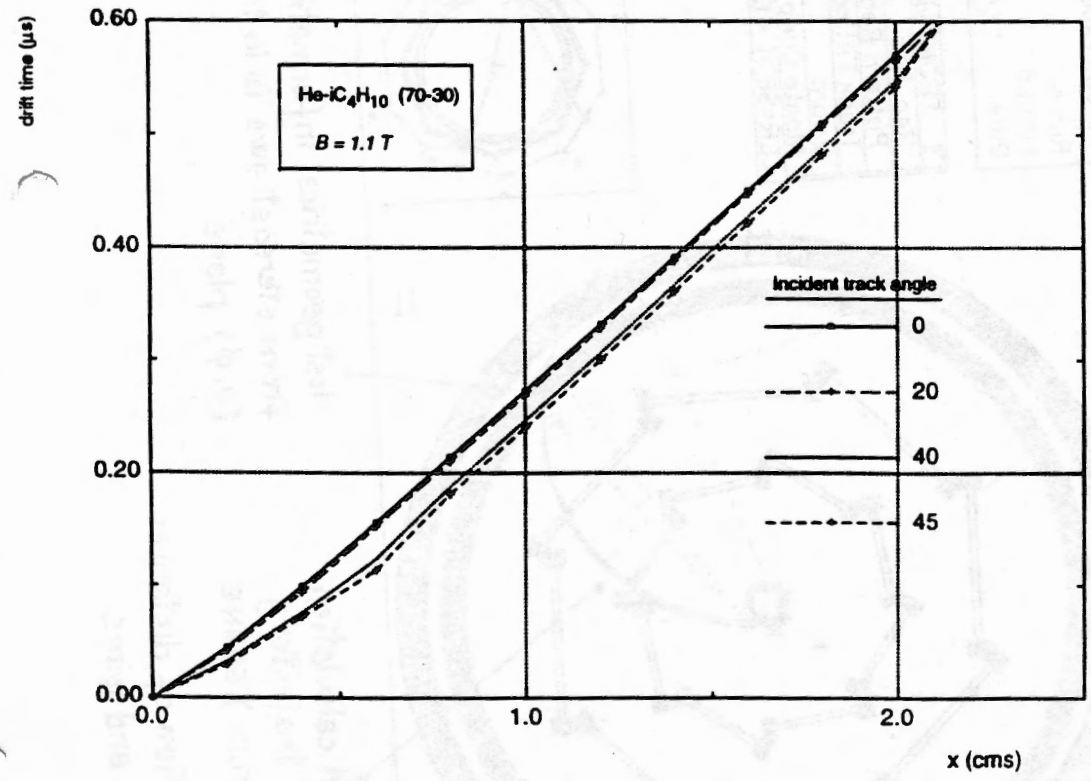

Fig. 10

Calculations with GARFIELD

Space - time relationship

Global track fitting

Possible improvement in resolution (1.2 - 1.3)

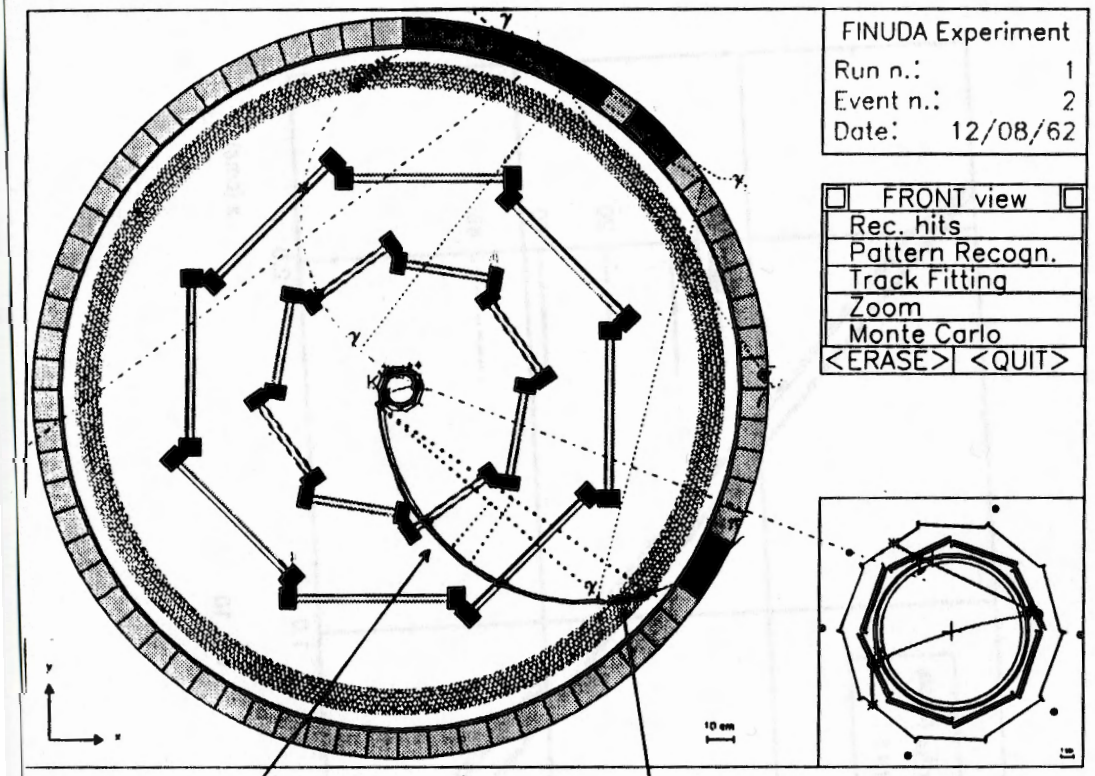

Numerical calculation of track trajectory (Runge-Kutta) GEANE

Minimization of distances from hits and wires

Most geometrical information from stereo straws is in the (ρ, ϕ) plane.

Status Report on

FI.NU.DA. experiment

The FINUDA Collaboration

T. Bressani

Frascati, L.N.F.

March 28, 1995

Summary

Introduction

Main efforts and activities of the last semester, are all finalised to the scope: FINUDA "in pit" around Summer '96.

- Conclude tests on sub-detector prototypes ⇨ final decision for mass production ⇨ tenders
- Freeze mechanical designs ⇨ tenders
- Two major changes from last presentation *(Technical Report)*

  1. Vertex detector design allows more space for beam pipe (ISIM/OSIM from hexagon/octagon to octagon/decagon); benefit also for reduction of machine induced background; present beam pipe diameter may be further increased without "dramatic" changes of the mechanical structure.

  2. Magnet yoke + cryostat will be fully assembled in Genova. Magnetic measurements will be performed with the Ansaldo Liquefaction Plant (no dewars!). Magnet will be transported as "a whole" (without end caps) and installed directly in the pit. Interference with the machine commissioning considerably reduced (we skip the "intermediate step" of the installation in the MEA Hall). Test on all sub-detectors, already mounted on the clepsydra, may be performed.

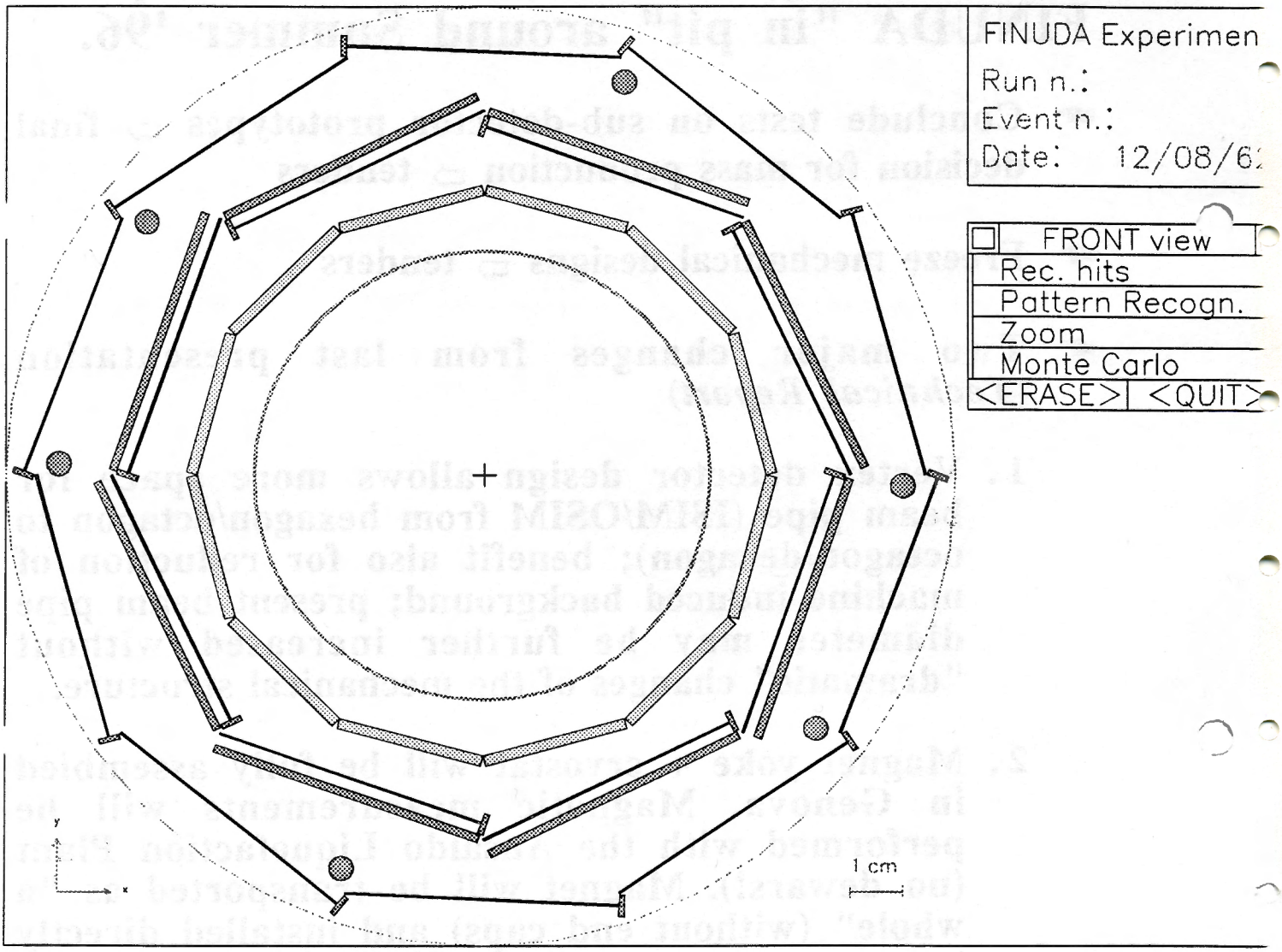
FINUDA Experimen
Run n.:
Event n.:
Date: 12/08/6
FRONT view
Rec. hits
Pattern Recogn.
Zoom
Monte Carlo
<ERASE>
<QUIT>
y
x
1 cm

LMDCs: conclusions and further checks

❶ Results fully consistent (≤) with design performances

❷ Calculations reliable

❸ Mechanics + electronics: OK

❶ Resolution + efficiency as a function of the incidence angle: beam test at CERN PS in June '95

❷ Lorentz angle: direct measurement with X-rays to check calculation;
however:
3 ways of controlling /changing it:
① electronical
② mechanical
③ % of the gas mixture

5. Monte Carlo simulation of the performance of the realistic detector configuration

- ✔ **Final FINUDA geometry**
- ✔ **Spectrometer acceptance**
- ✔ **Spectrometer momentum resolution**
- ✔ **Trigger efficiency and rates**

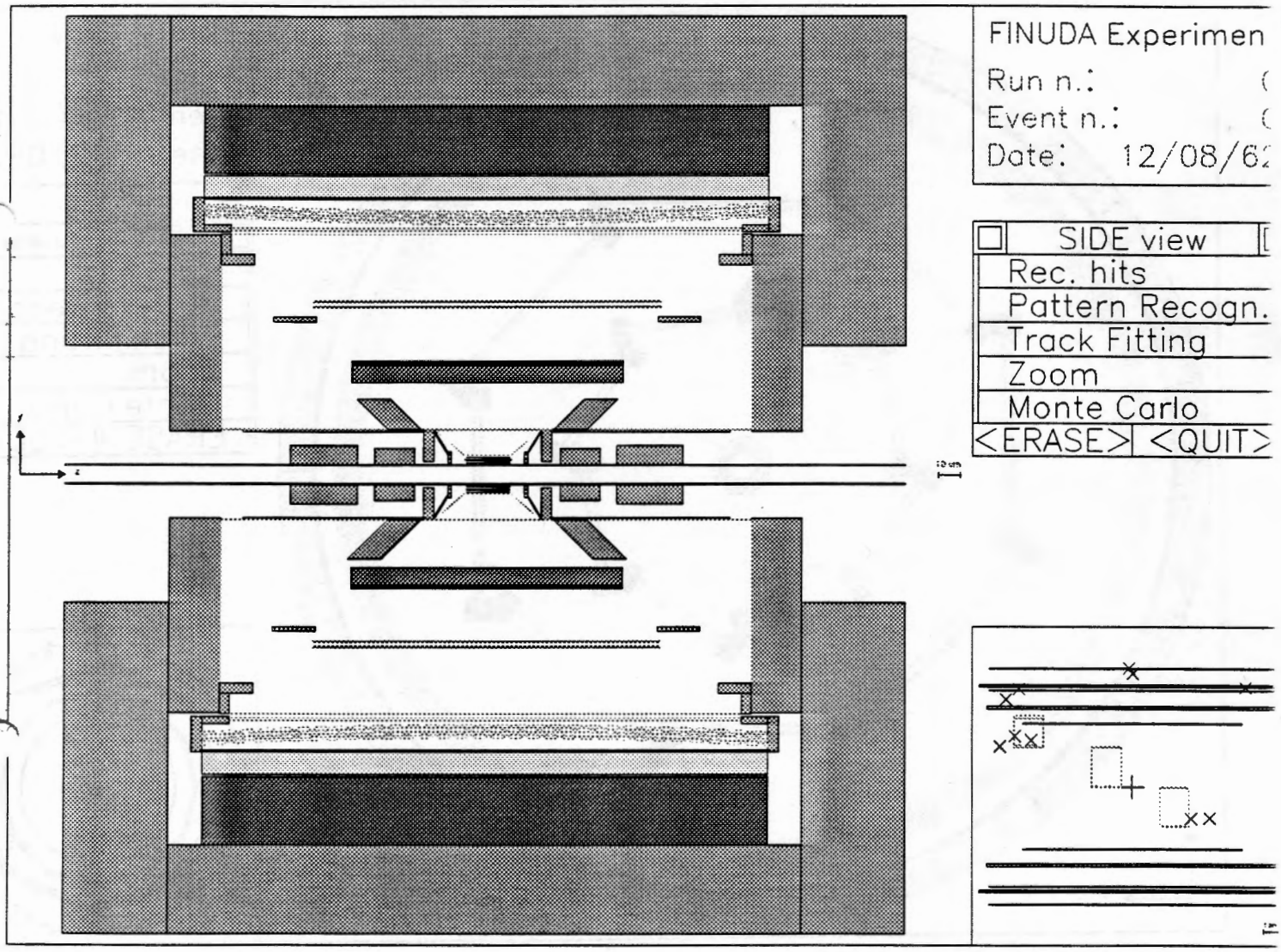
FINUDA Experimen
Run n.:
Event n.:
Date: 12/08/6
SIDE view
Rec. hits
Pattern Recogn.
Track Fitting
Zoom
Monte Carlo
<ERASE>
<QUIT>

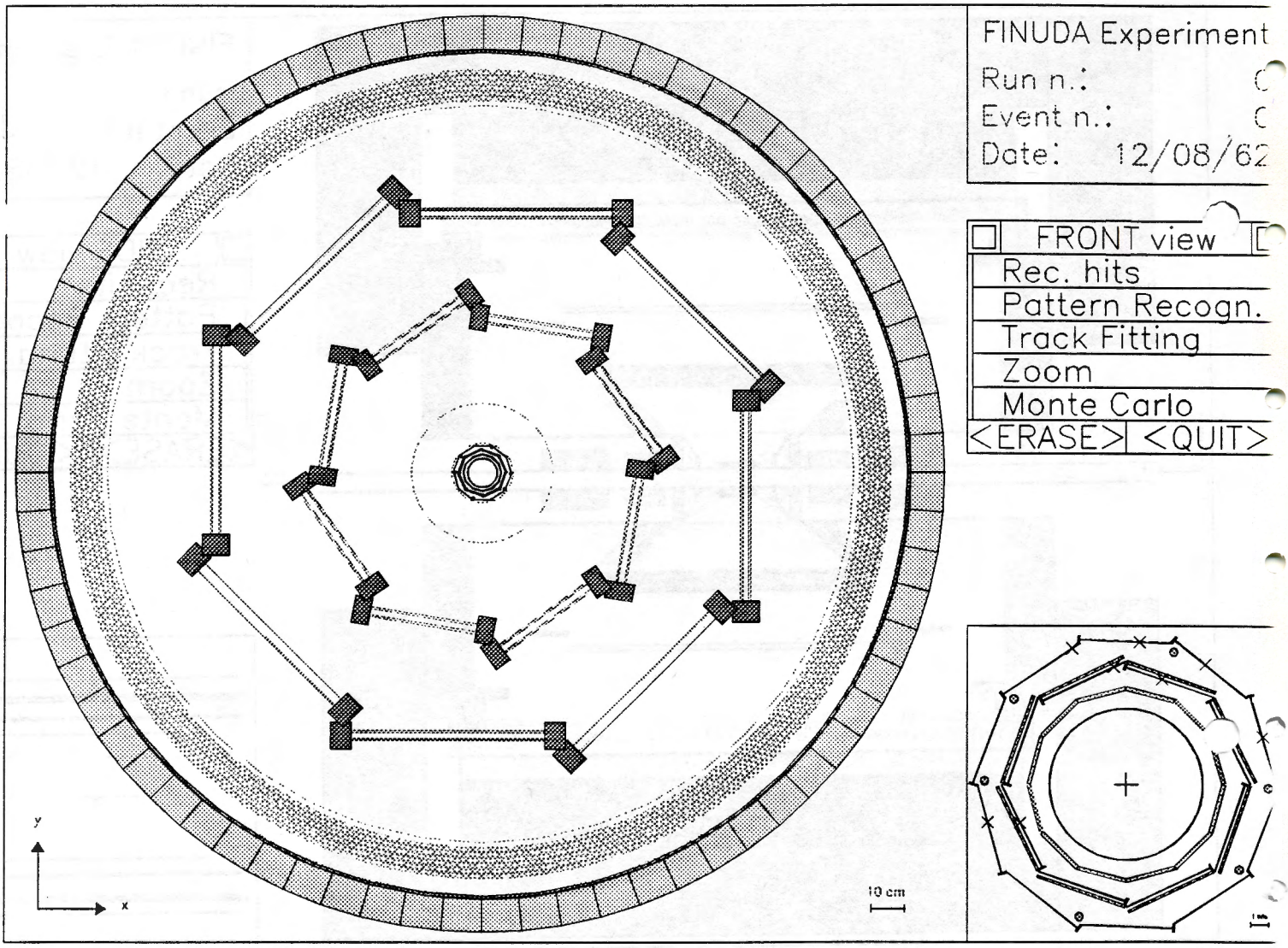
FINUDA Experiment
Run n.:
Event n.:
Date: 12/08/62
FRONT view
Rec. hits
Pattern Recogn.
Track Fitting
Zoom
Monte Carlo
<ERASE>
<QUIT>
y
x
10 cm

Spectrometer acceptance (straw tubes)

particle	full apparatus		geometric acceptance	
π^- 270 MeV/c	(45 ± 1)%	44%	(54 ± 1)%	53%
p 417 MeV/c	(32 ± 1)%	43%	(60 ± 1)%	63%
μ^+ 236 MeV/c	(31 ± 1)%	38%	(53 ± 1)%	53%

Technical report

Spectrometer acceptance (tofone)

particle	full apparatus	geometric acceptance
π^- 270 MeV/c	(40 ± 1)%	(48 ± 1)%
p 417 MeV/c	(29 ± 1)%	(56 ± 1)%
μ^+ 236 MeV/c	(21 ± 1)%	(40 ± 1)%

Momentum resolution

Assumed detector resolutions:

		σ		
μstrips	Rφ =	50 μm		
	z =	50 μm		
chambers	Rφ =	150 μm	(pessimistic!)	(100 μm)
	z =	1% wire	(1 ÷ 2 cm)	
straws	r =	100 μm		
	z =	1 mm	(pessimistic!)	(500 μm)

particle		momentum resolution (FWHM)	
π^+	270 MeV/c	0.28 %	(0.25 %)
p	417 MeV/c	0.79 %	(0.70 %)
μ^+	236 MeV/c	0.24 %	

Total radiation length	170000	cm
Helium	540000	cm
Air	30400	cm

Spectrometer size 102 cm (110 cm)

6. Machine induced background

Impact on:

- **TRIGGER**
- **PATTERN RECOGNITION**

Rate of particles per bunch lost , due to Touschek scattering,

in the Fi.Nu.Da. detector.

$A_{QF1} = A_{QD2} = 43$mm

A_{sc}/σ_x	A_{sc} (mm)	$N_Q(\varepsilon>0)$ (s^{-1})	$N_Q(\varepsilon<0)$ (s^{-1})	N_Q (s^{-1})	τ_{tot} (min)
8	23.5	$1.2\,10^4$	$3.0\,10^3$	$1.5\,10^4$	168
9	26.5	$3.4\,10^4$	$1.5\,10^4$	$5.0\,10^4$	198
10	29.4	$5.8\,10^4$	$3.6\,10^4$	$9.4\,10^4$	233

$A_{QF1} = A_{QD2} = 48$mm

A_{sc}/σ_x	A_{sc} (mm)	$N_Q(\varepsilon>0)$ (s^{-1})	$N_Q(\varepsilon<0)$ (s^{-1})	N_Q (s^{-1})	τ_{tot} (min)
8	23.5	$1.4\,10^3$	52.	$1.5\,10^3$	168
9	26.5	$8.6\,10^3$	$1.8\,10^3$	$1.0\,10^4$	198
10	29.4	$2.3\,10^4$	$9.4\,10^3$	$3.2\,10^4$	233

$A_{QF1} = A_{QD2} = 53$mm

A_{sc}/σ_x	A_{sc} (mm)	$N_Q(\varepsilon>0)$ (s^{-1})	$N_Q(\varepsilon<0)$ (s^{-1})	N_Q (s^{-1})	τ_{tot} (min)
8	23.5	225.	0.	225.	168
9	26.5	$1.7\,10^3$	52.	$1.7\,10^3$	198
10	29.4	$6.5\,10^3$	$2.2\,10^3$	$8.7\,10^3$	233

25/03/95 11.48

FINUDA Project (LNF/DAΦNE)

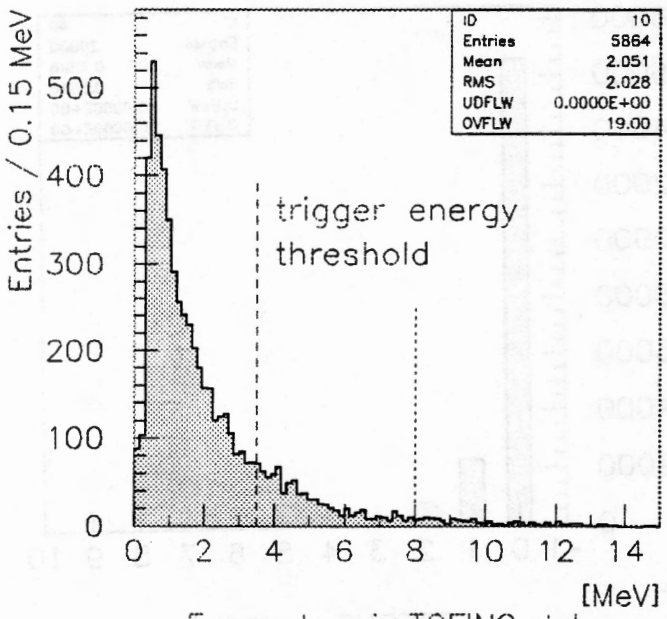

Energy loss in TOFINO slabs

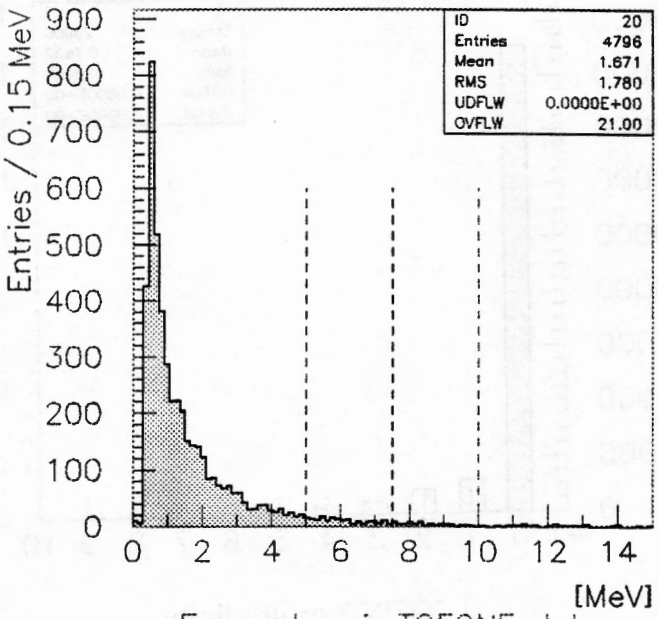

Energy loss in TOFONE slabs

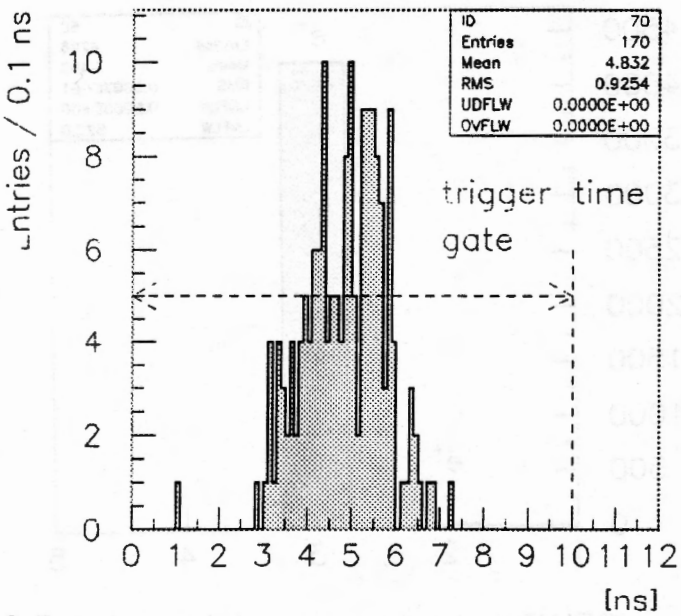

T.O.F. between internal and external scintillator barrels

Impact on trigger of the machine induced background (10000 showers)

25/03/95 11.48

FINUDA Project (LNF/DAΦNE)

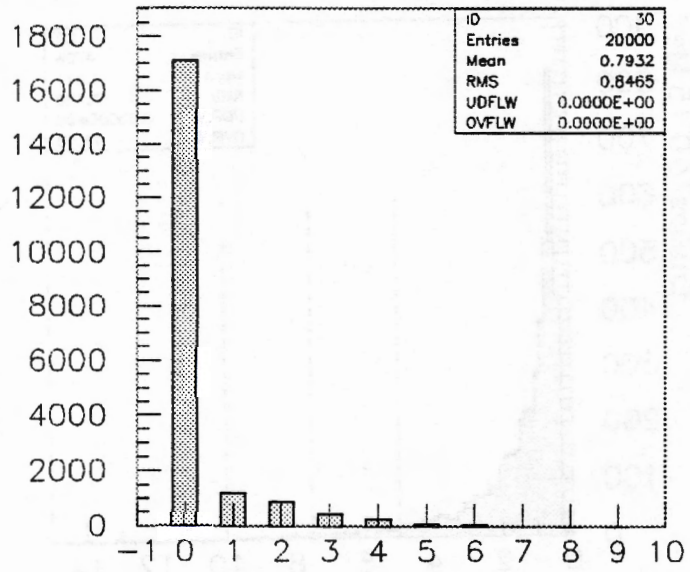

TOFINO multiplicity

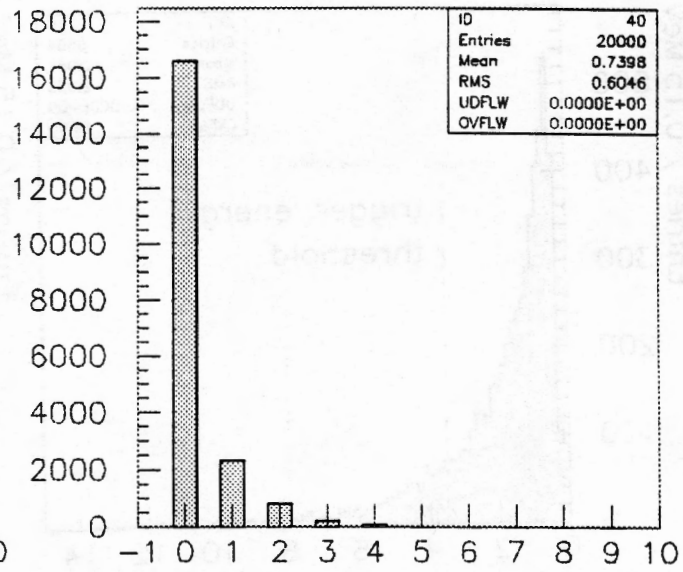

TOFONE multiplicity

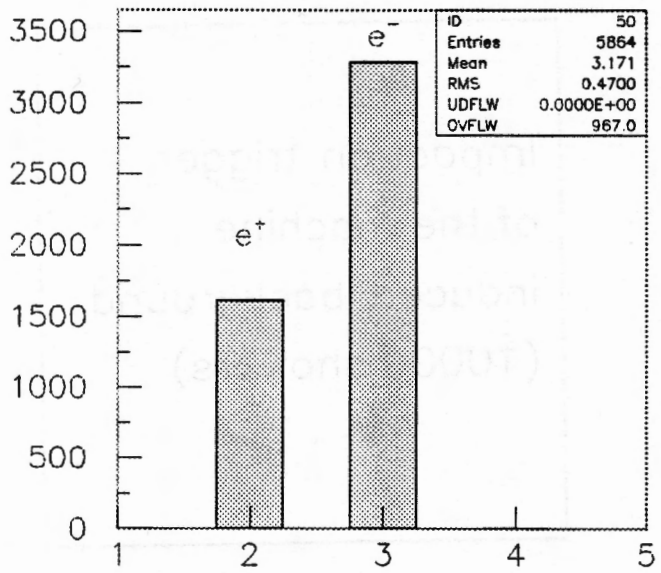

GEANT code of particles hitting TOFINO

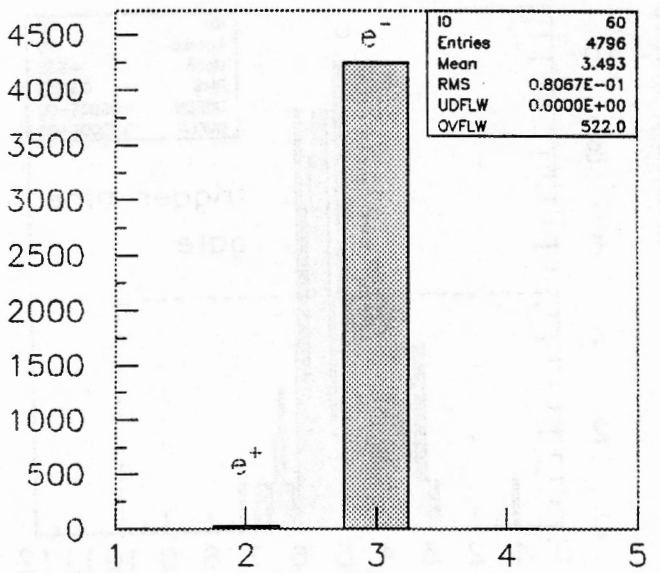

GEANT code of particles hitting TOFONE

Trigger rejection for machine induced background

Trigger conditions:

① Extended "back to back" topology

② Energy threshold on "BtoB" slabs ($\Delta E > 3.5$ MeV)

③ Time coincidence on tofone ($\Delta T < 10$ ns, $\Delta E > 5.0$ MeV)

Trigger rejection ⇨ 1.76×10^{-5}

at 0.6×10^{6} $\frac{\text{lost } e^{+}(e^{-})}{\text{sec}}$ ⇨ 11 $\frac{\text{trigger}}{\text{sec}}$

Asking 2 tofone slabs over threshold

$\Delta E > 5.0$ MeV ⇨ 0.4 trigger/sec

$\Delta E > 7.5$ MeV ⇨ 0.1 trigger/sec

25/03/95 12.45

FINUDA Project (LNF/DAΦNE)

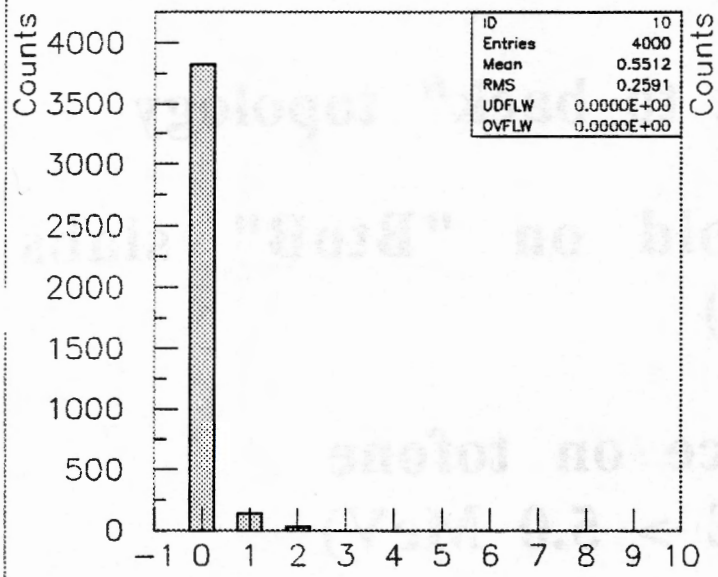

Hit frequency on internal μstrip modules

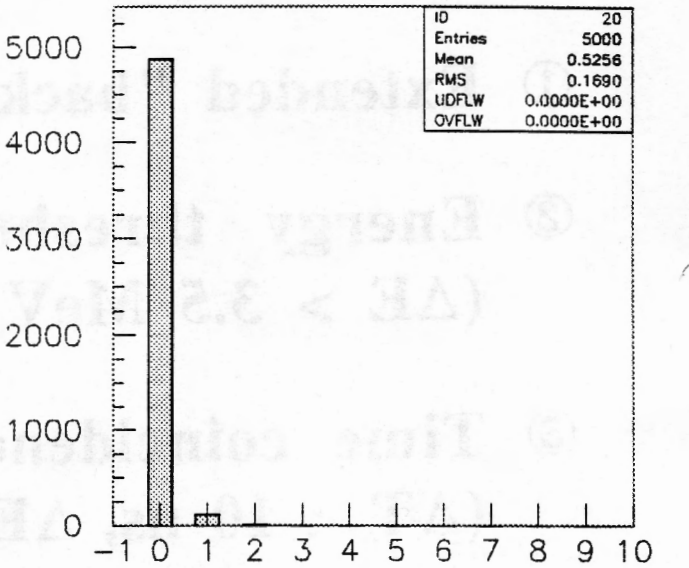

Hit frequency on external μstrip modules

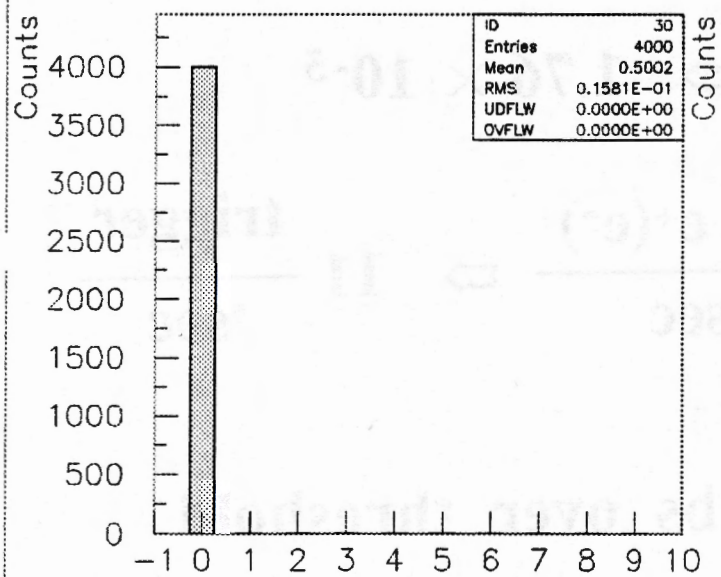

Hit frequency on internal drift chambers

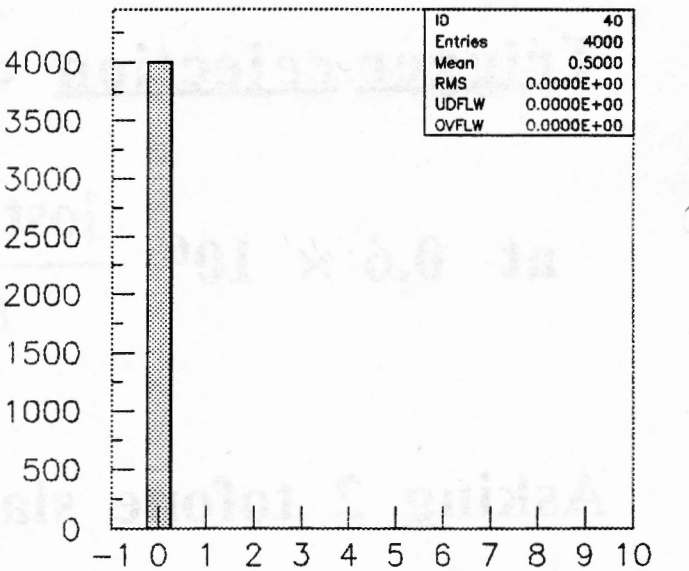

Hit frequency on external drift chambers

25/03/95 12.45

FINUDA Project (LNF/DAΦNE)

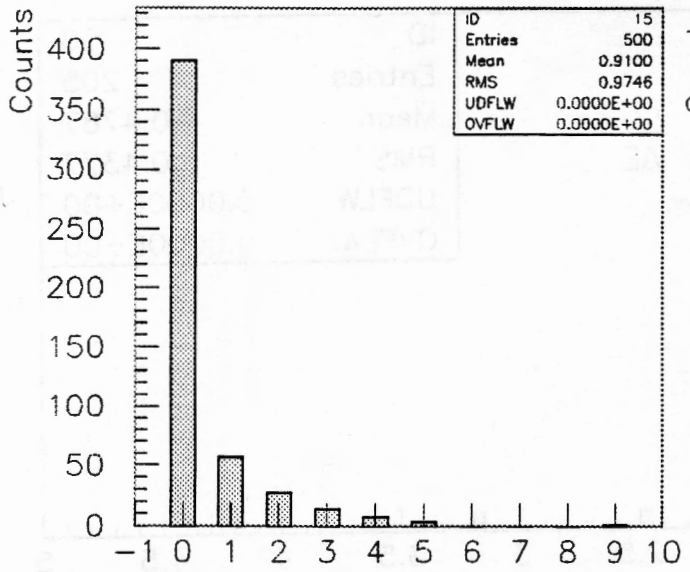

Hit multiplicity on internal μstrip array

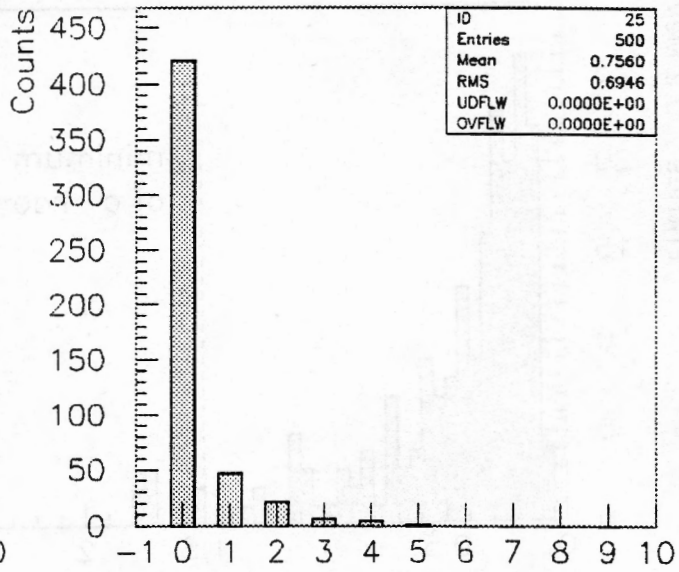

Hit multiplicity on external μstrip array

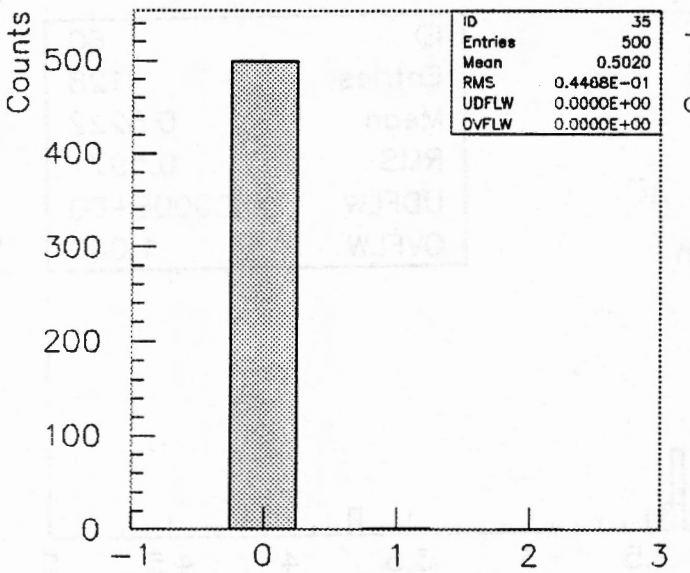

Hit multiplicity on internal drift chambers

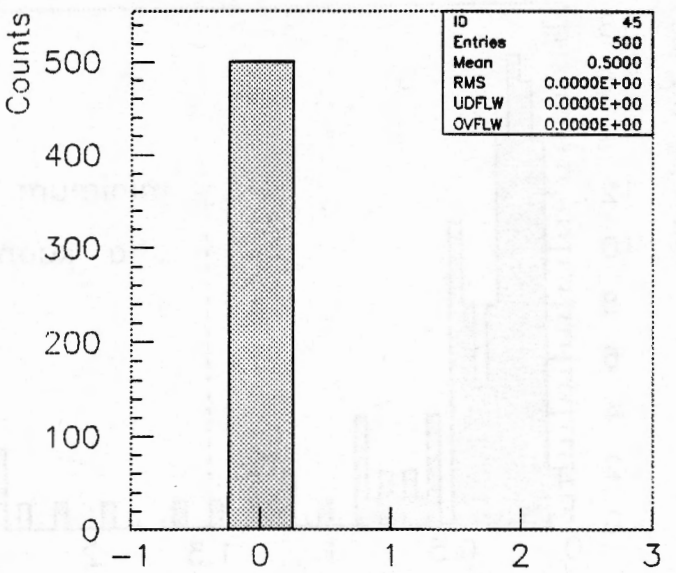

Hit multiplicity on external drift chambers

25/03/95 12.45

FINUDA Project (LNF/DAΦNE)

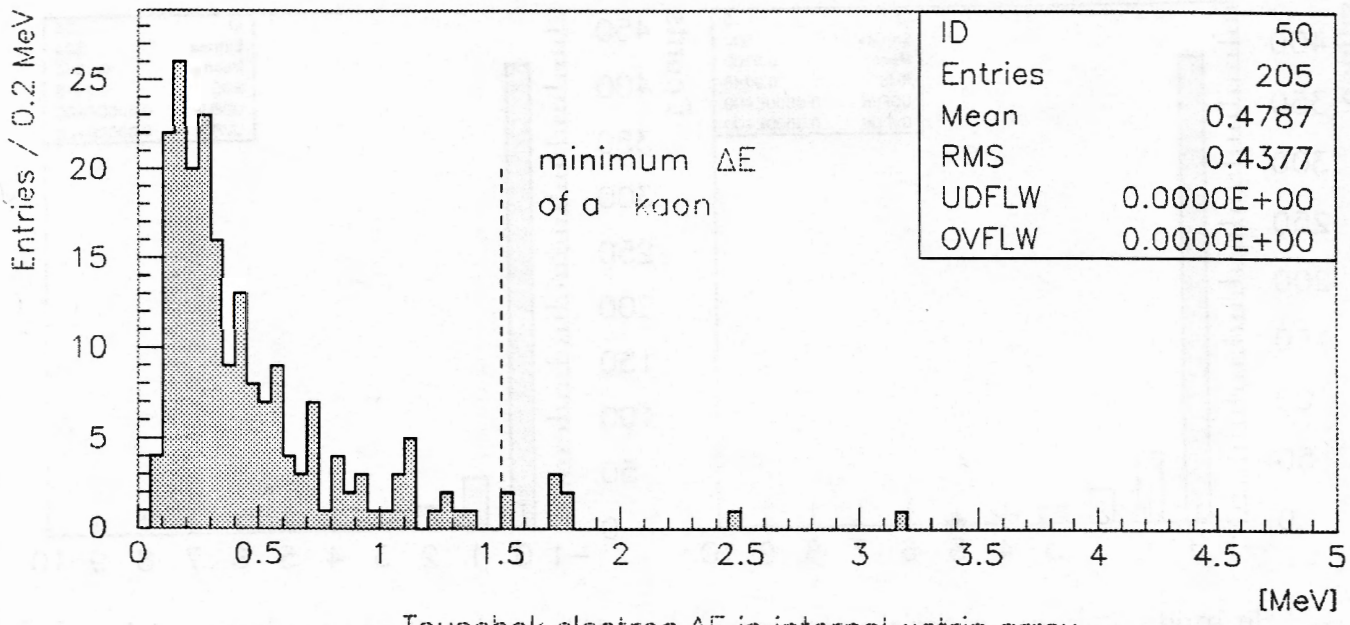

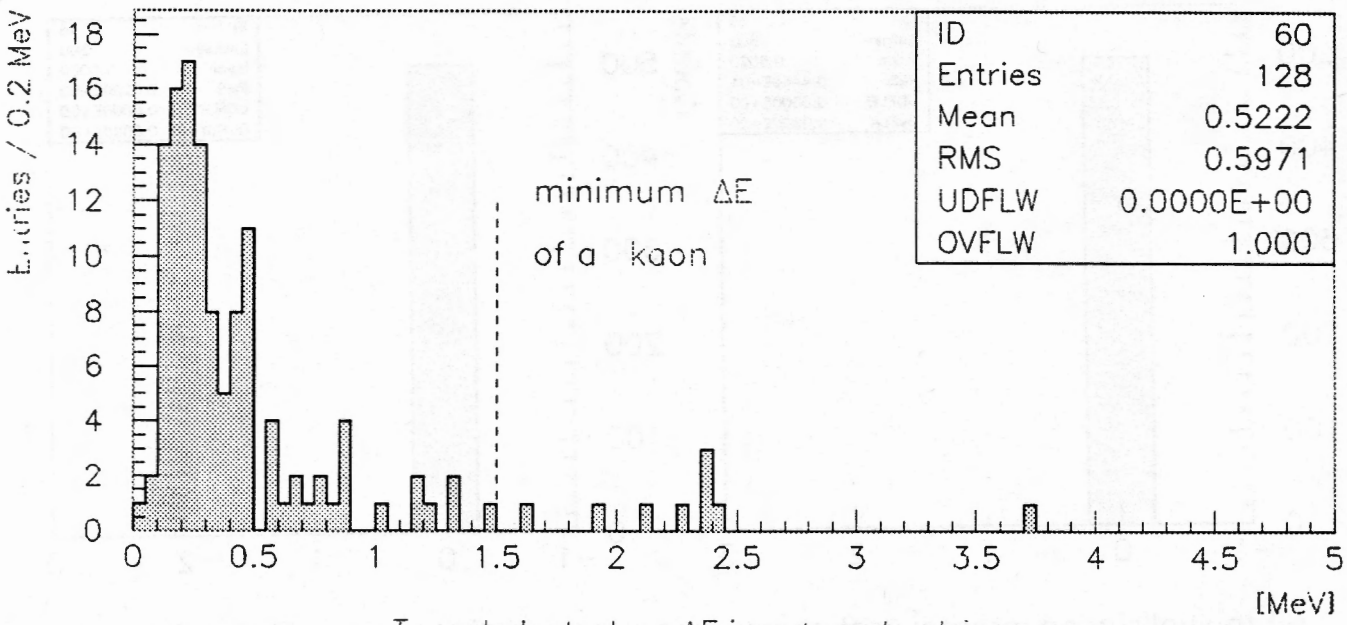

7. First Round Physics

The new octagonal ISIM/target arrangement allows, in principle, the positioning of 8 different targets.

The present idea for the first run arrangement is the following:

3 targets ^{12}C (graphite)	→ calibration + spectroscopy
3 targets ^{6}Li	→ non mesonic decay → → $\Delta I = 1/2$ rule validity
1 target ^{6}Li	→ control of ^{6}Li purity
1 target ^{27}Al	→ capture rate for heavier nuclei

We plan to run with this set-up for ≈ 150 machine/days, ≈ 30 of them for initial debugging and setting-up (total data taking time ≈ 120 days) at $\mathcal{L} = 10^{32}$ cm^{-2} s^{-1}

The choice of the target for the following run (of heavier mass) will be decided following the results of this first run and (presumably) following presentation and discussion with Scientific Committee of L.N.F..

The case of the ^{6}Li target

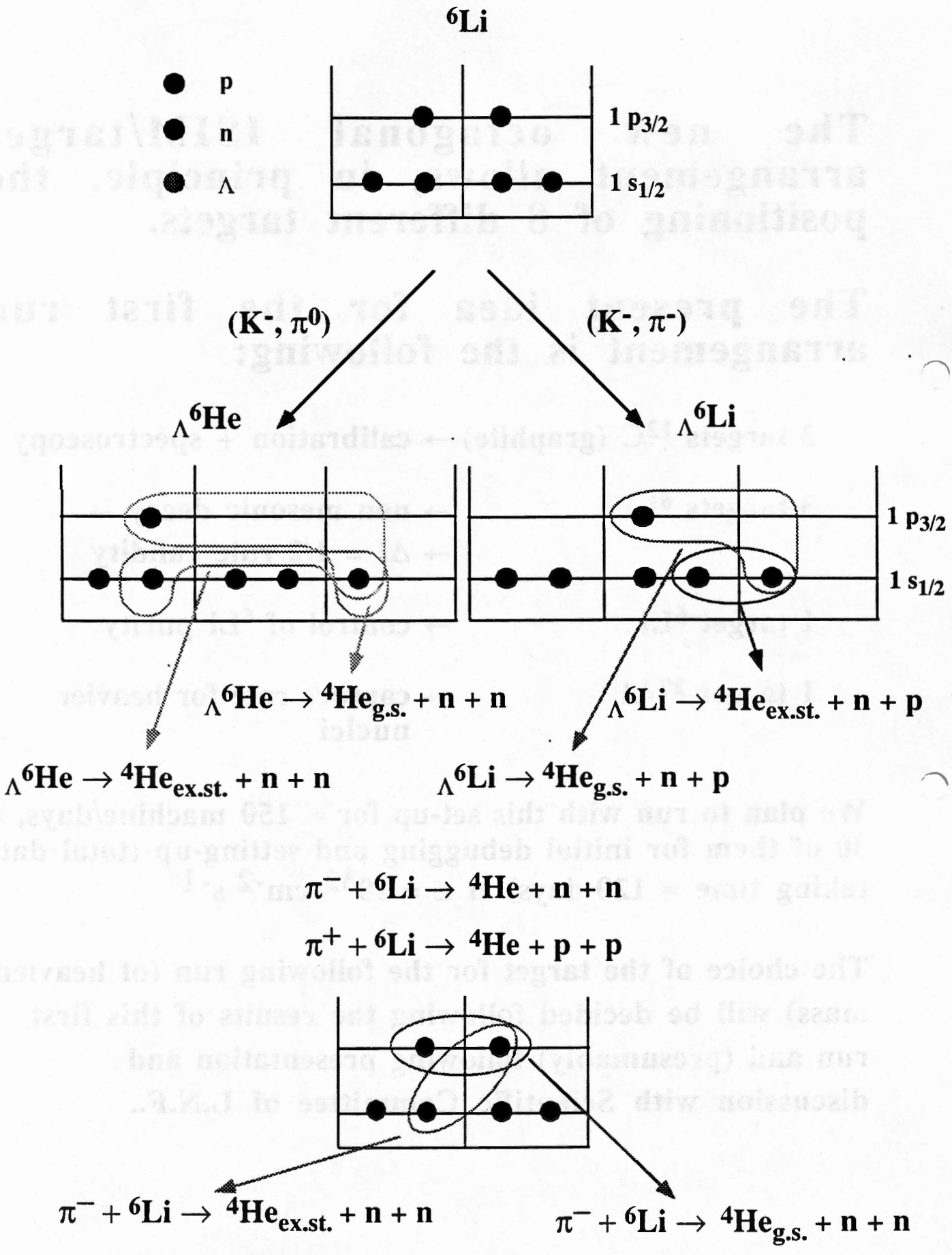

7. First Round Physics

The new octagonal ISIM/target arrangement allows, in principle, the positioning of 8 different targets.

The present idea for the first run arrangement is the following:

3 targets ^{12}C (graphite)	→ calibration + spectroscopy
3 targets ^{6}Li	→ non mesonic decay → → $\Delta I = 1/2$ rule validity
1 target ^{7}Li	→ control of ^{6}Li purity
1 target ^{27}Al	→ capture rate for heavier nuclei

We plan to run with this set-up for ≈ 150 machine/days, ≈ 30 of them for initial debugging and setting-up (total data taking time ≈ 120 days) at $L = 10^{32}$ cm^{-2} s^{-1}

The choice of the target for the following run (of heavier mass) will be decided following the results of this first run and (presumably) following presentation and discussion with Scientific Committee of L.N.F..

SPC

USERID: SPC ORIGIN: VSOXAZ CREATED: 06/18/95 14:52:35

FILENAME: TRIGGER LIST3820 CLASS: A FORMAT:C

SPOOLID: 607 RECS: 9292 COPY: 1 DUPLICATE: 1

PRINTED AT: CERNVM ID: R113 AT: 06/18/95 14:52:45

```
**********************************************************************
*
* THIS FILE WAS SENT BY BATCHV03 AT CERNVM WITH THE COMMAND:
* PRT3812 TRIGGER LIST3820 * ( EP22A XMIT FOR SPC       NOTIFY
* SPC AT VSOXAZ
*
**********************************************************************
```

Ciao Aldo,

ti lascio le pagine di relazione -

la stampa non è delle migliori, poi la copia da dare a Brennan la stampo da un'altra parte

la figura che ho inviato, è quella che ho ottenuto facendo la distribuzione in energia degli eventi trackek sulle slab di TOFNE.

Se va bene, poi faccio opera di collaggio

Alla Simonetta mando il file LATEX e la figura in *.PS, perché non mi ricordo come misemila -

Adesso vado -

ciao

Sviluppi della configurazione del trigger di FINUDA

A. Zenoni e C. Cattaneo

Fino alla versione 108 del programma di simulazione dell'esperimento FINUDA si é provata la seguente configurazione di trigger (*prima configurazione*):

1. **TOFINO**

   - richiesta di 2 slab colpite in configurazione back to back
   - almeno due slab del tofino sopra la soglia in energia (fissata a 2.5 MeV, con un errore del 5%)

2. **TOFONE**

   - almeno un colpo pronto sul TOFONE ($\sim$ 10 ns fissato con un errore di 0.5 10^{-9})

I risultati ottenuti per eventi ipernucleari, sono riassunti nella tabella 1.

Per quanto riguarda gli eventi di fondo Touschek, ipotizzando un rate di $6 \cdot 10^6$ $ev./sec$ con una luminositá di macchina di 10^{33} $cm^{-2}\,sec^{-1}$ si é verificato che il numero di eventi che passa il trigger in queste condizioni é cosí elevato ($\approx 10^3$ al secondo) da impedire una presa dati.

Si é quindi tentato di ottimizzare l'algoritmo di trigger, introducendo una soglia in energia ($5MeV$) sulle slab del TOFONE, richiedendo che un evento passi il trigger quando rilascia in almeno una slab del TOFONE un'energia superiore alla soglia fissata (dalla Fig. 1 si ricava che ponendo una soglia a $5MeV$ solo una piccola parte, rispetto al totale degli eventi di fondo Touschek, potrebbe fornire un segnale di trigger) e richiedendo che nel TOFINO il superamento della soglia in energia avvenga nelle slab in back to back (*seconda configurazione*). Per quanto riguarda gli eventi ipernucleari, il risultato é riassunto nella tabella 2.

Per quanto riguarda il fondo Touschek i risultati sono riassunti nella tabella 3.

Il fatto che nessun evento abbia passato il trigger non é indicativo, in quanto si é stimato che il fondo sia di $6 \cdot 10^6 c./sec$, quindi ben piú alto del numero di eventi generati. Operando statisticamente, si é stimato che il numero di eventi di fondo che passerebbero il trigger con almeno uno scintillatore del TOFONE sopra soglia é:

$$\frac{4}{5000} \cdot (\frac{115}{5000}) \cdot 6 \cdot 10^6 \approx 110 \, c./sec \qquad (1)$$

dove 4 é il numero di eventi che hanno passato il trigger nel TOFINO, 115 é il numero di eventi per cui vi é almeno uno scintillatore del TOFONE sopra soglia, $6 \cdot 10^6$ é il numero di eventi di fondo al secondo e 5000 é il numero di eventi generati per la simulazione.

Per abbassare ulteriormente il fondo, si é richiesto che gli scintillatori del TOFONE sopra soglia fossero almeno due. Il risultato per gli eventi buoni é descritto in tabella 1.

Per quanto riguarda gli eventi di fondo, operando come precedentemente detto, si ottiene che 4 eventi al secondo passerebbero il trigger.

Si puó quindi affermare che per costruire un trigger efficiente, le rischieste siano:

1. configurazione in back to back e superamento della soglia in energia negli scintillatori in back to back nel TOFINO

2. coincidenza pronta sul TOFONE e almeno due slab di TOFONE accese

In questo modo il numero di eventi di fondo viene abbassato notevolmente, mentre il numero di eventi ipernucleari rimane sufficientemente alto per un realistico tempo di presa dati.

Table 1: Efficienza di TRIGGER per eventi ipernucleari: prima configurazione

Efficienza per eventi con formazione di ipernucleo	
Tofino back to back × soglia in energia	81%
Coincidenza pronta sul TOFONE	46%
TRIGGER	39%
TRIGGER con π^- con 4 hits	29%
TRIGGER π^- in avanti con alta risoluzione	13%

Figure 1: Distribuzione in energia sugli scintillatori del TOFONE per eventi Tonschek

Table 2: Efficienza di TRIGGER per eventi ipernucleari: seconda configurazione

Efficienza per eventi con formazione di ipernucleo	
Tofino back to back × soglia in energia	74.3%
Coincidenza pronta sul TOFONE × soglia in energia	45.0%
TRIGGER	37.0%
TRIGGER con π^- con 4 hits	27.7%

FINUDA Experiment (L.N.F. / DAΦNE)

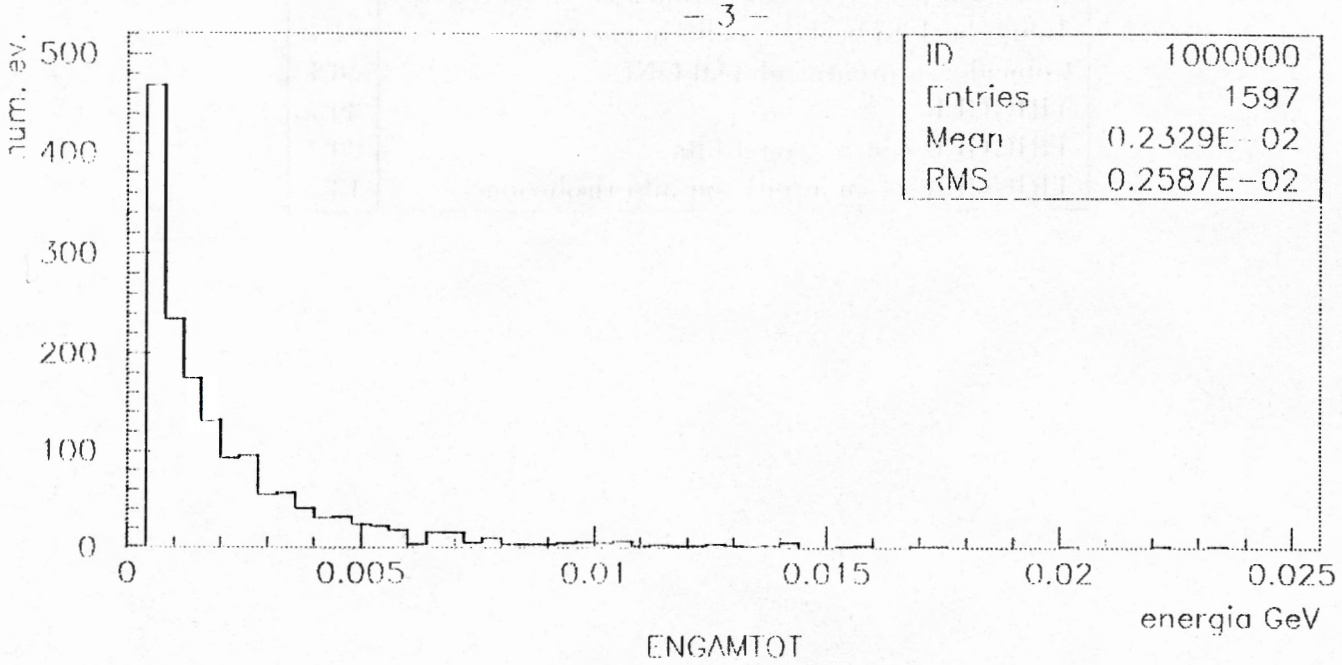

Table 3: Efficienza di TRIGGER per fondo Touschek - Seconda configurazione di TRIGGER

Numero di eventi generati	5000
Tofino back to back - soglia in energia	$8 \cdot 10^{-4}$%
Coincidenza pronta sul TOFONE	31.8%
Coincidenza pronta sul TOFONE × soglia in energia	2.3%
TRIGGER	0

Table 4: Efficienza di TRIGGER per eventi ipernucleari: configurazione definitiva

Efficienza per eventi con formazione di ipernucleo -	
Tofino back to back × soglia in energia	74.3%
Coincidenza pronta sul TOFONE × soglia in energia	45.0%
TRIGGER	34.6%
TRIGGER con π^- con 4 hits	26.4%